ornl

ORNL/TM-11281

OAK RIDGE NATIONAL LABORATORY

MARTIN MARIETTA

Metals and Ceramics Division Materials Sciences Program Annual Progress Report for Period Ending April 30, 1989

OPERATED BY
MARTIN MARIETTA ENERGY SYSTEMS, INC.
FOR THE UNITED STATES
DEPARTMENT OF ENERGY

ORNL/TM--11281

DE90 004371

ORNL/TM-11281
Dist. Category UC-404

Metals and Ceramics Division

METALS AND CERAMICS DIVISION MATERIALS SCIENCES PROGRAM ANNUAL PROGRESS REPORT FOR PERIOD ENDING APRIL 30, 1989

Compiled by
J. O. Stiegler, Manager, Materials Sciences Program

Date Published: September 1989

Prepared for the
U.S. Department of Energy
Office of Basic Energy Sciences
KC 02 01 01 0
KC 02 02 04 0
KC 02 01 05 0

Prepared by the
OAK RIDGE NATIONAL LABORATORY
Oak Ridge, Tennessee 37831-6285
operated by
MARTIN MARIETTA ENERGY SYSTEMS, INC.
for the
U.S. DEPARTMENT OF ENERGY
under Contract No. DE-AC05-84OR21400

Reports previously issued in this series are as follows:

ORNL–5089	Period Ending June 30, 1975
ORNL–5182	Period Ending June 30, 1976
ORNL–5311	Period Ending June 30, 1977
ORNL–5437	Period Ending June 30, 1978
ORNL–5589	Period Ending June 30, 1979
ORNL–5672	Period Ending June 30, 1980
ORNL/TM–7970	Period Ending June 30, 1981
ORNL/TM–8627	Period Ending December 31, 1983
ORNL/TM–9357	Period Ending June 30, 1984
ORNL/TM–10033	Period Ending December 31, 1985
ORNL/TM–10601	Period Ending June 30, 1987

Credits:
Composition and makeup: G. R. Carter

CONTENTS

ABSTRACT

This report summarizes the activities of the Materials Sciences Program in the Oak Ridge National Laboratory (ORNL) Metals and Ceramics Division for the period July 1, 1987, to April 30, 1989.

The program is directed at uncovering principles for the scientific design of materials. The efforts emphasize three classes of materials: high-temperature metallic alloys based on intermetallic compounds, structural ceramics, and radiation-resistant alloys. The principal elements of Materials Science and Engineering—synthesis/processing, characterization, properties, and performance—are incorporated in all of these programs to achieve a full understanding of the relationships among the elements. A first-principles theory provides understanding of the structure of alloy systems. Surfaces and interfaces of ceramic systems are investigated through ion beam and molecular beam epitaxy activities. Major emphasis is placed on structural characterization capabilities to furnish the link between processing and performance.

An important aspect of the program is the interaction with universities, industry, and other laboratories. Two cooperative research centers established to aid these interactions are Shared Research Equipment Program (SHaRE) and Oak Ridge Synchrotron Organization for Advanced Research (ORSOAR), which make our strong structural characterization capabilities available to researchers outside ORNL. The research activities and capabilities of these outside researchers are summarized in Chap. 1, "Structural Characterization," and Chap. 6, "Cooperative Research Centers." Other interactions with the scientific community are summarized in the appendixes.

Several major awards were given to staff members during the reporting period. C. T. Liu received the E. O. Lawrence Award presented by the Department of Energy in 1988. Teams led by Stan David received the grand prize in the International Metallographic Exhibit in both 1987 and 1988. John Vitek and Manfred Ruhle (Max Planck Institute) were awarded the 1987 Outstanding Paper Award by *Acta Metallurgica* for a pair of papers on "Diffraction Effects from Internal Interfaces"; and Mike Miller and Joe Horton received the companion award from *Scripta Metallurgica* for their paper entitled "An Atom Probe Field Ion Microscope Study of Boron-Decorated Boundaries in Ni_3Al."

1. STRUCTURAL CHARACTERIZATION

1.1 ANALYTICAL ELECTRON MICROSCOPY – *J. Bentley*

The microscopy and microanalysis task provides the core effort for state-of-the-art microstructural characterization of materials for the Basic Energy Sciences (BES) Materials Sciences Program. The facilities of the High Temperature Materials Laboratory add a substantial materials analysis capability to the division. The microscopy and microanalysis task involves both atom-probe field-ion microscopy (APFIM) and transmission electron microscopy (TEM), which centers on analytical electron microscopy (AEM). The electron microscopy work is described in this section; the APFIM work is described separately in Sect. 1.2, although in practice many of the research projects involve combined AEM and APFIM.

Three types of research are undertaken by the task: acquisition, installation, and optimization of instrumentation; development and evaluation of techniques and methods by application to basic materials science research; and application of advanced AEM to a wide range of materials, often in collaboration with other tasks.

The task is responsible for maintaining (and developing the capabilities of) the AEM (and APFIM) facilities of the Materials Science Section. Whereas these activities normally require a considerable effort, a larger than normal effort has been expended during this reporting period. A 120-kV Philips CM12/STEM AEM was delivered in August 1987, to replace our JEM 100CX and to function as a "workhorse" instrument. In January 1988, we removed our 300-kV Philips EM430T AEM and replaced it with a Philips CM30/STEM. Both CM instruments have fully equipped scanning systems including backscattered and transmission electron detectors, a full range of hybrid scanning modes, a choice of a video camera (for high-resolution imaging) or an electron energy loss spectrometer (EELS), and conventional energy-dispersive X-ray spectroscopy (EDS) analyzers. In addition, the CM12 is equipped with a secondary electron detector and a wide-angle video camera. Eventually, the X-ray detector on the CM12 will be of the windowless type (for light-element analysis). We exchanged EDS systems between the CM12 and CM30 to provide digital "imaging" on the CM30 and to allow interfacing to an EELS system with parallel collection (Gatan PEELS) that was added in the fall of 1988. However, the "serial" EELS was retained as an alternative for energy filtering. Other electron microscopes for which the task has responsibilities are a JEM 100C, a JEM 2000FX, and a Hitachi HU-1000 (which was out of service for much of the reporting period).

A large effort was required to deal with (1) extensive beam stability problems on the Philips EM400T/FEG and 300 kV Philips CM30 instruments; (2) EDS detectors and specimen holders requiring repeated repair; and (3) investigations (and revisions) of

our standard operating procedures and training requirements for facility use, in particular for the safe handling of radioactive specimens.

Strong collaborative efforts (many of which are presented in other sections of this report) continue with the BES tasks on structural ceramics, high-temperature alloy design, structure and properties of surfaces and interfaces, radiation effects, and the fundamentals of welding and joining and with other programs such as the fusion materials program. Collaborative research through the Shared Research Equipment (SHaRE) program again figured extensively in the AEM activities.

1.1.1 Electron Microscopy of Phase Transformations in Spinodal and Ordered Alloys[1,2] – *J. Bentley*

Examples illustrating the application of electron microscopy to phase transformations in spinodally decomposed and ordered alloys, the limitations of the methods, and potentially useful new techniques are reviewed. Conventional TEM and high-resolution electron microscopy (HREM) have been extensively applied to spinodally decomposed alloys. Stress relaxation in thin foils is important in understanding contrast mechanisms and in quantitative image interpretation. For HREM of systems with high strain, simulations that incorporate stress relaxation as well as microscope aberrations are required. For aligned structures with lower strain, stress relaxation may be less important but sensitivity to local changes in composition through lattice spacings is decreased. Surface effects can dominate diffraction and phase contrast in conventional imaging of spinodally decomposed alloys — through preferential etching in some isotropic structures and through relaxation-induced near-surface bending of lattice planes in highly strained structures. Potential image overlap problems are thus reduced, and wavelength measurement becomes fairly insensitive to foil thickness. There is great potential for application of high-spatial-resolution AEM to direct measurement of composition modulations in spinodally decomposed alloys. Conventional and high-resolution electron microscopy have been applied effectively to ordered alloys, particularly for long-period superlattice and domain characterization. A variety of methods for determination of long-range-order parameters have been developed and, whereas none is ideally suited for all applications, many have been successfully used where X-ray and neutron diffraction techniques were inapplicable. The development of techniques for order determination from wide-angle convergent beam electron diffraction (WACBED) patterns is expected. The atom location by channeling enhanced microanalysis (ALCHEMI) technique can provide quantitative sublattice occupancies in complex alloys. For many systems, however, corrections for ionization delocalization must be made.

Other complementary techniques should not be overlooked. In particular, APFIM has been shown to have some outstanding advantages for (1) the determination of the true three-dimensional morphology of isotropic and aligned modulated structures, (2) composition-profile determination at near-atomic resolution, and (3) order-parameter and site-occupancy determination, even in the presence of antisite defects.

1.1.2 AEM Characterization of Interfaces in Ceramics[3] – *J. Bentley*

Interfacial chemistry (and structure) determination in ceramics by state-of-the-art AEM is reviewed with illustrative examples. The main topics addressed are (1) the reliable detection of intergranular phases, (2) the measurement of grain boundary segregation in the absence of an intergranular phase, and (3) the characterization of intergranular phases. In the first section, the use and limitations of lattice imaging, Fresnel fringes, and Z-contrast methods are discussed with an emphasis on avoiding misleading results caused by artifacts such as grain boundary grooving during specimen preparation. In the second section, emphasis is on the spatial resolution and detection limits for analysis by EDS, EELS, and Z-contrast imaging. Comparisons with APFIM methods and results from metals are included. The third section covers the reliable determination of compositions with regard to secondary fluorescence effects, EELS fine structure analyses such as chemical bonding information from near-edge detail and radial distribution function (RDF) measurement by analysis of extended energy loss fine structure (EXELFS) analyses, and RDF measurement from electron diffraction patterns.

1.1.3 X-ray Detectors[4,5] – *J. Bentley*

The paper presents a summary of the session on X-ray detectors at the Aussois Workshop on electron beam-induced spectroscopies at high spatial resolution. The existing technology, the materials properties, and the operating characteristics of EDS detectors based on high-purity Ge, Si(Li), and HgI_2 and the various windows [conventional Be, ultrathin (UTW), thin windows that are able to withstand one atmosphere pressure, and "windowless" (WL)] were described. Several practical problems and malfunctions of EDS detectors were discussed at length including: self counting and high dead times caused by "flooding" with hard X-rays, incomplete charge collection caused by carrier deflection in the strong magnetic field of the objective lens, radiation shielding, shutters for protection from backscattered electrons, radiation hardening, and ice formation and removal for WL and UTW detectors. A UHV-compatible, compact, wavelength-dispersive spectrometer (WDS) for use in the specimen area of a 300-kV AEM was discussed along with more speculative concepts for WDS systems with fixed crystals and position-sensitive detectors.

The last ten years have seen the introduction of WL and UTW Si(Li) detectors; the use of time-variant pulse processing; the fast (1 μs) injection junction field effect transistor (IJFET) for better resolution, higher throughput rates, and improved pileup rejection of low-energy X-rays; progress in solving problems such as ice formation on WL and UTW detectors and protection from radiation damage by the use of shutters and "radiation hardened" crystals; the increase of collection angles typically from 0.04 to 0.2 sr; the successful incorporation on 300- and 400-kV AEMs; digital beam control for "mapping" and specimen-drift correction; high take-off-angle geometries for improved P/B ratios; UTW designs capable of sustaining a pressure of one atmosphere; and reliable Ge detectors with resolutions below 140 eV and K-line detectability from carbon to uranium. However, many improvements are still urgently required. The detector is still largely viewed as an addition to the microscope, the imaging performance of which

must be maintained. There is significant potential for a more optimized integration of EDS detectors into AEMs through changes in the objective lens design. In the near future, we can expect improved energy resolution, maybe 110 eV for a Ge detector, and the incorporation of WDS systems that perhaps include novel arrangements of complex multilayer diffracting "crystals" and position-sensitive detectors.

1.1.4 Sublattice Occupancies of Pd in $Cu_{0.5}Au_{0.5-x}Pd_x$ Alloys by ALCHEMI[6] – *J. Bentley and K. Hisatsune*[7]

X-ray diffraction of $L1_0$ ordered $Cu_{0.5}Au_{0.5-x}Pd_x$ ($0 < x < 0.25$) alloys shows that, whereas the unit cell volume decreases monotonically with increasing palladium content, the axial ratio c/a exhibits a maximum at about 4 at. % Pd, corresponding to local minimum and maximum values for a and c, respectively. Theoretical modeling that failed to predict the anomalous behavior assumed that Pd atoms were randomly interchangeable only with Au atoms. The ALCHEMI method was used to measure directly the sublattice occupancy of palladium.

Ion-milled specimens previously electropolished with an electrolyte of 10% perchloric acid in acetic acid were analyzed at 130 K with Philips CM12/STEM, EM400T/FEG, and CM30/STEM instruments and EDAX 9100/70 and 9900 energy-dispersive X-ray microanalysis systems. X-ray spectra were recorded at the symmetry position (channeling orientation) and near the tenth-order Bragg condition ("random" orientation) on the [001] and $[1\bar{1}0]$ systematic rows. The fraction (C) of Pd on Au sites was determined from $C = [R(Pd/Cu)-1]/[R(Au/Cu)-1]$, where $R(Pd/Cu) = (N_{Pd}/N_{Cu})_{channeling}/(N_{Pd}/N_{Cu})_{random}$, etc., and N_A is the integrated X-ray intensity for element A. The use of CuKα, PdKα, and AuLα peaks obviated the need for delocalization or absorption corrections.

A bright-field image showing twins on (011) and antiphase boundaries (APBs) in $Cu_{50}Au_{45}Pd_5$ is shown in Fig. 1.1.1(*a*). The twins, which are directly analogous to those formed in orthorhombic $YBa_2Cu_3O_{7-x}$ superconducting materials, relieve the transformation strains caused by the tetragonal distortion ($c/a = 0.93$) of the $L1_0$ structure. A selected area diffraction (SAD) pattern that exhibits "spot-splitting" caused by the two twins with [001] rotated by ~86.5° is shown in Fig. 1.1.1(*b*). The ion milling resulted in a disordered surface layer with different unit cell dimensions (and possibly composition) that gave rise to arrays of misfit dislocations [Fig. 1.1.1(*a*)] and to streaking in the diffraction patterns [Fig. 1.1.1(*b*)]. Alloys containing 15 and 25 at. % Pd have far fewer twins, which is probably because of different ordering temperatures relative to the annealing treatments.

Partial energy-dispersive X-ray spectra from a single domain in the $Cu_{50}Au_{45}Pd_5$ material are shown in Fig. 1.1.2. The differences in the AuLα/CuKα and PdKα/CuKα intensity ratios for the symmetry position on the [001] systematic row and a "random" orientation are clearly visible. Quantitative ALCHEMI analyses showed that the occupancies of Pd on the Au sublattice were 90 ± 2% and 105 ± 3% for the 5 and 25 at. % Pd alloys, respectively. X-ray diffraction and atom probe determinations are also planned.

ORNL PHOTO 5364-88

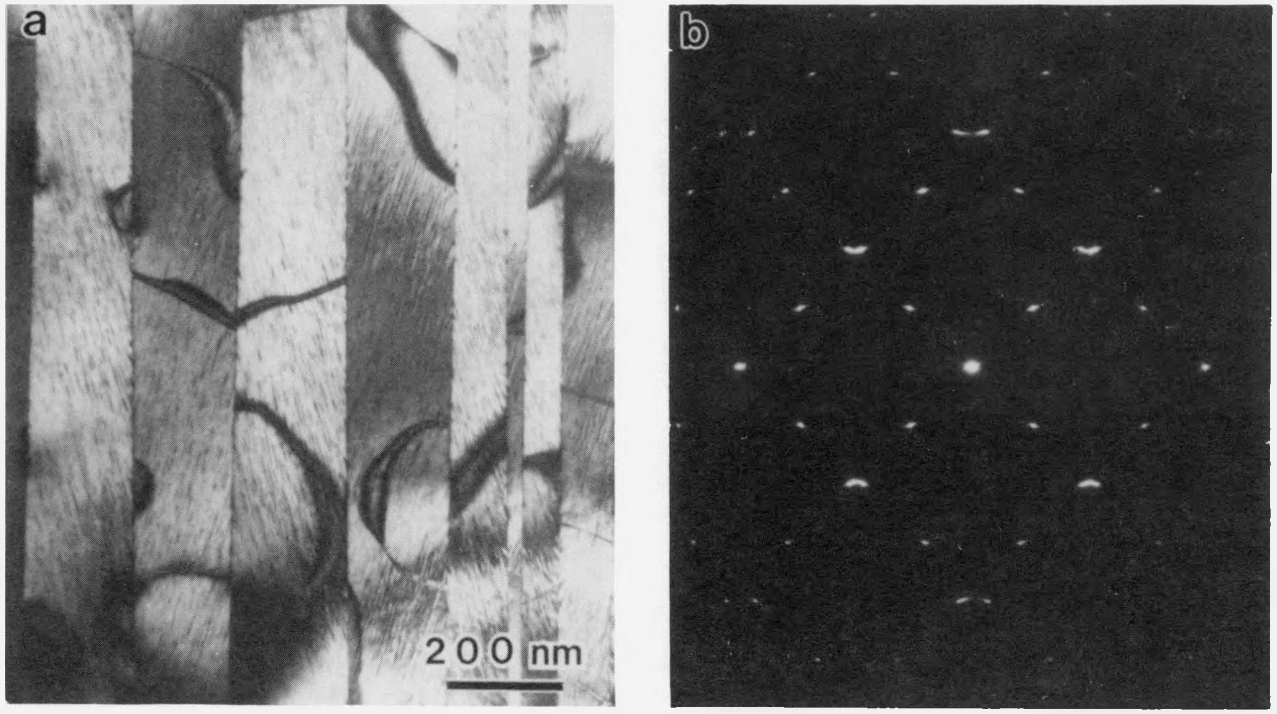

Fig. 1.1.1. (*a*) Bright-field image of $Cu_{50}Au_{45}Pd_5$ showing twins on (011) and APBs. Note presence of misfit dislocations resulting from disordered surface layer caused by ion milling. (*b*) [100] SAD pattern collinear with (*a*) showing "splitting" caused by two variants with [001] rotated by ~86.5°. Note streaking normal to misfit dislocations.

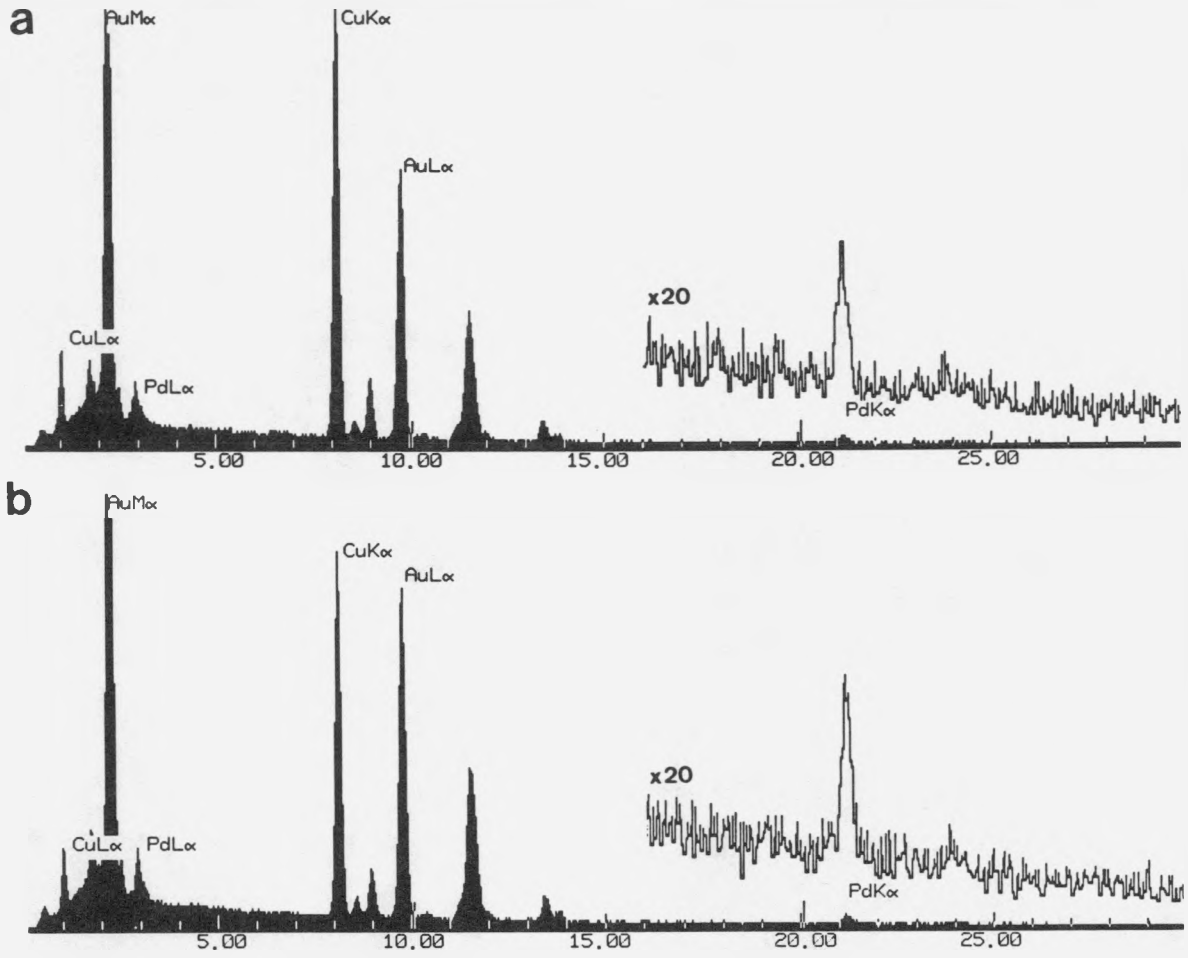

Fig. 1.1.2. Energy dispersive X-ray spectra from a single domain in $Cu_{50}Au_{45}Pd_5$. (*a*) symmetry position of [001] systematic row. Full scale = 12,000 and 600 counts/channel for solid and line spectra respectively. (*b*) "Random" orientation ($s_{0,0,10}>0$). Full scale = 10,000 and 500 counts/channel for solid and line spectra, respectively.

1.1.5 Radial Distribution Functions from Diffracted Electron Intensities[8,9] – *J. Bentley, P. Angelini, P. S. Sklad, and A. T. Fisher*

Many previous studies have shown the benefits of electronically recorded intensity profiles of electron diffraction patterns obtained with a TEM. The technique avoids the complex procedures involved in making densitometer traces from film, greatly expands the dynamic range, and allows energy filtering to remove inelastically scattered electrons that have lost more than a few eV. Potential applications for structural materials include surface oxide layers on metals and ceramics, surface-modified (ion-implanted) materials, intergranular amorphous phases in ceramics, and materials amorphized by in situ electron irradiation. For these applications, specimen preparation may limit available foil thicknesses. Therefore, besides refinement of practical experimental procedures, including the ability to obtain data with small focused probes (i.e., convergent-beam conditions), multiple scattering effects also have to be accounted for to confidently apply the method.

Most of the current measurements were made at 300 kV with a Philips CM30/STEM AEM equipped with a Gatan 607 EELS and EDAX 9900 microanalysis system, although a Philips EM400T/STEM with a field emission gun (FEG) was also used. A modified EELS (multichannel scaling) digital voltage "ramp" from the EDAX 9900 was input through an analog interface to the STEM unit operating in the post-specimen scanning (SCID) mode, thus preserving the available scan rotation, amplitude, and alignment functions of the CM30. A camera length of about 2 m, a scan amplitude of ~300 mrad, an EELS entrance aperture of 1 mm diameter, an energy window of 10 eV centered on the zero-loss peak, screen currents of up to 20 nA, and multiple scans totalling about 400 ms/channel were typically used. Direct pulse counting from the EELS photomultiplier detector was employed, with care taken to remain in the linear range and to avoid swamping the detector by exposure to the intense forward scattered beam. Generally, specimens were cooled to ~150 K to reduce contamination and thermal diffuse scattering while avoiding ice formation that occurred at lower temperatures. Thin polycrystalline evaporated films of gold or aluminum were used for calibrations. Data files were transferred to a personal computer for analysis with the ASYSTANT commercial software package. The intensity profiles I(s) were converted to reduced intensity functions $\phi(s) = s\{I-[N(X_a f_a^2+X_b f_b^2)]\}/N(X_a f_a+X_b f_b)^2 = 4\pi \int^{\infty} r[\rho(r)-\rho_0]\sin(sr)dr$, where $s = 4\pi\sin\theta/\lambda$, N is a scaling factor, f_a is the electron scattering factor for element a of concentration X_a, r is the interatomic distance, $\rho(r)$ is the radial density function, ρ_0 is the average atomic density, λ is the incident electron wavelength, and 2θ is the scattering angle. The Fourier (sine) transform provides the reduced density and radial distribution functions.

Experiments on evaporated carbon films of thickness $t = 0.1\lambda_p$ or $0.3\lambda_p$, where λ_p is the inelastic mean-free-path length, revealed that practically identical reduced-intensity functions and Fourier transforms were obtained for energy windows of 10 and 50 eV, indicating that at these thicknesses energy filtering may not be important and that criticisms of film-recorded (unfiltered) intensities may be unjustified. For the carbon film with $t = 0.3\lambda_p$, a broader intensity distribution (higher relative intensity at large scattering

angles) than for $t = 0.1\lambda_p$ was apparent. This is, of course, caused by multiple scattering. Peak positions in the Fourier transforms remained the same, but peak height ratios changed, indicating that, whereas bond length determination appears straightforward, estimates of coordination numbers are sensitive to thickness and that single scattering profiles, as assumed in the model, are required for accurate determinations. Intensity profiles for amorphous carbon obtained with an incident beam divergence of 16 mrad, while possessing broader peaks, gave peak widths and positions in the Fourier transforms almost identical to data obtained with a beam divergence of 0.5 mrad. Acceptable data were also obtained at 100 kV, although the intensity profiles were limited to smaller scattering vectors. Finally, data from SiC amorphized by ion implantation with chromium, although from thicker regions ($t = 0.36$ and $0.8\lambda_p$), gave Si-C and Si-Si (or C-C) peak positions that compared well with EXELFS data from the same material.

1.1.6 Structural Characterization of Cobalt Catalysts on a Silica Support[10] – *R. Srinivasan,[11] R. J. De Angelis,[11] P. J. Reucroft,[11] A. G. Dhere,[12] and J. Bentley*

In situ X-ray diffraction was used to characterize the structure of several cobalt catalysts on a silica support. The catalysts were reduced in flowing hydrogen at 350°C for about 16 h, and X-ray diffraction patterns were collected. After reduction, metallic cobalt was found to be present in the hcp and fcc forms in the ratio of 7:3 and 17% of the hexagonal close-packed planes were found to be faulted. If surface atoms adjacent to stacking faults are sources of active sites, the density of active sites was estimated to be 4.0×10^{19} per gram of cobalt.

1.1.7 Loss of Grain Boundary Segregant During Ion Milling[13] – *E. A. Kenik*

Bismuth segregates to grain boundaries in copper at intermediate temperatures (400–800°C). Currently, X-ray microanalysis is being used to measure the degree of equilibrium segregation as a function of boundary character. As part of that study, TEM specimens were prepared by several techniques to select the method that produced optimum specimens. Electropolishing produced specimens of marginal quality because of preferential grain boundary attack. On the other hand, ion-milling produced good, thin specimens with little or no boundary attack. However, X-ray microanalysis on specimens ion-milled at room temperature indicated no bismuth segregation, whereas analysis on electropolished specimens indicated bismuth segregation. A loss of bismuth from the ion-milled specimens was proposed to result from the high vapor pressure of bismuth at slightly elevated temperatures. The use of a liquid nitrogen cold stage during ion-milling minimizes the loss of bismuth. It is likely that beam heating during ion-milling is a contributing factor in this process and must be controlled. Similar loss of segregated phosphorus from boundaries was observed in room-temperature ion-milled specimens of type 304L stainless steel. In this case, electropolishing provided good specimens without preferential grain boundary attack, and X-ray microanalysis was performed on such specimens.

1.1.8 AEM of Phosphorus Segregation to Boundaries in Type 304L Stainless Steels – *E. A. Kenik*

X-ray microanalysis with ā 2.0-nm-diam probe has been used to detect segregation of phosphorus to boundaries in two different heats of Type 304L stainless steel. The first heat (supplied by C. L. Briant, General Electric Research and Development Center) contained 0.060 wt % P. Auger electron spectroscopy performed at GE indicated that for aging near 600°C this material exhibited ~15 at. % P at grain boundaries. AEM did not indicate the presence of any phosphorus-enriched precipitate at the grain boundaries. X-ray microanalysis indicated apparent phosphorus levels of ~1.2 at. % P. In addition, a slight increase in the chromium level and attendant decrease in the iron level were observed. The compositions were corrected for the size of the boundary segregant layer relative to that of the excited volume. Based on the assumption of a 0.2-nm-segregant layer, a grain boundary phosphorus level of ~15 at. % was calculated. The agreement between the Auger and AEM results may be somewhat fortuitous because the corrected phosphorus level is inversely related to the assumed segregant thickness. The assumed value of 0.2 nm is based on a single atomic layer of segregation at the boundary and typical interatomic spacings for common metals.

The second heat (supplied by Y. Kuriki, NKK Corporation, Japan) contained 0.012 wt % P and was aged at 750°C for 1 h. As a result of the lower phosphorus content of the steel, the apparent levels detected at the grain boundaries were lower (~0.50 ± 0.19 at. % P). A small increase in chromium and a corresponding decrease in iron at the grain boundaries was observed, similar to that observed for the other heat. To improve the detection limit for phosphorus, long acquisition times and summation of multiple analyses were required. As the minimum mass fraction (MMF) detectable for phosphorus was calculated as 0.15 wt % (0.27 at. %) P for individual analyses and 0.08 wt % (0.14 at. %) P for the summed analyses, the measured value of ~0.50 at. % P is statistically significant. A grain boundary composition of 6.7 at. % P was calculated after correcting for the size of the boundary segregant layer relative to that of the excited volume. Auger analysis of the grain boundary composition was not possible because the material could not be fractured intergranularly.

1.1.9 Phase Stability of Ni_2Al_3 Under Electron Irradiation[14-16] – *E. A. Kenik and M. Nastasi*[17]

In situ electron irradiations at 200, 300, and 1000 keV have been performed on Ni_2Al_3 at 100 and 300 K. At low doses, the Ni_2Al_3 partially disorders to a B2 structure with a lattice parameter of 0.284 nm, close to that extrapolated for β-NiAl at 60 at. % Al, the Ni_2Al_3 composition. The electron dose required to disorder the Ni_2Al_3 decreased with increasing accelerating voltage and possibly with decreasing temperature. At high doses, precipitation of aluminum from the B2 matrix occurs, along with radiation-induced sputtering and radiation-induced segregation. Mass loss was observed in some of the high dose irradiations at 300 kV and is illustrated for irradiation at 100 K in Fig. 1.1.3. The intensity of bremsstrahlung X-rays, which is proportional to the local mass thickness, indicated that the center of the irradiated area had decreased to half

ORNL PHOTO 5310-88

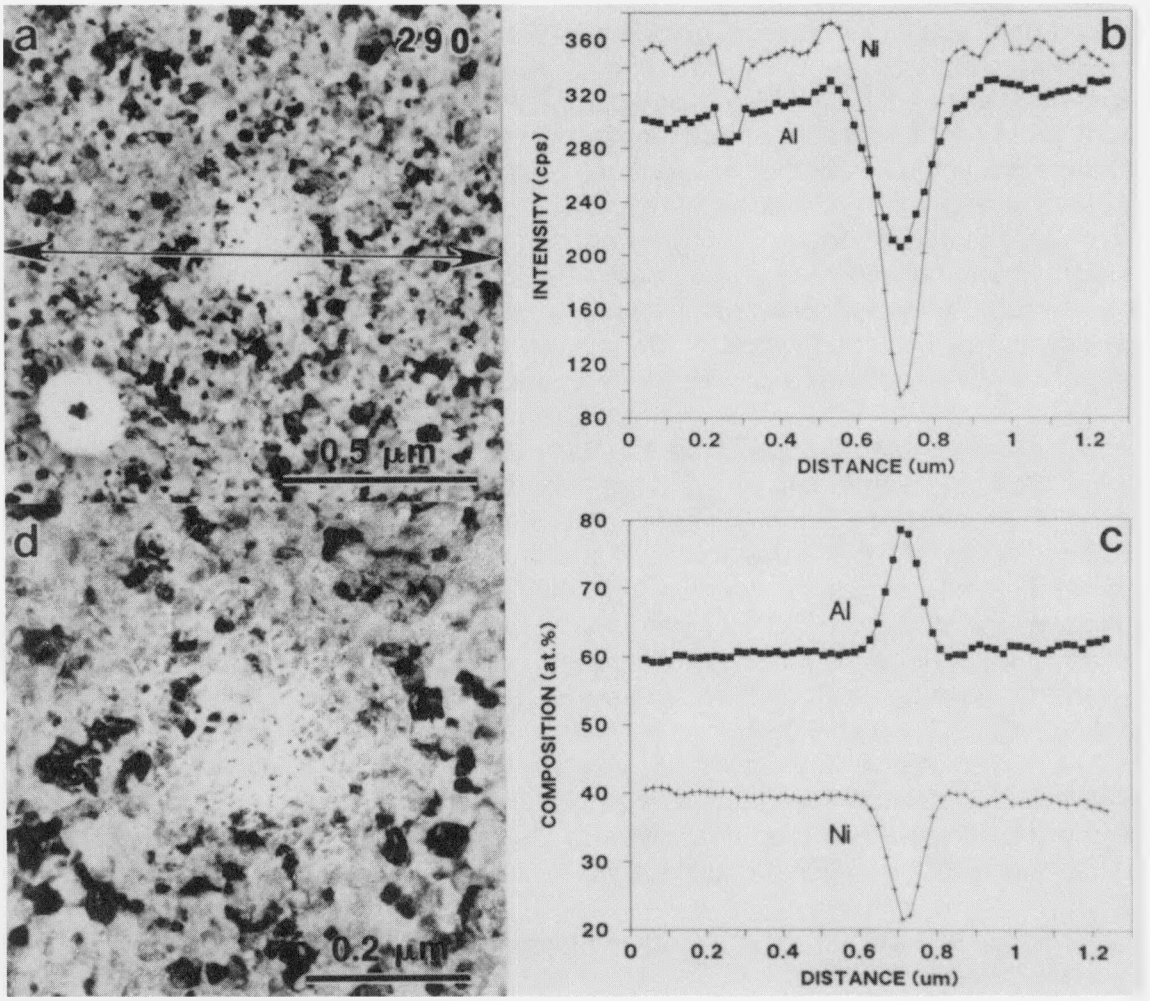

Fig. 1.1.3. Mass loss in Ni_2Al_3. (*a*) Area irradiated at 100 K with 300-keV electrons at a flux of 8×10^{24} electrons/m^2s to a dose of 290×10^{28} electrons/m^2, as indicated in figure. Arrow indicates location of X-ray line scan. (*b*) K X-ray intensities and (*c*) composition determined from X-ray line scan. (*d*) Central area at higher magnification and 2.4-μm underfocus showing lower mass thickness at irradiated grain boundaries.

the mass thickness of the unirradiated film. The data shown in Fig. 1.1.3(*b*) indicate that both aluminum and nickel K X-ray intensities decreased at the center of the irradiated area, indicating loss of both aluminum and nickel. In the composition profile [Fig. 1.1.3(*c*)], the center is enriched in aluminum (>75 at. % Al), indicating that nickel was lost preferentially. For Ni-Al alloys, preferential sputtering of aluminum is predicted from the larger kinetic energy transferred to aluminum and its presumably lower sublimation energy in the intermetallic compound. The discrepancy between the predicted and observed behavior probably results from radiation-induced segregation (RIS) driven by fluxes of point defects to sinks. At low temperatures, only self-interstitials are mobile and undersized atoms, such as nickel, will be transported via interstitial diffusion to defect sinks. The surfaces of the film would tend to become nickel enriched and sputtering from the electron-exit surface could result in preferential nickel loss as observed.

Figure 1.1.3(*d*) is a higher-magnification image of the center of the irradiated area underfocused by ~2.4 μm. The original grain boundaries appear lighter, indicating a local decrease in mass thickness, which may represent a bulk effect (composition or density difference) or a thickness effect (grain boundary grooving). Because grain boundaries in the adjacent unirradiated material do not exhibit this behavior, this effect must be associated with either RIS or sputtering. High-resolution EDS with an ~5-nm probe indicated that the grain boundaries near the center of the irradiated area exhibit Al/Ni ratios ~1.7 times higher than those of the adjacent matrix. This indicates that the local decrease in mass thickness apparent in Fig. 1.1.3(*d*) arises at least in part from a composition difference.

Lattice parameter changes for the B2 structure observed during irradiation are explained in terms of the radiation/sputtering-induced composition changes and the compositional dependence of the lattice parameter of β-NiAl. The B2 structure remains stable to a dose of 6×10^{28} electrons/m^2, with no amorphization detected. The appearance of essentially pure aluminum during irradiation indicates that $NiAl_3$, the intermediate phase in the Ni-Al phase diagram, is unstable under electron irradiation. This has been confirmed by separate irradiations of that phase.

1.1.10 In Situ Oxidation of Ni_3Al Alloys[18] – *K. R. Lawless,*[19] *J. V. Cathcart, and E. A. Kenik*

In situ high voltage electron microscopy (HVEM) oxidation studies have been performed to investigate the origin of dynamic embrittlement in Ni_3Al alloys. Microstructural changes were observed during oxidation at 600–750°C at oxygen pressures of 13–60 mPa. A thin, fine-grained oxide layer of polycrystalline γ-Al_2O_3 formed initially and showed preferred orientation with the underlying matrix. In thin areas, lateral diffusion of the rejected nickel resulted in metallic islands of essentially pure nickel (~5 at. % Al), which were thicker than the original matrix. At such a composition, the alloy was a random solid solution and no superlattice reflections were observed in diffraction patterns. In thicker regions, the matrix was similarly depleted of aluminum by the preferential oxidation of aluminum. This resulted in a triple-layer

structure; γ-Al_2O_3 outer layer, random solid solution of aluminum in fcc nickel, and the $L1_2$ ordered matrix. Larger, discrete γ-Al_2O_3 particles formed and grew into the matrix. These particles generally formed in a cube-on-cube orientation relation with the matrix, but on (100) oriented grains a (111) oriented oxide was also observed. Preferential formation of γ-Al_2O_3 occured at grain boundaries and resulted in penetration of the matrix. Dislocations were generated in the underlying metal as a result of the stresses generated by lattice mismatch of the oxide, matrix, and possibly the disordered solid solution. Several of the microstructural changes observed in these experiments may be relevant to the dynamic embrittlement in Ni_3Al alloys. These include the preferential oxidation of aluminum with the attendant disordering of the matrix and lateral diffusion of nickel, preferential grain boundary oxidation, and the generation of dislocations near the oxide layer.

1.1.11 Laser Enhanced Adhesion of Copper Films to Sapphire Substrates[20,21] – *E. A. Kenik, A. J. Pedraza,[22] M. J. Godbole,[22] D. H. Lowndes,[23] and J. R. Thompson[23]*

Strongly adherent films of copper on sapphire have been grown by alternating sputter deposition with pulsed laser treatment (PLT). Ultraviolet excimer lasers produce less damage to the films than do visible or infrared lasers. Single copper layers greater than 80 nm thick exhibit film damage and separation after PLT, whereas thinner films are adherent. AEM indicated the formation of an intermediate compound containing both aluminum and copper. Electron diffraction indicates that the structure of the intermediate compound depends on the atmosphere in which the laser treatment is performed. For PLT in argon, the copper appears to be incorporated into a distorted sapphire structure; whereas for PLT in air, the intermediate compound has the trirutile structure. Regions of strong copper-sapphire bonding and good thermal contact form early in the sequential deposition process and permit deposition of thick, adherent copper films. These regions are presumed to be related to the formation of the intermediate compound.

1.1.12 A Microscopic Evaluation of the Low-Temperature Aging of Type-308 Stainless Steel Weldments[24] – *K. B. Alexander, M. K. Miller, D. J. Alexander, and R. K. Nanstad*

Type-308 stainless steel is often used as weld filler metal in light-water reactor piping systems. In similar cast CF8-type steels, the ferrite phase has been shown to be responsible for the reported degradation in properties after long-term aging at temperatures between 300 and 400°C. Despite the relatively low volume fraction of ferrite in the type-308 materials, long-term aging at the maximum operating temperature (343°C) results in a significant loss in impact toughness. G-phase precipitation was detected by TEM in the ferrite of the aged welds, both in the matrix and on dislocations. Composition modulations in the aged ferrite consistent with spinodal decomposition were detected in atom probe composition profiles. A variety of statistical techniques were used to analyze the atom probe composition profiles. The spinodal decomposition of the ferrite into iron-rich and chromium-enriched regions is the most likely cause of the mechanical property degradation of these materials during aging.

1.1.13 Characterization of Amorphization of Ni-Ti Multilayers[25] – *K. B. Alexander, F. J. Walker, R. A. McKee, and F. A. List III*

The amorphous layers that form during the molecular beam epitaxy (MBE) deposition of nickel-titanium multilayers has been studied with the use of reflection high-energy electron diffraction (RHEED) and TEM. The amorphous layer thickness measured from RHEED and from both cleaved and liquid-nitrogen-cooled ion-milled TEM specimens is approximately 1.7 nm. Specimens prepared by ion-milling without liquid-nitrogen cooling resulted in an increase in the amorphous layer thickness. The amorphization process has also been studied with the use of specimens aged at temperatures between 200–350°C and by in situ heating in the transmission electron microscope.

1.1.14 Multilayer Ceramic Thin Films[26] – *K. B. Alexander, F. J. Walker, R. A. McKee, and F. A. List III*

Titanium oxide/aluminum oxide films have been deposited by MBE methods and characterized by RHEED and TEM techniques. Growth on silicon substrates below 973 K resulted in primarily amorphous multilayers. At 1323 K, the deposition of titanium in an oxygen atmosphere on (0001) Al_2O_3 substrates resulted in films of Ti_2O_3. These films consisted of small domains, up to 60 nm, slightly misoriented from a $[11\bar{2}0] \parallel [11\bar{2}0]$ orientation relationship. Two variants of Ti_2O_3 were observed because of multiple positioning during growth. Closing the titanium shutter during growth resulted in an oriented TiO_2 film.

1.1.15 Grain Boundary Chemistries in Yttrium-Based High-Temperature Superconductors[27,28] – *K. B. Alexander, D. M. Kroeger, J. Bentley, and J. Brynestad*[29]

In bulk, sintered ceramic high-temperature superconductor (high-T_c) materials, the grain boundaries, or portions of them are presumed to act as "weak links" to current flow. Knowledge of the structure and chemistry of the grain boundaries is therefore crucial to improving the properties of these materials. AEM has been used to show variations in yttrium segregation to local sites along a grain boundary in a specimen containing excess barium. Carefully prepared stoichiometric $Y_1Ba_2Cu_3O_{7-x}$ alloys and off-stoichiometric alloys have been examined by Auger electron spectroscopy. Stoichiometric alloys tend to exhibit excess copper at the grain boundary, whereas alloys with excess barium show excess yttrium at the boundaries. In general, the electron microscopy results agree with the Auger experiments. With the small probe size (2 nm) available with the Philips EM400T equipped with a field emission gun, variations in segregation along a grain boundary could be measured. In an off-stoichiometric alloy with 0.2% excess barium, when portions of the grain boundary that have the c-axis of one grain parallel to the grain boundary plane show excess yttrium, those portions of the grain boundary that deviate from this configuration have considerably more yttrium associated with them (see Fig. 1.1.4). This result clearly shows that preferential segregation occurs along the grain boundary in these materials.

ORNL PHOTO YP–8613

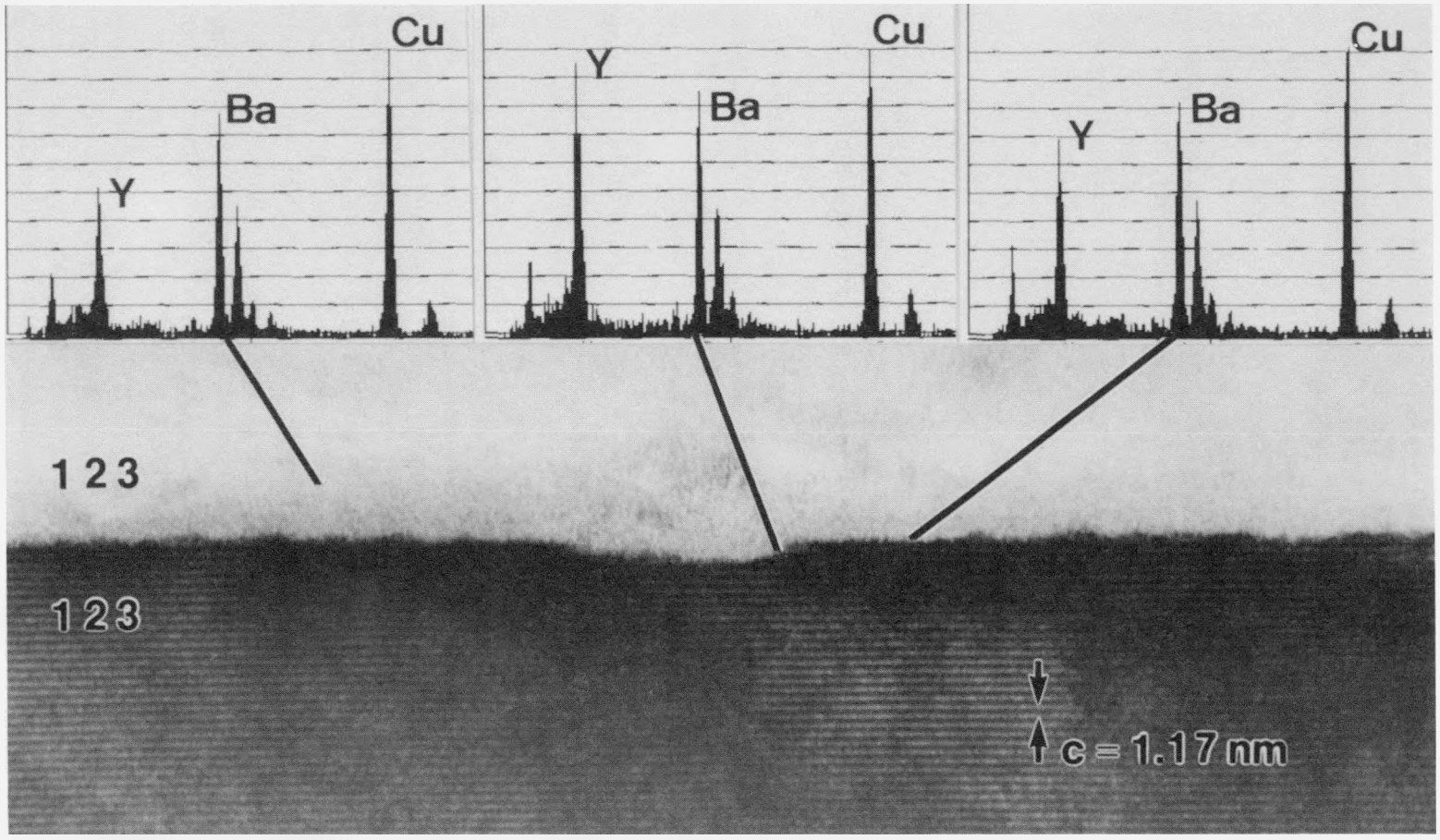

Fig. 1.1.4. Energy-dispersive X-ray microanalysis of a grain boundary in $YBa_{2.004}Cu_3O_{7-x}$. The steps along the grain boundary show more yttrium segregation than the flat portions which are parallel to the c-axis of the lower grain.

This study has shown the first experimental evidence of preferential segregation along a boundary in ceramic high-T_c materials.

1.1.16 Microstructural Characterization of α-Al_2O_3 Implanted with Iron[30] – *P. S. Sklad, J. D. McCallum, S. J. Pennycook,[23] C. J. McHargue, C. W. White,[23] and A. Perez[31]*

Rutherford backscattering spectroscopy (RBS), conversion electron Mössbauer spectroscopy (CEMS), AEM, and Z-contrast imaging in a scanning transmission electron microscope have been used to characterize the microstructure, the valence state, and the composition of Al_2O_3 implanted with iron. In as-implanted specimens, the iron resides in several different valence states. The results of CEMS investigations indicate that at high doses (6×10^{16} Fe^+/cm^2) approximately one half of the resident iron is in the Fe^0 state in the form of metallic iron clusters. This result is confirmed by conventional TEM analysis and Z-contrast imaging, both of which identified the 1- to 2-nm-diam clusters as α-Fe, Fig. 1.1.5.

It is also clear from RBS and AEM that the implanted iron undergoes significant redistribution during subsequent anneals in oxygen. The redistribution is accompanied by changes in the valence state of the iron (measured by CEMS). TEM examination of the microstructural evolution reveals that the changes in the iron distribution are the result of diffusion (mostly toward the surface) and the formation of precipitates both on the surface and in subsurface regions. Surface precipitates have been identified as α-Fe_2O_3, whereas subsurface precipitates have been identified as spinel. This phase development is consistent with the predictions of phase diagrams and also agrees with results of CEMS measurements.

The results of RBS measurements made on specimens annealed at high temperatures (≈1500°C) reveal that almost one half of the implanted iron is lost from the specimen. Transmission electron microscopy results show that the remaining iron is present in the form of subsurface precipitates of Fe_3O_4 containing aluminum as an impurity. There is no indication of the growth of precipitates on the specimen surface. These results suggests that the oxide is volatile under these conditions. The exact mechanisms involved in the diffusion and eventual loss of iron, with the corresponding change in valence state, are not well understood currently. Development of a mechanistic description of these processes must await the results of additional studies.

1.1.17 Amorphous to Gamma Transformation in Ion-Implanted Al_2O_3 (refs. 32,33) – *P. S. Sklad, J. C. McCallum,[23] C. J. McHargue, and C. W. White[23]*

Amorphous surface layers, free of implanted impurities, were produced on single-crystal α-Al_2O_3 substrates by implantation at –185°C with 2×10^{16} Al/cm^2 at 90 keV and 3×10^{16} O/cm^2 at 55 keV. The response of these amorphous layers to postimplantation annealing in the temperature range from 700 to 800°C was investigated by in situ TEM and conventional TEM of specimens annealed in bulk form. It was found that the amorphous Al_2O_3 transformed to the transitional γ phase along an irregular front. The

ORNL PHOTO 11108-88

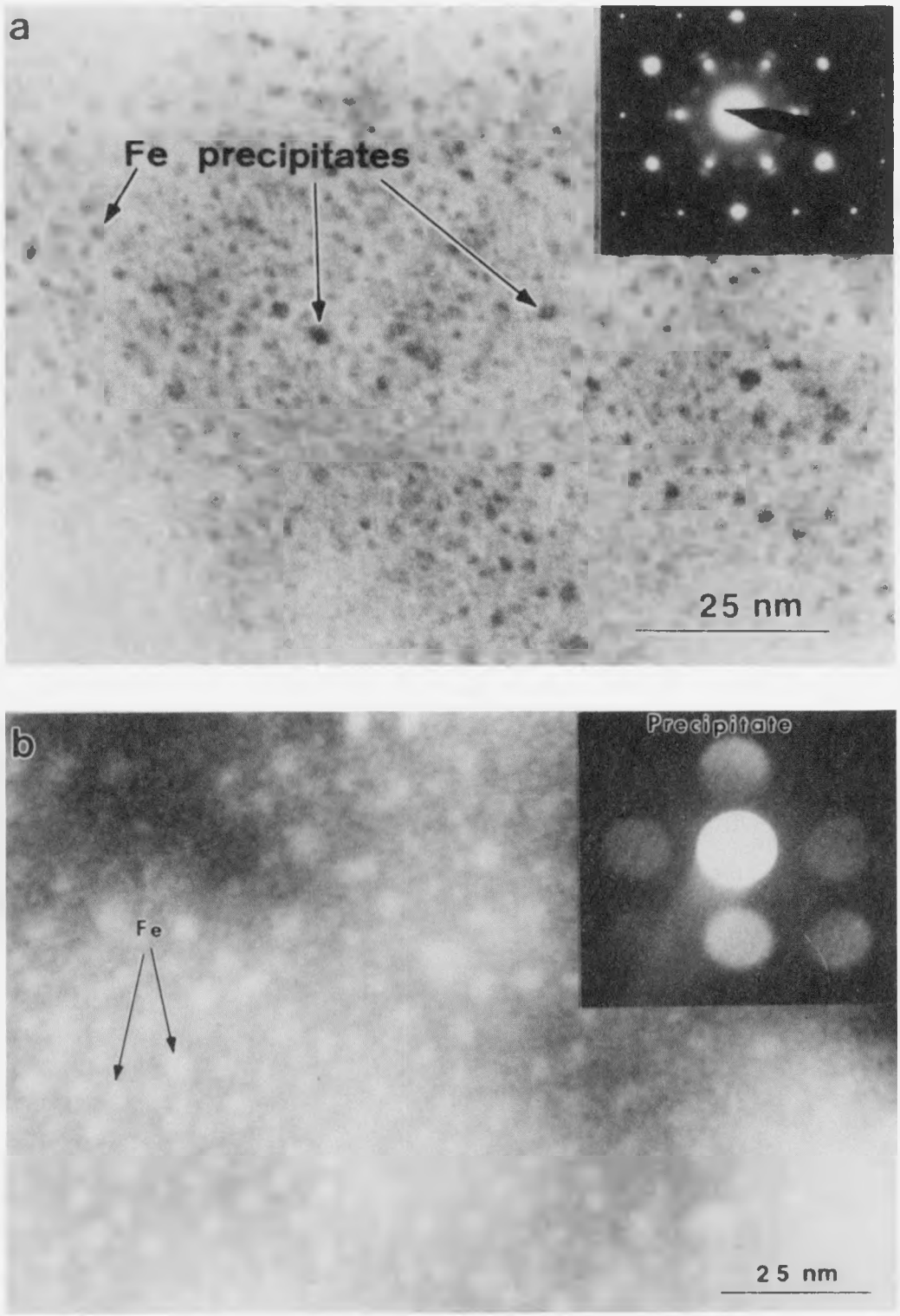

Fig. 1.1.5. As-implanted microstructure in α-Al_2O_3 implanted with 1×10^{17} Fe/cm^2 at ambient temperature. (*a*) TEM image and selected area diffraction pattern and (*b*) Z-contrast STEM image.

recrystallized material is columnar with the individual columns or domains being irregular in size and shape. The γ-Al_2O_3 is composed of two variants that are twin related and have the following orientation relationship with the substrate: $<110>_\gamma$ // $<10\bar{1}0>_\alpha$ and $(111)_\gamma$ // $(0001)_\alpha$. The temperature-dependent velocity of the amorphous-to-γ transformation front was measured by in situ TEM. Assuming a thermally activated process, the activation energy has been determined from an Arrhenius plot of velocity vs T^{-1}. Further experiments are under way to identify the rate controlling process(es) of the transformation.

1.1.18 The Preparation of TEM Specimens from Hazardous or Difficult Materials[34] – *P. S. Sklad*

The first, and often the most critical, step in any electron microscopy investigation is the preparation of an electron transparent specimen that is representative of the bulk material and in which the features of interest can be clearly observed and interpreted. However, for many materials of technological importance, specimen preparation procedures are far from routine. The application of standard, established techniques may be limited by material inhomogeneities; by physical constraints such as size or geometry; or by material constraints such as toxicity, radioactivity, or reactivity. Examples illustrating techniques for overcoming some of these difficulties are reviewed.

1.1.19 The Use of Analytical Electron Microscopy in the Study of Ion-Implanted Materials[35] – *P. S. Sklad*

Ion beam techniques are used extensively as a means of altering the surface-controlled properties of metallic, ceramic, and semiconductor materials. In most cases, the depth of implantation is limited to 1 or 2 μm. Determination of the microstructural and compositional changes that occur in regions located within a few hundred nanometers of the surface is essential to the understanding of the mechanisms responsible for the observed property changes. Electron microscopy, particularly AEM, is ideally suited for this purpose. In addition to standard imaging and diffraction techniques, other AEM techniques that prove valuable are EDS, EELS, and convergent-beam electron diffraction (CBED). These techniques allow direct measurement and quantification of the microstructure in terms of solute concentration profiles, second-phase formation, lattice damage, crystallinity of the implanted layer, and changes produced by postimplantation annealing. The depth distributions can be determined directly without recourse to energy-depth conversions (necessary for Rutherford backscattering) or sputtering rates (necessary for Auger electron spectroscopy or secondary ion mass spectroscopy). The results of AEM investigations can provide information necessary for interpreting the results from complementary techniques. Correlation of AEM observations with measured properties or predictions of theoretical models can form the basis on which ion-implantation techniques may be used to tailor the surface characteristics of materials.

1.1.20 Characterization of Amorphous Al_2O_3 by Extended Energy Loss Fine Structure (EXELFS) Analysis[36] – *P. S. Sklad, P Angelini, and J. Sevely*[37]

Investigations of the effects of ion implantation on the microstructure and properties of Al_2O_3 have demonstrated that under appropriate conditions amorphous surface layers are produced. However, other investigations have revealed differences in the response of amorphous Al_2O_3 to postimplantation thermal treatments. These differences, which are related to specifics of the implantation such as ion species, implantation temperature, and ion dose, suggest that fundamental structural and chemical differences exist in the as-implanted amorphous state. EXELFS analysis, which provides information on the near-neighbor distances around specific types of atoms, has been performed on several forms of Al_2O_3 to investigate these differences. The Al-O interatomic distance measured for a material made amorphous by implantation at –185°C with iron agrees with the value measured for α-Al_2O_3, the form into which it first crystallizes [see Fig. 1.1.6(*a*)]. In a similar way, the Al-O interatomic distance in material made amorphous by implantation at –185°C with a stoichiometric ratio of aluminum and oxygen agrees with the value measured for crystalline γ-Al_2O_3, the form into which it first crystallizes [see Fig. 1.1.6(*b*)]. The results of EXELFS analysis confirm the existence of underlying structural differences in amorphous materials originally thought to be similar. The relationship between these differences and the subsequent recrystallization behavior is a topic of continued investigation.

1.1.21 Evaluation of Amorphous and Crystalline SiC by Extended Energy Loss Fine Structure (EXELFS) Analysis[38] – *P. Angelini, P. S. Sklad, J. C. Sevely,*[37] *and D. K. Hssein*[37]

The characterization of SiC by the use of the EXELFS technique yields radial distribution functions (RDFs) that are sensitive to the structure and composition within near-neighbor distances of either C or Si atoms. EXELFS analyses of crystalline SiC are especially important to evaluate the method when comparisons with results from the amorphous state are to be made.

A commercially available SiC single crystal and SiC that had been made amorphous either by ion implantation with chromium or by irradiation with 300-kV electrons were examined in a Philips EM430T, operated at 300 kV, and equipped with a GATAN 607 EELS system and an EDAX 9100/70 X-ray energy dispersive spectroscopy system. Multiple EELS scans of the respective C and Si core absorption edges were acquired over a limited energy loss range, summed, background subtracted, and deconvoluted before EXELFS analyses were performed. Experimental parameters and analysis procedures were maintained as uniform as possible during the analyses.

Spectra were acquired at $t/\lambda \sim 0.4$, where t is the specimen thickness and λ is the plasmon mean free path length, to minimize surface effects caused by oxide layers and to maximize counting statistics while limiting multiple scattering effects. The modulations on the edges are less pronounced for amorphous than for crystalline SiC. A fourth-order polynomial, fit(E), was fitted through the core edge data to extract

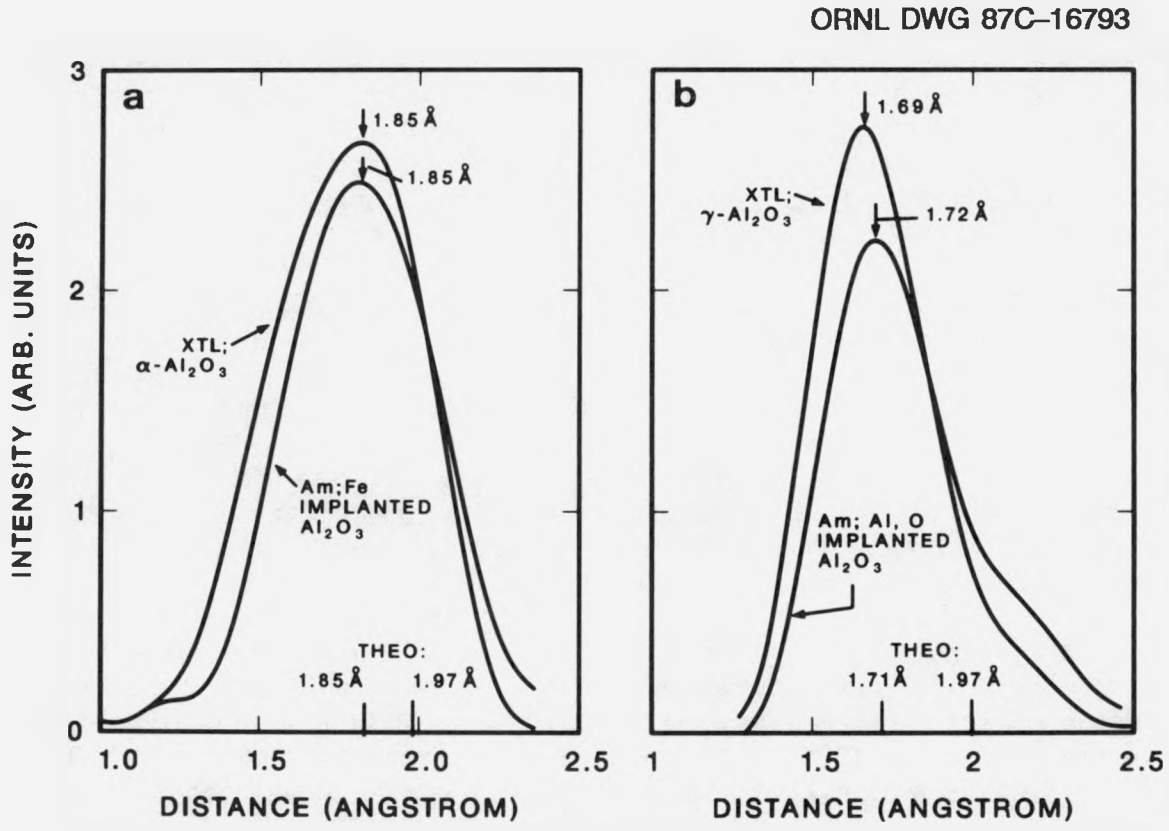

Fig. 1.1.6. First peak in the radial distribution functions for (*a*) crystalline α–Al_2O_3 and Al_2O_3 made amorphous by implantation with iron at –185°C and (*b*) crystalline γ–Al_2O_3 and Al_2O_3 made amorphous by implantation with a stoichiometric ratio of aluminum and oxygen at –185°C.

the modulations, with the energy range for the fitting starting ~30 eV above the edge energy. The EXELFS oscillation function $\chi(E)$ was then determined by calculating the ratio of the residual(E)/fit(E), where residual(E) = core edge data(E)–fit(E). After conversion from energy loss E to momentum k space and weighting of the oscillation function by k, the Fourier transform of $k\chi(k)$ was obtained. The modulus of the Fourier transform is related to the radial distribution function. Phase shift corrections must, however, be made to obtain interatomic distances. Phase shift corrections may be calculated or determined from the difference between known crystallographic structure data and the uncorrected EXELFS RDF results. Because the corrections depend on the choice of k_{min} and k_{max} used when taking the Fourier transform, it is important to perform analyses with similar parameters. The results of EXELFS analyses from both amorphous SiC specimens indicate that both the Si-C and the Si-Si (or C-C) distances have increased relative to the crystalline material by ~7% and that a loss in coordination of the Si-Si (or C-C) bond has occurred.

1.1.22 Analytical TEM Study of Yttria Stabilized Zirconia/Glass Composites[39,40] – *Y.-J. Lin,*[41] *P. Angelini, and M. L. Mecartney*[41]

Yttria-stabilized zirconia is a versatile ceramic material. In partially stabilized zirconia, the high toughness is mainly the result of the toughening effect of a tetragonal (t) to monoclinic (m) phase transformation in the vicinity of a crack. In commercial polycrystalline zirconia, often a significant amount of glassy grain boundary phase is present. This current research seeks to elucidate the effects of these grain boundary phases on the grain growth in yttria-stabilized zirconia ceramics.

Co-precipitated zirconia powders with 0, 3, 4, and 8 mol % yttria were mixed with 5 wt % of a borosilicate glass powder. The borosilicate glass was chosen because it would not scavenge yttria from the zirconia grains. Mixtures were cold pressed into pellets, sintered at 1400°C for 20 min, and then hot isostatic pressed (HIP) at 100 MPa and 1650°C for 100 min. TEM specimens were made by conventional methods. An Hitachi H600 and a Philips EM400T/FEG with an EDAX 9100 EDS system and a Gatan double-tilt cold stage were used for TEM examination.

The zirconia grains were surrounded by a substantial amount of the glass phase. The wetting angle of this glass phase eliminated the sharp corners and faceted grains commonly found in specimens without glass. The 8 mol % (cubic) specimen had the largest grains (~3.4 μm) and the 3 mol % (tetragonal) specimen had the smallest grains (~0.4 μm). The 0 mol % specimen (monoclinic at room temperature and tetragonal at the HIP temperature) had intermediate grain size (~1.5 μm). These results imply different grain growth rates for the tetragonal and cubic phases. The 4 mol % Y_2O_3-ZrO_2 specimen had a duplex structure containing both large and small grains, corresponding to the cubic and tetragonal phases. These observations on grain growth for this glass/zirconia composite are consistent with results from pure samples.

EDS analyses showed that the glassy grain boundary phase had negligible Y and low Zr (a few mol %) concentrations and that the yttria concentration often varied

significantly in the same grain for the 3 mol % Y_2O_3-ZrO_2 specimen. This implies that yttria partitioning is under way toward the equilibrium concentrations of yttria in the cubic phase (5.5 mol % Y_2O_3) and the tetragonal phase (2 mol % Y_2O_3). This partitioning may hinder the grain growth, accounting for the extremely small grain size for the 3 mol % Y_2O_3-ZrO_2 specimen.

Similar experiments were performed on co-precipitated zirconia powders containing 4 mol % yttria mixed with 5 wt % aluminosilicate glass powder. Phase partitioning into large cubic (7 mol % Y_2O_3) and small tetragonal (3 mol % Y_2O_3) zirconia grains was again observed. EDS analyses of the grain boundary phase indicated ~8 mol % yttria was present, in contrast to the negligible Y content of the borosilicate glass. The phase partitioning and extensive growth suggest that significant yttria solubility exists at high temperatures in both glasses.

1.1.23 Diffraction Effects Along the Normal to a Grain Boundary[42] – *J. M. Vitek, M. D. Vaudin,[43] M. Rühle,[44] and S. L. Sass[45]*

Much work has been done in recent years on studying the structure and properties of grain boundaries and interfaces in general. Included in these studies is work done by the authors on diffraction effects from grain boundaries along the reciprocal lattice direction that passes through the origin and is normal to a planar boundary. These studies considered the simplified case of kinematical diffraction effects caused by distortions normal to the planar interface in the boundary region.

Different methods were used by Vaudin, Sass, and co-workers, and by Vitek and Rühle to calculate the diffraction effects normal to interfaces. It has been noted both in literature and in personal communications that discrepancies existed between the results of these two groups. Specifically, disagreement was centered on three issues. First, differences were found between the calculated intensity distributions. These differences were attributed to the calculation procedures. Second, the effect of crystal shape on the diffraction calculations was disputed. Finally, the application of the results to experimental work and the interpretation of experimental results were matters of controversy.

The intent of this work was to clarify and resolve these differences, including some issues that have not been raised previously in the literature.

1.1.24 References

1. J. Bentley, *Ultramicroscopy* 30, 157-71 (1989).

2. J. Bentley, pp. 768-69 in *Proceedings of the 46th Annual Meeting of the Electron Microscopy Society of America*, G. W. Bailey, ed., San Francisco Press, San Francisco, 1988; invited presentation at EMSA meeting, Milwaukee, August 1988.

3. Summary of an invited presentation by J. Bentley at an International Symposium on Interface Structure and Reactions held in conjunction with the 41st Pacific Coast Regional Meeting of the American Ceramic Society, San Francisco, October 1988.

4. J. Bentley, *Ultramicroscopy* **28**, 211-12 (1989).

5. J. Bentley, pp. 235-36 in *Proceedings of the NSF/CNRS Workshop on Electron Beam Induced Spectroscopies with High Spatial Resolution*, C. Colliex and M. Issaacson, eds., presented at the workshop, Aussois, France, March 1988.

6. J. Bentley and K. Hisatsune, pp. 234-35 in *Proceedings of the 47th Annual Meeting of the Electron Microscopy Society of America*, G. W. Bailey, ed., San Francisco Press, San Francisco, 1989; presented at EMSA meeting, San Antonio, August 1989.

7. Nagasaki University, 7-1 Sakamoto-machi, Nagasaki 852, Japan.

8. J. Bentley et al., presented at the Materials Research Society Fall Meeting, Boston, November 1988.

9. J. Bentley et al., pp. 502-3 in *Proceedings of the 47th Annual Meeting of the Electron Microscopy Society of America*, G. W. Bailey, ed., San Francisco Press, San Francisco, 1989; invited presentation at EMSA Meeting, San Antonio, August 1989.

10. R. Srinivasan et al., submitted to *J. Catal.* (1988).

11. Department of Materials Science and Engineering, University of Kentucky, Lexington, Ky.

12. E. I. DuPont Company, 4501 North Access Road, Chattanooga, Tenn.

13. E. A. Kenik, pp. 493-95 in *Microbeam Analysis - 1989*, P. E. Russell, ed., San Francisco Press, San Francisco; presented at Microbeam Analysis Society Meeting, Asheville, N.C., July 1989.

14. E. A. Kenik and M. Nastasi, pp. 774-75 in *Proceedings of the 46th Annual Meeting of the Electron Microscopy Society of America*, G. W. Bailey, ed., San Francisco Press, San Francisco, 1988; presented at EMSA Meeting, Milwaukee, August 1988.

15. E. A. Kenik and M. Nastasi, *Ultramicroscopy* **30**, 181-7 (1989).

16. E. A. Kenik and M. Nastasi, pp. 333-38 in *Processing and Characterization of Materials Using Ion Beams*, L. E. Rehn, J. Greene, and F. A. Smidt, eds., *Materials Research Society Symposium Proceedings,* Vol. 128 (1989); presented at Materials Research Society Meeting, Boston, December 1988.

17. Materials Science and Technology Division, Los Alamos National Laboratory, P.O. Box 1663, Los Alamos, N.M.

18. L. R. Lawless, J. V. Cathcart, and E. A. Kenik, pp. 542-43 in *Proceedings of the 46th Annual Meeting of the Electron Microscopy Society of America*, G. W. Bailey, ed., San Francisco Press, San Francisco, 1988; presented at EMSA Meeting, Milwaukee, August 1988.

19. University of Virginia, Charlottesville, Va.

20. A. J. Pedraza, M. J. Godbole, E. A. Kenik, D. H. Lowndes, and J. R. Thompson, *J. Vac. Sci. Technol. A* **6(3)**, 1763-67 (1988).

21. M. J. Godbole, A. J. Pedraza, E. A. Kenik, and D. H. Lowndes, accepted for publication in *J. Mater. Res.* (September 1989).

22. University of Tennessee, Knoxville, Tenn.

23. Solid State Division, ORNL.

24. K. B. Alexander et al., to be published in *Mater. Sci. Technol.*; presented at the Workshop on Intermediate Temperature Embrittlement Process in Duplex Stainless Steels, Oxford, England, August 1989.

25. K. B. Alexander et al., pp. 452-53 in *Proceedings of the 46th Annual Meeting of the Electron Microscopy Society of America*, G. W. Bailey, ed., San Francisco Press, San Francisco, 1988; presented at EMSA meeting, Milwaukee, August 1988.

26. K. B. Alexander et al., to be published in *J. Am. Ceram. Soc.*; presented at an International Sympsoium on Interface Structure and Reactions held in conjunction with the 41st Pacific Coast Regional Meeting of the American Ceramic Society, San Francisco, October 1988.

27. K. B. Alexander et al., to be submitted to *J. Appl. Phys.*; presented at Materials Research Society Fall Meeting, Boston, November 1988.

28. K. B. Alexander et al., presented at SCANNING/EM West Meeting, Long Beach, Calif., April 1989.

29. Chemistry Division, ORNL.

30. P. S. Sklad et al., pp. 119–24 in *Characterization of the Structure and Chemistry of Defects in Materials*, B. C. Larson, M. Rühle, and D. Seidman, eds., *Mater. Res. Soc. Symp. Proc., Vol. 138* (1989); presented at MRS Fall Meeting, Boston, November 1988.

31. Université Claude Bernard, Lyon 1, Villeurbanne Cedex, France.

32. P. S. Sklad, pp. 654–55 in *Proceedings of the 47th Annual Meeting of the Electron Microscopy Society of America*, G. W. Bailey, ed., San Francisco Press, San Francisco, 1989; presented at EMSA meeting, San Antonio, August 1989.

33. P. S. Sklad et al., to be published in *Nucl. Instrum. Methods Phys. Res. B*; presented at Radiation Effects in Insulators-5, Ontario, Canada, June 1989.

34. P. S. Sklad, pp. 39-50 in *Specimen Preparation for Transmission Electron Microscopy of Materials*, J. C. Bravman, R. Anderson, and M. L. McDonald, eds., *Mater. Res. Soc. Symp. Proc.*, Vol. 115 (1988); invited presentation at MRS Fall Meeting, Boston, December 1987.

35. P. S. Sklad, pp. 149-56 in *Ion Implantation and Plasma Assisted Processes*, R. F. Hockman, H. Solnick-Legg, and K. O. Legg, eds., ASM Intl., Metals Park, Ohio (1988); presented at conference on Ion Implantation and Plasma Assisted Processes for Industrial Applications, Atlanta, May 1988.

36. P. S. Sklad et al., pp. 468-69 in *Proceedings of the 46th Annual Meeting of the Electron Microscopy Society of America*, G. W. Bailey, ed., San Francisco Press, San Francisco, 1988; presented at EMSA meeting, Milwaukee, August 1988.

37. Laboratoire d'Optique Électronique du CNRS, Toulouse, France.

38. P. Angelini et al., pp. 466-67 in *Proceedings of the 46th Annual Meeting of the Electron Microscopy Society of America*, G. W. Bailey, ed., San Francisco Press, San Francisco, 1988; presented at EMSA meeting, Milwaukee, August 1988.

39. Y.-J. Lin, P. Angelini, and M. L. Mecartney, pp. 572-73 in *Proceedings of the 46th Annual Meeting of the Electron Microscopy Society of America*, G. W. Bailey, ed., San Francisco Press, San Francisco, 1988; presented at EMSA Meeting, Milwaukee, August 1988.

40. Y.-J. Lin, M. L. Mecartney, and P. Angelini, pp. 515-17 in *Microbeam Analysis – 1989*, P. E. Russell, ed., San Francisco Press, San Francisco 1989; presented at Microbeam Analysis Society Meeting, Asheville, N.C., July 1989.

41. Department of Chemical Engineering and Materials Science, University of Minnesota, Minneapolis, Minn.

42. J. M. Vitek et al., *Scripta Metall.* **23**, 349-54 (1989).

43. Ceramics Division, National Institute of Standards and Technology, Gaithersburg, Md.

44. Department of Materials, University of California, Santa Barbara, Calif.

45. Department of Materials Science and Engineering, Cornell University, Ithaca, N.Y.

1.2 ATOM PROBE – *M. K. Miller*

During this period, the atom probe field-ion microscope (APFIM) has been successfully applied to a diverse range of projects. The research has characterized the microstructure of a variety of materials, developed new methods of analysis, and extended the range of materials that may be examined in the atom probe.

The atom probe has detected the formation of very diffuse solute atmospheres that formed during the early stages of decomposition in pressure vessel steels that were neutron-irradiated to low fluences. This new level of characterization was possible through the development of an innovative technique that is able to detect the early stages of solute clustering from the separations of atoms in the atom probe data chain.

Work on phase transformations within the low-temperature miscibility gap in the iron-chromium system has continued with an investigation into the change in morphology of the α and α' phases as a function of composition and temperature. A new method has been developed that permits the initial stage of phase separation to be distinguished from field evaporation micrographs.

The atom probe has been used in a variety of metallurgical applications. These projects included the microstructural characterization of a Udimet 720 nickel-base superalloy; characterization of the fine-scale decomposition in the Cape York, Twin City, and Santa Catharina iron-nickel meteorites; a study of the early stages of oxidation of nickel-zirconium intermetallic catalysis; an investigation of boron clustering in Ni_3Al; a study of the grain boundary chemistry of NiAl; and the identification of a B8-ordered BeFe phase in the iron-beryllium system. Several of these projects were performed collaboratively as part of the SHaRE program.

The applications of the atom probe have been extended from metallic specimens into both semiconducting and ceramic materials. Successful studies on a variety of high-temperature superconducting ceramic oxides, silicon carbide, and titanium diboride have been performed. To accomplish this, new methods of field-ion specimen preparation that used ion milling were developed.

Systematic studies were performed to provide information on the atom probe technique. These studies included an investigation of the effects of the presence of image gas on the accuracy of atom probe analyses and a comparison of the autocorrelation functions from atom probe and small angle neutron scattering (SANS) experiments.

The design and construction of the mapping atom probe (MAP) has continued during this period, with L. C. Emerson. This instrument is a combination of an imaging atom probe and a time-of-flight atom probe that enables the elemental identity and spatial coordinates of all atoms in a small volume of a field-ion specimen to be determined with near-spatial resolution.

In addition to the research activities, a monograph on the principles and applications of atom probe microanalysis was written in collaboration with Dr. G. D. W. Smith of Oxford University.[1,2] A book chapter on imaging materials at the atomic level, written with Dr. M. G. Burke of Westinghouse R&D Center, will be incorporated with contributions on other microanalytical techniques.[3,4]

1.2.1 Atom Probe Field-Ion Microscopy: A Technique for Microstructural Characterization of Irradiated Materials on the Atomic Scale[5-9] – *M. K. Miller, M. G. Burke,[4] and M. G. Hetherington[2]*

Irradiation is well known to adversely affect the mechanical properties of materials. This degradation in mechanical behavior is related to irradiation-induced changes in the microstructure. The APFIM, because of its near-atomic spatial resolution, is well suited to the characterization of the fine-scale features and the defects produced during irradiation. The technique is able to provide information on the size and morphology of precipitates and voids; chemistry of matrix and precipitates; solute clustering and partitioning behavior; and segregation to interfaces, boundaries, and other defects. The chemical and microstructural data provided by APFIM in conjunction with complementary small angle neutron scattering and analytical electron microscopy observations are essential to fully understand and model the effects of irradiation.

1.2.2 Solute Clustering and Precipitation in Pressure Vessel Steels under Low-Fluence Irradiation Conditions[7,8] – *M. K. Miller and M. G. Burke[4]*

After exposure to low- and intermediate-fluence neutron irradiation, a variety of reactor pressure vessel steels, including A533B-type surveillance specimens, Gundremmigen KRB-A ex-service plate, and test reactor irradiated materials, have been analyzed in the APFIM. A variety of ultrafine carbides and nitrides were also observed in the matrix of the neutron-irradiated A533B and Gundremmigen steels. These ultrafine precipitates were observed both before and after irradiation.

Phosphorus was found to be the most significant element in both trepanned and test-reactor-irradiated KRB-A material. Examination of the ion-by-ion evaporation sequences indicated that the features that gave rise to the statistically high significance results were very diffuse solute-enriched regions. Therefore, these regions are best described as "pre-clusters" or atmospheres. In some cases, copper and nickel were found to be associated with the phosphorus atmospheres.

Although no discrete, copper-enriched precipitates were detected in these materials, either from the atom probe data or from the field-ion micrographs, one copper-enriched atmosphere was intersected in the trepanned KRB-A material. Phosphorus was found to be associated with this copper-enriched atmosphere.

The very diffuse nature and the number of solute atoms associated with these atmospheres suggest that they are the precursor to the clusters and precipitates that have been observed in pressurized water reactor pressure vessel steels irradiated to higher fluences. The APFIM results from several different irradiated pressure vessel

steels seems to indicate that there is a progression in solute clustering and precipitation behavior. Very diffuse atmospheres form during the early stages of neutron irradiation. These atmospheres then become enriched in solute and turn into clusters. These clusters finally develop into precipitates only after long-term exposure at high fluence or during higher temperature thermal aging treatments.

The results of the microstructural analyses indicated that a variety of mechanisms should be invoked to explain the changes in mechanical properties of these materials during neutron irradiation.

1.2.3 Statistical Analysis of the Early Stages of Phase Decomposition[10] – *M. K. Miller and M. G. Hetherington*[2]

A new method for analyzing atom probe ion-by-ion data for the early stages of phase separation or clustering has been developed. The separation of the solute atoms μ in the atom probe data chain has been shown to be an effective parameter to investigate clustering in low-solute-content alloys. For a large sample size, the mean separation of any distribution of solute atoms, $\hat{\mu} = (1 - p)/p$, depends only on the solute content p and is not influenced by the distribution of the solute in the data chain. Clustering influences the individual separations of solute atoms (i.e., if the solute atoms are clustering, then the average separation between similar atoms will be smaller). The variance of the separations of similar atoms in the experimental atom probe ion-by-ion data chain may be used to detect deviations from a random distribution when compared with the estimated variance for the random data set. The experimental and estimated variances may be determined from

$$\hat{\sigma}^2 = (\Sigma\mu^2)/N_B - \hat{\mu}^2$$

and

$$\sigma^2 = (1 - p)/p^2 , \qquad (1)$$

where N_B is the number of B atoms. A useful parameter to determine whether clustering has occurred is the significance or the difference of the estimated and experimental variances divided by the standard error $\hat{\tau}$ of the estimated variance, that is,

$$\text{significance} = (\hat{\sigma}^2 - \sigma^2)/\hat{\tau} , \qquad (2)$$

where $\hat{\tau} = \sqrt{q(1+6q+q^2)/p^4/N_B}$, and $q = 1 - p$. Values of significance that are greater than 2 indicate that phase separation or clustering has occurred. This method has been successfully applied to solute clustering in irradiated pressure vessel steels and model alloys, boron clustering in Ni_3Al, and the early stages of decomposition in iron-chromium alloys.

1.2.4 A Comparison of Autocorrelograms Determined from Small Angle Neutron Scattering and Atom Probe Data[11] – *S. Spooner[12] and M. K. Miller*

Microscopy and small angle scattering (SAS) analysis are complementary means of characterizing the structure of an alloy. The interpretation of scattering or diffraction data requires the fitting of a structure model because it is not possible to reconstruct real space images from diffraction intensity because of the "phase problem." Direct space structure determined from field-ion microscopy (FIM) and electron microscopy is often necessary for interpretation of SAS data. A direct comparison of methods may be compared by the examination of autocorrelation functions of atom probe composition profiles and autocorrelation functions calculated from SAS.

SAS methods employ a relatively large sample size so that it is possible to determine structure model parameters with very high statistical precision. The atom probe sample volume is exceedingly small. However, when composition profiles are measured over hundreds of atomic diameters in a sufficiently fine-scale microstructure, the sampling process can be statistically significant. In this case, it becomes possible to compare diffraction and the direct space APFIM measurements. A comparison has been made of the autocorrelograms obtained from analysis of small-angle neutron-scattering and APFIM data. The two methods were found to be complementary to one another in the interpretation of fine-scaled microstructures. The global character of the spatial structure was given effectively in the SANS autocorrelation function, whereas the small lag autocorrelation values appear to be more accurate in the APFIM results.

1.2.5 APFIM Investigation of Planar Defects in High-Temperature Superconductors[13] – *M. K. Miller, A. J. Melmed,[14] and K. L. More*

One of the major limitations of superconducting oxide materials is the inability of polycrystalline specimens to carry high critical current densities. There are several possible reasons why the grain boundaries might be poor superconductors, including the presence of microcracks, contamination or impurity segregation to the grain boundaries, and the presence of a nonsuperconducting grain boundary phase. A combined FIM and field emission microscopy study of $RBa_2Cu_3O_{7-x}$, where R is Y, Yb, or Sm, high-temperature superconducting oxides, has been performed. High quality field-ion hydrogen and argon images have been obtained. The oxide was usually found to exhibit a characteristic striped pattern in both hydrogen and argon field-ion images. These stripes were usually uniform in intensity. The presence of planar defects have been observed as stripes that have a different intensity or as an individual stripe that abruptly changes intensity. A thin phase was also observed at grain boundaries, as shown in Fig. 1.2.1. This boundary phase imaged darkly in both field-ion and field emission images taken below the critical superconducting transition temperature. The presence of these defects possibly degrades the electrical properties of the bulk material.

ORNL PHOTO 9447-87

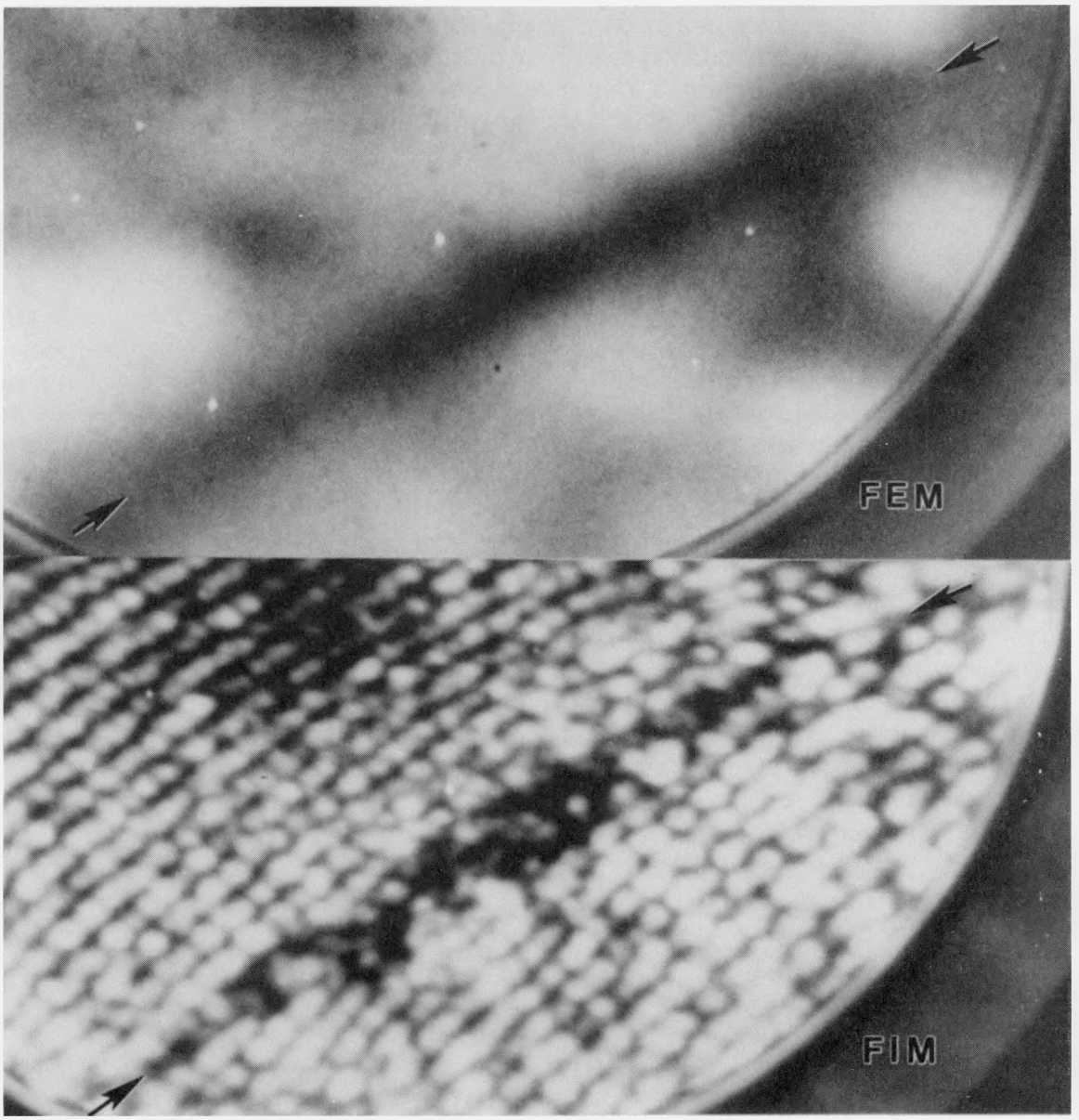

Fig. 1.2.1. Complementary field-ion micrograph and field emission micrograph of a grain boundary in $YBa_2Cu_3O_{7-x}$ high-temperature superconducting oxide showing a darkly imaging 3-nm-thick boundary phase. Specimen temperature was 40 K.

1.2.6 FIM Simulation of $RBa_2Cu_3O_{7-x}$ Superconductors[15] – *M. K. Miller and K. L. More*

Field-ion microscopy has been successfully performed on several $RBa_2Cu_3O_{7-x}$ high-temperature superconducting oxides. In most cases, the field-ion images exhibited a characteristic striped pattern. This imaging behavior is quite different from most metallic systems in which a typical ring pattern is obtained. In these oxides, only the most prominent poles exhibit the normal ring structure. The striped patterns have been observed both above and below the critical superconducting transition temperature and are observed irrespectively of whether hydrogen, argon, or neon is used as the image gas.

Computer-simulated field-ion images of the orthorhombic and tetragonal structures of $RBa_2Cu_3O_{7-x}$ superconductors have been obtained. No significant differences were found between the orthorhombic and tetragonal structures. However, these simulations indicated that several possible selective imaging species could be responsible for the characteristic striped field-ion images. These possibilities include Cu1, R, Cu1+O1 and Cu2+O2+O3+R combinations.

1.2.7 Microstructural Characterization of Udimet 720: A Nickel-base Alloy[16] – *K. L. More and M. K. Miller*

The microstructure and chemical composition of Udimet 720, a nickel-base superalloy, has been characterized with a variety of techniques, including APFIM, TEM, and secondary ion-mass spectroscopy. The microstructure of the alloy after a standard four-stage heat treatment consisted of a γ matrix and a dispersion of large and small spherical coherent γ' precipitates. The elemental partitioning between these phases was determined. Chromium, cobalt, and molybdenum preferentially partitioned to the γ phase; whereas, nickel, aluminum, and titanium partitioned to the γ' phase. Boron and carbon segregation to the γ/γ' interfaces was observed. Coarse carbide and boride precipitates formed on the grain and twin boundaries. Significant boron segregation to grain and twin boundaries was also observed.

1.2.8 Atom Probe Investigation of the Oxidation of Ni-Zr Intermetallic Compounds[17] – *E. M. Perry,[18] D. L. Cocke,[18] and M. K. Miller*

Intermetallic compounds of nickel and zirconium are inexpensive materials that have potential applications as catalysts for hydrogenation, methanation, and isomerization. The initial stages of oxide formation on three Ni-Zr intermetallic compounds have been examined by atom probe mass spectrometry. Ni_5Zr, Ni_7Zr_2, and Ni_3Zr were oxidized at temperatures up to 573 K and oxygen pressures ranging from ≈5 to 50 Pa. Atom probe composition depth profiles of the oxide layer and underlying bulk alloy provided information on alloy stoichiometry, oxide layer structure, and oxide stoichiometry. Interesting oxide structures have been observed, particularly for Ni_5Zr. An oxygen-depleted region was observed below a thin overlayer that contained O, Ni, and Zr. The overall oxygen content of the oxide layers was much less than expected for the known formation of ZrO_2 at these temperatures and oxygen pressures.

1.2.9 Atom Probe Study of Phase Decomposition in the Cape York Meteorite[19] – *M. K. Miller and K. F. Russell*

A combined APFIM, optical microscopy, and scanning electron microscopy (SEM) characterization of the Cape York iron-nickel meteorite has been performed. Iron-nickel meteorites are a unique material for studying phase decomposition in the iron-nickel system because of their extremely slow cooling rates of approximately 1°C per 10^6 years. This slow cooling rate enables low-temperature transformations to proceed. The majority of iron-nickel meteorites have a characteristic Widmanstätten structure comprising of kamacite and plates of taenite. Kamacite is a body-centered cubic iron phase containing approximately 7% nickel in solid solution. Taenite generally refers to a face-centered cubic austenite that contains more than 25% nickel. However, taenite plates are made up of several regions. Previous microprobe investigations have shown that the nickel profile across taenite plates has a characteristic M shape ranging from ~50% at the edge to less than 25% in the center of the plate. This profile arises as a result of the slow cooling process. Several different regions have been identified within the taenite plate, including a thin, clear taenite (CT1) $L1_0$-ordered FeNi region at the edge, followed by a cloudy zone (CZ), a second clear taenite (CT2) region, and a plessite or a martensitic region in the center. The CZ has been shown to be a mixture of globular $L1_0$-ordered FeNi in a honeycomb of either martensite, kamacite, or a disordered face-centered cubic phase. The CT2 region contains between approximately 28 and 24% nickel and is either an $L1_2$-ordered Fe_3Ni phase or an ultrafine-scale mixture of $L1_0$-ordered Fe-Ni and martensite. These two cases are difficult to distinguish with TEM because the extra reflections produced in electron diffraction patterns from the variants of an $L1_0$-ordered phase are equivalent to those produced in an $L1_2$-ordered crystal. The atom probe results indicate that an Fe-28 at. % Ni region in the taenite plate had composition modulations of ~10 nm periodicity and amplitude fluctuations from 50 at. % Ni to ~15 at. % Ni, as shown in Fig. 1.2.2. This investigation has revealed that this region in the taenite plate had phase-separated to form an ultrafine scale duplex microstructure of $L1_0$-ordered FeNi and a low-nickel face-centered cubic phase.

1.2.10 Atom Probe Field-ion Microscopy Study of Phase Separation in the Twin City and Santa Catharina Meteorites[19,20] – *M. K. Miller and K. F. Russell*

An APFIM investigation has been performed on the high-nickel Twin City and Santa Catharina meteorites. SEM analysis of the Twin City meteorite revealed an average matrix composition of 26.1 at. % Ni. The Santa Catharina meteorite is heavily weathered and variable in composition. SEM analysis revealed that the matrix composition of the unweathered sample used in this study was 29.5 at. % Ni. Atom probe analysis of the matrix of both meteorites revealed ultrafine-scale phase separation into high- and low-nickel regions. The diameters of the isolated, roughly spherical high-nickel regions were ~2 nm in the Twin City meteorite and 10 nm in the Santa Catharina meteorite. The interparticle spacing was 7.5 and 20 nm in the Twin City and Santa Catharina meteorites, respectively. The brightly imaging precipitates had a composition of ~50% nickel, and the matrix had a composition of between 11 and 15% nickel. The ordered nature of these brightly imaging precipitates was evident by the alternating bright

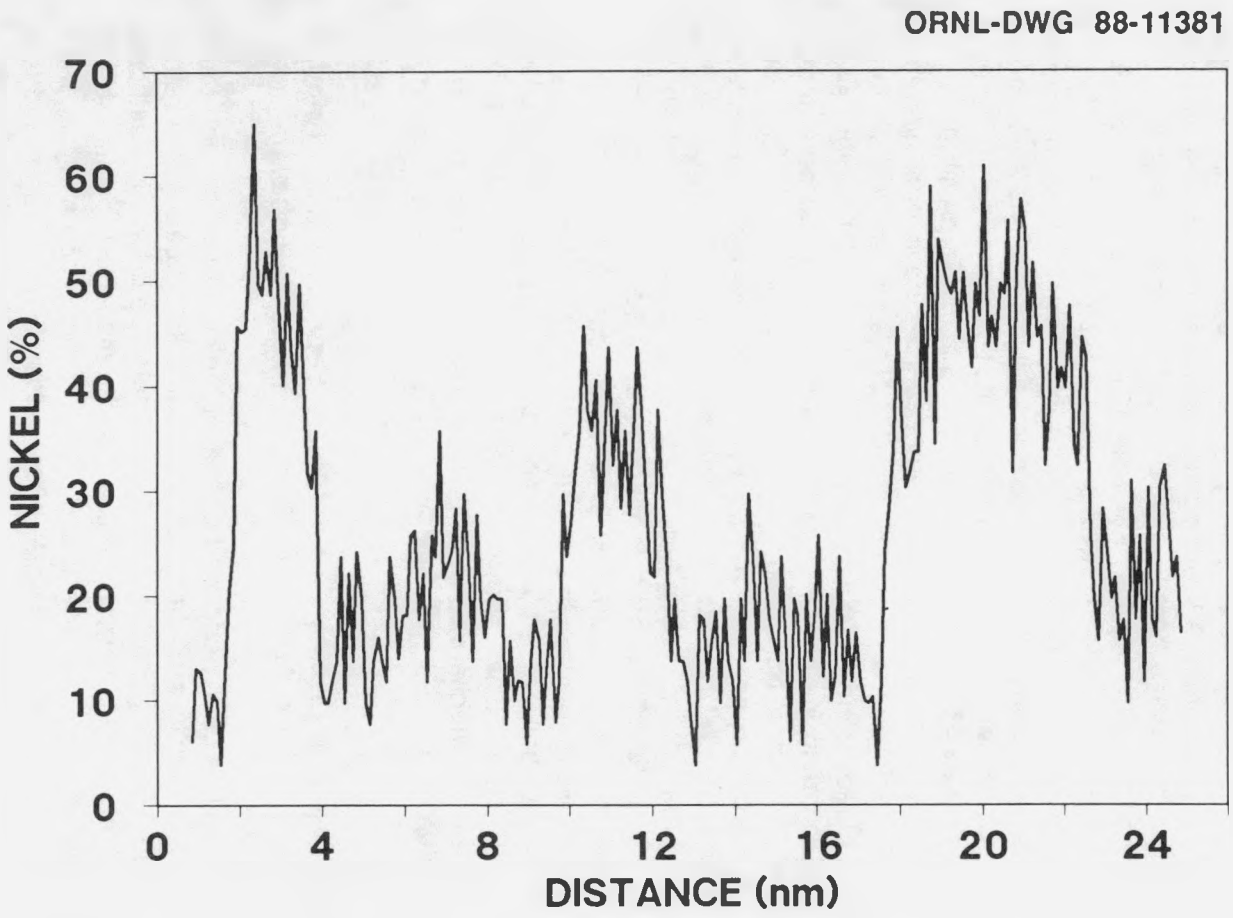

Fig. 1.2.2. Atom probe composition profile through a taenite region containing approximately 28.0 at. % Ni in the Cape York iron-nickel meteorite. Fine-scale phase separation into 50 at. % Ni and 15 at. % Ni regions is evident.

and dim imaging behavior of the (002) planes in the field-ion micrographs. Atom probe plane-by-plane analysis revealed that these bright and dim (002) planes alternated between essentially pure iron and pure nickel. The precipitates were found to have a cube-on-cube relationship with the face-centered cubic matrix. In some cases, where the precipitates had coalesced, antiphase boundaries were evident from the mismatching of the bright and dim planes across the boundary. In the Santa Catharina meteorite, the volume fraction of the precipitate was determined to be ~50%. These results indicate that the matrix of these meteorites is a mixture of an $L1_0$-ordered FeNi phase and a low-nickel face-centered cubic phase.

1.2.11 Effect of Aluminum Level on Boron Clustering in Ni_3Al [21] – *J. A. Horton, M. K. Miller, C. T. Liu, E. P. George, and J. Bentley*

APFIM has been used to investigate boron clustering in a series of Ni_3Al alloys containing 24, 25, and 26 at. % Al and boron levels of up to 1 at. %. Boron clusters were detected in the 25 and 26% Al alloys, as shown in Fig. 1.2.3, but not in the 24% material. The boron clusters generally consisted of 2 or 3 boron atoms with a maximum of 10 atoms. The occurrence of the clustering coincides with the higher rate of boron strengthening as measured by the increase in yield stress as a function of boron content and the reduced level of boron segregation to grain boundaries. The levels of boron and nickel were found to be highly variable on grain boundaries in rapidly solidified materials, and no consistent indication of nickel enrichment with boron segregation was found. These results suggest that cosegregation of nickel and boron may not be necessary for the ductilization of Ni_3Al by boron because the rapidly solidified material is also ductilized by boron and exhibits segregation of only boron to the grain boundaries.

1.2.12 Grain Boundary Chemistry of NiAl [22] – *P. P. Camus, I. Baker,[23] J. A. Horton, and M. K. Miller*

Atom probe analyses performed at the grain boundaries in Ni-49 at. % Al indicated a majority of regions that contained almost no aluminum and a few regions that were neither enriched or depleted in aluminum. The widths of the depleted zones were less than 0.5 nm. It is proposed that the aluminum depletion could be responsible for the enhanced ductility and the change in fracture mechanism that occurs in this intermetallic alloy compared with NiAl alloys that are further from stoichiometry.

1.2.13 Identification of an Ordered Hexagonal BeFe Phase[24-27] – *M. K. Miller and M. G. Burke*[4]

The complementary techniques of APFIM and TEM have been employed to identify an ordered equiatomic BeFe phase in the iron-beryllium system. Aging at 650°C has resulted in the formation of an additional phase in an Fe-25 at. % Be alloy. APFIM has revealed that the composition of this phase is equiatomic BeFe. Both FIM and TEM techniques have shown that this phase has an ordered hexagonal crystal structure. The comparison of actual and computer-simulated field-ion micrographs and electron

Small clusters of boron were observed in the 25 and 26% Al alloys but not in the 24% Al material. ~15% of the boron in the matrix was in the clusters.

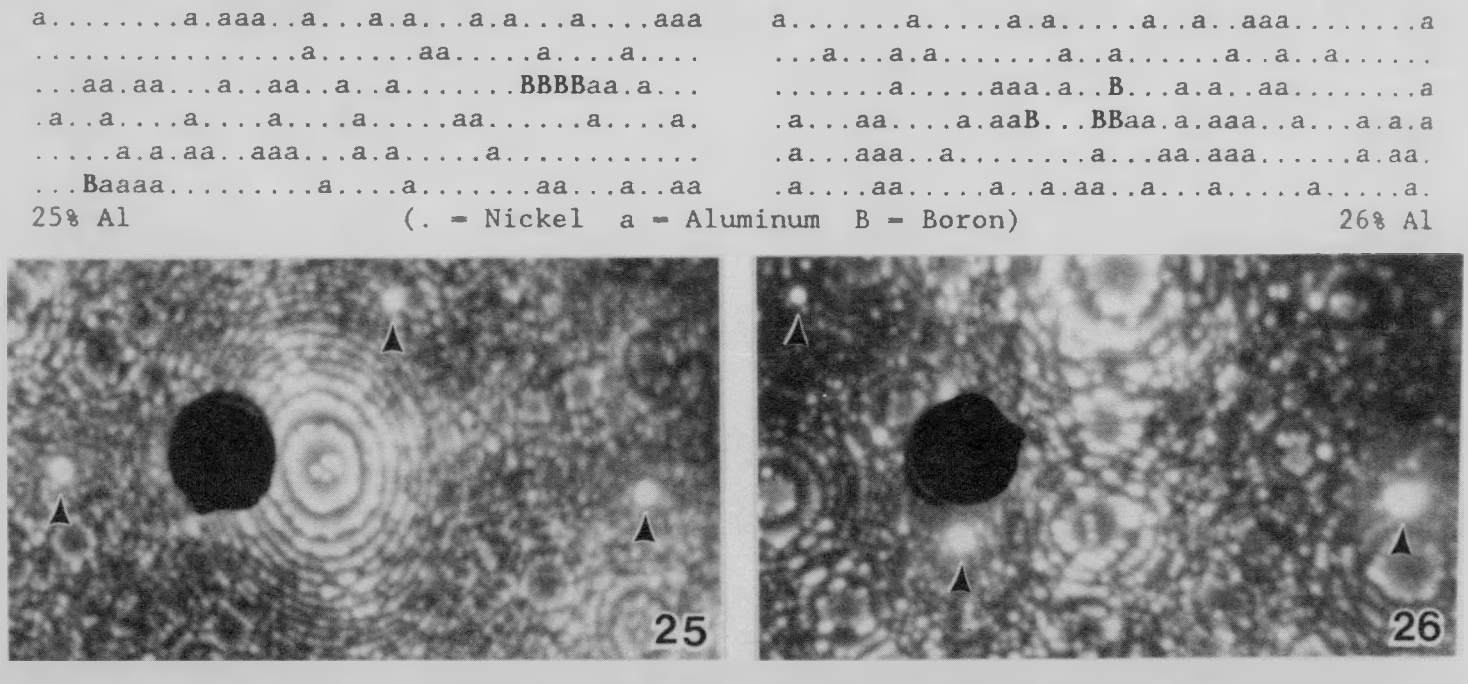

These clusters would reduce the amount of boron that is available to segregate to boundaries and precipitate in the grain boundary phase. Their presence might increase the flow stress of the matrix by increased pinning of dislocations and thereby make the grain boundaries more sensitive to failure.

Fig. 1.2.3. Field-ion micrographs of (*a*) Ni-25 at. % Al - 0.24 at. % B and (*b*) Ni-26 at. % Al-0.24 at. % B, showing brightly imaging boron clusters. Corresponding character plots show short portions of the atom probe ion-by-ion data chains and also reveal the boron clusters.

diffraction patterns with the equiatomic composition indicate that the crystal structure of this BeFe phase was B8.

1.2.14 Field Evaporation and Field-Ion Microscopy Study of the Morphology of Phases Produced as a Result of Low-Temperature Phase Transformations in the Iron-Chromium System[28,29] – *M. K. Miller*

The morphology of the phases produced in iron-chromium alloys upon aging within the low-temperature miscibility gap has been characterized by field evaporation microscopy and FIM. Upon aging alloys of this system within the miscibility gap, the body-centered cubic solid solution phase separates into an iron-rich α phase and a chromium-enriched α' phase.

The series of high-purity iron-chromium alloys that were used in this study contained 14, 17, 19, 24, 30, and 45% Cr. These alloys were examined after solution treatment above the miscibility gap and after subsequent isothermal aging in the temperature range 470 to 560°C for up to 11,000 h.

The phase contrast exhibited in the field evaporation micrographs was more pronounced than that exhibited in the field-ion micrographs, especially in the low-volume-fraction alloys and during the early stages of phase separation.

The morphology of the α and α' phases was found to change with composition and aging temperature. At the lower chromium levels, the morphology of the phases consisted of isolated roughly spherical islands of the α' phase embedded in an α matrix. As the chromium level increased, this morphology smoothly changed into an isotropic network, where both the α and α' phases were highly interconnected.

1.2.15 Precision Ion Milling of Field-Ion Specimens[29] – *K. B. Alexander, P. Angelini, and M. K. Miller*

Field-ion specimens of ceramic (TiB_2, SiC), semiconducting (Si), and metallic (308 stainless steel) materials have been successfully prepared by precision ion milling. The instrument used for this operation was a Gatan model 645 precision ion milling system (PIMS). This instrument features a focussed argon ion beam, 1-2 μm in diameter, and a secondary electron imaging system. Ion milling is performed with the specimen blank mounted in a TEM stage that was modified for examination of field-ion specimens. Because the specimen needle may be imaged with secondary electrons during the ion milling operation, the position and time spent under the ion beam may be adjusted to sculpt the specimen blank into a desired end form. The use of a TEM specimen holder also facilitates repeated ion milling and TEM examination and has been applied to bring a desired feature, such as a grain boundary, into the analyzable region of the field-ion specimen. This ion milling method also permits resharpening of blunt or fractured specimens.

1.2.16 Pulsed Laser Atom Probe Characterization of Silicon Carbide[29] – *P. Angelini, K. L. More, A. Cerezo, and M. K. Miller*

Field-ion specimens of both bulk and whisker silicon carbide materials have been fabricated by conventional ion milling and by milling in a Gatan model 645 precision ion milling system. FIM and field evaporation of both α-SiC and β-SiC materials have been successfully demonstrated. High-quality field-ion micrographs were obtained in which the normal ring structure was evident. Because field-ion micrographs could be taken immediately after pulsed field evaporation, the effects of preferential field evaporation of silicon that occurred under ramped field evaporation were eliminated. However, because of the high electrical resistivity of silicon carbide, conventional voltage pulsed field evaporation was not practical and pulsed laser field evaporation was required. Chemical analyses were conducted at Oxford University in the pulsed laser atom probe that is equipped with a high-power Neodymium-YAG laser. A series of atom probe experiments were performed to investigate whether the wavelength of the laser radiation or the specimen temperature (40 to 100 K) significantly influenced the performance of the instrument or the accuracy of the composition determinations. No significant variations in performance were found. The full-width-at-half maximum (FWHM) mass resolution of 0.4 amu was only slightly inferior to voltage pulsed field evaporation of metals. However, the background noise level was considerably higher. Within the statistical accuracy of the analyses, the compositions were found to be stoichiometric SiC. These experiments also revealed that laser power required to field evaporate these SiC specimens was greater than that of other semiconducting materials.

1.2.17 Effects of Image Gas on Atom Probe Analysis[30] – *M. K. Miller and K. F. Russell*

In addition to improving the mass resolution of an atom probe, the incorporation of an energy-compensating lens makes it possible in principle to perform elemental analysis while viewing the field-ion image without significantly increasing the low background noise level. In an energy-compensated atom probe, the lens is set to transmit only ions with the energy of the standing plus pulse voltages. The random noise from the image gas forming the field-ion image and projected from the specimen is filtered out because these gas ions have only the standing component of the voltage. Therefore, these ions are not transmitted through the energy-compensating lens to the detector. Field adsorbed image gas atoms on the surface of the specimen can be desorbed with the energy of the standing plus pulse voltages and will produce an additional set of peaks in the spectrum at the mass-to-charge ratios characteristic of the image gas rather than as random background noise. These additional peaks are ignored in the compositional determinations. The background neutral image gas atoms in the vacuum system do not have sufficient energy to produce a signal at the detector. However, the presence of these gas atoms will affect the performance of the instrument through several other processes. The effects of the image gas may be separated into three main categories: (1) those affecting the field ionization and evaporation processes at the specimen, (2) those affecting the probability of a genuine ion from the specimen colliding with or being deflected by a gas atom during its flight through the drift tubes and the energy-compensating lens, and (3) those affecting the performance of the single atom detector.

A systematic study of the performance of an energy-compensated atom probe as a function of image gas pressure was performed. The three inert image gases that were investigated in this study were helium, neon, and argon. The image gas pressure was varied between the background base pressure of 2×10^{-11} and 1×10^{-3} mBar. The highest pressure used was the maximum possible experimentally because of potential electrical breakdown in the single atom detector.

The results indicated that, at the typical image gas pressures where field-ion images are normally obtained, the mass resolution of the atom probe is seriously degraded both in terms of the FWHM of the mass spectra and the increased number of ions in the tails of the mass spectra, the number of afterpulses produced in the single-atom detector is increased, and the accuracy of the compositional determination is affected. It is, therefore, recommended that atom probe analyses be performed with the minimum of image gas present.

1.2.18 Atom Probe Field-Ion Microscopy and Related Topics: A Bibliography 1978-87[31] – *M. K. Miller and A. R. McDonald*

A bibliography containing approximately 2400 references on the topics of FIM, field emission microscopy, APFIM, and liquid metal ion sources has been prepared. The bibliography covers the period 1978 to 1987.

1.2.19 References

1. M. K. Miller and G. D. W. Smith, "Atom Probe Microanalysis: Principles and Applications to Materials Problems," to be published by Materials Research Society.

2. Department of Metallurgy and Science of Materials, University of Oxford, England.

3. M. K. Miller and M. G. Burke, "Atom Probe Field-Ion Microscopy: Imaging at the Atomic Level," invited chapter in *Imaging of Materials*, D. B. Williams, R. Gronsky and A. R. Pelton, eds., Oxford University Press, Oxford, England, in press.

4. Westinghouse R&D Center, Pittsburgh.

5. M. K. Miller, M. G. Hetherington, and M. G. Burke, invited review, *Metall. Trans.* (1989), in press.

6. M. G. Burke and M. K. Miller, presented at TMS/ASM Fall Meeting, Chicago, Ill., September 1988.

7. M. K. Miller and M. G. Burke, *Proceedings of the 14th International Symposium on the Effects of Radiation on Materials, ASTM, Andover, Mass., June 1988*, to be published in ASTM STP 1046, N. H. Packan, R. E. Stoller, and A. S. Kumar, eds.

8. M. G. Burke and M. K. Miller, *J. Phys.* **49-C6**, 283-88 (1988); presented at the 35th International Field Emission Symposium, Oak Ridge, Tenn., July 1988.

9. M. K. Miller, invited paper, presented at the Workshop on Mechanisms of Embrittlement of Pressure Vessel Steels, International Group on Irradiation Damage Mechanisms in Pressure Vessel Steels, Harwell, England, October 1988.

10. M. K. Miller and M. G. Hetherington, *J. Phys.* **49-C6**, 427-32 (1988); presented at the 35th International Field Emission Symposium, Oak Ridge, Tenn., July 1988.

11. S. Spooner and M. K. Miller, *J. Phys.* **49-C6**, 405-10 (1988); presented at the 35th International Field Emission Symposium, Oak Ridge, Tenn., July 1988.

12. Solid State Division, ORNL.

13. M. K. Miller, A. J. Melmed, and K. L. More, *J. Phys.* **49-C6**, 447-52 (1988); presented at the 35th International Field Emission Symposium, Oak Ridge, Tenn., July 1988.

14. National Institute of Standards and Technology, Gaithersburg, Md.

15. M. K. Miller and K. L. More, *J. Phys.* **49-C6**, 483-88 (1988); presented at the 35th International Field Emission Symposium, Oak Ridge, Tenn., July 1988.

16. K. L. More and M. K. Miller, *J. Phys.* **49-C6**, 391-96 (1988); presented at the 35th International Field Emission Symposium, Oak Ridge, Tenn., July 1988.

17. E. M. Perry, D. L. Cocke, and M. K. Miller, *J. Phys.* **49-C6**, 385-90 (1988); presented at the 35th International Field Emission Symposium, Oak Ridge, Tenn., July 1988.

18. Department of Chemistry, Texas A&M University.

19. M. K. Miller and K. F. Russell, *J. Phys.* **49-C6**, 397-402 (1988); presented at the 35th International Field Emission Symposium, Oak Ridge, Tenn., July 1988.

20. M. K. Miller and K. F. Russell, invited paper, presented at the TMS-AIME meeting, Las Vegas, Nev., February 1989.

21. J. A. Horton, M. K. Miller, C. T. Liu, E. P. George, and J. Bentley, pp. 89-97 in *High-Temperature Ordered Intermetallic Alloys III*, C. T. Liu, A. I. Taub, N. S. Stoloff, and C. C. Koch, eds., *Proc. Mater. Res. Soc. Symp.* **133** (1989).

22. P. P. Camus, I. Baker, J. A. Horton, and M. K. Miller, *J. Phys.* **49-C6**, 329-33 (1988); presented at the 35th International Field Emission Symposium, Oak Ridge, Tenn., July 1988.

23. Dartmouth College.

24. M. K. Miller and M. G. Burke, *Proceedings of the 2nd International Conference on Solid-Solid Phase Transformations, Phase Transformation '87, Cambridge, July 1987*, G. W. Lorimer, ed., Institute of Metals, England, 1988, pp. 199-202.

25. M. G. Burke and M. K. Miller, *J. Phys.* **49-C6**, 373-78 (1988); presented at the 35th International Field Emission Symposium, Oak Ridge, Tenn., July 1988.

26. M. G. Burke and M. K. Miller, *Ultramicroscopy* **30**, 199-209 (1989).

27. M. G. Burke and M. K. Miller, *Proceedings of the 46th Electron Microscopy Society of America, 1988, Milwaukee*, G. W. Bailey, ed., San Francisco Press, pp. 780-81.

28. M. K. Miller, *Proceedings of the 2nd International Conference on Solid-Solid Phase Transformations, Phase Transformation '87, Cambridge, July 1987*, G. W. Lorimer, ed., Institute of Metals, England, 1988, pp. 39-43.

29. K. B. Alexander, P. Angelini, and M. K. Miller, *Journal de Physique (Paris)*, in press.

30. M. K. Miller and K. F. Russell, *J. Phys.* **49-C6**, 81-7 (1988); presented at the 35th International Field Emission Symposium, Oak Ridge, Tenn., July 1988.

31. M. K. Miller and A. R. McDonald, *Atom Probe Field-Ion Microscopy and Related Topics: A Bibliography 1978–87,* ORNL/TM-11157, April 1988.

1.3 X-RAY DIFFRACTION RESEARCH – *C. J. Sparks*

Our technical progress this year includes an emphasis on interfaces that we have studied both at our recently completed rotating-anode single-crystal facility at ORNL and at our X-ray scattering facility at the National Synchrotron Light Source (NSLS). The high brightness at our synchrotron facility has benefited every experiment. Among the highlights was our study of buried interfaces from metal overlayers on ceramic substrates by reflection X-ray diffraction techniques.

As our progress in both acquiring and analyzing X-ray diffraction data from thin films and interfaces improves, we are also developing new X-ray diffraction methods that are sensitive to the near-interface region of thick films. By measuring residual coherence between film and substrate, we can determine to what depth the film is commensurate with the structure of the substrate. That is, we can know how well the atoms in the overlayer are aligned with respect to the atoms in the substrate. We have applied this method to gallium arsenide and copper on silicon crystal substrates and are examining other systems being grown by molecular beam epitaxy (MBE) techniques in collaboration with our surfaces and interfaces group. For example, by tuning the synchrotron X-ray energy near to an absorption edge of the overlayer, we can determine which part of the interface scattering is produced by displaced substrate atoms and which is produced by the overlayer. In this way, we can obtain information on the structure of a buried interface not possible by any other method.

In collaboration with researchers from the University of Illinois (H. Zable, H. Morkoc, and N. Lucas), we have studied thin films of GaAs (~250 to 900 Å thick) deposited on (100) silicon single-crystal substrates. Our findings show that the strain arising from the lattice mismatch of 4% is mostly accommodated in the first few GaAs planes at the silicon interface. Only about 10% of this strain is distributed through the bulk of the film. More-detailed information of the interface is now being derived from models fitted to the measured X-ray scattering rods associated with the interface. Even clean surfaces give rise to sufficient X-ray scattering that reconstruction of those surfaces as a function of temperature can be measured. In a collaboration with other synchrotron radiation users, we have found that the clean tungsten (001) surface undergoes an order-disorder change in surface structure at ≈230 K. Above that temperature, finite-sized domains form that are fluid-like and have no long-range order. Hydrogen coverage can be described with the lattice-gas model.

This surface and interface sensitivity of intense synchrotron X-ray sources provided information on near-surface strain distributions and the near-surface strain-induced phase transformations in ceramic materials. In collaboration with Hwang and Houska of Virginia Tech, both glancing-angle and low-energy X-ray techniques were applied to increase surface sensitivity to measure strain gradients from polished and severely ground, fully stabilized zirconia. Maximum strains approaching 6% at the surface were measured and found to fall rapidly, approaching zero strain at about 0.1 μm for the polished surface and 1 μm for the severely ground surface. Measurements of strain-induced transformation showed that pin-on-disk wear testing of a partially stabilized zirconia sample produced more of the high-temperature cubic and tetragonal phases

than polished samples. The variation in the amount and distribution of the high-temperature phases is explained in terms of surface heating followed by rapid cooling by the underlying substrate.

We are also supporting the effort on high-temperature superconductors. Recently, the superconducting temperature was raised even higher using the thallium-containing materials $Tl_2Ca_2Ba_2Cu_3O_{10+\delta}$. Both the synthesis of this material and unraveling the crystal structure is a prerequisite for understanding and controlling its properties. After successful fabrication, both X-ray and neutron powder diffraction were used to determine the structure. However, there remains the problem of low critical current density in bulk-sintered polycrystalline samples. X-ray diffraction measurements on the thallium-bearing compounds was used to help control the chemistry in the synthesis of these materials to achieve a single-phase product. Elimination of other phases is essential for the proper evaluation of the critical current density J_C. The intragrain J_C values were large (near 10^7 A/cm^2 at 4.2 K in 10 kOe) and decreased exponentially with temperature. These features are qualitatively very similar to those found in the corresponding $YBa_2Cu_3O_{7-\delta}$ compounds. Increasing the low intergranular transport is a major concern under study at several laboratories.

A very exciting advancement has been made in the use of X-ray scattering to understand the magnetic structure of materials. The magnetic cross section for X-ray scattering is about 10^{-7} or 10^{-8} of that for charge scattering from the electrons. When the X-ray energy is in resonance with an absorption edge, where strong electric multipole transitions take place between atomic core states and the exchange-split Fermi edge states, dramatic enhancements of the magnetic scattering can occur. We have shown that in uranium arsenic (UAs), the magnetic X-ray intensity is enhanced by 10^7 when the X-ray energy is in resonance with the M_{IV} edge of uranium. New insights into the magnetic structure of both surfaces and materials will result from this advancement.

The tetragonal DO_{22} compound Al_3Ti has recently received attention as a possible structural material because of its low density, 3.4 g/cm^3, and its good oxidation resistance. Al_3Ti has the disadvantages, however, that it is a line compound and is extremely brittle at room temperature, presumably because of the lack of slip systems associated with the crystal symmetry. It is known that stable cubic $L1_2$ ternary compounds having the stoichiometry $Al_{75-x}Z_xTi_{25}$ exist, where Z is Cu, Ni, or Fe and x = 8 to 12.5. Cubic alloys based on these compounds have several attractive features and may be more easily made ductile because the $L1_2$ structure provides more slip systems for plastic deformation. At ~1350°C, the melting point of these alloys is much higher than other aluminum-based alloys. Preliminary studies have indicated the alloys have good oxidation resistance and retain their strength, as indicated by hot hardness, much better than even Ti-6Al-4V, a widely used titanium alloy. Because an understanding of the factors influencing the stability of the DO_{22} and $L1_2$ structures is desirable, alloys of $Al_{75-x}Fe_xTi_{25}$, where x = 0 to 12 at. % Fe, were fabricated by splat cooling and examined primarily with X-ray diffraction to determine the crystallographic phases present, as well as their composition, volume fraction, lattice parameters, and sublattice occupation. The tetragonal DO_{22} structure of Al_3Ti dissolved 0.8 ± 0.4 at. %

Fe, with additional iron partitioned to the $L1_2$ structure containing 6.2 ± 0.4 at. % Fe, and is completely transformed to the $L1_2$ structure with the addition of about 6 at. % Fe. The lattice parameters of both phases were independent of iron concentration up to about 6 at. %. At 8 at. % Fe, the iron was found to be predominantly distributed on the nominal aluminum sublattice, which also contained about 5 at. % Ti. The Al_3Ti composition was similarly found to contain about 5 at. % Ti on the aluminum sublattice. All compositions, including a single crystal of $Al_{67}Fe_8Ti_{25}$, were found to be brittle.

Because 25% of our synchrotron radiation beam time goes to general users, we sometimes find ourselves involved in experiments that give us insights into unfamiliar fields of advanced chemistry and physics that could someday have interesting applications in materials science. The study of two-dimensional structures of organic films only a few monolayers thick follows the phase transformations as a function of film thickness and temperature. The crystalline phase melts and dislocations play a part in forming a liquid. Insights to the structure and wetting behavior of these 2-D films provide new information on a host of practical applications, from paint for corrosion resistance to multilayers developed for specific properties. This work was done in collaboration with Harvard University.

We continue to advocate that the unique properties of an X-ray microprobe will provide new insights to materials via microcharacterization. Our invited talk at the Materials Research Society[1,2] gave an overview of the desirable characteristics of an X-ray microprobe compared with small electron beams. Because detectable limits and energy deposition are reduced by 10^{-3} to 10^{-5} when comparing X rays with electrons, every effort should be made to build an X-ray microprobe using an undulator source on a 6-8 GeV ring.

1.3.1 X-Ray Scattering

1.3.1.1 X-Ray Diffraction Study of a Thin GaAs Film on Si(100) (ref. 3) – *A. S. Bommannavar,[4] C. J. Sparks, A. Habenschuss,[5] G. E. Ice, A. Dhere,[6] H. Morkoc,[7] and H. Zabel[7]*

Thin GaAs films grown on single-crystal silicon substrates are shown to have a nearly linear strain gradient through their thickness because of lattice mismatch. The GaAs films, ~900 Å thick, are strained to accommodate the 4% smaller Si lattice. Previous studies showed a small change in the average lattice spacing of the GaAs films, but ours is the first to analyze the broadening of the Bragg reflections to show that a strain gradient exists between the surface and interface of the GaAs film. Only 10% of the lattice mismatch is accommodated by strain in the bulk of the GaAs film. We found that the remaining 90% is dissipated in the first few GaAs planes at the silicon interface. This is the first qualitative evidence for the existence of a strain gradient in GaAs films grown epitaxially on single-crystalline substrates. A large effort is being made by the electronics industry to lessen the effects of the lattice mismatch and thermoelasticity differences between GaAs and the silicon substrates to improve performance of these semiconductor heterostructures.

1.3.1.2 X-Ray Characterization of Heteroepitaxial GaAs on Si(001) (ref. 8) – *H. Zabel,[7] N. Lucas,[7] H. Morkoc,[7] and C. J. Sparks*

The epitaxial growth of GaAs on Si(001) substrates combines all the major problems of heteroepitaxial structures. These include antiphase domains from the deposition of polar GaAs on nonpolar Si substrates, large lattice parameter mismatch between both structures, and mismatch of the thermal expansion coefficients. Recent X-ray results on the density of antiphase domains, strain and strain relaxation, and of the anisotropy of the thermal expansion of GaAs films induced by the Si substrate have been reviewed.

1.3.1.3 X-Ray Study of W(001) With and Without Hydrogen[8] – *K. Evans-Lutterodt,[9] R. J. Birgeneau,[9] E. D. Specht, J. W. Chung,[9] J. D. Brock,[9] M. S. Altman,[10] P. J. Estrup,[10] I. K. Robinson,[11] and A. A. MacDowell[11]*

We have carried out synchrotron X-ray diffraction studies of the clean W(001) surface reconstruction transition as a function of temperature and of the room-temperature phases and phase transitions of W(001) with submonolayer coverages of hydrogen. For clean W(001), we find that below the transition temperature of ≈230 K, the $(\sqrt{2} \times \sqrt{2})$R 45° diffraction peaks have an intrinsic width, larger than the instrumental resolution, corresponding to finite-sized domains. Nevertheless, we are able to measure one and one-half decades of change in diffraction linewidth, and three decades in the amplitude. The detailed dependences of the surface peak widths are consistent with the predictions of the two-dimensional XY model with cubic anisotropy to leading order. We also find that the clean surface structure is commensurate at all temperatures measured, above and below the transition temperature. For hydrogen-covered W(001), our data suggest a simple picture in which at very low coverages there is a trade-off with increasing coverage (analogous to that in a two-phase coexistence region), between hydrogen-poor and hydrogen-rich regions until a uniform but still disordered $(\sqrt{2} \times \sqrt{2})$R 45°-H is attained. With further increase in coverage, the surface layer exhibits a commensurate transition which, rather than being a solid-solid transition as previously assumed, is actually a lattice-gas melting transition into a domain-wall fluid phase. Such surface domain-wall fluid phases should occur commonly in chemisorbed systems.

1.3.1.4 Residual Strain Gradients in a Fully Stabilized Zirconia Sample[12] – *Bing Hwang,[13] C. R. Houska,[13] G. E. Ice, and A. Habenschuss[5]*

Diffraction profiles of polished and severely ground fully stabilized zirconia (FSZ) samples are examined for the asymmetry that results from a d-spacing gradient extending from the free surface into undisturbed bulk material. Variations in residual strain or chemical composition could account for this depth gradient. The latter is eliminated by X-ray photoelectron spectroscopy (XPS). A maximum compressive strain of approximately 4% is obtained at the surface of the ground sample; it decreases gradually to zero at greater depths. The overall compressive zone is ~ 1 μm. A similar but smaller compressive zone is found in the polished sample.

Although the maximum strains are large, they are reasonable for ceramic materials in compression. Such large residual elastic strains would be relaxed by plastic deformation in metals. Understanding residual stress is an important step toward designing ceramics toughened against crack propagation initiated by large elastic stresses.

1.3.1.5 X-Ray Analysis of the Near-Surface Phase Distribution Applied to Wear on a PSZ Disk[14] – *Bing Hwang,[13] C. R. Houska,[13] G. E. Ice, and A. Habenschuss[5]*

X-ray diffraction methods were used to determine the depth distribution of any phase in a multiphase sample by using either different wavelengths or symmetrical and asymmetrical diffraction optics or a combination of the two. Measurement of X-ray intensity ratios from different phases as a function of the known wavelength or diffraction geometry reveals the unknown depth distributions of the phases. The depth distribution of phases is demonstrated on a partially stabilized zirconia (PSZ) sample subjected to a pin-on-disk wear tester to induce a near-surface phase transformation. In an earlier study,[15] the debris collected from a prolonged pin-on-disk test of this MgO-PSZ was found to be highly defective with only the high-temperature cubic form. Diffraction patterns were made with 2.48 Å X rays and unscrambled into symmetrical peaks with Pearson-VII functions.

The distribution of the high-temperature cubic and tetragonal phases shows that even the preliminary polishing process may produce surface heating and somewhat rapid cooling, enhancing the high-temperature cubic and tetragonal phases near the surface. Further enhancement to greater depth of the high-temperature phases of ZrO_2 is found after wear testing.

1.3.1.6 Structure and Superstructure of the Superconductor $Tl_2Ca_1Ba_2Cu_2O_8$ by Neutron and Electron Diffraction[16] – *A. W. Hewat,[17] E. A. Hewat,[18] J. Brynestad,[19] H. A. Mook,[20] and E. D. Specht*

Neutron powder diffraction has been used to refine the structure of the high-T_C superconductor $Tl_2Ca_1Ba_2Cu_2O_8$ to determine the precise oxygen coordination and the effective valence of copper. The results are in excellent agreement with the Dupont X-ray structure, confirming the possible substitution of about 9% of the Ca sites with Tl in our sample. The Tl sites may be either 3% Tl-deficient or 7% Ca-substituted. The apparent valence of copper is 2.22. Oxygen in the center of the Tl square implies an average valence of less than 3 for Tl; it is, therefore, not surprising that this oxygen is disordered toward the midpoint of the shortest Tl-Tl distance. High-resolution electron images and diffraction reveal a quite different superstructure to the 5 x 5.4 Å superstructure seen in $Bi_2Sr_1Ca_2Cu_2O_8$. Very weak and diffuse superlattice spots may be the result of a charge density wave in the TlO plane with period 6 x 3.8 Å.

1.3.1.7 Superconductivity, Intergrain and Intragrain Critical Current Densities of $Tl_2Ca_2Ba_2Cu_3O_{10+\delta}$ and $Tl_2Ca_1Ba_2Cu_2O_{8+\delta}$ Materials[21] – *J. R. Thompson,[20] J. Brynestad,[19] D. M. Kroeger, Y. C. Kim,[21] S. T. Sekula,[20] D. K. Christen,[20] and E. D. Specht*

Bulk-sintered and powdered samples of the high-temperature superconductive compounds $Tl_2Ca_2Ba_2Cu_3O_{10+\delta}$ and $Tl_2Ca1Ba_2Cu_2O_{8+\delta}$ having Tc values (magnetic midpoint) of 125 and 97 K, respectively, have been synthesized. The materials were characterized by X-ray diffraction, metallographic, and electron microprobe analyses. Both the intergrain and intragrain critical current densities J_C were studied by direct transport measurements at 77 K and through extensive magnetization measurements. The primary results and conclusions are that (1) the intragrain J_C values were large (near 10^7 A/cm^2 at 4.2 K in 10 kOe) and much larger than the transport values; (2) both sintered and powdered materials exhibited large flux creep; (3) and the intragrain J_C decreased exponentially with temperature as $J_C(T) = J_C(0) \exp(-T/T_0)$, where T_0 is an empirical characteristic temperature. These features are qualitatively very similar to those found in the corresponding $Y_1Ba_2Cu_3O_z$ compounds.

1.3.1.8 X-Ray Resonance Exchange Scattering in UAs[23] – *E. D. Isaacs,[11] D. B. McWhan,[11] C. Peters, G. E. Ice, D. P. Siddons,[24] J. B. Hastings,[24] C. Vettier,[17] and O. Vogt[25]*

A resonant enhancement of magnetic scattering was first found on tuning through the L_{III} absorption edge of holmium,[26] and much larger enhancements have been predicted for the M_{IV} and M_V edges in 4f and 5f materials.[27]

Resonant enhancement of the magnetic X-ray scattering cross section in UAs has been investigated by tuning the incident X-ray energy through the uranium M_{IV} and M_V absorption edges. At the M_{IV} edge, the intensity for the (0,0,5/2) magnetic reflection is enhanced by 10^7 relative to the nonresonance component far above the edge and is a remarkable 1% of the intensity at the (0,0,2) charge peak. At the M_V edge, the enhancement is 10^5. The dramatic enhancement at M edges arises from strong electric multipole transitions between atomic core states and the exchange-split Fermi edge states. This remarkable enhancement in magnetic X-ray scattering may provide new insights into the magnetic structure of both surfaces and materials.

1.3.1.9 Phase and Microstructure of Fe-Modified Al_3Ti[28] – *W. D. Porter, K. Hisatsune,[29] C. J. Sparks, W. C. Oliver, and A. Dhere[6]*

Studies of the phase stability between the tetragonal DO_{22} structure of Al_3Ti and the cubic $L1_2$ phase formed by the substitution of Fe for 10% of the Al led to the measurement of site-occupation parameters. This research contributes to a program focused on creating useful engineering materials by enhancing the ductility of the usually brittle intermetallic compounds that have desirable high-temperature properties. Efforts are made to convert noncubic structures to cubic structures to enhance the deformation modes for increased ductility. The structures of Al_3Ti may be described as the stacking of two cubic $L1_2$ unit cells with an antiphase boundary between them.

Unlike the $L1_2$ structure, the DO_{22} structure permits Al-Al first-neighbor pairs, suggesting that there may not be a large energy barrier to mixing of the Al and Ti sites. X-ray powder diffraction of intensity ratios (I superstructure/I fundamental) gave a Bragg-Williams long-range order parameter of $S = 0.78_4$. This corresponds to about 5% of the Al sites being wrongly occupied with Ti atoms and, consequently, 15% of the Ti sites being wrongly occupied with Al atoms. For the polycrystalline $Al_{67}Fe_8Ti_{25}$ sample, X-ray energies just below the FeK edge and 2 to 5 keV above the edge effected a change in the real part of the iron atomic scattering factor by 6 electron units. X-ray intensity ratios (I superstructure/I fundamental) changed by about 15%. Such a large change in the intensity ratio provides for sufficient accuracy to determine that 6 ± 2 at. % or 75% of the 8 at. % Fe addition resides on the Al sublattice, 25% of the Fe addition occupying sites on the Ti sublattice. Although intensity measurements for two different X-ray energies are sufficient to determine the site occupations of a ternary alloy with two sublattices, we used the redundancy to test the precision of our measurements. Our results also showed that the Al and Ti atoms were mixed on the two sublattices with 15_4% of the Ti sites occupied by Al atoms, which is similar to the results on Al_3Ti.

1.3.1.10 Synchrotron Studies of the First-Order Melting Transitions of Hexatic Monolayers and Multilayers in Freely Suspended Liquid-Crystal Films[30] – *S. Amador,[31] P. S. Pershan,[31] H. Stragier,[32] B. D. Swanson,[32] D. J. Tweet,[32] L. B. Sorensen,[32] E. B. Sirota,[33] G. E. Ice, and A. Habenschuss[5]*

Synchrotron X-ray diffraction has been used to study the surface and the interior hexatic-to-liquid (smectic-I to smectic-C) melting transitions of freely suspended liquid-crystal films of N-[4'-(n-heptyl) benzylidene]-4-(n-heptyl)aniline (70.7) five molecular layers thick. Both the surface hexatic monolayers and the interior hexatic layers melt via hysteretic first-order transitions. After the two surface layers undergo a first-order transition to the smectic-I phase, the surface hexatic correlation length ξ evolves smoothly from ~100 to ~300 Å with a roughly square-root $\xi \sim |T\text{-}T_C|^{1/2}$ form.

1.3.1.11 Focusing Error in the X-Ray Johann Spectrometer[34] – *C. N. Koumelis[35] and C. J. Sparks, Jr.*

The focusing error in the Johann X-ray spectrometer is calculated step by step for an ideal crystal completely opaque to the radiation. Parameters are given that permit choices to be made between X-ray source size and energy resolution. How location of the X-ray source and the focus contribute to the energy resolution for X-ray crystal spectrometers are better understood. This work contributes to our understanding of the resolution achievable with X-ray spectrometers and to the trade-offs between intensity and energy resolution.

1.3.2 References

1. C. J. Sparks and G. E. Ice, "X-Ray Microprobe for the Microcharacterization of Materials," pp. 223-33 in *Synchrotron Radiation in Materials Science Symposium*, Vol. 143, Materials Research Society, Boston, Mass., 1988.

2. C. J. Sparks, "Synchrotron Radiation Provides for New Information about Surfaces and Interfaces from Profile Analysis," paper presented at Charles Barrett Symposium TMS Fall Meeting, Chicago, Ill., 1988, and seminar given at University of Missouri, Columbia, Mo., 1988.

3. A. S. Bommannavar, C. J. Sparks, A. Habenschuss, G. E. Ice, A. Dhere, H. Morkoc, and H. Zabel, "X-Ray Diffraction Study of a Thin GaAs Film on Si(100)," in *Mater. Res. Soc. Symp. Proc.* **102**, 223-27 (1988).

4. NSLS, Brookhaven National Laboratory.

5. Chemistry Division, ORNL.

6. E. I. duPont, Chattanooga, Tenn.

7. University of Illinois, Urbana, Ill.

8. Accepted for publication in *J. Vac. Sci. Technol. A* (1989).

9. Department of Physics, Massachusetts Institute of Technology, Cambridge, Mass.

10. Department of Physics, Brown University, Providence, R.I.

11. AT&T Bell Laboratories, Murray Hill, N.J.

12. B. Hwang, C. R. Houska, G. E. Ice, and A. Habenschuss, *J. Appl. Phys.* **63**, 11 (1988).

13. Department of Materials Engineering, Virginia Polytechnic Institute and State University, Blacksburg, Va.

14. B. Hwang, C. R. Houska, G. E. Ice, and A. Habenschuss, *Adv. Ceram. Mater.* **3**, 180 (1988).

15. S. Rao and C. R. Houska, *Acta Crystallogr.* **A42**, 14 (1986).

16. A. W. Hewat, E. A. Hewat, J. Brynestad, H. A. Mook, and E. D. Specht, *Physica C* **152**, 438-44 (1988).

17. Institut Laue-Langevin, 156X, 38042 Grenoble, Cedex, France.

18. CEA, IRDI, D. LETI, CENG, 85X, 38041 Grenoble, Cedex, France.

19. Chemistry Division, ORNL.

20. Solid State Division, ORNL.

21. J. R. Thompson, J. Brynestad, D. M. Kroeger, Y. C. Kim, S. T. Sekula, D. K. Christen, and E. D. Specht, *Phys. Rev. B* **39**, 6652 (1989).

22. Department of Physics, University of Tennessee, Knoxville, Tenn.

23. E. D. Isaacs, D. B. McWhan, C. Peters, G. E. Ice, D. P. Siddons, J. B. Hastings, C. Vettier, and O. Vought, submitted to *Phys. Rev. Lett.* (1989).

24. Brookhaven National Laboratory, Upton, N.Y.

25. ETH, Zurich, Switzerland.

26. Doon Gibbs, D. R. Harshman, E. D. Isaacs, D. B. McWhan, D. Mills, and C. Vettier, *Phys. Rev. Letts.* **61**, 1241 (1988).

27. J. P. Hannon, G. T. Trammell, M. Blume, and Doon Gibbs, *Phys. Rev. Lett.* **61**, 1245 (1988).

28. High-Temperature Ordered Intermetallic Alloys, *Mater. Res. Soc. Symp. Proc.* **133** (1988).

29. School of Dentistry, Nagasaki University, Nagasaki 852, Japan.

30. S. Amador, P. S. Pershan, H. Stragier, B. D. Swanson, D. J. Tweet, L. B. Sorenson, E. B. Sirota, G. E. Ice, and A. Habenschuss, *Phys. Rev. A* **39**(5), 2703 (1989).

31. Division of Applied Sciences and Department of Physics, Harvard University, Cambridge, Mass.

32. Department of Physics, FM-15, University of Washington, Seattle, Wash.

33. Exxon Research and Engineering Company, Corporate Research Laboratories, Route 22 East, Annandale, N.J.

34. C. N. Koumelis and C. J. Sparks, Jr., *Univ. Athens* (Greece) **61**, 315-52 (1986).

35. University of Athens, Greece.

2. HIGH-TEMPERATURE ALLOY RESEARCH

2.1 THEORETICAL STUDIES OF METALS AND ALLOYS – *W. H. Butler*

Recent progress in the theory of many electron systems and in techniques for dealing with disorder, together with advances in computing, have made it possible to calculate and to understand many properties of materials in terms of the most basic laws of physics. The Theory Group participates in this progress and exploits it to develop a fundamental theoretical basis for materials science. The Theory Group also strives to provide theoretical leadership to many of the experimental programs at ORNL.

During the reporting period, important progress was made in several areas:

We continued to investigate improvements in density functional theory (the fundamental framework that undergirds most modern first-principles calculations in solid state physics) by investigating nonlocal exchange-correlation functionals. This work is described in Sect. 2.1.1. We also initiated a program to calculate the quasi-particle self energies and dielectric response functions of narrow-band materials.

Our work on the theory of alloys has matured to the point where it is possible to calculate most of the ground-state properties of random alloys from first principles. Current work emphasizes ordering, phase stability, and the interplay between chemical and magnetic effects (Sect. 2.1.2). During the reporting period, we tested our theory for electrical resistivity and found that it is very accurate even for strongly scattering alloys (Sect. 2.1.3).

Parameter free, first-principles density functional theory calculations of the properties of surfaces and interfaces were used to study the effects of absorbates and overlayers on the atomic, electronic, and magnetic structures of a number of systems (Sect. 2.1.4). The detailed mechanism by which H adsorbed on a W surface induces its reconstruction was elucidated, as was the mechanism by which S poisons the catalytic activity of a Ni surface.

We performed a number of first-principles calculations of the electronic structure of high-temperature superconductors, including the first calculations of the total energy, bulk modulus, and equilibrium lattice constant of La_2CuO_4. We also carefully investigated the validity of the local-density approximation to density functional theory (LDA-DFT) for these materials. Although LDA-DFT gives a good description of most ground-state properties, including the equilibrium lattice constant and the bulk modulus, it has so far proved inadequate in explaining the magnetic properties of La_2CuO_4. We also developed simple force models to describe the structure and stability of $YBa_2Cu_3O_7$ and $YBa_2Cu_3O_6$ (Sect. 2.1.5).

We continued our studies of the effects of impurities on the bonding forces between atoms at grain boundaries. We completed a comprehensive study of dopants in Ni, and we began new projects aimed at increasing the speed of our calculations and the size of the clusters that we can treat (Sect. 2.1.6).

During the past decade, under the relentless assault of LDA-DFT, nature has been forced to reveal how the electrons in materials control most of their equilibrium properties. Mechanical properties, however, have proved to be extremely resistant to first-principles calculations. Dislocation motion is a very difficult problem to model from an electronic structure point of view. During the reporting period we believe we made a breakthrough in this difficult and important area by combining first-principles calculations of the elastic properties and fault energies with a continuum analysis of dislocation motion. The two approaches complement each other very nicely and provide an explanation of the anomalous high-temperature strength that is observed in some alloy systems (Sect. 2.1.7).

2.1.1 Advances in Density Functional Theory and in Techniques for Calculating Electronic Structure – *G. S. Painter, F. W. Averill,[1] and F. W. Kutzler[2]*

The calculation of the properties of a material from first principles requires the solution of the many-electron Schrödinger equation. In principle, the solution to this equation would provide answers to all of the questions we can ask about the properties of materials. In practice, when more than one electron is involved, it is not feasible to solve this equation exactly. Consequently, approximations must be used. Usually, an effective-field approach is used. The Schrödinger equation is solved separately for each electron, the effects of the other electrons being taken into account by assuming that they determine an effective field in which the electron under consideration moves. One contribution to this effective field is obvious: the electrostatic field resulting from the charges on the other electrons (the electrons also experience the electrostatic field of the nucleus). However, other nonclassical contributions (known as exchange and correlation) are of less obvious origin and are much more difficult to calculate.

An important result was obtained in the 1960s by Hohenberg, Kohn, and Sham,[3] who showed that the effective field method of solving the many-electron Schrödinger equation could be made exact if the functional dependence of the exchange and correlation energy on the electron density were known. Although the exchange and correlation energy functional is not known exactly, a body of results obtained in work by the Theory Group, as well as by others, demonstrates that it can be approximated rather well by the exchange and correlation energy of a homogeneous electron gas. The effective-field approach based on the result of Hohenberg, Kohn, and Sham[5] is known as density functional theory (DFT). The version of DFT in which the exchange-correlation energy is replaced by a local function calculated for an electron gas is known as the local density approximation (LDA). If spin polarization is allowed, it is known as the local spin density approximation (LSDA).

The LDA and LSDA have been extremely successful. They form the basis for most modern first-principles calculations in solid state physics. The LDA and LSDA give particularly good values for interatomic separations and for vibrational frequencies. It has been known for several years, however, that binding energies calculated using LSDA could be in error by several tenths of an electron volt per atom.

To improve on LSDA, we have developed techniques that allow us to implement and assess exchange-correlation energy functionals of arbitrary complexity, including so-called "nonlocal functionals" in which the exchange and correlation contribution to the effective field seen by an electron at one point depends not only on the magnitude of the electron density at that point but also on the density variations at that point. We have developed procedures to incorporate these gradient corrections to the LSDA in our atomic cluster codes, and we have carried out tests of the nonlocal corrections to the spectroscopic constants of several atoms and molecules. In a comprehensive set of calculations (Sect. 2.1.1.1), we have found significant corrections ($\sim$10% for O_2 and N_2 and $\sim$20% for F_2) to the binding energies of diatomic molecules, with rather slight effects on equilibrium separations. Our studies identified a cooperative effect of nonlocality in the exchange-correlation functional and nonsphericity in the charge density, which lowers the total energy of open-shell atoms. Inclusion of this effect greatly improves the calculated binding energies of diatomic molecules (Sects. 2.1.1.2 and 2.1.1.3) by reducing errors in worst cases by 50% (O_2 and F_2).

A remarkable part of DFT is the Hohenberg-Kohn theorem, which states that the total energy of any system of electrons is a unique functional of their density. Therefore, if this energy functional and the electron density were known, it would be possible to obtain the total energy by performing a simple integration. Currently, however, DFT calculations require the solution of the one-electron Schrödinger equation. The primary reason for this requirement is that we do not have a good expression for the kinetic energy functional. (We know the electrostatic part of the functional and have a good approximation for the exchange-correlation part.) Recently, attempts have been made to circumvent the solving of the Schrödinger equation by assuming that the kinetic energy functional could be represented by an expansion in terms of the gradient of the electron density. During the reporting period, we collaborated with researchers at other institutions to assess the validity of these techniques and found significant errors in this representation of the kinetic energy (Sect. 2.1.1.4). We also identified the source of the exchange-energy error as originating in the functional for exchange itself, rather than in the local-spin density (LSD) electron density.

Although DFT is rigorously a ground-state theory and not a theory for the excitation spectrum, it has been shown that DFT is correct within symmetry classes. Thus, energy differences between states of different symmetry should be correctly given by DFT. We studied the applicability of the local and nonlocal LSDA to interconfigurational energies in the important case of transition metal atoms and found inclusion of nonlocal terms marginally significant in determining these energies (Sect. 2.1.1.5).

Although first-principles calculations are an important part of materials science theory, it is equally important to extract concepts and rules of thumb from these calculations that can be applied quickly and heuristically even in complicated systems. During the reporting period, we extended our concept of the orbital force to obtain a new way of describing the chemical bond. We associated with each electronic orbital a dynamic force that describes the change in the total force in a cluster resulting from a change in the electron density in the orbital. We calculated dynamic orbital forces for various states of first-row diatomic molecules and showed that correct predictions could be made by the associated orbital force about whether the bond length contracted or expanded when the occupation of these orbitals change (Sect. 2.1.1.6).

An important factor in maintaining a forefront status in this field is the development of efficient and accurate techniques for carrying out calculations. In optimizing the augmented Gaussian orbital cluster approach, which forms the basis of our microchemical studies (Sect. 2.1.4), new multidimensional integration methods have been developed. The most recent scheme, which has broad generality in many regards, has been described in the literature (Sect. 2.1.1.7).

2.1.1.1 Nonlocality in the Density-Functional Description of Bonding in Li_2, N_2, O_2 and F_2 (ref. 4) – *F. W. Kutzler[2] and G. S. Painter*

The fully self-consistent implementation of the nonlocal-density functional of Langreth and Mehl has been used in conjunction with the augmented Gaussian method to calculate the potential-energy curves and dissociation energies of N_2, Li_2, O_2, and F_2. The nonlocal functional gives ground-state potential-energy curves in very good agreement with experiment. We compare these nonlocal results with other local-density calculations, and examine the effect of nonlocal-potential self-consistency on the dissociation energy.

2.1.1.2 Cooperative Effect Between Nonlocal-Density Functionals and Nonspherical Charge Densities in Atomic Total Energies[5] – *F. W. Kutzler[2] and G. S. Painter*

When the total energies of atoms having nonspherical charge densities are calculated using both nonlocal functionals and nonspherical charge densities, the energies are lower than when either nonlocality of nonsphericity is used separately. Within the LDA the inexact treatment of self-interaction negates most or all of the effect of a nonspherical treatment, resulting in only minor changes in total energy. The lower atomic reference energy improves binding energies of first-row dimers, which are overbound by both local and nonlocal functionals when spherical charge densities are used.

2.1.1.3 Energies of Atoms with Nonspherical Charge Densities Calculated with Nonlocal-Density Functional Theory[3] – *F. W. Kutzler[2] and G. S. Painter*

Calculations using nonlocal-density functional theory show that the total energies of atoms in states characterized by partially filled degenerate subshells are substantially

lower when the charge density is not spherically averaged. This is in contrast to the case of local density theory in which spherical and nonspherical treatments of atoms give essentially identical energies. A cooperative effect of nonlocality in the exchange-correlation functional and nonsphericity in the charge density lowers the atomic total energies and greatly improves the calculated binding energies of B_2, C_2, O_2, and F_2.

2.1.1.4 Chemical Bond as a Test of Density-Gradient Expansions for Kinetic and Exchange Energies[6] – *J. P. Perdew,[7] M. Levy,[8] G. S. Painter, S. Wei,[7] and J. B. Lagowski[9]*

Errors in kinetic and exchange contributions to the molecular bonding energy are assessed for approximate density functionals by reference to near-exact Hartree-Fock values. From the molecular calculations of Allan et al.[10] and of Lee and Ghosh[11], it is demonstrated that the density-gradient expansion does not accurately describe the noninteracting kinetic contribution to the bonding energy, even when this expansion is carried to fourth order and applied in its spin-density-functional form to accurate Hartree-Fock densities. In a related study, it is demonstrated that the overbinding of molecules such as N_2 and F_2, which occurs in the LSDA approximation for the exchange-correlation energy, is not attributable to errors in the self-consistent LSD densities. Contrary to expectations based on the Gunnarsson-Jones nodality argument, it is found that the LSDA for the exchange energy can seriously overbind a molecule, even when bonding does not create additional nodes in the occupied valence orbitals. LSD and exact values for the exchange contribution to the bonding energy are displayed and discussed for several molecules.

2.1.1.5 Interconfigurational Energies in Transition Metal Atoms Using Nonlocal-Density Functional Theory[12] – *F. W. Kutzler[2] and G. S. Painter*

The functional of Langreth, Mehl, and Hu[13] (LMH) and the generalized gradient approximation (GGA) of Perdew and Yue[14] have been used to calculate s-d transition energies, 4s-ionization energies, and 3d-ionization energies for the 3d-transition metal atoms. These calculations have been compared with results from the local-density functional of Vosko, Wilk, and Nusair.[15] By comparison with experimental energies, we find the nonlocal functionals are marginally more successful than local density in calculating energy differences between transition metal atoms. The GGA approximation is somewhat better than the LMH functional for most of the metals studied, although there are several exceptions.

2.1.1.6 Dynamic Orbital Forces and Molecular Geometry in the Density-Functional Formalism[16] – *G. S. Painter and F. W. Averill[1]*

The eigenvalues of the single-particle equations of DFT were shown to define dynamic orbital forces that can serve, in the Mulliken sense, as a semiquantitative basis for understanding chemical binding. LSD calculations for first-row diatomic molecules demonstrated that the type of bond-length change accompanying a change

in occupation number of a given one-electron orbital can be predicted with consistent accuracy by the associated dynamic orbital force.

2.1.1.7 Pseudospherical Integration Scheme for Electronic Structure Calculations[17] – *F. W. Averill[1] and G. S. Painter*

Contemporary electronic-structure methods avoid shape approximations but in doing so encounter the difficult problem of integral evaluation over complicated interstitial volumes. In this paper, we present a simple and efficient technique for applying rapidly convergent Gaussian product formulas to general interstitial regions. As in the recent methods of Boerrigter, te Velde, and Baerends,[18] the technique is based on partitioning space into Voronoi cells and atomic spheres. In the current work, introduction of a general pseudospherical local-coordinate system unifies the integration procedures and effects a simplified approach. A systematic procedure is derived from determining the number of Gaussian points required for a specified level of numerical precision.

2.1.2 Ordering, Phase Stability, and Magnetism in Alloys – *G. M. Stocks, D. M. Nicholson, W. H. Butler, W. A. Shelton,[19] D. D. Johnson,[20] and F. J. Pinski[19]*

During the past few years the theory of the ground state (T = 0 K) properties of metals and alloys has progressed to the point where it is possible to contemplate formulating a full finite-temperature theory of ordering and phase stability in metallic alloys. The central difficulty in obtaining such a formulation is the necessity of including, on an equal footing, contributions to the free energy arising from the electronic energies and contributions from the entropy of configurational rearrangements. In addition, the vibrational and magnetic degrees of freedom and their interactions with the compositional fluctuations must be considered.

During the last few years, we have been developing theoretical and computational techniques that allow us to obtain such a first-principles theory. Our approach can be divided into two parts.

The first part is a theory of the energy and ground-state properties of random alloys. The density-functional-theory Korringa-Kohn-Rostoker coherent-potential-approximation (DFT-KKR-CPA) theory, which was developed by us and our collaborators at the Universities of Cincinnati, Bristol (UK), Warwick (UK), and Sandia National Laboratories, allows us to calculate the total energy of a random substitutional alloy within DFT at a level that had previously been possible only for pure metals and ordered compounds.

The second part of the theory is its extension to finite temperature by including the entropy of configurational rearrangement. This has been done both within the mean-field theory of Gyorffy[21] and Stocks and by the calculation of interchange potentials of a lattice gas using model that can then form the basis of cluster variation method (CVM) calculations or Monte Carlo statistical simulations.

We have also used the mean-field theory to calculate the phase diagram of Pd(c)Rh(1-c) entirely from first principles. The bare mean-field theory phase diagram is in qualitative agreement with experiment. When corrections for the effects of the electron-phonon interaction are included and the mean spherical approximation is used to correct some of the deficiencies inherent in mean-field statistical mechanics, the agreement becomes quantitative.

We have also used the mean-field theory to study the nature of the interchange interactions in Al(c)Ag(1-c) alloys by calculating the short-range order (SRO) diffuse scattering for a number of fcc alloys. With increasing Ag content, the calculated SRO diffuse-scattering patterns change from signifying clustering to signifying a propensity of ordering of the CuPt type. In terms of an Ising model description, this implies a change in sign in near-neighbor interchange potential as a function of composition. Clustering in Al-rich alloys is consistent with Guinier-Preston zone formation in these alloys. Furthermore, it suggests that the zone formation is driven by concentration fluctuations rather than by elastic effects as has been suggested in the past.

In the past we have developed a theory of finite-temperature magnetism in the pure metal 3d-transition metal ferromagnets that generalizes the spin-polarized DFT theory of the magnetic ground state. In the disordered local moment (DLM) theory of the finite-temperature paramagnetic state, it is assumed that local (single-site) moments exist but that their orientation (up/down in the simplest picture) is disordered and as a consequence the total macroscopic moment is zero. The ferromagnetic transition temperature is signaled by the lining up of the local moments. The disorder in the orientation of the local moment inherent in the paramagnetic DLM state is treated using spin polarized DFT-KKR-CPA. The phase transition is treated using a mean field approximation analogous to that referred to in the preceding paragraph in the case of compositional fluctuations. Conventional Stoner-type paramagnets are signaled by the vanishing of the local moment in the DLM state.

In magnetic alloys, it is essential that both magnetic and compositional fluctuations be considered. We have begun a detailed study of the joint effects of chemical and magnetic disorder in fcc Ni(c)Fe(1-c) alloys. In the INVAR region of the phase diagram, it is found that the energies of random alloys of the fully aligned ferromagnetic state, the DLM state, and the Stoner paramagnetic state become essentially degenerate, suggesting the onset of a magnetic instability. That this instability is strongly coupled to the lattice is suggested by the observation that the equilibrium lattice spacings for the three states are different.

Using the ground-state DFT-KKR-CPA theory, we have calculated the equilibrium lattice spacings and heats of mixing of Cu(c)Zn(1-c) alloys in the fcc phase. These calculations go beyond our early calculations on this system in that they include angular momentum components up to f-wave. The concentration variation of the lattice spacing is in excellent agreement with experimental values. The heats of mixing are slightly skewed to Cu-rich alloys and are about 50% of those obtained experimentally. Early

attempts to estimate the effects of short-range order on the experimental results suggest that these effects may explain a substantial fraction of the difference.

We have published the proceedings of the NATO Advanced Study Institute (ASI) on "Alloy Phase Stability" that we organized in Maleme, Crete, Greece,[22] in 1987. The book *Alloy Phase Stability* (edited by G. M. Stocks and A. Gonis[23]) comprises the lecture notes and contributed talks presented at the ASI. Covered topics include: alloy design, experimental probes of the atomic and electronic structure, thermodynamics and statistical mechanics, semiphenomenological and model Hamiltonian electronic theories of phase stability, first-principles theories of alloy phase stability, and the effects of strain and microscopic defects on phase stability.

2.1.2.1 Configurational Energies and Effective Cluster Interactions in Substitutionally Disordered Binary Alloys[24] – *A Gonis,[23] X.-G. Zhang,[25] A. J. Freeman,[25] P. Turchi,[23] G. M. Stocks, and D. M. Nicholson*

The determination of configurational energies in terms of effective cluster interactions in substitutionally disordered alloys based on what is known about the alloy electronic structure is examined within the methods of concentration wave (CW), the generalized perturbation method (GPM), and, for the first time, the embedded-cluster method (ECM). It is shown that the ECM provides the exact summation to all orders of the effective cluster interaction expansions obtained in the partially renormalized GPM. The connection between the various methods (CW, GPM, and ECM) is discussed and illustrated by means of numerical calculations for model one-dimensional tight-binding (TB) systems and for TB Hamiltonians chosen to describe Pd-V alloys. These calculations, and the formal considerations presented in the body of the paper, show the complete equivalence of converged GPM summations within specific clusters and the ECM. In addition, it is shown that an exact expansion of the configurational energy can be obtained in terms of fully renormalized effective cluster interactions. In principle, these effective cluster interactions can be used in conjunction with (1) statistical models to determine stable ordered structures at low temperatures and (2) alloy phase diagrams.

2.1.2.2 First-Principles Study of Ordering Properties of Substitutional Alloys Using the Generalized Perturbation Method[26] – *P. E. A. Turchi,[23] G. M. Stocks, W. H. Butler, and D. M. Nicholson*

Ab initio calculations of effective cluster interactions that make up the ordering energy of a substitutional alloy are reported. Tendencies toward ordering or phase separation and, more generally, phase stability in PdV and PdRh substitutional alloys are discussed. The study is based on an extension of the generalized perturbation method to systems describable by muffin-tin Hamiltonians in the framework of the multiple-scattering formalism in conjunction with the Korringa-Kohn-Rostoker coherent potential approximation. Future applications of the method are discussed.

2.1.2.3 Theory of Random Alloys[27] – *F. J. Pinski,[19] D. M. Nicholson, G. M. Stocks, W. H. Butler, D. D. Johnson,[20] and B. L. Gyorffy[21]*

We review the theory of random substitutional alloys that we have developed from microscopic quantum mechanics. This theory is based on the understanding of the electron "glue" that is responsible for cohesion. We describe how many properties can be calculated from first-principles theories, (i.e., only the atomic numbers and the concentrations of elements are required inputs). These properties include the equilibrium volume, short-range order parameters, phase diagrams, magnetic properties, and transport coefficients. Two types of mean-field approximation are used in these calculations. Density functional theory is used to reduce the "many-electron" problem to that of a single electron moving in a mean field as a result the other electrons, and the coherent-potential approximation is used to replace the disordered potential field of the random alloy by an effective potential.

2.1.2.4 Electronic Structure of Random Alloys and the Theory of Ordering Processes[28] – *G. M. Stocks, D. M. Nicholson, F. J. Pinski,[19] D. D. Johnson,[20] and A. Gonis[23]*

We consider some of the approaches toward obtaining an understanding of alloy phase stability within the context of ab initio density functional theory. We show recent results of calculations, using the concentration functional theory of Gyorffy and Stocks, of the spinodal for Pd_cRh_{1-c} alloys. We also show results for short-range order diffuse scattering patterns in Al_cAg_{1-c} that show that the intersite interactions change from clustering to ordering with increasing silver content. The implications of these results for the phase diagram of Al_cAg_{1-c} alloys and for Guinier-Preston zone formation in aluminum-rich alloys are briefly discussed. In conclusion, some conjectures about what the future might hold regarding first-principles theories of phase stability are made.

2.1.2.5 Electronic Structure and the State of Compositional Order in Metallic Alloys[22] – *B. L. Gyorffy,[21] D. D. Johnson,[20] F. J. Pinski,[19] D. M. Nicholson, and G. M. Stocks*

The theory of phase transitions in metallic alloys is reviewed. Phenomenological theories such as that of Landau are explained as are semimicroscopic theories based on pair-potentials. A detailed explanation of the modern, fully microscopic mean-field theory of compositional order in alloys is given. A first-principles microscopic Cahn-Hilliard theory is derived based on the KKR-CPA.

2.1.2.6 Configurational Energies in Terms of Effective Cluster Interactions in Binary Substitutional Alloys: Connection Between the Embedded Cluster Method and the Generalized Perturbation Method[22] – *P. E. A. Turchi,[23] A. Gonis,[23] X. Zhang,[25] and G. M. Stocks*

Starting from the formal expansion of the configurational energy in terms of fully renormalized effective cluster interactions, it is shown that the (ECM) and the GPM lead to identical expressions for the energy of a given alloy configuration within the coherent

potential approximation (CPA). Correction terms associated with fluctuations in the reference medium can be calculated in both methods. Numerical results are presented for a model tight-binding Hamiltonian, which clearly indicate the significance of multisite cluster interactions in the determination of the tendencies toward ordering or phase separation and phase stability in alloys.

2.1.2.7 White Paper on Ab Initio Theory Alloy Phase Stability[29] – *G. M. Stocks*

During the last few years it has become clear that DFT provides an excellent foundation for describing the ground state properties of metallic alloys. In particular, the LDA to DFT has been used to calculate total energies, equilibrium lattice spacings, bulk moduli, heats of formation of ordered alloys, and heats of transformation all with good results. Recent work has extended LDA and DFT to random (substitutional) metallic alloys, where the electronic structure is calculated using the ab initio Korringa-Kohn-Rostoker coherent-potential approximation (KKR-CPA). Given this new availability of parameter-free methods that can treat pure metals, ordered intermetallic compounds, and disordered solid solutions on an equal footing, it is appropriate to consider the possibility of obtaining an ab initio theory of alloy phase stability based on DFT.

2.1.2.8 Chemical Disorder and Magnetism in Alloys[30] – *F. J. Pinski*[19]

Many alloys exist as solid solutions rather than as compounds. For transition metal alloys, these solid solutions can exist at a variety of temperatures and pressures. Many of these alloys have important technological applications, such as in the steel and magnetic recording media industries. One can think of these solid solutions, A_cB_{1-c}, as consisting of two types of atoms, A and B, randomly located on an underlying lattice. In this notation, c denotes the concentration of type A atoms, that is, the fraction of all atoms that are type A. Standard band theory techniques, which are often applied to crystal materials, cannot be applied here because of the broken symmetry introduced by the random location of the atoms in the alloy. Band theory requires long-range order (i.e., a unit cell that repeats throughout space) and is not applicable to these solid solutions.

2.1.2.9 Effects of Chemical and Magnetic Disorder in $Fe_{0.50}Mn_{0.50}$ (ref. 31) – *D. D. Johnson,*[20] *F. J. Pinski,*[19] *and G. M. Stocks*

We present the results of first-principles calculations of the total energy and spin-polarized electronic structure of disordered fcc $Fe_{0.50}Mn_{0.50}$. These self-consistent calculations were performed using the KKR-CPA, using the LSDA to treat exchange and correlation. We use a lattice constant of a = 6.80 a.u.; information about stability can be inferred from calculated pressure and energy. The moments on the Fe and Mn sites are large but antiparallel to each other, resulting in a small net magnetization. A comparison of the electronic structure is made for fcc Fe, Mn, and FeMn in both the ferromagnetic and disordered local moment states.

2.1.2.10 Local-Density Theory of Magnetism and Its Interrelation with Compositional Order in Alloys[22] – *J. B. Staunton,[32] B. L. Gyorffy,[21] D. D. Johnson,[20] F. J. Pinski,[19] and G. M. Stocks*

These lectures focus on the spin polarized electronic structure of both magnetic metals and alloys. This was shown to provide the basis for a first-principles description of the mechanism driving the magnetic phase transition in pure metals at finite temperatures, and in alloys it demonstrates how compositional ordering depends on the state of magnetic order. It remains to combine these treatments of magnetic and compositional fluctuations and obtain a parameter-free microscopic theory of magnetic and compositional ordering in alloys. The prospect of understanding a wide range of magnetic properties of alloys is in sight.

2.1.2.11 On Positron Annihilation in Concentrated Random Alloys and Superconducting Cuprates[33] – *Z. Szotek,[34] W. M. Temmerman,[34] B. L. Gyorffy,[21] and G. M. Stocks*

We discuss an application of a generalization of the Lock-Crisp-West theorem to concentrated random alloys. Using a theory developed for binary random alloys, we explore a possibility of positron localization in the new high-temperature superconductors.

2.1.2.12 NATO ASI on Alloy Stability[22] – *G. M. Stocks and A. Gonis[23]*

This book contains the lecture notes and contributed papers presented at the NATO Advanced Study Institute (ASI) on Alloy Phase Stability which was held June 14-17, 1987, in Maleme-Chania, Greece. The ASI was cross disciplinary and brought together scientists with interests ranging from practical alloy design to first-principles theories of the properties of alloys. The main lecture courses were presented by internationally recognized experts in their fields. The main body of the book consists of their lecture notes. The book is divided into sections according to subject matter:

Sect.	Subject
1	Alloy design
2	Experimental probes of atomic and electronic structure
3	Thermodynamics and statistical mechanics
4	Electronic theories of phase stability; semiphenomenological and model Hamiltonians
5	Electronic theories of phase stability; first-principles theory
6	Effects of strain and macroscopic defects on phase stability
7	General

2.1.3 Transport in Metals and Alloys – *W. H. Butler, G. M. Stocks, D. M. Nicholson, J. C. Swihart,[35] R. H. Brown,[36] P. B. Allen,[37] and F. J. Pinski[19]*

One of the fundamental properties of materials is their response to electric and magnetic fields. Recently, we developed a theory for the electrical conductivity of alloys based on the KKR-CPA. This theory includes the effects of "vertex corrections" and is applicable even in the strong scattering regime, where the usual theories based on the Boltzmann equation cannot be used.

The theory of the electrical conductivity of strongly scattering disordered systems is extremely complex and our theory, necessarily, makes some approximations. During the reporting period we tested our theory by calculating the electrical resistivity of vanadium-aluminum alloys in two ways. One calculation employed the KKR-CPA theory. The other calculation may be likened to a simulation because it involved an exact calculation of the electrical resistivity, subject to the constraints that the calculations were performed for finite systems. The same potentials were used in both calculations, and the same technique for representing the wave functions was used in both calculations.

It was very gratifying to observe that the electrical resistivity calculated from the simulation was (within the statistical limits) consistent with that calculated from the KKR-CPA theory (Sects. 2.1.3.1, 2.1.3.2, and 2.1.3.3). The simulation was made possible by our extension of KKR theory so that it can treat systems consisting of hundreds of atoms per unit cell. In the future we plan to use this technique to study the electronic structure of complex systems such as those containing grain boundaries and dislocations.

2.1.3.1 Resistivity of Strong-Scattering Alloys: Absence of Localization and Success of Coherent-Potential Approximation Confirmed by Exact Supercell Calculations in $V_{1-x}Al_x$[38] – *R. H. Brown,[36] P. B. Allen,[37] D. M. Nicholson, and W. H. Butler*

A supercell procedure for exact evaluation of the one-electron Kubo-Greenwood formula is applied to the resistivity p of $V_{1-x}Al_x$ alloys and compared with a KKR-CPA calculation. The results of these calculations agree well, consistent with the observation of delocalized eigenstates, in spite of the very high resistivity ($\rho \approx 200$ $\mu\Omega$ cm).

2.1.3.2 A First-Principles Calculation of the Resistivity and Thermopower in Strong-Scattering Alloys[39] – *R. H. Brown,[36] P. B. Allen,[37] D. M. Nicholson, and W. H. Butler*

We investigate the concentration and short-range order dependence of the zero-temperature resistivity and thermopower for substitutionally disordered alloys from a first-principles approach. The alloy disorder is simulated by calculating the electronic structure of a large supercell (typically, 200 to 250 atoms) with periodic boundary conditions. For the strong-scattering alloys we consider, the electron mean-free path is much less than the supercell dimension, causing artificial effects of periodicity to be

negligible. In spite of strong scattering, there is no evidence for localized states near E_F. The resistivity and thermopower are averaged over several configurations, resulting in statistical error bounds of approximately $\pm$10%. The concentration-dependent resistivity of substitutional $V_{1-x}Al_x$ alloys agree well with KKR-CPA calculations. This confirms the accuracy of KKR-CPA theory.

2.1.3.3 A First-Principles Calculation of the Electronic Structure and Transport Properties of a Strong-Scattering Disordered Alloy[5] – *R. H. Brown,[36] P. B. Allen,[37] D. M. Nicholson, and W. H. Butler*

There is significant disagreement concerning the accuracy of CPA transport calculations of strong-scattering alloys. We report on a direct calculation of the electronic structure and conductivity of a strong-scattering, disordered alloy and compare our results with the KKR-CPA results.

2.1.3.4 A Comparison of Supercell and Coherent-Potential Approximation Methods in Substitutionally Disordered Alloys[40] – *R. H. Brown,[36] W. H. Butler, and D. M. Nicholson*

The calculated conductivity and thermopower from KKR-CPA and supercell methods are compared. The convergence of the supercell calculation with cell size is examined. Each approach is examined in the regime where its applicabi-lity is questionable. The supercell method is tested in weak-scattering AgPd alloys to check for periodic boundary effects. The KKR-CPA is investigated near the band limits in strong-scattering VAl alloys where eigenstate localization effects may become evident.

2.1.3.5 Electrical Resistivity of Random Transition Metal Alloys[5] – *W. H. Butler, D. M. Nicholson, J. C. Swihart,[35] and F. J. Pinski[19]*

We report on calculations of the electrical resistivity of several solid-solution transition metal alloys including PdAg, NiMo, PdMo, and FeNi. The calculations are performed using the KKR-CPA theory for transport in alloys. This theory includes the electronic structure at the level of the CPA and properly includes matrix elements. It reduces to the Boltzmann equation in the limit of weak scattering. It does not include localization effects or the effects of short-range order. Agreement with experimental results appears to be very good.

2.1.3.6 Electron-Phonon Interaction Effects in Tantalum[41] – *A. Al-Lehaibi,[35] J. C. Swihart,[35] W. H. Butler, and F. J. Pinski[19]*

The results of calculations for a number of electron-phonon interaction effects for tantalum are presented. The calculations are based on Korringa-Kohn-Rostoker energy bands, Born-von Karman phonons, and the rigid-muffin-tin approximation for the electron-phonon matrix element. The calculated Eliashberg spectral function α^2F is compared with the earlier tunneling data of Shen[42] and the proximity tunneling data of Wolf et al.[43] The calculated and tunneling transverse-phonon peaks agree well, but the

height of the tunneling longitudinal-phonon peak is smaller than the calculated results. The calculated electron-phonon coupling parameter λ is 0.88, which is larger than the λ determined from superconducting tunneling and superconducting T_c measurements, but is slightly smaller than the λ determined from electronic specific-heat measurements. Calculated phonon linewidths along various symmetry directions are presented. The temperature dependence of the electrical resistivity resulting from phonon scattering is calculated in the lowest-order variational approximation and it agrees with experimental results. The point-contact spectral function of Kulik, $G(\omega)$ is determined and compared with $\alpha^2F(\omega)$. The agreement between calculated and measured electronic specific heat and high-temperature electrical resistivity gives strong support to the validity of the rigid-muffin-tin approximation for electron-phonon matrix elements. The main disagreement between calculated and measured results is for superconducting properties for which an ad hoc Coulomb interaction μ must be used.

2.1.4 Surfaces and Interfaces – *C. L. Fu*

A precise and detailed understanding of the physical and electronic structure of surfaces and interfaces in materials is extremely important in both science and technology because many important materials properties are determined or strongly influenced by surface effects. Corrosion, catalysis, and brittle fracture are examples of important materials properties that cannot be understood without detailed knowledge of the properties of surfaces and interfaces.

Recently, we have made great progress in this area by extending DFT calculations to treat surfaces and interfaces. It is now possible, for example, to calculate the electronic and magnetic properties of free surfaces from first principles. We can also determine how the atomic positions relax from the ideal positions in the truncated solid because of the creation of the surface or interface. It is known that many solid surfaces and interfaces are "reconstructed" (i.e., their symmetry is different from that of the bulk). This effect can also be investigated from first principles by comparing the energy of the reconstructed surface with that of the relaxed unreconstructed surface.

These calculations were made possible by the development of highly precise full-potential electronic structure codes based on the full potential augmented plane wave method (FLAPW) and the mixed-basis pseudopotential methods of solving the LDA-DFT equations. Both of these techniques are applicable to perfectly ordered systems, but because the electronic and structural properties of the bulk material are recovered only a few atomic layers beneath a metal surface and the charge density extends only a few angstroms above the surface, it is sufficient to model a surface by a system consisting of an infinite set of slabs of material, each 5 to 15 atoms thick, separated by vacuum layers of similar thickness.

An excellent example of the power and precision of our techniques for calculating the properties of surfaces from first principles is provided by our study of the interaction between hydrogen and the tungsten (001) surface by the FLAPW method (Sect. 2.1.4.1). For an H coverage of 0.5, we found that the (001) surface of W is reconstructed. We

also found excellent agreement between calculated and experimental values for the surface vibrational modes that involve a symmetrical H stretching motion. This work represents the first ab initio study of absorbate-induced reconstruction on metallic surfaces.

The nickel surface-sulfur system has immense technological importance. The surfaces of the nickel group metals are often used as catalysts and a major problem in this application of these materials is poisoning of the catalytic activity by environmental sulfur. We calculated the effects of sulfur on the electronic, magnetic, and structural properties of a Ni (100) surface and discovered the detailed changes in electronic structure that are responsible for the poisoning (Sect. 2.1.4.2). The calculated Ni-S distance (1.36 Å) is in excellent agreement with experiment.

The ability to treat surfaces and to treat overlayers of foreign atoms on surfaces makes it possible to investigate a number of interesting phenomena. What happens, for example, to the magnetic moment of an element such as iron or nickel when it consists of a single overlayer on a nonmagnetic substrate? Together with colleagues at Northwestern University, we have performed several first-principles FLAPW calculations on such overlayer-substrate systems. Our studies of Fe overlayers on a Au substrate is described in Sect. 2.1.4.3, Ni on Cu(111) is described in Sect. 2.1.4.4, and Ni on Ag is described in Sect. 2.1.4.5. We have also considered a system with two overlayers, W(110) covered by Fe covered by Ag (Sect. 2.1.4.6). The size of the magnetic moment of a transition metal atom is a complicated function of its environment.

Generally, we observe the magnetic moment of an atom at a surface to be higher than one in the bulk. [Sect. 2.1.4.7 describes our study of surface magnetism of fcc Co(001) for example] this is consistent with the observation that magnetic moments are generally higher in atoms than in solids, and that the volume of magnetic phases are generally larger than corresponding paramagnetic phases. There are other important factors, however, such as the hybridization with substrate electronic states.

2.1.4.1 Total Energy Determination of the H-Induced c(2X2)-W(001) Multilayer Surface Reconstruction[5] – *C. L. Fu and A. J. Freeman*[23]

The effect of H (θ – 0.5)-induced c(2X2) W(001) surface reconstruction is determined using the precise all-electron FLAPW method. The reconstructed surface, corresponding to the $\bar{M}_5$<10> distortion, is found to have a surface atom displacement of 0.25 Å and a reconstruction energy of 60 meV per adsorbed H. Further, we predict a substantial subsurface reconstruction, which allows the release of strain caused by the reconstructed surface layer. The calculated total energy minimum path from the relaxed p(1X1) phase to the c(2X2) structure indicates a possible first-order transition and the coexistence of reconstructed and unreconstructed domains. The reconstruction is driven by the instability of surface states near E_F and the bonding of W-H-W "dimers." Possible coupling of $\bar{M}_5$ and $\bar{M}_1$ surface phonons, calculated symmetrical H stretching frequency, and electronic structure are presented and discussed.

2.1.4.2 Covalent Bonding of Sulfur on Ni(001): The Prototype Adsorbate Poisoner[44] – *C. L. Fu, and A. J. Freeman*[23]

The effects of sulfur, as a prototypical poisoner, on the structural, electronic, and magnetic properties of Ni(001) is investigated with the highly precise full-potential linearized augmented plane-wave method. The poisoning is found to be caused by local Ni-S covalent bond formation and the "lone-pair" density polarization on the S site. A nearly magnetically dead Ni surface layer ($0.12\mu_B$) is obtained. The indirect long-range (screening) interaction is manifested in a layer-dependent oscillatory on-site charge transfer between e_g and t_{2g} symmetry states for Ni inner layers.

2.1.4.3 Monolayer Magnetism: Electronic and Magnetic Properties of Fe/Au(001)[45] – *C. Li,*[23] *A. J. Freeman,*[23] *and C. L. Fu*

A highly precise all-electron LSD FLAPW calculation has determined the electronic and magnetic properties of an Fe monolayer adsorbed on an Au(001) substrate. The magnetic moment of the Fe atom is found to be $2.97\mu_B$ [i.e., enhanced by 30% from the bulk value and very close to that determined previously for the surface layer of Fe(001) itself ($2.96\ \mu_B$)]. As a result of Au d-band hybridization with the Fe d-band, Au interface atoms have a small moment of $+0.03\ \mu_B$. Although the Fe magnetic moment is strongly *enhanced*, the contact hyperfine field at the Fe nucleus is substantially *reduced* to -213 kGauss, a result of the large positive conduction electron contribution, which is rather sensitive to the atomic environment.

2.1.4.4 Surface Magnetism of the Clean Ni(111) Surface an of a Ni Monolayer on Cu(111)[46] – *C. L. Fu and A. J. Freeman*[23]

Results of highly precise all-electron LSD FLAPW calculations on a (1) close-packed seven-layer Ni(111) slab and (2) p(1X1) Ni monolayer on Cu(111) are presented. For Ni(111), we find an enhancement of the magnetic moment for both the surface (to $0.63\ \mu_B$) and subsurface Ni layers (from a center layer value of $0.58\ \mu_B$). In contrast, a slight decrease of the magnetic hyperfine field at the surface is obtained. Although the magnetism is suppressed for monolayer-Ni/Cu(111) as a result of sp(Cu)-d(Ni)interactions, we find that the Ni overlayer is not magnetically "dead" but has a sizable but reduced moment of $0.34\ \mu_B$/atom.

2.1.4.5 Structural, Electronic, and Magnetic Properties of a Ni Monolayer on Ag(001): Ni Adsorption vs Ag Surface Segregation[47] – *S. C. Hong,*[23] *A. J. Freeman,*[23] *and C. L. Fu*

The structural, electronic, and magnetic properties of a p(1X1) Ni overlayer on Ag(001) are investigated with use of the highly precise all-electron total-energy FLAPW method. Although the Ni-Ag bond length remains essentially the same as that of p(1X1) Ni/Cu(001), we found that the Ni magnetic moment ($0.57\ \mu_B$) is enhanced by 50% from that ($0.39\mu_B$) of Ni/Cu(001) as a result of the effect of negative pressure. Nevertheless, the magnetic moment is reduced by about 20% compared with that ($0.70\mu_B$) of the

surface layer in Ni(001) because of hybridization coupling of Ni and Ag. The magnetic hyperfine field is found to be reduced at the interface because of the direct contribution from conduction electrons. Self-consistent charge and spin densities, work function, single-particle energy bands, and layer-projected density of states for Ni/Ag(001) are also presented. The negligible exchange splitting observed in the photoemission experiment of Thompson et al.[48] is explained in terms of possible Ni subsurface layer formation (Ag segregation to the surface), which is found from separate self-consistent calculations to have a lower total energy and a very small (nearly "dead") magnetic moment ($\leq 0.02\mu$).

2.1.4.6 Structural, Electronic, and Magnetic Properties of Clean and Ag-Covered Fe Monolayers on W(110)[49] – *S. C. Hong,[23] A. J. Freeman,[23] and C. L. Fu*

The structural, electronic, and magnetic properties of magnetic Fe transition-metal atoms as an overlayer on a nonmagnetic transition metal W(110) and the effects of a Ag covering on the magnetism of Fe/S(110) are determined by means of the highly precise self-consistent all-electron FLAPW method, based on the LSDA. The interlayer spacings of Fe-W and Ag-Fe are determined from total-energy calculations. We find that the Fe atoms are relaxed downward (compared with the average of the Fe-Fe and W-W bulk bond lengths) by 9.5 % and 4.0 % for clean and Ag-covered Fe/W(110), respectively. We find that the hybridization of the W and Fe d-bands plays an important role in determining the magnetism of the Fe/W(110) systems. The magnetic moment ($2.18\mu_B$) and the magnitude of the Fermi-contact hyperfine field (–148 kG) of the Fe in relaxed Fe/W(110) are greatly reduced compared with those of the unrelaxed Fe/W(110) (by $0.38\mu_B$ and 46 kG, respectively). The Ag covering increases the magnitude of the Fermi-contact term of the Fe by 29 kG by encouraging the indirect covalent spin polarization of the s-like electrons. If one includes estimates of the dipolar and unquenched orbital-angular-momentum contributions, then our calculated values of the hyperfine field are found to be in remarkable agreement with recent conversion-electron Mössbauer-spectroscopy experimental values.

2.1.4.7 Electronic Structure and Surface Magnetism of fcc Co(001)[50] – *C. Li,[23] A. J. Freeman,[23] and C. L. Fu*

A FLAPW all-electron LSD of the electronic and magnetic properties of both five- and nine-layer fcc Co(001) ferromagnetic films is reported. The surface magnetic moment of $1.85\mu_B$ is 13% larger than that of the bulk value as a result of the narrowing of the 3d band at the surface. The effect of the surface is found to be short-ranged, with changes in charge and spin densities localized mostly to the surface layer. The subsurface Co atom layers have magnetic moments equal to $1.64\mu_B$ (i.e., a value very close to that of bulk fcc Co), indicating a short range effect of the surface on the magnetism (i.e., one-atomic-layer screening length). A contact magnetic hyperfine field calculation indicates that the core electron contribution is, as usual, precisely proportional to the magnetic moment, whereas the valence electron contribution is rather sensitive to the atomic environment. The total energy results yield a surface energy for the fcc Co(001) surface equal to 4.1 J/m^2.

2.1.4.8 Enhanced Surface and Interface Magnetism of bcc Ni Overlayers on Fe(001)[47] – *J. I. Lee,[23] A. J. Freeman,[23] and C. L. Fu*

The surface and interface magnetism of metastable bcc Ni as an overlayer on Fe(001) is investigated using the highly precise FLAPW method. Two systems – a monolayer overlayer of Ni (1Ni/Fe) and a bilayer (2Ni/Fe) coverage on Fe(001) – are investigated and compared. The effect of the Ni-Fe hybridization on the electronic and magnetic properties is examined. We find that the magnetic moments at the interface Ni (0.7 ~ 0.8 μ_B) and Fe (2.7 μ_B) sites are enhanced relative to their corresponding bulk values. A manifestation of the moment enhancement at the interface Fe-site is a positive contribution to the hyperfine field from the valence electrons. The magnetic moment (0.72 μ_B) of the surface Ni atom of 2Ni/Fe is found to be reduced from that (0.83 μ_B) of the surface Ni atom on 1Ni/Fe.

2.1.5 High-T_C Superconductors – *G. M. Stocks, W. H. Butler, G. S. Painter, N. F. Wright, W. A. Shelton,[19] and C. L. Fu*

From the outset, understanding the properties of the new class of ceramic high critical temperature (high-T_C) superconducting materials discovered in 1986 posed serious theoretical difficulties. Many of the same difficulties remain today, not the least of which is discovering the mechanism responsible for the pairing. Beyond this, however, these materials fall into a class that is close to the metal-insulator transition. For these materials, it is not yet clear whether the modern theoretical solid state physics machinery of LSD-DFT is applicable. Indeed, in the oxides of the late-transition metals that are also close to the metal insulator transition (the so-called Mott insulators), LSD-DFT yields either metals or narrow-gap semiconductors rather than the experimentally observed insulators.

Density functional theory is, in principle, a theory of the ground-state properties of any material. Consequently, it should be applicable to calculating the cohesive energy, equilibrium lattice spacing, elastic moduli, and vibrational and magnetic structure of the high-T_C materials. Furthermore, although density functional theory is not a theory for the quasi-particle spectrum, it is often possible to interpret the band structure resulting from LSD-DFT calculations as the electron quasi-particle spectrum and to use the LSD-DFT band structure as a basis for interpreting spectroscopic experiments.

In collaboration with W. M. Temmerman, Z. Szotek, and G. Y. Guo (Daresbury Laboratory); B. L. Gyorffy (University of Bristol); and P. A. Sterne (Lawrence Livermore Laboratory), we have calculated the ground-state properties and electronic structures of a number of the high-T_C materials and their parent compounds using the atomic-sphere-approximation linearized-muffin-tin-orbital (ASA-LMTO) method (Sects. 2.1.5.1 and 2.1.5.2). We have calculated the energies, equilibrium volumes, and Bulk moduli of La_2CuO_4 and $La_{1.5}Sr_{0.5}CuO_4$ using the ASA-LMTO method (Sect. 2.1.5.3). An ordered supercell containing a double-formula unit was used to simulate the disordered Sr-doped compound. The calculated equilibrium volumes are in good agreement with experimental values, indicating that LSD-DFT provides a useful starting point for treating

the energetics of these materials. We also found local charge redistributions that result in holes in the p-band of the out-of-plane oxygen atoms that invalidate the use of the rigid-band and virtual crystal approximations for treating the effects of alloying.

We have performed LSD-DFT calculations to search for the experimentally observed antiferromagnetic ground state of La_2CuO_4 (Sects. 2.1.5.4, 2.1.5.5, and 2.1.5.6). On the basis of our most converged calculations, we obtain a magnetic moment that is either very small or zero. We also find a metallic-like band structure rather than the observed insulator. We find that the magnitude of the magnetic moment decreases with increasing k-point sampling (accuracy) in the Brillouin zone integration, pointing to the need for great care in performing calculations of the magnetic structure in these materials. The failure of LSD-DFT to yield the antiferromagnetic ground states of La_2CuO_4 and $YBa_2Cu_3O_6$ remains the most important apparent failure of the theory in the area of the high-T_C materials (Sect. 2.1.5.7).

We have calculated the band structure for positrons in the high-T_C superconductors $YBa_2Cu_3O_7$ and $YBa_2Cu_3O_6$ using the ASA-LMTO method. On the basis of our results, we argue that it is very unlikely that oxygen vacancies will trap positrons in these compounds (Sect. 2.1.5.8).

We have developed a new complex lattice KKR-CPA code that is able to treat the electronic structure of the disordered perovskite structure, high-T_C superconductors. We have used this code to study the effects of alloying on the electronic structure of $BiBa_XK_{1-X}$ and $BaBi_XPb_{1-X}$. In these materials the bands near the Fermi energy are made up of a Bi-s/O-p bonding/antibonding complex. In $BiBa_XK_{1-X}$ where the alloying of K occurs on the "inactive" Ba sublattice, the effects of the alloying on the bands close to the Fermi energy are well described by the rigid band model. For $BaBi_XPb_{1-X}O_3$, where the alloying occurs on the active Bi sublattice, alloying produces significant nonrigid band effects.

Because of the strong electron correlations that are believed present in the high-T_C materials, many workers advocate a totally different starting point than that provided by a mean-field theory such as DFT. The expectation is that, if the mechanism responsible for the high-T_C behavior results from the strong electron-electron interaction, this mechanism will be most easily discovered within a simple model Hamiltonian that allows this interaction to be treated without making the mean-field approximation inherent in DFT. The simple model Hamiltonian most commonly used in this approach is called the Hubbard Hamiltonian. A great deal of work has been devoted to searching for superconducting solutions of the Hubbard model with a half-filled band and a repulsive intrasite electron-electron interaction, the situation that is thought by many to best approximate the high-T_C materials. So far, this work has not produced a convincing new candidate mechanism to explain high T_C behavior.

We have also considered the Hubbard Hamiltonian approach. However, we have studied the case where the intrasite electron-electron interaction is attractive because of the small body of opinion that suggests that this model is more appropriate to the

high-T_C materials. In collaboration with B. L. Gyorffy (University of Bristol, UK) and J. B. Staunton (University of Warwick, UK) we have investigated the nature of in the Hubbard model with attractive interactions (Sect. 2.1.5.9). For sufficiently large values of the interaction, we find a qualitatively new feature. A new state in which the superconducting gap loses its site-to-site coherence becomes possible. In this state, globally, there is no superconducting gap and, hence, no superconductivity; however, a disordered local gap (DLG) remains. The superconducting transition is signaled by intersite coherence in the phase of the local-gap parameter. This model then gives local electron pairing in the normal state. Observation of such pairing above Tc would be the clearest indication of the applicability of this model to high-T_C materials.

Although understanding the mechanism responsible for high superconducting transition temperatures in the oxide superconductors is currently the most exciting challenge in theoretical solid state physics, understanding the chemistry and stability of these compounds may be the key to their technological application. We have developed simple models that can explain the stability of these materials (Sects. 2.1.5.10, 2.1.5.11, 2.1.5.12, and 2.1.5.13), and we plan to extend these models to simulate the processing of these materials.

2.1.5.1 Electronic Structure of Y-Ba-Cu Oxides and Fluorides[51] – *W. M. Temmerman,[34] Z. Szotek,[34] P. J. Durham,[34] G. M. Stocks, and P. A. Sterne[23]*

We have calculated the electronic structure of the superconducting $YBa_2Cu_3O_7$ and the nonsuperconducting $YBa_2Cu_3O_6$ compounds. We find that, on reducing the oxygen content, the Cu in the O-Cu-O linear chains becomes insulating. We have also studied some hypothetical $YBa_2Cu_3F_2O_6$ systems to examine the effect of fluorine on the Cu-O_5 pyramids and the O-Cu-O chains.

2.1.5.2 Ground-State Properties and Electronic Structure of High-T_C Superconductors[52] – *G. M. Stocks, W. M. Temmerman,[34] Z. Szotek,[34] G. Y. Guo,[34] and P. J. Durham[34]*

We report the results of calculations of the ground-state properties (equilibrium volume, bulk modulus, and antiferromagnetism) and the electronic structure of a number of high-T_C superconductors and related materials. The calculation are based on the LDA and were performed using the ASA-LMTO method.

2.1.5.3 Density Functional Theory Total Energies and Equilibrium Volumes of La_2CuO_4 and $La_{1.5}Sr_{0.5}CuO_4$[53] – *G. M. Stocks, W. M. Temmerman,[34] Z. Szotek,[34] and P. A. Sterne[23]*

We have calculated the total energy and equilibrium volumes of La_2CuO_4 and $La_{1.5}Sr_{0.5}CuO_4$ using the LDA-DFT. The calculations were performed using the ASA-LMTO method under the constraint of a fixed c/a ratio. The calculated equilibrium volumes are in good agreement with experimental values, indicating that DFT provides a useful starting point for a discussion of the energetics of this class of superconductor.

In the strontium compound, we find local charge redistributions that result in holes in the p-band of the out-of-plane oxygen atoms. These local charge rearrangements invalidate the use of the rigid band and virtual crystal models for describing alloying.

2.1.5.4 On the Metal-Semiconductor Transition and Antiferromagnetism in La_2CuO_4[54] – *G. Y. Guo,[34] W. M. Temmerman,[34] and G. M. Stocks*

The spin-polarized self-consistent ASA-LMTO calculations of the total energy, magnetic moment, and electronic band structure of the La_2CuO_4 compound in both tetragonal and orthorhombic structures have been performed. A band model to explain the semiconductivity and antiferromagnetism in La_2CuO_4 has been quantitatively investigated.

2.1.5.5 Electronic Structure and Antiferromagnetism in La_2CuO_4[55] – *P. A. Sterne,[23] C. S. Wang,[56] G. M. Stocks, and W. M. Temmerman[34]*

Self-consistent spin-polarized energy bands have been calculated for tetragonal and orthorhombic La_2CuO_4. No stable antiferromagnetic order is found in either the stoichiometric compound or oxygen-deficient La_2CuO_3. Constraining the occupancy of Brillouin zone boundary states leads to a small antiferromagnetic moment in both systems that is rapidly quenched by Ba doping.

2.1.5.6 Local-Spin-Density Calculations for the High-T_C Superconductors[57] – *W. M. Temmerman,[34] G. Y. Guo,[34] Z. Szotek,[34] and G. M. Stocks*

In this paper we present LSD calculations for La_2CuO_4 and $YBa_2Cu_3O_6$. We find both La_2CuO_4 and $YBa_2Cu_3O_6$ to be antiferromagnetic semimetals having a very small or nearly nonexistent moment. The value of this moment depends on the Brillouin zone integration sampling and on the angular momentum expansion of the Cu and O sites in the CuO_2 layers. Expanding the Wigner-Seitz spheres by 10% or including the breathing mode failed to make La_2CuO_4 an antiferromagnetic semiconductor.

2.1.5.7 On the Validity of the Band Model for High-T_C Superconductors[58] – *W. M. Temmerman,[34] G. Y. Guo,[34] Z. Szotek,[34] P. J. Durham,[34] and G. M. Stocks*

The discovery of high-T_C superconductivity in cupric oxides has led, among other things, to numerous electronic band structure studies of these compounds. The foundation of these calculations is DFT and they are implemented with the LDA or LSDA. In this article we will review what we have learned from these calculations regarding the electronic structure of the family of high-T_C materials. To answer this, we have to find out how relevant the LSD/LDA is for the electronic properties of cupric oxides. It is well known that the application of LDA-DFT for transition metal oxides is fraught with difficulty and controversy. Although the LDA describes the variation of the equilibrium volume through the 3d transition metal oxides, including the volume expansion associated with Mott insulators, the theory fails to describe FeO and CoO as antiferromagnetic insulators, and in the case of NiO and MnO where the LDA does yield

an insulating ground state, the band gap is grossly underestimated. Evidently the high-T_C materials are systems that are on the verge of undergoing a Mott transition; consequently, it is necessary to be circumspect regarding the applicability of LDA-DFT both in the metallic (superconducting) and magnetic insulating states.

2.1.5.8 Do Oxygen Vacancies Trap Positrons in the Superconducting Cuprates $YBa_2Cu_3O_7$ and $YBa_2Cu_3O_6$?[59] – *Z. Szotek,[34] W. M. Temmerman,[34] B. L. Gyorffy,[21] and G. M. Stocks*

We have calculated the band structure for positrons in the high-temperature superconductors $YBa_2Cu_3O_7$ and $YBa_2Cu_3O_6$ using the ASA-LMTO method. On the basis of our results, we argue that it is very unlikely that oxygen vacancies will trap positrons in these compounds.

2.1.5.9 Local Pairing and Superconductivity in the Hubbard Model with Attractive Interactions[40] – *B. L. Gyorffy,[21] J. B. Staunton,[32] and G. M. Stocks*

We have investigated the nature of pairing in the Hubbard model with an attractive interaction (negative U). For sufficiently large values of the interaction, such that the magnitude of the interaction is greater than the band width, we find a qualitatively new feature. The usual Hartree-Fock-Gor'kov approximation, BCS-like solution, substantially overestimates the stability of the long-range ordered superconducting state. A new state in which the gap loses site-to-site coherence becomes possible. In this state there is, globally, no gap; however, a disordered local gap (DLG) remains. This disordered DLG state bears the same relationship to the BCS state as the DLM state does to the Stoner state in the theory of magnetism. This DLG model can be developed has a phenomenological model of local pairing and as such may have relevance to high-T_C materials.

2.1.5.10 Ionic Models for $YB_2Cu_3O_7$[60] – *N. F. Wright, G. S. Painter, W. R. Busing,[61] and W. H. Butler*

Simple ionic models are applied to $YBa_2Cu_3O_7$. It is found that additional forces are needed to constrain the barium and the planar coordinated copper atoms to be stable in their observed positions. These additional forces are compared with forces calculated from first principles. It is observed that the restoring forces are small for motion of the "in chain" oxygen atoms that are perpendicular to the chains.

2.1.5.11 Calculation of the Madelung Energy for the High-T_C Superconductor $YBa_2Cu_3O_7$[62] – *R. C. Ward,[63] K. A. Ritley,[64] N. F. Wright, and W. H. Butler*

Determining the nature of the stability of the high-T_C superconductor $YBa_2Cu_3O_7$ will be important to its manufacture and use. We present a calculation of the Madelung, or electrostatic energy, of this high-T_C superconductor using a method for determining the electrostatic potential in an ionic lattice resulting from Ewald. We also present a variation of the Ewald method that we have used to determine the interionic potential

surfaces of this material and present a plausible explanation for the presence of Cu-O chains in terms of the electrostatic forces.

2.1.5.12 Ionic Models for $YBa_2Cu_3O_7$ and $YBa_2Cu_3O_6$[65] – *N. F. Wright, W. H. Butler, and G. S. Painter*

Simple ionic models consisting of electrostatic and short-range repulsive interactions are used to investigate the structural stability of $YBa_2Cu_3O_7$ and related compounds. In this model it is found that the relative charge on the "in-plane" and "in-chain" copper ions is constrained by the position of the barium ion. Additional nonionic forces must be postulated to hold the in-plane copper ions in position. These models are being extended by allowing for ionic polarizabilities. Results from these models are being compared with those of first-principles calculations.

2.1.5.13 Point Dipole Model for the Structural Stability of $YBa_2Cu_3O_7$[40] – *N. F. Wright and W. H. Butler*

A point dipole model is used to investigate the structural stability of $YBa_2Cu_3O_7$. This model includes electrostatic interactions arising from point dipoles and short-range repulsive interactions. The requirements for the stabilization of the lattice differ in this model from those for a point ion model. The total charge on the "in-plane" copper ions relative to the charge on the "in-chain" copper ions is constrained because of the resulting forces on the barium ions. For the dipole model, a greater fraction of charge must be present on the in-chain copper than for the ion model. Additional nonionic restoring forces must be included in a point ion model to stabilize the copper-oxygen planes. This is not required in the point dipole model. The differences between these two models will be examined, and resulting estimates of atomic polarizabilities will be compared with free-atom calculations. The predictions for the two phonon spectra will be compared with experimental values. The applicability of these potential parameters for simulations will be discussed.

2.1.6 Microchemical Bonding Effects - *G. S. Painter, F. W. Averill,[1] F. W. Kutzler,[2] and W. H. Butler*

Perfect crystallinity with no structural disorder is an exceptional state of matter, rarely encountered outside the laboratory. It is more common for even "pure" materials to contain atomic impurities and to display structural disorder, traits that greatly complicate theoretical treatment. During the past seven years, we have developed powerful refined techniques for calculating the properties of atomic clusters within DFT, with the goal of addressing impurity effects in solids. The augmented Gaussian orbital cluster method allows the total energy and interatomic forces in clusters of atoms to be calculated from first principles using only the atomic numbers as input. This rigorous technique forms the basis of our studies of the local bonding characteristics in free atomic clusters (as produced in molecular beams) and cluster models of defect regions of solids (grain boundaries, impurity sites, etc.).

As an extension of our earlier studies of the effects of boron and sulfur impurities in atomic cluster models of interstitial and grain boundary sites in nickel, augmented Gaussian orbital calculations were completed for other first-row impurities. Rigorous LSD calculations of the total energies and interatomic forces revealed the following properties: (1) both Li and F significantly dilate and destabilize the octahedral Ni host cluster; (2) the remaining first-row members are stably bound with binding energies in the order Be < O < N < B < C, producing the largest strain of the host and C and N the least; and (3) the species B, N, and C enhance the maximum restoring force of the host atoms (by 30% for C) (Sects. 2.1.6.1-2.1.6.3).

It is recognized that impurities and dopants are often the determining factors in materials performance, and these calculations provided an atomic-level quantum basis for understanding the different effects produced by first-row impurities in Ni. Results are specific to the small host cluster, but the effects on the mechanical properties are so profound that they are expected to be manifest at the macroscopic level. Reasons underlying the differences in the series are now understood in terms of competing atom size strain energy and covalency factors. These quantum mechanical results were found to be consistent with the ranking of grain-boundary segregant effects of first-row atoms in the pair-bonding empirical approach.

The augmented Gaussian basis cluster technique forms the basis for two new project areas directed toward first-principles studies of complex solids (i.e., those systems where delocalization effects are large and/or the structural disorder places them outside the scope of our band theory-based methods).

In one case we implemented the interacting fragments approach of Harris,[66] which was developed to calculate the coupling energy of weakly interacting fragments. We investigated the basis for the success of this approximate functional, and we developed an extension of the Harris method, which we call the self-consistent atomic fragments approach. This method has greater accuracy than the Harris method and applies to strongly interacting systems as well (Sect. 2.1.6.4).

A second project focuses on the development of precise classical interatomic potentials that are valid for molecules, surfaces, and solids. These interatomic potentials are obtained by fitting to binding energy curves calculated from first principles using DFT. For nickel it appears that fitting to the binding energy curves for a small number of small clusters is sufficient to allow the prediction of an arbitrary configuration of nickel atoms.

2.1.6.1 Supercomputers in Materials Science Theory[67] - *G. S. Painter*

It has been recognized for over half a century that the physical and chemical properties of materials ultimately depend on the electronic bonding interactions among the component atoms, as described by quantum theory. But understanding the cohesive properties of materials remained a challenge to theorists until the breakthroughs in theoretical technique and computer performance achieved during the

past decade and a half. As a result, the total energy of most crystalline solids can now be calculated, greatly advancing scientists' understanding of the cohesive properties of such materials.

There are two important factors underlying these advances. One is refinement of LSDA, a theoretical concept that relates the total energy of an atomic system to the electronic charge density. The second is great improvement in computer capacity and performance. The LSDA provides a reliable and tractable framework for describing the interactions between electrons during bonding, while recent advances in computer design have provided the means to carry out the complex calculations involved in first-principles studies.

Using these advanced tools, the LSDA concept and supercomputers, materials scientists have made great progress in understanding cohesion in materials where the atoms occupy ordered sites on an underlying crystal lattice. However, some of the most interesting materials science problems have remained beyond the scope of contemporary theoretical techniques because most materials contain impurities, defects, and areas of structural disorder. Only in the last few years have the advanced computer programs and computer power been developed to treat such problems. Materials science theorists are now beginning to understand the atomic-level factors that are important in designing materials that have specific improved mechanical properties.

2.1.6.2 Impurity Effects on Metallic Cohesion: Lithium-Row Atoms in Nickel Clusters[68] – *G. S. Painter and F. W. Averill*[1]

We present results from a theoretical study of the localized bonding in atomic clusters consisting of octahedral nickel hosts and interstitial atoms from the lithium row of the Periodic Table. Trends in impurity binding energies and the effects of impurities on the elastic properties of the host are established by comparison of total energies and interatomic forces of the doped clusters with results for the bare host. Properties of the host cluster are strongly dependent on impurity atom type. An orbital analysis identifies the microchemical mechanisms through which the elastic properties of the host respond to changes in impurity-host bond character, from strongly electropositive lithium to strongly electronegative fluorine. The tendency of Li and F to form ionic bonds destabilizes and weakens the Ni host cluster. A bonding mode which is predominantly covalent characterizes the remainder of the first-row series. A nonuniform variation of impurity-induced strain and elastic properties of the host is found in which midrow atoms B, C, and N effected an appreciable strengthening of the host. Trends in the stability and strengthening character of the midrow series of atoms is a result of competing atom size and covalency effects. There is good qualitative correspondence between the trends and relative effects of different impurities in this study and the observed effects of first-row impurities on the cohesive properties of metallic host interfaces. This relationship suggests that the microchemical properties of the cluster model may serve to identify atomic-level factors important in understanding macroscopic impurity effects in grain-boundary segregation.

2.1.6.3 Effects of First-Row Impurities on the Cohesive Properties of Nickel Clusters[5] – *G. S. Painter and F. W. Averill*[1]

To understand the influence of impurities on transition metal interfacial cohesion, we have carried out LSD calculations of the total energies and interatomic forces in atomic cluster models of impurity-containing grain boundary sites in nickel. The presence of the 2p-core plays an important role in differentiating second-row from first-row impurities in the way they affect the cohesive properties of host environments. A more subtle competition of atomic size and covalency factors underlies effects within the first-row series. Impurity binding energies and the degree of cohesive enhancement produced in host clusters reach a maximum for carbon and a minimum for oxygen. These trends are explained in terms of the valence orbital characteristics of the impurities.

2.1.6.4 A Study of the Harris Functional and Related Methods for Calculating Total Energies in Density Functional Theory[69] - *F. W. Averill*[1] *and G. S. Painter*

The simplified energy functional of Harris[66] has given results of useful accuracy well outside the limits of weakly interacting fragments for which the method was originally proposed. In the current study, we discuss the source of the frequent good agreement of the Harris energy with full Kohn-Sham self-consistent results. A procedure is described for extending the applicability of the scheme to more strongly interacting systems by going beyond the frozen-atom fragment approximation. A gradient force expression is derived, based on the Harris functional, that accounts for errors in the fragment charge representation. Results are presented for some diatomic molecules, illustrating the points of this study.

2.1.7 Mechanical and Elastic Properties of High-Temperature Alloys - *C. L. Fu and M. H. Yoo*

The strength of a crystalline solid generally decreases with increasing temperature because of the reduction of the elastic constants and the thermally assisted motion of dislocations. One outstanding exception to this general rule is the anomalous yield and flow behavior of certain ordered intermetallic compounds such as Ni_3Al, which become stronger as they are heated. Associated with this intrinsic property of thermal strengthening, however, is low ductility resulting from brittleness of grain boundaries. Therefore, fundamental understanding of the physical mechanisms responsible for the anomalous flow stress and intergranular fracture is of utmost importance for the development of advanced materials for structural applications.

Over the past three decades, many theories have been proposed to explain the flow-stress behavior of intermetallic compounds, but these have met with only limited success. The main deficiencies of these theoretical models have been (1) the lack of a comprehensive theory that simultaneously takes into account both the energetic and kinetic aspects of crystal dislocations and (2) the lack of first-principles quantum-mechanical calculations to test and verify the models. The elastic constants of crystals,

for example, are difficult to calculate from first principles because the elastic energies involved are smaller than the total energy of the crystal by a factor of approximately 10^{-7}.

Currently, the most precise way to evaluate the electronic structure is to solve the Kohn-Sham equations in the LDA. One of the most accurate approaches to solving the local-density equations is the FLAPW method. This method is specially designed to accurately treat surfaces and interfaces. This method makes it possible to calculate from first principles the physical quantities that are difficult to measure experimentally, such as local strain energies and surface and interfacial energies, but are essential for the interpretation of the mechanical properties of alloys.

The work described in this section is aimed at a comprehensive theoretical understanding of the strength of the ordered intermetallic compounds in terms of the motion of dislocations. We have carried out (Sect. 2.1.7.1) a systematic analysis of the elastic constants of ordered $L1_2$ alloys based on anisotropic elasticity theory and first-principles quantum-mechanical calculations. The calculated shear anisotropy factors were used to determine the angular forces acting on dislocations. In ordered alloys, dislocations generally occur in pairs because a single dislocation would create a semi-infinite half plane with antisite disorder (energetically unfavorable nearest-neighbor configurations). The second dislocation "repairs" the broken bonds caused by the first so that the stacking fault is confined to the region between the dislocations. Anisotropy of the shear elastic constants can cause these dislocation pairs to assume a nonplanar configuration that impedes their motion. This effect is called the "cross-slip pinning mechanism."

Our calculations showed that Ni_3Al, a material that shows the high-temperature strengthening effect, has sufficient shear anisotropy to cause a nonplanar configuration of the dislocations. Pt_3Al, on the other hand, is a very similar material that does not show the high-temperature strengthening effect. Our calculations show that its shear anisotropy is much lower than that of Ni_3Al.

In addition to shear anisotropy, a second fundamental material property is central to the cross-slip pinning mechanism, the stacking-fault energy. We have performed first-principles calculations of the various stacking faults that can occur in $L1_2$-ordered alloys and have used these, together with our calculations of the elastic shear anisotropy, to develop a criterion for the existence of the high-temperature strengthening effect via the cross-slip pinning mechanism (Sect. 2.1.7.2).

In addition to slip caused by the motion of dislocations through a crystalline solid, many materials can deform by twinning. We calculated the six independent elastic constants of TiAl from first principles and used these to examine the orientation dependence of the free energy change associated with twin formation on the compressive stress axis (Sect. 2.2.2.13). We found that the primary (111) [112] twin is favored over a wide range of orientations. We also calculated the twin boundary energy from first principles to study the twinning and fracture relation in TiAl. We found that

localized slip and twinning is effective in stopping a (110) crack in TiAl. This prediction is consistent with experimental results.

2.1.7.1 All-Electron Total-Energy Theory of Crystal Elasticity: $L1_2$-Ordered Alloys[70] – *C. L. Fu and M. H. Yoo*

First-principles calculations of the ground-state linear elastic constants for Ni_3Al and Pt_3Al are presented. It is found that, although the bulk modulus of Pt_3Al (B = 292 GPa) is larger than that of Ni_3Al (B = 175 GPa), a far smaller shear-anisotropy factor for Pt_3Al is predicted (A = 1.3 and A = 2.9 for Pt_3Al and Ni_3Al, respectively). The anomalous (positive temperature dependence of flow stress in Ni_3Al and its absence in Pt_3Al are discussed in terms of the current results.

2.1.7.2 Stacking Fault Energies, Crystal Elasticity, and Their Relation to the Mechanical Properties of $L1_2$-Ordered Alloys[71] – *C. L. Fu and M. H. Yoo*

First-principles calculations of the stacking fault energies of Ni_3Al and the linear elastic constants of Ni_3Al and Pt_3Al are presented. The anomalous (positive) temperature dependence of flow stress in Ni_3Al and its absence in Pt_3Al are fully rationalized in terms of the current results and cross-slip pinning mechanism. It is found that the elastic shear anisotropic factor plays an equally (or even more) important role as the anisotropy of antiphase-phase boundary energy in determining the plastic flow behavior of $L1_2$-ordered alloys.

2.1.8 References

1. Judson College, Elgin, Ill.

2. Department of Chemistry, Tennessee Technological University, Cookeville, Tenn.

3. Abstract of *Phys. Rev. Lett.* 59(12), 1285-8 (1987).

4. Abstract of *Phys. Rev.* B37(6), 2850-5 (1988).

5. Abstract of paper presented to the American Physical Society Meeting, New Orleans, Mar. 21-25, 1988.

6. Abstract of *Phys. Rev.* B37(2), 838-43 (1988).

7. Department of Physics and Quantum Theory Group, Tulane University, New Orleans, La.

8. Department of Chemistry and Quantum Theory Group, Tulane University, New Orleans, La.

9. Department of Physics, University of Toronto, Ontario, Canada.

10. N. L. Allan, C. G. West, D. L. Cooper, P. J. Grout, and N. H. March, *J. Chem. Phys.* **83**, 4562 (1985).

11. C. Lee and S. K. Ghosh, *Phys. Rev. A* **33**, 3506 (1986).

12. Abstract of paper submitted to *Phys. Rev.*

13. D. C. Langreth and M. J. Mehl, *Phys. Rev.* **B28**, 1809 (1983), and errata, *Phys. Res.* **B29**, 2310 (1984); E. D. Hu and D. C. Langreth, *Phys. Scripta* **32**, 391 (1985).

14. J. P. Perdew and W. Yue, *Phys. Rev.* **B33**, 8800 (1986).

15. S. H. Vosko, L. Wilk, and M. Nusair, *Can. J. Phys.* **58**, 1200 (1980).

16. Abstract of *Phys. Rev.* **B35**(14), 7713-16 (1987).

17. Abstract of *Phys. Rev.* **B39**(12), 8115-21 (1989).

18. P. M. Boerrigter, G. te Velde, and E. J. Baerends, *Int. J. Quantum Chem.* **33**, 87 (1988).

19. Department of Physics, University of Cincinnati, Cincinnati, Ohio.

20. Sandia National Laboratories, Livermore, Calif.

21. University of Bristol, Bristol, UK.

22. Abstract presented to NATO ASI Series on Alloy Phase Stability, Chania, Crete, Greece, June 14-27, 1987.

23. Lawrence Livermore National Laboratory, Livermore, Calif.

24. Abstract of *Phys. Rev.* **B36**(9), 4630-46 (1987).

25. Physics Department, Northwestern University, Evanston, Ill.

26. Abstract of *Phys. Rev.* **B37**(10), 5982-85 (1988).

27. Abstract of paper presented to the Third International Conference on Supercomputing, Boston, Mass., May 15-20, 1988.

28. Abstract of *Mater. Sci. Forum* **37**, 161-72 (1989).

29. Abstract presented at Workshop on Advanced Computation and Simulation of Complex Materials Phenomena, National Research Council, Mar. 24-26, 1987, LaJolla, Calif.

30. Abstract of *Projects in Scientific Computing*, pp. 30-31, Pittsburgh Supercomputing Center, Pittsburgh, 1987.

31. Abstract of *J. Appl. Phys.* **63**(8), 3490-2 (1988).

32. University of Warwick, UK.

33. Abstract presented at 20th Polish Seminar on Positron Annihilation, Piechowice, Poland, May 15-21, 1988.

34. SERC, Daresbury Laboratory, Warrington, UK.

35. Physics Department, Indiana University, Bloomington, Ind.

36. Physics Department, Luther College, Decorah, Iowa.

37. Department of Physics, SUNY, Stony Brook, N.Y.

38. Abstract of *Phys. Rev. Lett.* **62**(6), 661-4 (1989).

39. Abstract of *Mater. Res. Soc. Symp. Proc.* **141**, 91-6 (1989).

40. Abstract presented at American Physics Society Meeting, St. Louis, Mo., Mar. 20-24, 1989.

41. Abstract of *Phys. Rev.* **B36**(8), 4103-11 (1987).

42. L. Y. L. Shen, *Phys. Rev. Lett.* **24**, 1104 (1970).

43. E. L. Wolf, R. J. Noer, D. Burnell, Z. G. Khim, and G. B. Arnold, *J. Phys.* **F11**, L23 (1981).

44. Abstract of paper to be published in *Phys. Rev. Lett. B.*

45. Abstract of *J. Magn. Magn. Mater.* **75**, 201-8 (1988).

46. Abstract of *J. de Phys.* **C8**(12), 1625-6 (1988).

47. Abstract of paper submitted to *Phys. Rev. B.*

48. M. A. Thompson, M. Inellion, and J. L. Erskine, *Bull. Am. Phys. Soc.* **31**, 675 (1986).

49. Abstract of *Phys. Rev.* **B38**(17), 156-63 (1988).

50. Abstract of *J. Magn. Magn. Mater.* **75**, 53-60 (1988).

51. Abstract of *J. Phys. F: Met. Phys.* **17**, L319-27 (1987).

52. Abstract presented at International Conference on High-Temperature Superconductors and Materials and Mechanisms of Superconductivity, Interlaken, Switzerland, Feb. 29-Mar. 4, 1988.

53. Abstract of *Supercond. Sci. Technol.* **1**, 57-63 (1988).

54. Abstract of *J. Phys. C: Solid State Phys.* **21**, L103-8 (1988).

55. Abstract of *High-Temp. Supercond.* **99**, 353-6 (1988).

56. Dept. of Physics, University of Maryland, College Park, Md.

57. Abstract of *Phys. Scripta* **T25**, 78-79 (1989).

58. Abstract presented at International Symposium on the Electron Structure of High T_c Superconductors, Rome, Italy, Oct. 4-7, 1988.

59. Abstract of *J. Phys. C: Solid State Phys.* **21**, L509-14 (1988).

60. Abstract of *High-Temp. Supercond.* **99**, 539-42 (1988).

61. Chemistry Division, ORNL, Oak Ridge, Tenn.

62. Abstract of paper submitted to *Am. J. Phys.*

63. Computer and Telecommunications Division, ORNL, Oak Ridge, Tenn.

64. Sonoma State University, Rohnert Park, Calif.

65. Abstract presented at MRS Spring Meeting, San Diego, Calif., Apr. 24-29, 1989.

66. J. Harris, *Phys. Rev.* **B31**, 1770 (1985).

67. Abstract of *ORNL Review* **21**(3), 14-16 (1988).

68. Abstract of *Phys. Rev.* **B39**(11), 7522-35 (1989).

69. Abstract of a paper prepared for submission to *Phys. Rev.*

70. Abstract of *Philos. Mag. Lett.* **58**, 199-204 (1988).

71. Abstract of Materials Research Society 1988 Fall Meeting, Boston, Mass., Nov. 28-Dec. 2, 1988.

2.2 ALLOYING BEHAVIOR AND DESIGN – *C. T. Liu*

The objective of this task is to further understand the physical metallurgy and mechanical behavior of ordered intermetallics, with emphasis on fundamental alloy variables that control low-temperature ductility and fracture and high-temperature strength and deformation behavior. This understanding will lead to the development of scientific bases for design of new-generation materials for structural use. Research in this task is currently focused on nickel aluminide (Ni_3Al) and titanium trialuminides ($TiAl_3$), which have been selected as model materials for the study of brittle fracture and anomalous temperature dependence of deformation behavior.

During this reporting period, important progress has been made in several areas. Recently, both atom probe and STEM experiments have indicated that boron and nickel cosegregate to grain boundaries in Ni_3Al. The excess nickel resulting from this cosegregation is expected to cause local disordering at the grain boundaries, which in turn is expected to facilitate slip transfer across the grain boundaries, and has therefore been cited as a mechanism for the dramatic ductilizing effect of boron in Ni_3Al. However, so far only a few boundaries in a limited number of samples have been chemically analyzed, and it is not clear whether the results obtained are general in nature. We are therefore using Auger electron spectroscopy (AES) to sample a relatively large number of grain boundaries in each specimen and are studying the effects of stoichiometry and boron content on the nickel and aluminum contents of grain boundaries. Within the scatter of our results, the boundaries of the boron-doped alloys have nickel and aluminum compositions that are very similar to those of the corresponding boron-free alloys. Therefore, our results indicate no strong tendency for boron-nickel cosegregation. This finding agrees with the results of an almost completed study of boron atom clustering in Ni_3Al with 25 and 26 at. % Al using the imaging atom probe at ORNL. About 10 to 15% of the boron resides in clusters, the level of which is essentially independent of both heat treatment and boron concentration. No indication of cosegregation of boron and nickel was found, instead a high degree of variability was present.

In an effort to gain a better understanding of the combined effects of grain boundaries and oxidation on the ductility of Ni_3Al alloys, specimens with a range of grain sizes ($\sim$20-200 μm) were preoxidized in air and then tested in tension in vacuum. Preoxidation did not affect the ductility of the finest-grained material at 600 or 760°C, whereas it caused severe embrittlement of the largest-grained material, especially at 760°C. A continuous, thin aluminum-rich oxide layer, which formed on the fine-grained samples, protected the underlying alloy from oxygen penetration, thus preventing any loss of ductility. On the other hand, the nickel-rich oxide that formed on the large-grained samples allowed oxygen to penetrate along grain boundaries, causing severe embrittlement. It follows that the grain boundaries act as short-circuit paths for rapid diffusion of aluminum atoms from the bulk to the surfaces and are thus responsible for the difference in oxidation behavior between fine- and large-grained materials. This study leads to development in heat-treatment schemes, which control oxide formation on specimen surfaces and eliminate the preoxidation embrittlement in the large-grained specimens.

Alloys having the ordered cubic $L1_2$ crystal structure have been shown to exist in the ternary system $(Al,X)_3Ti$, where X is Cu, Ni, or Fe. Current interest is high in these trialuminide alloys because of their high symmetry, low density, high melting point, and good oxidation resistance. Unlike Ni_3Al, which has the same $L1_2$ crystal structure, these alloys fracture by transgranular cleavage at room temperature and exhibit no tensile ductility. A selected area electron channeling pattern (SAECP) technique has been developed that allows the crystallographic orientation of individual cleavage facets to be determined. In this manner, the cleavage planes of $(Al,Fe)_3(Ti,V)$ alloys have been investigated in both the directionally solidified and randomly oriented conditions. The predominant cleavage plane is found to be the {110} type, with limited evidence of {111} and other low-index planes. The observations are of interest because (1) these alloys cleave predominantly on the {110} planes and not {100} or {111}, as do $L1_2Ni_3Ge$ and Ni_3Al alloys, and (2) the alloys exhibits more than one type of cleavage plane.

The force couplet model (FCM) was introduced to explain the temperature dependence of flow stress in ordered intermetallic alloys. We recognized, for the first time, that the elastic anisotropy is more important than the anisotropy of the antiphase boundary (APB) energy in describing the anomalous yield behavior of $L1_2$ alloys. We calculated, also for the first time, the elastic constants of Ni_3Al and Pt_3Al using the first-principles all-electron total-energy approach. The anomalous temperature dependence (positive) of flow stress in nickel-based $L1_2$ alloys and its absence in platinum-based $L1_2$ alloys are fully rationalized by the FCM using the ab initio elastic constants (in collaboration with the theoretical studies).

The dislocation core structures in Ni_3Al have been determined by atomistic simulation studies using the embedded atom method (EAM). The stable equilibrium configurations of screw superpartials, 1/2[101], are found to be a (111) planar dissociation on the (111) APB plane. On the (010) slip plane, a nonplanar dissociation, which is at stable equilibrium, occurs on either the (111) or the (111) plane. Our preliminary calculations to study the effect of an applied stress show that the mobility of a superdislocation is much higher on the (111) plane than on the (010) plane (in collaboration with M. S. Daw and M. I. Baskes at SNL).

The role of interaction between slip dislocations and [110] tilt boundaries in crack nucleation is investigated theoretically for the face-centered cubic (fcc) and $L1_2$ structures. When the slip activity at the boundary is impeded, cleavage fracture on the (111) plane is predicted rather than intergranular fracture. Intergranular fracture can be initiated when a symmetric double pileup of primary slip dislocations from both sides of the boundary occurs simultaneously. The available experimental data on slip/grain boundary interaction and intergranular fracture are in good agreement with the current results.

The interrelationships between twinning and generalized plastic flow or fracture toughness in ordered intermetallic compounds are studied by taking the specific example of TiAl. The six independent elastic constants were determined by using the

first-principles total-energy approach. The free-energy change of twin formation was evaluated based on Eshelby's ellipsoidal inclusion method. The effectiveness of localized slip and twinning to stop a (110) crack is predicted to be higher than that to stop a (001) crack, which is consistent with the available experimental data.

The mechanical properties microprobes (MPMs) are prototype systems that have been developed to measure properties from submicron volumes of material. The differential MPM was invented at ORNL and is capable of measuring both elastic and plastic properties continuously as the volume of material being tested expands. A patent application for this measuring technique has been filed. Recent work has improved the accuracy and dynamics of this testing technique. Funding has been obtained to build a high-temperature MPM. This is a very challenging undertaking. Most of the design concepts have been finished. A ultrahigh-vacuum manipulator with 5° of sample manipulation has been designed, fabricated, and delivered.

Section 2.2.1 describes progress in understanding intergranular fracture, boron segregation and alloy design of ductile nickel aluminides. Section 2.2.2 describes both experimental and modeling work on dislocation structures and anomalous temperature dependence of deformation behavior. Section 2.2.3 concerns creep and cavitation in Ni_3Al alloys. Section 2.2.4 is devoted to our effort on studying trialuminides based on $TiAl_3$, $ZrAl_3$, $NbAl_3$, and $ScAl_3$. Section 2.2.5 describes our research on recent development of MPM and its applications to characterization of mechanical properties from submicron volumes of materials.

2.2.1 Ductility and Fracture Behavior of Nickel Aluminides

2.2.1.1 Grain-Boundary Design of $L1_2$-Ordered Intermetallic Alloys[1] – *C. T. Liu*

This paper summarizes recent research on intergranular fracture and alloy design of $L1_2$-ordered Ni_3X intermetallics. The grain boundaries in Ni_3Al, Ni_3Ga, Ni_3Si, and Ni_3Ge are intrinsically brittle, and boron additions are effective in ductilizing the first three alloys but not Ni_3Ge. The beneficial role of boron is to increase grain-boundary cohesive strength, to enhance plastic flow in the boundary region, and to disorder grain boundaries. Boron is ineffective in ductilizing Ni_3X alloys in which $X \geq 25\%$. The room-temperature ductility of undoped Ni_3Al can be improved also by change in grain shape from equiaxed to columnar.

2.2.1.2 Comparison of Grain Boundary Compositions in Boron-Doped and Boron-Free Ni_3Al [2] – *E. P. George, C. T. Liu, and R. A. Padgett*

It has recently been reported that boron attracts excess nickel to the grain boundaries in Ni_3Al (cosegregation of nickel and boron), effectively disordering them. This is expected to increase the mobility of grain boundary dislocations and/or to increase the number of allowed dislocation reactions at the grain boundaries and is, therefore, cited as a possible mechanism by which boron improves the room-temperature ductility of Ni_3Al. However, only a limited number of grain boundaries in

a limited number of samples have been analyzed so far (mainly because of the limitations of the techniques used); therefore, the results obtained to date are not general in nature. In this study, we have used AES (a technique that allows us to sample a relatively large number of grain boundaries in each specimen) to analyze the grain boundary compositions of boron-free and boron-doped Ni_3Al alloys containing 24 and 25.2 at. % Al.

On average, the grain boundaries in the 24% Al, boron-free alloy were slightly nickel-enriched (~22% Al), whereas the boundaries in the 25.2% Al, boron-free alloy were slightly aluminum-enriched (~26% Al), a result which is in agreement with predictions of embedded-atom calculations. The grain boundary compositions of the boron-doped alloys were not significantly different from those of the corresponding boron-free alloys, indicating no strong tendency for cosegregation of nickel and boron. These results do not rule out the existence of disordered grain boundaries. However, if nickel-enrichment is used as an indication of disorder at the grain boundaries, our results suggest that the grain boundaries in the boron-free, Ni-24Al alloy may also be disordered as are those in the boron-doped, Ni-24Al alloy.

2.2.1.3 Free Surface Segregation in Boron Doped Ni_3Al [3] – *C. L. White, C. T. Liu, and R. A. Padgett, Jr.*

Surface segregation in boron-doped Ni_3Al alloys containing 24-26 at. % Al has been studied for temperatures between 600 and 1000°C. As in earlier studies, boron was not observed to segregate to free surfaces at 1000°C, whereas sulfur was observed to segregate strongly. Between 600 and 800°C, both boron and nitrogen, as well as sulfur, were observed to segregate to surfaces damaged by sputter ion etching. Boron and nitrogen did not segregate strongly to well-annealed surfaces in this temperature range, however, indicating possible effects of chemical order, defect structure, and/or nickel enrichment on the extent of interfacial boron segregation.

2.2.1.4 Effect of Aluminum Level on Boron Clustering in Ni_3Al [4] – *J. A. Horton, M. K. Miller, C. T. Liu, E. P. George, and J. Bentley*

In alloys containing 0.24% B, atom-probe field-ion microscopy (APFIM) revealed the presence of boron clusters in Ni-25 at. % Al and Ni-26 at. % Al but not in Ni-24 at. % Al. The observed boron clusters generally consisted of two to three boron atoms and a maximum size of 10 atoms. Quench rates that ranged from rapid solidification to furnace cooling had little effect on the clustering. The occurrence of the clustering coincides with a higher rate of boron strengthening as measured by an increase in the yield stress per atomic percent boron, and it also coincides with a reduced amount of boron segregation to grain boundaries. The levels of nickel and boron were highly variable on grain boundaries in rapidly solidified material and, therefore, no consistent indication of nickel enrichment at the grain boundaries associated with boron segregation was found. This result suggests that cosegregation of nickel with boron may not be necessary for the ductilization of Ni_3Al by boron

because the rapidly solidified material is also ductilized by boron and exhibits segregation of only boron to the grain boundaries.

2.2.1.5 Effects of Grain Size and Test Temperature on Ductility and Fracture Behavior of a B-Doped Ni_3Al Alloy[5] – *M. Takeyama and C. T. Liu*

Effect of grain size on ductility and fracture behavior of boron-doped Ni_3Al (Ni-23Al-0.5Hf, at. %) was studied by tensile tests using a strain rate of $3.3 \times 10^{-3} s^{-1}$ at temperatures to 1000°C under a high vacuum of $<1 \times 10$ Pa. At temperatures below 700°C, the alloy showed essentially ductile transgranular fracture with more than 30% elongation, whereas it exhibited ductile grain-boundary fracture in the temperature range 700 to 800°C. In both cases, the ductility was insensitive to grain size. On the other hand, at temperatures above 800°C, the ductility decreased from about 17 to 0% with increasing grain size. The corresponding fracture mode changed from grain-boundary fracture with dynamic recrystallization to brittle grain-boundary fracture. The ductile transgranular fracture at lower temperatures is explained by stress concentration at the intersection of slip bands. The grain-size dependence of ductility is interpreted in terms of stress concentration at the grain boundaries. Finally, it is suggested that the temperature dependence of ductility in this alloy might be related to the thermal behavior of boron segregated to the grain boundaries.

2.2.1.6 Effect of Grain Shape on Environmental Embrittlement in Ni_3Al Tested at Elevated Temperatures[6] – *C. T. Liu and B. F. Oliver*[7]

This paper describes the effect of grain shape on environmental embrittlement in boron-doped Ni_3Al (24 at. % Al). The alloy showed severe embrittlement when tested at 600 and 760°C in air. The embrittlement can be alleviated by control of grain shape, and the material with a columnar-grained structure produced by directional levitation zone remelting shows good tensile ductilities when tested in oxidizing environments. The columnar-grained structure with vertical grain boundaries minimizes the normal stress and, consequently, suppresses nucleation and propagation of cracks along the boundaries.

2.2.1.7 Effect of Preoxidation and Grain Size on Ductility of a Boron-Doped Ni_3Al at Elevated Temperatures[8] – *M. Takeyama and C. T. Liu*

The ductility of preoxidized Ni_3Al (Ni-23Al-0.5Hf-0.2B, at. %) specimens having various grain sizes ($17 \sim 193$ μm) was evaluated by means of tensile tests at 600 and 760°C in vacuum. It was found that the preoxidation does not affect the ductility of the finest-grained material at either temperature, whereas it causes severe embrittlement in the largest-grained material, especially at 760°C. A continuous, thin aluminum-rich oxide layer, which forms on the fine-grained samples, protects the underlying alloy from oxygen penetration, preventing any loss of ductility, whereas the nickel-rich oxide that forms on the large-grained samples allows oxygen to penetrate along grain boundaries, causing severe embrittlement. The grain boundaries act as short-circuit paths for rapid diffusion of aluminum atoms from the bulk to the surfaces, and this is responsible for

the difference in oxidation behavior between fine- and large-grained materials. The embrittlement of large-grained samples can be eliminated through control of oxide formation on Ni_3Al surfaces.

2.2.1.8 Effect of Grain Size on Yield Strength of Ni_3Al and Other Alloys[9] – *M. Takeyama and C. T. Liu*

This paper analyzes the effect of grain size on yield strength of ordered Ni_3Al and Zr_3Al and mild steels that show Lüders band propagation after yielding, using the Hall-Petch relation, $\sigma_y = \sigma_o + k_y d^{-1/2}$, and the new relation proposed by Schulson et al., $\sigma_y = \sigma_o + k d^{-(p+1)/2}$ (ref. 10). The major emphasis is placed on the analysis of Ni_3Al data obtained from published and new results, with a careful consideration of the alloy stoichiometry effect. All data, except for binary stoichiometric Ni_3Al prepared by powder extrusion, fit the Hall-Petch relation, whereas the data from boron-doped Ni_3Al and mild steels do not follow the Schulson relation. However, no conclusion can be made simply from the curve-fitting using either relation. The results are also discussed in terms of Lüders strain and alloy preparation methods. On the basis of the Hall-Petch analysis, the small slope k_y is obtained only for hypostoichiometric Ni_3Al with boron, which would be related to a stronger segregation of boron in nickel-rich Ni_3Al. In addition, the potency for the solid solution strengthening effect of boron is found to be much higher for stoichiometric Ni_3Al than for hypostoichiometric alloys.

2.2.1.9 Deformation and Fracture Experiments in Transmission Electron Microscopes[11] – *J. A. Horton*

Direct observations of dislocations emitted by crack tips have been made with a transmission electron microscope (TEM) during in situ straining experiments. The observations include nearly perfect screw dislocations emitted from mode III shear cracks in materials such as stainless steel and copper, perfect edge dislocations emitted from mode I cracks in aluminum, and mixed-character dislocations emitted from mode II cracks in molybdenum. Recent in situ deformation experiments involving superlattice dislocation interactions in the intermetallic alloy Ni_3Al will also be described.

2.2.1.10 Grain Boundary Chemistry of NiAl[12] – *P. P. Camus, I. Baker,[13] J. A. Horton, and M. K. Miller*

Atom-probe analyses performed at the grain boundaries in Ni-49 at. % Al indicated a majority of regions that contained almost no aluminum and a few regions that indicated neither enrichment nor depletion of aluminum. The widths of the depleted zones were less than 0.5 nm. It is proposed that this aluminum depleted zone could be a cause of the enhanced ductility and change in fracture mechanism that occurs in this intermetallic alloy compared with NiAl alloys further from stoichiometry.

2.2.1.11 Strength and Ductility of Intermetallic Compounds[14] – *D. P. Pope[15] and C. T. Liu*

This paper reviews recent research on strength, ductility, and fracture in ordered intermetallic alloys. A great deal is now known about the physical metallurgy and mechanical properties of $L1_2$ intermetallic compounds, especially the flow and fracture properties. However, there are many potentially useful intermetallics having other crystal structures about which relatively little is known, and more research effort should be concentrated on those alloys. We hope that the knowledge gained about $L1_2$ intermetallics from this recent massive effort will provide a basis for understanding the properties of these more complex materials.

2.2.1.12 Phase Stability and Alloy Design of Ordered Intermetallics[16] – *C. T. Liu*

Ordered intermetallics have many attractive high-temperature properties; however, low ductility and brittle fracture limit their use for structural applications. The embrittlement in intermetallics is mainly caused by low crystal symmetry and insufficient number of slip systems, poor cleavage strength, and intrinsic and extrinsic grain-boundary weakness. Experimental studies of ordered phase stability and grain-boundary structure have led to substantial improvement in the ductility and fracture toughness of several ordered intermetallics, including $(Co,Fe)_3V$, $(Ni,Fe)_3V$, $(Co,Ni,Fe)_3V$, Fe_3Al, Ni_3Al, Ni_3Ga, and Ni_3Si. Currently, the control of ordered structures and grain-boundary properties is mainly based on some empirical and/or phenomenological relationship. The first-principles calculations have advanced to the stage that they are able to help us to understand the electron structure and phase stability and to design ductile ordered intermetallic alloys for structural use at elevated temperatures.

2.2.1.13 Aluminides for Structural Use[17] – *J. O. Stiegler and C. T. Liu*

The search for the new high-temperature structural materials has renewed interest in intermetallic compounds. Recent interest has been centered primarily on aluminides of nickel, iron, and titanium. These materials possess a number of attributes that make them attractive for high-temperature applications. However, all of these aluminides suffer from low-temperature embrittlement, which has been severe enough to preclude their use as structural materials. In several cases, metallurgical solutions have been discovered that offer the possibility of engineering applications. Although an impressive amount of work has been done on titanium aluminides, relatively little information has been released because of defense applications of these alloys. Consequently, this article will deal in more detail with only the aluminides of nickel and iron and with alloys derived from them.

2.2.1.14 Ordered Intermetallic Alloys[18] – *C. T. Liu and J. O. Stiegler*

Physical metallurgy and mechanical behavior of ordered intermetallic alloys based on $(Fe,Co,Ni)_3V$ and Ni_3Al are reviewed in this article. Both alloys can be made highly ductile and fabricable, offering the potential for further macroalloying to produce alloys

for specific applications. Because of their high strength and relatively low density, they have potential for turbine disk, vane, nozzle, combustor, and possibly blade applications. They also may be suitable for components for Stirling engines, high-temperature valves, coal-conversion systems, steam turbines, and possibly for high-temperature process heat applications such as the gas-cooled reactor.

2.2.2 Deformation, Dislocation Structure and Anomalous Yielding in Ordered Intermetallics

2.2.2.1 Micromechanisms of Yield and Flow in Ordered Intermetallic Alloys[19] – *M. H. Yoo, J. A. Horton, and C. T. Liu*

The stability and mobility of active slip systems in superlattice structures, for both cubic and noncubic crystals, are theoretically investigated based on the energetics and kinetics of dislocation dissociations. The main concept of the force couplet model for the positive temperature dependence of yield and flow stress is introduced. Two sources of the glide resistance in ordered lattices are the fault dragging mechanisms and the cross-slip pinning mechanism. The effective fault energy consists of two terms related to the chemical and mechanical instability of a shear fault [antiphase boundary (APB) or superlattice intrinsic stacking fault (SISF)]. Dependence of the yield stress on the orientation and the sense of applied stress stems from the signs and magnitudes of the glide and nonglide stresses. As the effective fault energy is altered by solute segregation and/or high nonglide stress, the two glide resistance mechanisms are affected differently. In Ni_3Al and β-CuZn, the anomalous yield strength, strain rate sensitivity, in situ deformation TEM observations, and nonstoichiometry effect are discussed in view of the current model.

2.2.2.2 Temperature Effect on Superdislocation Dissociation on a Cube Plane in Ni_3Al[20] – *P. Veyssiere,*[21] *M. H. Yoo, J. A. Horton, and C. T. Liu*

Temperature dependence of the apparent APB energy on cube planes is studied using weak-beam determination of dissociation distances of superdislocations originating from deformation at 20, 650, and 850°C. It is difficult to assess how closely the observed dependence applies to the true cube ABP energy because of the uncertainty associated with lattice resistance to the motion of superpartials. It is estimated that the true energy of conservative APB on {001} is liable to decrease with temperature by as much as 30% between room temperature and 850°C.

2.2.2.3 Effect of Prestress on Tensile Yield Strength of a Ni_3Al Alloy[22] – *M. H. Yoo and C. T. Liu*

An experimental technique of prestressing and quenching was employed to elucidate the nature of pinning points responsible for the anomalous yield strength of Ni_3Al. The apparent number density of pinning points at room temperature was found to be unaffected by the prestressing and quenching from elevated temperatures. This

result is consistent with the cross-slip-pinning (CSP) model in that cross-slipped segments act as pinning points on the leading superpartial dislocations.

2.2.2.4 Geometry of Glide in Ni_3Al at Temperatures Above the Flow Stress Peak[23] – *P. M. Hazzledine, M. H. Yoo, and Y. Q. Sun*[24]

At temperatures above the flow stress peak in Ni_3Al, the slip system is <010>{001}. At higher temperatures, still a second system, <101> {001}, also operates. Both types of dislocation form glide loops that dissociate into 1/2 <110> APB-linked partials, and both glide loops show ranges of elastic instability. Three types of dislocation may lower their energy further by a second dissociation on {111} planes: the screw <110> forms a Kear-Wilsdorf lock, the edge <110> forms a Lomer-Cottrell lock, and the 45° <010> forms a B5 lock. Interactions between <110> and <010> dislocations give rise to two more dislocations with nonplanar cores, the <110> lock and the <111> lock. All these locked dislocations are slow moving or immobile and all, except for the <111> lock, have been observed in the electron microscope. The formation of <110> and <111> locks and the mixing of the two slip systems through interactions between them give an explanation for the high-temperature work-hardening peak found in Ni_3Al.

2.2.2.5 Superlattice Dislocation Structures in Ordered Intermetallic Alloys[25] – *J. A. Horton, P. Veyssiere,*[21] *I. Baker,*[13] *and M. H. Yoo*

Superlattice dislocations have been characterized by TEM in several ordered alloys, including Ni_3Al with no boron and Ni-24 at. % Al with boron additions. Specimens were either bulk-deformed at various temperatures or were deformed in the electron microscope at room temperature. Comparisons of dislocation structures in bulk-deformed specimens quenched from the test temperature will be made to specimens slowly cooled and to that produced by in situ deformation where the analysis is made under load. The relative stability and formation mechanism of superlattice intrinsic stacking fault coupled dislocations vs antiphase boundary coupled dislocations will be discussed.

2.2.2.6 Stability of Superdislocations and Shear Faults in $L1_2$ Ordered Alloys[26] – *M. H. Yoo*

Stability of superdislocations, superpartials, and APBs and/or SISFs between superpartials in $L1_2$ ordered alloys is analyzed within the framework of anisotropic linear elasticity theory. In the case of primary slip system, {111} <101>, the tangential component of elastic interaction between two superpartials is zero along the edge orientation, but along the screw orientation, it is of comparable magnitude to the radial component (e.g., 0.62 and 2.30 for APB- and SISF-type dissociations, respectively), which is associated with climb dissociation of fractional Shockley edge partials. Discussion is presented on dislocation microstructure (TEM), on core structure of superdislocations (atomistic simulation), and on possible intrinsic effects associated with positive and negative temperature dependences of the anomalous flow behavior of Ni_3Al.

2.2.2.7 Slip, Twinning, and Fracture at a Grain Boundary in the $L1_2$ Ordered Structure – A $\Sigma = 9$ Tilt Boundary[27] - *M. H. Yoo and A. H. King*[28]

The role of interaction between slip dislocations and a $\Sigma = 9$ tilt boundary in localized microplastic deformation, cleavage, or intergranular fracture in the $L1_2$ ordered structure has been analyzed by using the anisotropic elasticity theory of dislocations and fracture. Screw superpartials cross slip easily at the boundary onto the (111) and the (001) planes at low and high temperatures, respectively. Transmission of primary slip dislocations onto the conjugate slip system occurs with a certain degree of difficulty, which is eased by localized disordering. When the transmission is impeded, cleavage fracture on the (111) plane not intergranular fracture, is predicted to occur, unless a symmetric double pileup occurs simultaneously. Absorption (or emission) of superpartials occurs only when the boundary region is disordered. Slip initiation from preexisting sources near the boundary can occur under the local stress concentration. Implications of the current result on the inherent brittleness of grain boundaries in Ni_3Al and its improvement by boron segregation are discussed.

2.2.2.8 Interaction of Slip with Grain Boundary in the $L1_2$ Ordered Structure – A $\Sigma = 9$ Tilt Boundary[29] – *M. H. Yoo and A. H. King*[28]

The role of slip/grain boundary interaction in intergranular fracture has been analyzed for a $\Sigma = 9$ tilt boundary in $L1_2$ ordered alloys by use of the anisotropic elasticity theory of dislocations and fracture. Screw superpartials cross slip easily at the boundary onto the (111) and the (001) planes for low and high temperatures, respectively. Transmission of primary slip dislocations onto the conjugate slip system occurs with some difficulty, which is eased by localized disordering. Unless a symmetric double pileup occurs simultaneously, cleavage fracture rather than intergranular fracture is predicted to occur on the (111) plane. Absorption (or emission) of superpartials occurs only when the boundary region is disordered. The inherent weakness of grain boundaries in Ni_3Al and its improvement by boron segregation are discussed.

2.2.2.9 Deformation Twinning in Superlattice Structures[30] – *M. H. Yoo*

The role of twinning in deformation and fracture behavior of ordered intermetallic compounds has been investigated from a viewpoint based on the crystallography of twinning. The conjugate relationship between the order twinning the active slip system at elevated temperatures is identified in all the ordered structures considered. Implications of this conjugate relationship on the strength and ductility of ordered alloys are discussed.

2.2.2.10 Atomistic Simulation of Superdislocation Dissociation in Ni_3Al[31] – *M. H. Yoo, M. S. Daw,*[32] *and M. I. Baskes*[32]

The purpose of this paper is to determine the core structure of <101> screw superdislocations in Ni_3Al using EAM. First, the bulk properties and fault energies of

Ni_3Al pertinent to superdislocations are discussed. Second, the initial and boundary conditions for the atomic cell are specified. Third, the calculated results of both spontaneous dissociations and stable equilibrium configurations are presented. Finally, discussion is given on the comparison of the current results with the two previous results, including the effect of applied stress on dislocation mobility.

2.2.2.11 Intergranular Fracture by Slip/Grain Boundary Interaction[33] – *M. H. Yoo and A. H. King*[28]

The role of interaction between slip dislocations and [110] tilt boundaries in crack nucleation has been analyzed for the fcc and $L1_2$ structures. Dislocation absorption into the boundaries is orientation-dependent according to the elastic anisotropy. When the transfer of slip across the boundary is impeded, cleavage fracture is predicted on the (1T1) plane. Intergranular fracture can be initiated when a symmetric double pileup of primary slip dislocations from both sides of the boundary occurs simultaneously. The available experimental data on slip/grain boundary interaction and intergranular fracture are in good agreement with the current predictions.

2.2.2.12 Deformation and Fracture in Ordered Superlattice Structures[34] – *M. H. Yoo*

One of the important problems in materials science is to explain why certain intermetallic and nonmetallic compounds are intrinsically strong but weak at interfaces. This chapter presents an overview of the recent advancement in mechanistic understanding of the problem in ordered intermetallic alloys. The force couplet model successfully predicts the outstanding issues on deformation behavior, including the anomalous (positive) temperature dependence of yield strength. Crystallographic and elastic analyses of slip/grain boundary interaction characterize the importance of both cohesive energy and localized microplasticity of grain boundaries in intergranular fracture. Discussion will be given on further research needed in this area, including solid solution strengthening and fracture toughness.

2.2.2.13 Deformation Twinning in Ordered Intermetallic Compounds[35] – *M. H. Yoo, C. L. Fu, and J. K. Lee*[36]

Mechanistic understanding of deformation twinning in ordered superlattice structures is reviewed, and the interrelationships between twinning and generalized plastic flow or fracture toughness are discussed. Although general discussions refer to all the fcc-based and bcc-based cubic and noncubic ordered intermetallic alloys, specific calculations of the energetic and kinetic aspects of deformation twinning are made for TiAl. The importance of the twin-slip conjugate relationship on high-temperature mechanical properties is emphasized. Discussion is given of possible effects of macroalloying and microalloying on twinning propensity.

2.2.3 Creep and Cavitation in Nickel Aluminides

2.2.3.1 Coble Creep in a Powder-Metallurgical Nickel Aluminide of Composition Ni-22.8Al-0.6Hf-0.1B (at. %)[37] – *J. H. Schneibel and W. D. Porter*

Coble creep, which is controlled by mass transport along grain boundaries has been identified in a powder-metallurgically prepared nickel aluminide with the nominal composition Ni-22.8Al-0.6Hf-0.1B (at. %). Diffusional creep rates as a function of temperature T, stress σ, and grain size L are well described by $= 33\delta_b D_b \Omega\sigma/(kTL^3)$, where $\delta_b D_b = 3 \times 10^{-6}\ m^3 s^{-1} \times \exp[-(313\ kJ/mol)/(RT)]$, where δ_b is the diffusional grain boundary width, D_b is the grain boundary diffusivity, R is the gas constant, and T is the absolute temperature. The activation energy of 313 kJ/mol is unusually high compared with that for volume diffusion.

2.2.3.2 Evolution of Dislocation Structure During Inverse Creep of a Nickel Aluminide: Ni-23.5Al-0.5Hf-0.2B (at. %)[38] – *J. H. Schneibel and J. A. Horton*

A well-annealed polycrystalline nickel aluminide of composition Ni-23.5Al-0.5Hf-0.2B (at. %) shows inverse creep behavior at 1033 K and 250 MPa. The minimum creep rate does not correspond to a steady-state creep condition. The increase in the creep rate with strain and time is accompanied by an increase in the volume fraction of dislocation-containing regions. The inverse transient can be eliminated by prestraining the sample at room temperature. It is absent in the diffusional creep regime.

2.2.3.3 Inverse Creep in Ni_3Al[39] – *P. M. Hazzledine and J. H. Schneibel*

Two recent papers have reported that when Ni_3Al is crept in the temperature region of the yield stress anomaly, the initial rapid creep rate first declines then increases before fracture or reaching a steady state. In the first stage, primary octahedral slip occurs, and in the second stage, slip takes place on a secondary octahedral plane and on its cube cross slip plane, in contradition to Schmid's law. This unexpected slip behavior and the inverse creep are both compatible with the dislocation structures developed in constant strain rate tests of Ni_3Al. During inverse creep, two sets of dislocations that share a common cube cross slip plane interact in such a way as to unlock each other's structure, thereby causing the strain rate at constant stress to increase with strain.

2.2.3.4 Influencing the Shape of Creep Cavities in Nickel Aluminides by Stress Changes[40] – *L. Martinez*[41] *and J. H. Schneibel*

A nickel aluminide of composition Ni-23.5Al-0.5Hf-0.2B (at. %) is found to develop intergranular cavities having quasi-equilibrium shapes when it is creep-deformed at high temperatures and low stresses. When the temperature is lowered and the stress significantly increased (by a factor of 10), crack-like noses form at the tips of the original quasi-equilibrium cavities. Although this observation is in general agreement with previously published computer simulations, certain complications are found as well. The

experimental and theoretical relationships between growth rates and size at the crack-like noses are inconsistent, and growth-rates vary from nose to nose. Possible reasons for these effects are discussed.

2.2.3.5 Coble Creep and Cavitation in a Powder Metallurgical (PM) Nickel Aluminides of Composition Ni-22.8Al-0.6Hf-0.1B (at. %)[42] – *W. D. Porter and J. H. Schneibel*

The creep behavior of a fine-grained nickel aluminide powder metallurgy product with a composition of Ni-23.5 at. % Al-0.5 at. % Hf-0.2 at. % B has been measured as a function of stress, temperature, and grain size. The specimens had an initial grain size of 12 to 14 μm, which could be increased to 30 μm by annealing at 1273 K. At 1033 and 1140 K, the steady-state strain rate is almost proportional to the stress up to about 150 MPa, which indicates that diffusional creep is rate controlling. The grain size dependence of the creep rate, for a given stress and temperature, indicates Coble creep (i.e., grain boundary diffusion control). The value of the grain boundary diffusivity estimated from our creep data is in agreement with previous estimates for a cast nickel aluminide of the above composition. It appears that grain boundary mass transport in such alloys is anomalously slow compared with that in other metals and alloys.

2.2.3.6 Coble Creep, Cavity Sintering, and Cavity Growth[43] – *J. H. Schneibel and L. Martinez*[41]

The close relationships between Coble creep, cavity sintering, and cavity growth are discussed. The measurement of size distributions of crack-like cavities is useful for determining grain boundary and surface diffusivities. In nickel aluminide (Ni_3Al) intermetallics, the grain boundary diffusivity determined in this manner agrees well with that obtained from Coble creep measurements. A critical comparison of the zero-creep technique and the "zero-growth" technique (critical cavity radius determination) to measure surface free energies is given.

2.2.3.7 Crack-Like Creep Cavitation in a Nickel Aluminide[44] – *J. H. Schneibel and L. Martinez*[41]

Intergranular creep cavitation in a single-phase nickel aluminide of composition Ni-23.5Al-0.5Hf-0.2B (at. %) has been examined for different creep times, stresses, and grain sizes. The lengths and thicknesses of the observed crack-like cavities were measured on metallographic sections. From the cavity size distributions, cavity growth rates were determined. Estimates for grain boundary and surface diffusivities were obtained by fitting a model of creep-enhanced crack-like diffusive growth to the measured cavity growth rates and thicknesses. Complications arising from coalescence and plastic deformation of the cavities are discussed.

2.2.3.8 Numerical Modelling of Cavity Growth Controlled by Diffusion and Plasticity[45] – *L. Martinez[41] and J. H. Schneibel*

We present the results of numerical calculations of a model for cavity growth controlled by surface and grain boundary diffusion and plasticity. The cavities initially evolve in a quasi-equilibrium mode and further transform to develop a crack-like shape. During the quasi-equilibrium mode, the cavity growth rate diminishes as the diameter increases, and in the crack-like mode, the growth rate becomes essentially size-independent. The numerical data are compared with analytical calculations based on models with similar assumptions and some experimental results.

2.2.3.9 Cavity Nucleation Under Time-Dependent Stress Concentrations[46] – *H. Trinkaus[47] and M. H. Yoo*

Intergranular cavity nucleation under creep-induced microscale stress concentrations is studied in the framework of the formal theory of nucleation under time-dependent supersaturation presented in an earlier paper. The energetic and kinetic conditions for significant cavity nucleation and the conditions for permanent cavity stability during stress relaxation are established. For a suddenly activated slip/grain boundary interaction, the kinetic condition for significant nucleation is operative, constituting a Hall-Petch type relationship for cavitation. Expressions for the total number density of cavities nucleated during a single stress pulse and for the average cavity nucleation rate resulting from a randomly fluctuating stress are derived. The results provide explanations for some observations in creep cavitation not previously understood.

2.2.4 Structure and Properties of Trialuminides (Al_3X)

2.2.4.1 Aluminum-Based Cubic Intermetallics Having the $L1_2$ Structure[48] – *W. D. Porter and W. C. Oliver*

It has long been known that additions of Cu, Ni, or Fe to the intermetallic compound Al_3Ti result in a shift from the DO_{22} to the $L1_2$ crystal structure. The resulting pseudobinary ordered cubic intermetallic is of interest because of its crystal structure, low density, high melting point, and potential oxidation resistance. However, these compounds are brittle, and some ductility must be developed if they are to be used for structural applications. The current study was undertaken to investigate the effects of composition, microstructure, and processing techniques on the mechanical properties of these ternary aluminum-based intermetallic alloys. The alloys were produced by arc melting and were characterized by optical microscopy, analytical electron microprobe, and X-ray diffraction. Microprobe, RT microhardness, and hot hardness results will be discussed.

2.2.4.2 Phase and Microstructure of Fe-Modified Al_3Ti[49] – *W. D. Porter, K. Hisatsune,*[50] *C. J. Sparks, W. C. Oliver, and A. Dhere*[51]

Previous work has shown that Al_3Ti of the DO_{22} crystal structure can be stabilized in the cubic Ll_2 structure by the partial substitution of Al by Cu, Ni, or Fe. These alloys are of interest because of their high degree of symmetry, low density (<4 g/cm^3), high melting point (~1350°C), and oxidation resistance. X-ray diffraction data shows that a crystal of the composition $Al_{67}Fe_8Ti_{25}$ is single-phase Ll_2. A series of cast and splat-quenched alloys of the stoichiometry $Al_{75-x}Fe_xTi_{25}$ in which x = 0 to 10 was studied to follow the formation of the Ll_2 phase. The Ll_2 phase was present in the splat-quenched materials containing more than 0.5 at. % Fe, and the relative fractions of Ll_2 and DO_{22} phases and their compositions were analyzed by X-ray diffraction and electron microprobe. Structural changes of rapidly solidified samples were followed as a function of annealing treatment. Phase stability, compositional changes, and brittleness of the alloys will be discussed.

2.2.4.3 Identification of Cleavage Planes in an Al_3Ti-Base Alloy by Electron Channeling in the SEM[52] – *E. P. George, W. D. Porter, and D. C. Joy*

Selected area electron channeling patterns were used to identify the cleavage planes in a polycrystalline Al_3 Ti-based alloy having the $L1_2$ structure. To do this unambiguously in the scanning electron microscope (SEM), one needs to know that the cleavage facet from which any given channeling pattern is obtained is indeed normal to the electron beam. We accomplished this by utilizing a recently developed technique in which an optical microscope with a short depth of focus is inserted in the SEM column and used to measure the elevations of several points on the cleavage facets. By appropriately tilting and rotating the sample and using the optical microscope to measure elevations, it was possible to orient the facets normal to the beam. The cleavage planes in a cast and extruded alloy having an equiaxed grain structure were compared with those in a directionally solidified (DS) alloy of the same composition. Of the eight cleavage facets examined in the DS material, six were of the {110} type and two were of the {111} type. Of the six facets examined in the cast and extruded material, two each were of the {110} and {111} types and one each were of the {100} and {013} types. Although it cannot be said that all possible cleavage planes have been identified in this alloy, the availability of several low-strength cleavage planes apparently exacerbates its brittleness.

2.2.4.4 Cleavage Fracture in an Al_3Ti-Based Alloy Having the Ll_2 Structure[53] – *E. P. George, W. D. Porter, H. M. Henson, W. C. Oliver, and B. F. Oliver*[7]

Selected area electron channeling patterns were used to identify the cleavage planes in a polycrystalline Al-23Ti-6Fe-5V alloy, which is an Al_3Ti-based alloy having the $L1_2$ structure. Such alloys are of scientific and technological interest because they fracture by brittle transgranular cleavage, despite the availability of more than five independent slip systems in the Ll_2 structure and their relatively low hardness when compared with ductile Ll_2 alloys such as Ni_3Al. Homogenized bars of the levitation zone

melted and directionally solidified alloy were fractured at room temperature in three-point bending. The fracture surfaces, which consisted almost entirely of brittle transgranular cleavage facets, were examined in a SEM equipped to take channeling patterns. An optical microscope with a short depth of focus was inserted in the SEM column just below the objective lens, and by focusing it on several points on the cleavage facets, it was possible to orient the facets normal to the optic axis of the SEM prior to taking the channeling patterns. Of the eight cleavage facets examined in this study, six were of the {110} type and two were of the {111} type. Although it cannot be said that these are the only two cleavage planes in this alloy, the availability of more than one plane with low cleavage strength contributes to the brittleness of this alloy. These results are examined in the light of theoretical treatments of cleavage fracture, and comparisons are made with earlier studies on other $L1_2$ materials.

2.2.4.5 Microstructure and Fracture Toughness of Powder-Processed Al_3Nb[54] – *J. H. Schneibel, P. F. Becher, and J. A. Horton*

Intermetallic alloys with the nominal compositions Al-24.5Nb, Al-25Nb, and Al-25.5Nb (at. %) were fabricated by hot-pressing of prealloyed powders in graphite dies in vacuum. The hot-pressed disks contained substantial porosity even at processing temperatures of 0.95 T_m, where T_m is the absolute melting point. In addition to some copper and silicon contamination, significant concentrations of oxygen and carbon were measured in Al-25.5Nb. Alpha alumina precipitates, as well as niobium-enriched precipitates, were identified. The fracture toughness of precracked bend specimens with the nominal composition Al-25.5Nb was found to be 2.5 ± 0.5 MPa $m^{1/2}$. Possibilities for improving this value are discussed.

2.2.4.6 Microstructure and Mechanical Properties of $L1_2$-Structure Alloys Based on Al_3Zr[55] – *J. H. Schneibel and W. D. Porter*

The tetragonal compound Al_3Zr can be transformed into the cubic $L1_2$ structure by additions of Cr, Fe, Ni, or Cu. This result is interpreted in terms of Pettifor's structure map. The transformation is accompanied by substantial softening. The significant porosity of cast buttons that develops during the homogenization required to produce the $L1_2$ structure is attributed to the Kirkendall effect. Al-5.5Fe-25Zr (at. %) specimens with the $L1_2$ structure can be deformed at room temperature in compression, and their yield stress has been determined as a function of temperature. Al-Fe-Zr is nevertheless a brittle material. This is illustrated for a Al-Fe-V-Zr $L1_2$-structure compound, the fracture toughness of which is only slightly higher than that of sintered SiC. Evidence is presented to suggest that $L1_2$ formation is accompanied by an increase in toughness. Significant improvements in the mechanical properties of Al_3Zr-type alloys may possibly be achieved by improved processing.

2.2.4.7 Cleavage Fracture in Al_3Sc[56] – *J. H. Schneibel, E. P. George, and J. A. Horton*

Al_3Sc, an intermetallic compound that has the cubic $L1_2$ structure, serves as a model material for cubic compounds based on trialuminides. As evidenced by the

fracture of large-grained polycrystals, it fractures by cleavage in a brittle manner. Out of a total of 18 cleaved grain facets analyzed so far by the selected area channeling pattern technique, 16 were {011} and 2 were {001} oriented. Because Auger analysis revealed no segregation of impurities to cleavage planes in this material, the cleavage appears to be an intrinsic effect. Consistent with this is the low value of K/G ($\sim$1.3), where K and G are bulk and shear modulus, respectively.

2.2.4.8 Fracture Studies of Trialuminides[57] – *E. P. George, W. D. Porter, and J. H. Schneibel*

Trialuminides, especially those based on the light element titanium, have several attractive properties (high melting point, low density, good oxidation resistance, etc.) that make them ideally suited for high-temperature structural applications. However, their low-temperature brittleness has so far precluded their successful exploitation. Among the approaches that have been tried to ductilize trialuminides is macroalloying to control crystal structure: specifically, alloying elements have been identified that convert the noncubic crystal structures of several trialuminides to the cubic $L1_2$ structure. Concurrently, strict compositional control has successfully lowered the hardness of some trialuminides to levels below that of other ductile $L1_2$ alloys (like Ni_3Al). Surprisingly, however, even the relatively soft trialuminides having the $L1_2$ structure undergo brittle cleavage fracture despite the availability of more than five independent slip systems. We will summarize here results of research into this unusual fracture behavior. Among the topics to be covered are a new technique using selected area channeling patterns to identify planes of low cleavage strength, examples illustrating the use of this technique to a couple of different trialuminides, possible reasons for low cleavage strength, and preliminary results of fracture toughness measurements.

2.2.5 Mechanical Properties Microprobe

2.2.5.1 Characterizing the Hardness and Modulus of Thin Films Using a Mechanical Properties Microprobe[58] – *W. C. Oliver and C. J. McHargue*

A new ultralow-load microindentation system has been acquired by the Metals and Ceramics Division. The system's spatial resolution and its data-acquisition capabilities allow the determination of several mechanical properties from submicrometer volumes of materials, hence the term mechanical properties microprobe (MPM). In this paper, we demonstrate the ability of such a system to measure the modulus and hardness of an ion-implanted sapphire specimen. The implantation process results in an amorphous surface layer 155 nm thick. The hardness and modulus of the amorphous Al_2O_3 are 10 GPa and 200 GPa, respectively. This represents a 60% reduction in hardness and 50% reduction in modulus compared with the unimplanted material.

2.2.5.2 Mechanical Properties of Nanometre Volumes of Material: Use of the Elastic Response of Small-Area Indentations[59] – *J. B. Pethica[60] and W. C. Oliver*

A new, differential method for determining the stiffness of a submicron indentation contact area is presented. This allows measurement of elastic modulus as well as

plastic hardness continuously during a single indentation and without the need for discrete unloading cycles. Some of the new experiments that become possible with this technique, especially at the nanometer scale, are described. We show quantitatively that electropolished tungsten reproducibly exhibits the ideal theoretical lattice strength at small indentation loads.

2.2.5.3 The Influence of Thickness and Wavelength on the Mechanical Properties of a Compositionally Modulated Ceramic Thin Film[61] – *W. C. Oliver, F. A. List, and R. A. McKee*

The hardness and modulus of thin (<1 μm) ceramic films have been investigated using the differential mechanical properties microprobe (DMPM). The DMPM consists of a computer-controlled ultralow-load indentation system having a special system that allows the elastic stiffness of the contact to be determined continuously during the indentation process. The films were deposited in a molecular beam epitaxy (MBE) system utilizing unique high-temperature effusion cells. The specimens have been studied. The first is a wedge-shaped layer of amorphous Al_2O_3 on a silicon substrate. The thickness of the layer varies from 0 to 900 nm at the two extreme sides of a 7.6-cm (3-in.) silicon wafer. The effect of layer thickness on the hardness and modulus as measured with the DMPM has been quantified for this system. The second specimen is made up of 38 repetitions of alternating layers of crystalline TiO_2 and amorphous Al_2O_3. The wavelength of the composition modulation and the thickness of the film varies uniformly from 0 to 38 nm and from 0 to 1460 nm, respectively, across the 7.6-cm (3-in.) diameter of the silicon substrate.

2.2.5.4 Thin Film and Near-Surface Characterization Using a Mechanical Properties Microprobe[62] – *W. C. Oliver and C. J. McHargue*

Ion implantation of materials to improve their mechanical properties is a rapidly expanding industry. Such surface treatments result in very thin (<500 nm) surface films. These films can have extraordinary mechanical properties because of the tremendous variety of structures and compositions available via ion implantation. The MPM has been developed to determine the properties of such thin films. In this paper we will discuss the application of the MPM to several ion-implanted material systems.

2.2.5.5 Nanoindentation of Silver—Relations Between Hardness and Dislocation Structure[63] – *G. M. Pharr[64] and W. C. Oliver*

The depth dependence of hardness in a well-annealed single crystal of silver has been characterized in nanoindentation experiments. The work is based on similar experiments performed by Chen and Hendrickson but extends their results to indent depths on the nanometer scale. The hardness is generally found to increase with decreasing depth, with a rather sharp increase observed at depths of less than 50 nm. Using etch pitting to reveal the surface dislocation structure after indentation, the sharp rise in hardness is found to be associated with the disappearance of dislocation rosette patterns and any signs of near-surface dislocation activity, thereby suggesting

that very-small-scale indentation plasticity may take place by nondislocation mechanisms. However, order-of-magnitude calculations show that possible alternatives, specifically, diffusional mechanisms, are too slow to make significant contributions. It is suggested that for very small indents, either the surface dislocation debris is quickly annealed out before it can be observed or indentation plasticity is accommodated entirely by subsurface dislocation activity.

2.2.5.6 Mechanical Characterization Using the Differential Mechanical Properties Microprobe[65] – *W. C. Oliver and J. B. Pethica*[60]

The MPM is used to generate load/displacement data continuously during an indentation experiment. Such data can be used to calculate the hardness as a function of depth if the elastic accommodation of the indenter displacement is small or if one assumes a constant apparent modulus. The hardness and apparent modulus of the sample can be calculated at any point during the indentation process at which the contact stiffness as well as the indenter load and displacement are known. Normally, the contact must be unloaded to some degree to measure the stiffness of the contact. Hence, if elastic effects are large and the apparent modulus of the sample is not constant as a function of depth, the indentation process must be interrupted at each depth for which the properties are to be measured. A new technique will be discussed that allows the contact stiffness to be measured continuously without interrupting the loading process. Using this technique, hardness and apparent modulus can be calculated as a function of depth from a single indentation. Results from three sets of specimens will be presented.

The first set of specimens are ion-implanted ceramic specimens. The surface hardness of sapphire can be tailored for various applications using ion implantation. The hardness and modulus of these thin (typically 100-nm-thick) films are measured using the DMPM.

The second set of specimens consists of various hard carbon and diamond-like films. The hardness and modulus of these films can be obtained from DMPM results.

Finally, results obtained from a naturally occurring radiation-damaged zircon geological sample stone will be presented. The 570-million-year old sample has trace levels of uranium and thorium that have resulted in regions of the sample being radiation damaged. The properties of these regions are measured using the DMPM and correlated with the composition as measured with an electron beam microprobe using wavelength dispersive spectrometry.

2.2.5.7 Thin-Film and Near-Surface Characterization Using a Mechanical Properties Microprobe[66] – *D. L. Joslin,*[67] *C. J. McHargue, and W. C. Oliver*

An ultralow-load microindentation system will be described and examples of its applications given. The system's spatial resolution and its data-acquisition capabilities allow the determination of several mechanical properties from volumes of material having

submicron dimensions. Research with this instrument has led to improved techniques for determining the plastic and elastic properties of materials from microindentation experiments. The techniques have been applied to thin layers created by ion implantation of metals and ceramics, radiation-damaged materials, and thin hard coatings. Changes in hardness and modulus of elasticity have been measured in films as thin as 100 nm.

2.2.5.8 Determination of the Mechanical Properties of Diamond and Diamond-Like Films by the UltraLow-Load Indentation Technique[68] – *M. E. O'Hern, C. J. McHargue, R. E. Clausing, and W. C. Oliver*

Diamond and diamond-like films deposited at Oak Ridge National Laboratory were characterized with the MPM and compared with a natural diamond characterized by the same method. The diamond films were 75 μm thick and has a micrograin structure, whereas the natural diamond had a <100> orientation. The diamond-like film (or hcc) was rf glow discharge deposited to a thickness of about 0.2 μm. Results of the current study are given, and future work is discussed.

2.2.5.9 New Techniques Using the Mechanical Properties Microprobe[69] – *W. C. Oliver*

Two new uses for the MPM will be discussed. First, a new technique that allows the hardness and apparent modulus of a thin-film substrate combination to be determined continuously during indentation is presented. Second, a new technique for characterizing the properties of interfaces between the fibers and matrix of a ceramic/ceramic composite will be discussed. Techniques for determining the dynamic shear strength of such boundaries have been established. In addition, preliminary results indicate that similar tests may be useful in determining fiber matrix bonding and the residual stress state of the fiber.

2.2.5.10 Elastic Displacement During Indentation of Ceramics and Glasses[70] – *G. M. Pharr[84] and W. C. Oliver*

Load-displacement behavior during the indentation of several ceramics and glasses by a triangular pyramid diamond indenter has been experimentally measured and analyzed for comparison with models for the elastic displacements produced by indentation. The materials investigated included fused silica, soda lime glass, and single crystals of silicon, germanium, sapphire, and quartz. Data from the unloading portions of the load-displacement curves are compared with theoretical predictions for indenters of three ideal geometries — (1) a cylindrical flat punch, (2) a cone, and (3) a paraboloid of revolution. The data are generally in best agreement with the paraboloid geometry. The results have implications for the experimental determination of elastic moduli and hardness from load-displacement measurement during indentation.

2.2.6 References

1. Abstract from an invited paper in *Proc. Symp. Interfac. Struct. Prop. Des.* **122**, 429-41, M. H. Yoo, W.A.T. Clark, and C. L. Briant, eds., Materials Research Society Publication, 1988.

2. Abstract of a paper to be published in *Scr. Metall.* (1989).

3. Abstract from *Acta Metall.* **36**, 2229-38 (1988).

4. Abstract from an invited paper to be published in *Proc. Symp. High Temp. Ord. Intermetal. Alloys III*, **133**, C. T. Liu, A. I. Taub, N. S. Stoloff, and C. C. Koch, eds., Materials Research Society Publication, 1989.

5. Abstract from *Acta Metall.* **36**, 1241-49 (1988).

6. Abstract from *J. Mater. Res.* **4**, 294-99 (1989).

7. Department of Materials Science and Engineering, University of Tennessee, Knoxville.

8. Abstract from a paper to be published in *Proc. Symp. High Temp. Ord. Intermetal. Alloys III*, **133**, C. T. Liu, A. I. Taub, N. S. Stoloff, and C. C. Koch, Materials Research Society Publication, 1989.

9. Abstract from *J. Mater. Res.* **3**, 665-74 (1988).

10. Schulson et al., *Acta Metall.* **33**, 1587 (1985).

11. Abstract published in *J. Met.* **40**, 7 (1988).

12. Abstract from *J. de Phys. Colloque* **C6** Supplement au N°11, Tome 49 (1988).

13. Thayer School of Engineering, Dartmouth College, Hanover, N.H.

14. Abstract from a chapter in the book, *Superalloys, Supercomposites and Superceramics*, pp. 583-624, J. K. Tien and T. Caulfield, eds., Academic Press, New York, 1989.

15. Department of Materials Science and Engineering, University of Pennsylvania, Philadelphia, Pa.

16. Abstract from an invited paper in *Alloy Phase Stab.* **163**, 7-21, G. M. Stocks and A. Gonis, eds., NATO ASI Series E, Kluwer Academic Publishers, Boston, 1989.

17. Abstract from *Encyclopedia of Materials Science and Engineering*, pp. 3-9, R. W. Cahn, ed., Pergamon Press, New York, 1988.

18. Summary from *McGraw-Hill Yearbook of Science and Technology*, pp. 80-83, McGraw Hill Book Company, New York, 1987.

19. Abstract from *Acta Metall.* **36**, 2935-46 (1988).

20. Abstract from *Philos. Mag. Lett.* **59**, 61-68 (1989).

21. LEM, CNRS-ONERA, B.P. 72, 92322 Chatillon Cedex, France.

22. Abstract from *J. Mater. Res.* **3**, 845-47 (1988).

23. Abstract of a paper accepted for publication in *Acta Metall.* (1989).

24. Department of Metallurgy, Oxford University, United Kingdom.

25. Abstract from a paper presented at the TMS-AIME Annual Meeting, Phoenix, Ariz., Jan. 25-29, 1988.

26. Abstract from *Acta Metall.* **35**, 1559-69 (1987).

27. Abstract from *J. Mater. Res.* **3**, 848 (1988).

28. Department of Materials Science and Engineering, State University of New York at Stony Brook, Stony Brook, N.Y.

29. Abstract from *MRS Proc.* **122**, 305 (1988).

30. Abstract from *J. Mater. Res.* **4**, 50 (1989).

31. Abstract from a paper to be published in ASM Symp. Proc. on Atomistic Modelling in Materials-Beyond Pair-Potentials, Plenum Press, 1989.

32. Theoretical Division, Sandia National Laboratories, Livermore, Calif.

33. Abstract from a paper to be published in Symp. Proc. on Interface Science and Engineering, ASM World Materials Conf., September 1988.

34. Abstract of a paper to be published in *1988 ASM Materials Science Seminar Book, Science of Advanced Materials*, Chicago, Ill., Sept. 24-30, 1988.

35. Abstract from a paper to be published in *MRS Sym. Proc.* **133** (1989).

36. Department of Metallurgical Engineering, Michigan Technological University, Houghton, Mich.

37. Abstract from *J. Mater. Res.* **3**, 403-6 (1988).

38. Abstract from *J. Mater. Res.* **3**, 651-55 (1988).

39. Abstract from a paper to be presented at the TMS-AIME Fall Meeting, October 1-5, 1989, Indianapolis, Ind.

40. Abstract from a paper presented at TMS-AIME Symposium on Intermetallics, January 25-29, 1988, Phoenix, Arizona.

41. Institute of Physics, University of Mexico, 62190 Cuernavaca, Mexico.

42. Abstract from a paper presented at the PM Aerospace Materials Conference, Lüzern, Switzerland, Nov. 2-4, 1987.

43. Abstract of a paper to be published at the 90th Annual Meeting of the American Ceramic Society, Cincinnati, Ohio, May 1-5, 1988.

44. Abstract from a paper accepted for publication in *Acta Metallurgica*.

45. Abstract from a paper presented at 118th TMS-AIME Annual Meeting, Feb. 27-March 2, 1989, Las Vegas, Nev.

46. Abstract from *Philos. Mag. A* **57**, 543-64 (1988).

47. Institut für Festkorperforschung der Kernforschungsanlage Jülich, Postfach 1913, D-5170 Jülich, Federal Republic of Germany.

48. Abstract from a paper presented at the TMS-AIME Annual Meeting, Phoenix, Ariz., Jan. 25-29, 1988.

49. Abstract from a paper to be published in *MRS Proc.* **133** (1989).

50. School of Dentistry, Nagasaki University, Nagasaki 852, Japan.

51. E.I. du Pont, Chattanooga, Tenn.

52. Abstract of a paper to be published in *MRS Proc*. **133** (1989).

53. Abstract from *J. Mater. Res.* **4**, 78 (1989).

54. Abstract from *J. Mater. Res.* **3**, 1272-76 (1988).

55. Abstract of a paper to be published in *MRS Proc*. **133** (1989).

56. Abstract of a paper to be presented at the TMS-AIME Fall Meeting, Oct. 1-5, 1989, Indianapolis, Ind.

57. Abstract of an invited paper presented at a seminar at University of Tennessee, Knoxville, Tenn., on March 14, 1989.

58. Abstract from *Thin Solid Films* **161**, 117-22 (1988).

59. Abstract from *MRS Proc.* **130**, 13-23 (1989).

60. Department of Metallurgy and Science of Materials, Parks Road, Oxford OX1 3PH, England.

61. Abstract from *MRS Proc.* **130**, 99-104 (1989).

62. Abstract from *Proceedings of the Symposium on Ion Implantation and Plasma Assisted Processes for Industrial Applications*, pp. 157-61, ASM Publication, 1989.

63. Abstract from *J. Mater. Res.* **4**, 91-101 (1989).

64. Department of Materials Science, Rice University, P.O. Box 1892, Houston, Tex.

65. Abstract from a paper presented at the 1989 Spring Meeting of the Society for Experimental Mechanics, Cambridge, Mass.

66. Abstract from a paper presented at NATO Advanced Study Institute, Ciocco, Italy, August 1988.

67. The University of Tennessee, Knoxville, Tenn.

68. Abstract from a paper presented at the 1989 MRS Spring Meeting, San Diego, Calif., April 1989.

69. Abstract from a paper presented at the ASM Annual Meeting, Detroit, Mich., Nov. 7, 1988.

70. Abstract from a paper presented at the American Ceramic Society, Cincinnati, Ohio, May 1988.

2.3 FUNDAMENTALS OF WELDING AND JOINING – *S. A. David and J. M. Vitek*

The purpose of the fundamental Welding Science Program is to investigate the physical metallurgy of weldments and to develop the capability to predict weld metal microstructure and properties. The program consists of four major parts relating to the study of (1) solidification behavior of weld metal; (2) mathematical modeling, and its verification, of welding processes; (3) correlation of thermal history and phase stability of weldment microstructure; and (4) activities related to coordination of BES welding programs and ORNL-industry cooperative programs.

The development of weld metal microstructure is being examined with respect to solidification substructure, grain structure, and solute redistribution. The intent of these studies is to develop a unified solidification theory for weld metal microstructures at both conventional and extremely rapid cooling rates. Our recent investigations have shown that significant microstructural modifications can occur during rapid solidification of austenitic stainless steel weld metals. These microstructural modifications are being examined in terms of rapid solidification theories involving large undercoolings and nucleation kinetics. In addition, because many of the details of the microstructural development during welding in polycrystalline materials are lost, a fundamental study of the weld pool solidification behavior in single crystals has been initiated. The interplay between the shape of the weld pool, weld microstructure, and the growth crystallography is being examined using Fe-15Ni-15Cr alloy single crystals.

A program on weld modeling has been initiated to develop a comprehensive modeling capability to predict weld metal microstructure and properties from first principles of transport phenomena. A computational and experimental study was carried out to quantitatively understand the influence of the heat flow and the fluid flow in the transient development of the weld pool during gas tungsten arc (GTA) and laser welding of type 304 stainless steel. The calculated results are being compared with experimental findings with regard to weld pool size and shape for several conditions to verify the model's accuracy in describing weld pool fluid flow phenomena.

A cooperative research program with Massachusetts Institute of Technology, Pennsylvania State University, and Idaho National Engineering Laboratory is also under way to relate modeling studies of transport phenomena to weld microstructures.

The phase stability studies of both austenitic and ferritic steels are directed toward understanding the transformation behavior of the materials during welding and after aging over a range of service temperatures. Mechanical properties after aging are being evaluated to develop structure-property relationships for these steels.

ORNL has been assigned the task of coordinating the BES welding programs. Yearly meetings of all the BES welding program contractors have been arranged, and coordination of the BES welding programs has been implemented. A yearly newsletter describing the BES Welding Science Program and results has also been published.

2.3.1 Effect of Rapid Solidification on Stainless Steel Weld Metal Microstructures and Its Implications on the Schaeffler Diagram[1-3] – *S. A. David, J. M. Vitek, and T. L. Hebble*

An investigation was carried out to determine the effect of rapid solidification on the weld metal microstructure of austenitic stainless steels and its implication on the ferrite constitution diagram. A wide variety of stainless steels were laser-beam welded at different welding speeds and laser power levels. The results indicate that both weld-pool cooling rate and the postsolidification solid-state cooling rates have a profound effect on the microstructures. For the steels investigated, the microstructures ranged from duplex austenite (γ) + ferrite (δ) to fully austenitic or fully ferritic. These microstructures were found to be sensitive to both cooling rates and composition. The observed results are rationalized based on rapid solidification theory.

Observations of this investigation indicate that solidification rates and postsolidification cooling rates have a profound effect on the observed microstructures, thus making it impossible to predict the microstructures of rapidly cooled weld metal from conventional constitution diagrams. The influence of the observations made in this investigation on the Schaeffler diagram have been demonstrated, and possible corrections to the constitution diagram incorporating the cooling rate effects have been proposed.

2.3.2 Development of Microstructures in Fe-15Ni-15Cr Single-Crystal Electron Beam Welds[4] – *M. Rappaz,[5] S. A. David, J. M. Vitek, and L. A. Boatner[6]*

A detailed analysis of the microstructures produced in an autogenously welded single crystal of Fe-15Ni-15Cr was performed to investigate the relationship between growth crystallography and solidification behavior. Electron beam welds were made at various speeds on the (001) surface of single crystals, in either the [100] or [110] directions. A geometrical analysis was carried out to relate the dendrite growth velocities in the three <100> directions to the weld velocities for the different crystallographic orientations examined. From this analysis, the preferred dendrite trunk directions were determined as a function of the solidification front orientation based on a minimum velocity or minimum undercooling criterion. A thorough examination of the weld microstructures and a comparison with the geometrical relationships developed in this work permitted a three-dimensional reconstruction of the weld-pool shape to be performed. In addition, the dendrite spacings were measured and the variation in spacings as a function of growth velocity was compared with theoretical predictions. It was found that the range of velocities over which dendritic growth is expected agreed with the experimental findings, and furthermore, that the change in dendrite spacing with growth velocity varied as predicted by theory. These results clearly demonstrate the effect of crystallography on the microstructural development during weld-pool solidification. The results also show that the resultant microstructures and pool shapes can be explained by geometrical analysis in conjunction with existing solidification models.

2.3.3 Heat Transfer During Nd:YAG Pulsed-Laser Welding and Its Effect on Solidification Structure of Austenitic Stainless Steels[7] – *T. Zacharia, S. A. David, J. M. Vitek, and T. DebRoy*[8]

Theoretical and experimental investigations were carried out to determine the effect of process parameters on weld metal microstructure of austenitic stainless steels during pulsed-laser welding. Laser welds made on four austenitic stainless steels at different power levels and scanning speeds were considered. A transient-heat-transfer model that takes into account fluid flow in the weld pool was employed to simulate thermal cycles and cooling rates experienced by the material under various welding conditions. The weld metal thermal cycles and cooling rates are related to features of the solidification structure. For the conditions investigated the observed fusion zone structure ranged from duplex austenite (γ) + ferrite (δ) to fully austenitic or fully ferritic.

Unlike welding with a continuous-wave laser, pulsed-laser welding results in thermal cycling from multiple melting and solidification cycles in the fusion zone, causing significant postsolidification solid state transformation to occur. There was microstructural evidence of significant recrystallization in the fusion zone structure that can be explained on the basis of the thermal cycles. The current investigation clearly demonstrated the potential of the computational model to provide detailed information regarding the heat transfer conditions experienced during welding.

2.3.4 Laser Beam Welding of High-Manganese Stainless Steels—Examination of Alloying Element Loss and Microstructural Changes[9] – *P. A. A. Khan,*[8] *T. DebRoy,*[8] *and S. A. David*

Alloying element loss and microstructural modifications of high-manganese austenitic stainless steels resulting from laser beam welding were examined. Welds were fabricated using both high- and low-power carbon dioxide lasers. Variables studied were welding speed, laser power, and shielding gas flow rate.

Pronounced decrease in the concentration of manganese was observed when specimens were welded at low laser powers. The rate of vaporization of alloying elements such as iron and manganese was found to increase significantly with laser power. However, the decrease in the concentration of manganese was less pronounced when the welds were made at high laser power. The composition change was not significantly influenced by either the welding speed or the shielding gas flow rate. The effective weld-pool temperature for vaporization was insensitive to changes in the welding variables. A slight reduction in the concentrations of dissolved oxygen and nitrogen was observed at the surface of the welded specimens. At low laser power, the welded region had a duplex austenitic and ferritic microstructure at low welding speeds and fully austenitic structure at higher welding speeds. However, at high laser powers, the weld microstructure was duplex at all welding speeds.

2.3.5 The Aging Behavior of Types 308 and 308CRE Stainless Steels and Its Effect on Mechanical Properties[10-13] – *J. M. Vitek and S. A. David*

The aging behavior of types 308 and 308CRE stainless steels has been examined over a range of temperatures (475–850°C) for aging times up to 10,000 h. Both the homogenized and the as-welded initial conditions were studied. At elevated aging temperatures (>550°C), aging of type 308 steel resulted in precipitation of carbides and the transformation of ferrite to sigma phase when ferrite was initially present or the formation of sigma phase in initially ferrite-free material. The elevated-temperature aging of type 308CRE steel resulted in the precipitation of titanium-rich carbides, nitrides, and sulfides and the transformation of ferrite to sigma phase. The distribution of precipitates was affected by the initial condition of the materials. The elevated-temperature creep properties, in particular the improved properties of type 308CRE, were related to the precipitate distribution. For low-temperature (<550°C) aging of welded type 308 steel, precipitation of G-phase within the ferrite was observed, as well as the decomposition of ferrite into alpha and alpha prime. With the help of a novel mechanical properties microprobe (MPM), which was capable of determining the hardness of the minor constituent ferrite phase, the hardness behavior as a function of aging could be related to the microstructures. These results are interpreted in terms of the potential susceptibility of these alloys to 475°C embrittlement.

2.3.6 Effect of Cooling Rate on Ferrite in Type 308 Stainless Steel Weld Metal[14] – *J. M. Vitek and S. A. David*

Weld filler metals such as type 308 stainless steel generally solidify as primary ferrite, and during cooling the ferrite transforms to austenite. This transformation is normally not carried out to completion, resulting in some residual ferrite retained in the final as-welded microstructure. The effect of cooling rate on residual ferrite content and composition was evaluated by heating as-welded material to 1300°C (2372°F) and then cooling it to room temperature at fixed rates that varied from 0.16 to 693°C/s (0.29 to 1247°F/s). As the cooling rate increased, the amount of retained ferrite increased, the ferrite's chromium content decreased, and its nickel content increased. The influence of the width of the elongated ferrite grains on the cooling rate effect was determined by examining ferrite regions of different sizes. Calculations using a simple diffusion model reproduced the experimental results qualitatively. The diffusion calculations provided additional information on the sensitivity of ferrite composition to cooling rate and ferrite width. The results of the current investigation can be combined with modeling results on cooling rates of welds to allow one to predict the amount and composition of ferrite in welds. Such information is necessary to understand the stability of ferrite under multiple-pass welding conditions or during elevated-temperature applications.

2.3.7 Microstructural Characterization and Properties of 3Cr-1.5Mo-0.1V Thick Section Electron Beam Welds[15] – *S. A. David, J. F. King, and J. M. Vitek*

Single-pass, full-penetration, thick-section (10 cm) electron beam weldments of high integrity were made of 3Cr-1.5Mo-0.1V steel using a 100 kW Sciaky electron beam welder. The weldment was characterized using microhardness measurements, Charpy V-notch impact, tensile, and guided bend tests. Microstructural characterization was done using both optical and electron microscopy.

The mechanical properties results showed the electron beam weldments had properties that matched those of the base metal. A hardness minimum within the heat-affected zone (HAZ) was observed on either side of the fusion zone. Such a minimum is commonly observed in ferritic steel weldments, although this region was very narrow compared with the weldments made by other conventional processes. Microstructural characterization of the weld revealed that the fusion zone and immediately surrounding HAZ contained retained austenite between the bainite laths. Further away from the fusion zone, the HAZ structure consisted of bainite and proeutectoid ferrite, which corresponded to the drop in the microhardness and resulted in a minimum. Tempered bainite was observed beyond this minimum in the HAZ.

2.3.8 References

1. S. A. David, J. M. Vitek, and T. L. Hebble, "Effect of Rapid Solidification on Stainless Steel Weld Metal Microstructures and Its Implications on the Schaeffler Diagram," *Weld. J.* 55(10), 289s-300s (October 1987).

2. S. A. David and J. M. Vitek, "Microstructural Modification During Laser Welding," to be published in *Proceedings of International Conference on Materials Processing*, Hyderabad, India, January 14-20, 1988.

3. J. M. Vitek and S. A. David, "Laser Welding of Stainless Steel Weld Filler Metals at High Cooling Rates," to be published in *Proceedings of 4th International Colloquium on Welding and Melting by Electrons and Laser Beam*, Cannes, France, September 1988.

4. M. Rappaz, S. A. David, J. M. Vitek, and L. A. Boatner, "Development of Microstructures in Fe-15Ni-15Cr Single Crystal Electron Beam Welds," *Metall. Trans. A* (in press).

5. M. Rappaz, Laboratoire de Metallurgie, Ecole Polytechnique Fédérale de Lausanne, Switzerland.

6. L. A. Boatner, Solid State Division, Oak Ridge National Laboratory.

7. T. Zacharia, S. A. David, J. M. Vitek, and T. DebRoy, "Heat Transfer During Nd:YAG Pulsed Laser Welding And Its Effect on Solidification Structure of Austenitic Stainless Steels," *Metall. Trans. A* **20A**, 1125-38 (1989).

8. P. A. A. Khan and T. DebRoy, Department of Materials Science and Engineering, Pennsylvania State University, University Park, Pa.

9. P. A. A. Kahn, T. DebRoy, and S. A. David, "Laser Beam Welding of High-Manganese Stainless Steels — Examination of Alloying Element Loss and Microstructural Changes," *Weld. J.* **67**(1), 1s-7s (January 1988).

10. J. M. Vitek and S. A. David, "The Aging Behavior of Types 308 and 308CRE Stainless Steels and Its Effect on Mechanical Properties," pp. 157-171 in *Properties of Stainless Steels in Elevated Temperature Service*, MPC-Vol. 26, PVP-Vol. 132, ed. M. Prager, American Society of Mechanical Engineers, New York, 1987.

11. S. A. David, J. M. Vitek, J. R. Keiser, and W. C. Oliver, "Use of a Mechanical Properties Microprobe in the Study of Weld Metal Transformations," *Metall. Trans. A* **18A**, 1996-9 (November 1987).

12. J. M. Vitek and S. A. David, "The Aging Behavior of Homogenized Type 308 and 308CRE Stainless Steel," *Metall. Trans. A* **18A**, 1195-1201 (July 1987).

13. S. A. David, J. M. Vitek, J. R. Keiser, and W. C. Oliver, "Nanoindentation Microhardness Study of Low-Temperature Ferrite Decomposition in Austenitic Stainless Steel Welds," *Weld. J.* **66**(8), 235 (August 1987).

14. J. M. Vitek and S. A. David, "The Effect of Cooling Rate on Ferrite in Type 308 Stainless Steel Weld Metal," *Weld. J.* **67**(5), 95s-102s (May 1988).

15. S. A. David, J. F. King, and J. M. Vitek, "Microstructural Characterization and Properties of 3Cr-1.5Mo-1V Thick Section Electron Beam Welds," pp. 61-66 in *Power Beam Processing, Electron, Laser, Plasma-Arc*, Proceedings of the International Power Beam Conference held at San Diego, California, May 2-4, 1988, ed. E. A. Metzbower and D. Hauser, ASM International, Metals Park, Ohio, 1988.

3. STRUCTURAL CERAMICS

P. F. Becher

The research within this task includes collaborative studies with colleagues at ORNL in the Metals and Ceramics, Chemistry, and Engineering Technology Divisions; Texas A&M University; CSIRO-Melbourne, Australia; Rutgers University; North Carolina State University; and elsewhere.

The underlying mechanisms of mechanical, optical, electrical, or other behavior of ceramic materials are very dependent on microstructure and composition. Subtle changes in microstructure and/or composition can result in a transition in the material's response through changes in controlling mechanisms. Recognizing this, we have incorporated research on the control of microstructure and composition with studies of mechanical (e.g., toughening, fracture, and creep) behavior. Because dense ceramics are produced primarily by densification of powder compacts, we are analyzing the interactions between particulate (powder) systems to develop fundamental descriptions of how the dispersion and consolidation of single- and multiple-phase particulate systems can be regulated to develop desired microstructures and compositions during subsequent densification processes. Analytical electron microscopy (AEM) is employed to develop understanding of both the microstructural and compositional evolution during densification and the role of these in studies of toughening, fracture, and creep processes. This interactive approach provides a critical basis for developing analytical descriptions of mechanical behavior and the chemistry and physics required to develop the necessary microstructural/compositional characteristics.

3.1 TOUGHENING BEHAVIOR AND MECHANISMS IN CERAMICS

Two major areas of toughening behavior have been addressed in our research — transformation toughening and whisker/fiber reinforcement. Advances in each of these are briefly described in the following sections. Pertinent scientific issues concerned with the development of critical microstructural characteristics/designs during fabrication are discussed in the final section.

3.1.1 Transformation Toughening Behavior – *P. F. Becher, C. H. Hsueh, M. V. Swain,[1] and G. M. Begun[2]*

The fact that microstructure, in particular grain size, can influence the martensitic transformation behavior of zirconia ceramics is an important, although often overlooked, characteristic. The basis for such microstructural scaling effects on the martensitic transformation is also a subject of debate. By employing solutions that define the

relationship between temperature and stress associated with the martensitic transformation, we have defined a grain-size-dependent transformation behavior that is consistent with experimental observations of a variety of transformation phenomena.[3]

To understand such behavior, we first note that a key determinant in the transformation toughening contribution is the magnitude of the external stress required to transform the tetragonal ZrO_2 phase to the monoclinic phase. This is important because decreasing the stress required for the transformation results in increasing the size of the transformation-zone generated by the crack tip stress field. This is the basis for increasing the fracture toughness in zirconia ceramics and composites. This feature of the martensitic transformation in zirconia is, of course, analogous to the toughness increases achieved by crack-tip plasticity in metallic systems brought about by lowering the yield stress. As shown in our earlier studies,[4] thermodynamic considerations of the transformation allow one to describe the observed transformation toughening vs temperature behavior and relate such behavior to the transformation characteristics (e.g., transformation temperature and stress).

In the case of constrained tetragonal grains or particles, the internal strain energy changes associated with the transformation inhibit the transformation. During cooling, the tetragonal-to-monoclinic transformation can be initiated even though no external stress is applied. Under these conditions, the transformation starts when the temperature T is less than the martensite start temperature M_s, Fig. 3.1.1. In dense zirconia ceramics containing tetragonal particles or grains, the total energy change U_T now required for the transformation is the sum of the chemical free energy $\Delta G^{t\text{-}m}{}_c$ and internal strain energy ΔU_i changes. Figure 3.1.1 also shows that M_s must also be $<T_o$, which is the temperature at which $\Delta G^{t\text{-}m}{}_c = 0$.

When $T > M_s$, $\Delta U_T > 0$ and additional energy must be supplied to transform the tetragonal phase. The source of this additional energy can, of course, be the external strain energy derived from the applied stress acting on the system. The amount of external strain energy required ΔU_{SE} is

$$\Delta U_{SE} = \sigma_A \epsilon = \Delta U_T , \qquad (1)$$

where σ_A and ϵ are the applied stress and the resultant total strain, respectively.

When $T = M_s$, the transformation occurs spontaneously and $\Delta U_{SE} = 0$, so that

$$\Delta U_i = \Delta S(M_s - T_o) , \qquad (2)$$

noting that the change in entropy for the tetragonal-to-monoclinic transformation $\Delta S < 0$. This relation points out that ΔU_i changes as a result of variations in M_s

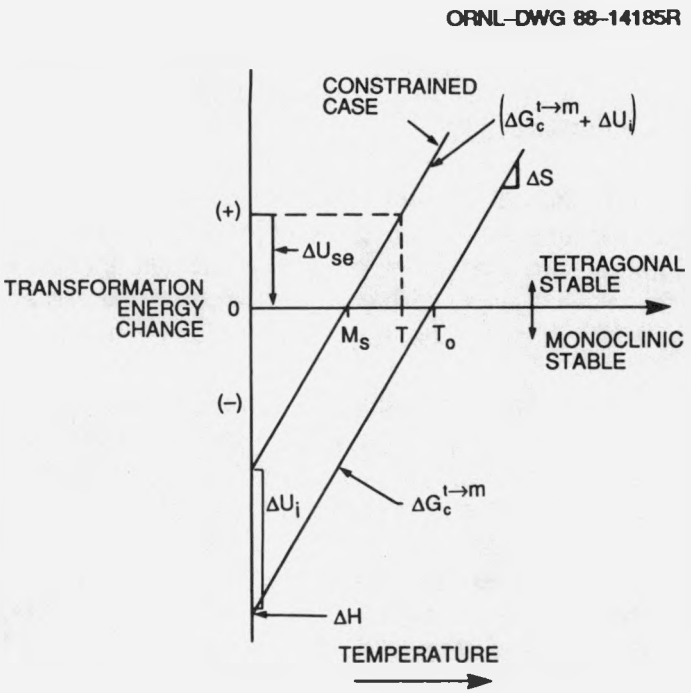

Fig. 3.1.1. Energy is required (+) to transform polycrystalline tetragonal zirconia (constrained case) at temperatures $>M_s$. Required energy can be supplied by action of external applied stress.

because ΔS and T_o are material constants. Thus, the effects of microstructure and alloying will be reflected in the M_s temperature.

Combining these conditions, we find that the tetragonal phase is the stable phase when $T > M_s$, with external strain energy of the magnitude

$$\Delta U_{SE} = \Delta S(T_o - T) + \Delta S(M_s - T_o) = \Delta S(M_s - T) , \qquad (3)$$

required for the transformation, Fig. 3.1.1.

Let us now examine further the internal strain energy term which, unlike $\Delta G^{t\text{-}m}_c$, is not a material constant and is affected by alloying and microstructure. The sources of the internal strain energy changes are the volumetric 3ϵ and shear τ strains associated with a transformation triggered by the applied tensile σ_A and shear τ (i.e., $\tau = \cos\phi\ \sigma_A$) stresses. (Note that ϕ is the angle between the applied stress axis and the shear plane/direction.) The internal strain energy change, Eq. (1), is the sum of these two stress-strain terms,

$$\Delta U_i = \tau\gamma + \sigma_A\epsilon = \sigma_A(\epsilon + \gamma/\cos\phi) , \quad (4)$$

in the absence of any other stresses.

The magnitude of the external applied stress required to drive the transformation can be reduced by internal tensile stresses present in the materials. There are several sources of these internal stresses, including thermal expansion anisotropy and transformations. In the case of MgO-PSZ ceramics, internal tensile stresses are also generated by the formation of delta-phase during low-temperature anneals.

In tetragonal phase polycrystalline zirconias, the anisotropy in crystallographic thermal expansion coefficients, σ_A vs σ_C, provides additional local thermal expansion anisotropy (TEA) stress σ_r, which can impose tensile stress on grain boundaries and assist the transformation.[5] The level of these stresses at $T << T_{SR}$, the temperature below which diffusive processes no longer relieve the stress, is directly related to the thermal expansion anisotropy and the magnitude of T_{SR} and the elastic modulus.[6] Studies show that the thermal expansion anisotropy of yttria-doped tetragonal zirconia and the associated TEA stresses at a given temperature increase with decrease in yttria content.[5] Thus, under identical test and microstructural conditions, decreasing the yttria content would diminish the external stress required to transform the polycrystalline tetragonal zirconia.

The transformation of polycrystalline tetragonal zirconias involves laths/variants that behave as mechanical twins do and can similarly produce very extensive permanent deformations. For coupled transformations, stress concentrations at twin-grain boundary intersections produce pileup stresses and promote the transformation of the adjacent grains. Electron microscopy studies have suggested that the growth of such variants/twins involves dislocation motion. Several models have been derived to show that the twinning shear can be generated by leading-edge twin dislocations. These models lead to stress concentrations because of twin/variant-grain boundary intersections that have the form of a Hall-Petch pileup stress,

$$\sigma_{pu} = \sigma_o + k\, d^{-1/2} , \quad (5)$$

where σ_o is a constant, k is a constant, and d is the tetragonal phase grain size. The σ_o term will be altered by the type and amount of alloying element used.

To initiate the transformation, we require a stress equal to the critical transformation stress σ_c^T. The stress required is the sum of the external σ_A and internal stresses (e.g., the TEA stresses σ_r and the grain boundary pileup stresses σ_{pu}),

$$\sigma_c^T = \sigma_A + \sigma_r + \sigma_{pu} . \quad (6)$$

At M_s, no external stress ($\sigma_A = 0$) is required to transform the material, and in the presence of the internal stresses, the internal strain energy change becomes

$$\Delta U_i = (\sigma_o + kd^{-1/2} + \sigma_r)(\epsilon + \gamma/\cos\phi) , \quad (7)$$

which is obtained by substituting the term $(\sigma_r - \sigma_{pu})$ for σ_A in Eq. (4). Combining Eqs. (2) and (7), we now can define the martensite start temperature in terms of grain size,

$$M_s = T_o + (\gamma\delta k/\Delta S)d^{-1/2} + (\sigma_o + \sigma_r)(\delta/\Delta S) , \quad (8)$$

where $\delta = \epsilon + \gamma/\cos\phi$. As seen in Fig. 3.1.2, our experimental observations for polycrystalline zirconias containing 12 mol % ceria support the $d^{-1/2}$ dependence of the M_b, which is equivalent to the M_s temperature in this material.

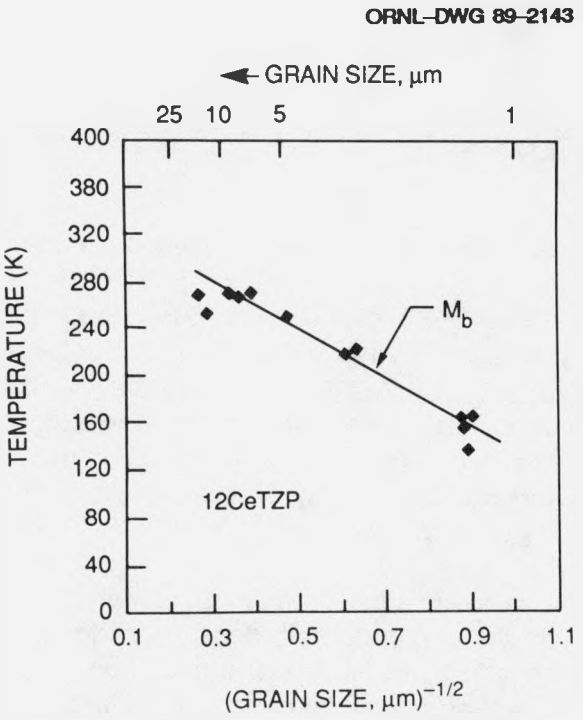

Fig. 3.1.2. The martensite start temperature M_b for the tetragonal to monoclinic transformation increases with increase in the grain size of the polycrystalline tetragonal zirconia.

This then provides a rationale for microstructural scaling effects on the martensitic transformation in polycrystalline zirconia. This also emphasizes the fact that one can tailor the transformation by grain size control and use measurements of the transformation temperature as a measure of this. Note that if we also include the influence of solute content on the TEA stresses σ_r, we can define the M_s temperature in terms of both grain size and solute content.

The critical issue then is how to enhance the transformation toughening contribution. We can illustrate this by combining the above results with a previous analysis that showed that the toughness increase resulting from the stress induced transformation ΔK^T_{IC} is greatest when the external strain energy required is least or when T approaches M_s for the case of $T > M_s$.[4] The transformation toughening contribution is then defined as

$$\Delta K^T_{IC} = AB^{1/2}(\epsilon)^2 V_f E K^m_{IC}/\Delta S(M_s - T) , \qquad (9)$$

where A and B are geometric constants, V_f is the volume fraction of tetragonal phase that is transformed, and K^m_{IC} is the fracture toughness of the untransformed parent phase.[4] For a fixed composition, E, ϵ, and K^m_{IC} are constants at a given test temperature. Substitution of Eq. (8) into Eq. (9) yields

$$\Delta K^T_{IC} = AB^{1/2}(\epsilon)^2 V_f E K^m_{IC}/\{(T - T_o)\Delta S + \delta[(\sigma_o + \sigma_r) + \gamma k d^{-1/2}]\} , \qquad (10)$$

which defines the grain size dependence of the transformation toughening contribution.

When T is constant, $T_o - T$ and S are constants, and if the material composition is made constant, σ_o, γ, σ_r, ϵ, and k will each be constants. Thus, one can show that for a given composition (e.g., 2 mol % Y_2O_3 TZP) the transformation toughening contribution will be increased by increasing the size of the tetragonal grains. The experimental data for polycrystalline tetragonal zirconias containing either 12 mol % ceria or 2 mol % yttria provide distinct support for the predicted grain size effect on the transformation toughening contribution, Fig. 3.1.3.

The analysis of the grain-size-dependent martensitic transformation in polycrystalline zirconias provides an important description for the microstructural design of monolithic zirconias and input for the design of composite materials. The twinning-dislocation pileup mechanism defining the grain-size-dependent coupled martensitic transformations in zirconias is a new approach but one consistent with various observations. Finally, the analytical approach also includes a basis for including some aspects of alloying behavior (e.g., those related to thermal expansion anisotropy). This provides a framework for constitutive relationships for the design of transformation toughened ceramics and composites.

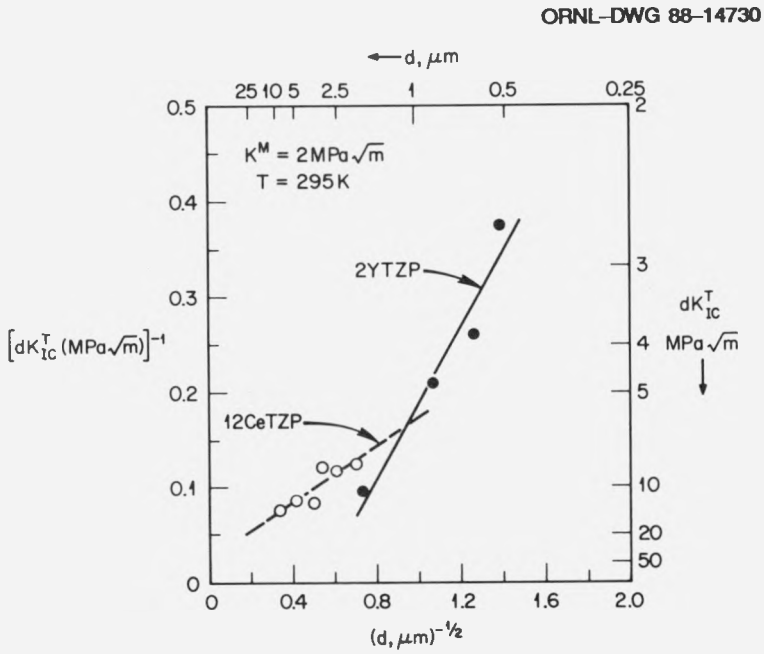

Fig. 3.1.3. The transformation toughening contribution at room temperature exhibits a substantial increase with increase in size of the tetragonal grains in both ceria (12 mol %) and yttria (2 mol %) doped polycrystalline zirconias.

3.1.2 Some Considerations of Nonideal Transformation-Zone Profile[7] – *C. H. Hsueh and P. F. Becher*

The nonideal transformation-zone profile, in which the volume fraction of transformed particles decreases with the increase in the lateral distance from crack surfaces, is considered for the stress-induced phase transformation in ceramics containing zirconia. It is shown that one source of this nonideal transformation-zone profile can be the size distribution of the transforming particles/grains. The effect of particle-size distribution on the transformation-zone profile emerges by considering the particle-size dependence of the critical stress required to induce the transformation. The stress can be the dilatational or shear component or the combination of these stresses. The nucleation argument indicates that larger particles are more readily transformed. Also, the requirement of minimum total free energy predicts that larger particles can be transformed at lower stresses. The model described in Sect. 3.1.1 yields a size dependent transformation condition based on a pileup stress. Because particle-size distributions always exist in ceramics and the stress decreases with the increase in distance from the crack tip, the volume fraction of particles that transform is expected to decrease with the increase in distance from crack surfaces as the crack grows, which in turn results in a nonideal zone profile.

The prediction of the nonideal transformation-zone profile can be achieved for a given particle-size distributions and constitutive equations for particle-size dependence of the toughness. The trends of nonideal transformation-zone profiles revealed in the sample calculation are expected to obtain for other particle-size distributions and other constitutive equations for particle-size dependence of the toughness, albeit that specific transformation-zone profiles must be material dependent. However, the derivation of the equation of toughening resulting from the nonideal zone profile is general in nature and is not limited by the type of particle-size distributions or the functional dependence of the toughness on the particle size.

3.1.3 Crack-Tip Toughening by Inclusions with Pairs of Shear Transformations[8] – *S. –J. Chang[9] and P. F. Becher*

The deviatoric transformation strain of an inclusion is modeled by applying an equivalent distribution of dislocations along a surface that exhibits a discontinuous change in the transformation strains. This method is applied to qualitatively model the twin structures generated in transformation-toughened ceramics. For this case, the transformation shear strain of the inclusion is assumed to consist of a number of symmetrical pairs of (twinning) shears in a rectangular grain. The elastic energy is derived and expressed in terms of elementary functions. For the case of one pair of shears, the inclusion-induced-toughening effect in the presence of a crack is calculated by applying a recent solution of the crack-dislocation interaction problem. Numerical results show that the toughening resulting from the shear in the inclusions (as compared with that resulting from dilatation) is significant, particularly when the inclusion is located within a distance of the crack tip equal to or less than several grain sizes. Moreover, the toughening depends strongly on the orientation of the inclusion relative to the crack.

3.1.4 Whisker-Reinforcement Toughening Behavior – *P. F. Becher, C. H. Hsueh, P. Angelini, and K. Alexander*

Ceramics reinforced with strong whiskers and fibers can exhibit very high toughness and strength. The toughening mechanisms associated with the ceramic whiskers/fibers involve (1) elastic bridging of the crack, (2) interfacial debonding coupled with frictional bridging, (3) pullout, and possibly (4) crack deflection. In fact, we have shown that during fracture, one or all of these mechanisms may be operating. A key feature in this is the matrix-whisker interface. Theoretical studies of frictional whisker/fiber sliding illustrate how the interfacial shear strength can be altered by differences in thermal expansion coefficients and elastic properties between matrix and fiber and by the interfacial friction coefficient. The analyses further show that thin interface layers can alter the radial clamping stress on the whiskers and decrease the interfacial friction stress. These aspects allow us to alter the interface characteristics and enhance frictional bridging and pullout. In addition, the interfacial friction stress established during tensile and compression loading were shown to be neither equivalent nor constant along the fiber length because of Poisson's effect. Thus, evaluation of interfacial sliding properties in various composites can only be made under well-defined loading-configuration and sample-thickness conditions.

AEM studies are used to provide critical insight into the interface characteristics and their modification in conjunction with the above theoretical results. For instance, AEM results show that the amorphous oxide surface layer on SiC whiskers can be replaced by a carbonaceous surface film vs a hyperstoichiometric region with appropriate heat treatments. These surface layers, of course, allow us to modify the interfacial properties of the composite and either enhance or diminish frictional bridging/sliding and pullout of the whisker in the matrix as noted previously.

The analytical models of composite toughening behavior provide a framework with which to explore the contributions of other mechanisms. For example, we can now describe and evaluate the effects of matrix-toughening processes. First, both experimental and theoretical results demonstrate the substantial improvements achieved by combining transformation toughening and whisker reinforcement. In this case, the coupled toughening effects, in fact, are synergistic and the result is greater than the sum of the parts. On the other hand, the coupled toughening response of microcrack toughening and whisker reinforcement are additive. Second, the toughness achieved by whisker reinforcement can be amplified by matrix grain bridging. A toughness of 8 MPa $m^{1/2}$ could be obtained with only 5 vol % SiC whiskers in a 15-μm-grain-sized alumina vs 20 vol % in a 2-μm-grain-sized alumina because matrix grain bridging is activated in the larger-grained alumina, Fig. 3.1.4. Third, crystallizing the amorphous grain boundary phases introduced by the use of sintering additives also increases the toughness of whisker-reinforced ceramics. The combination of analytical models and experimental observations provide important insights into the design of toughened systems.

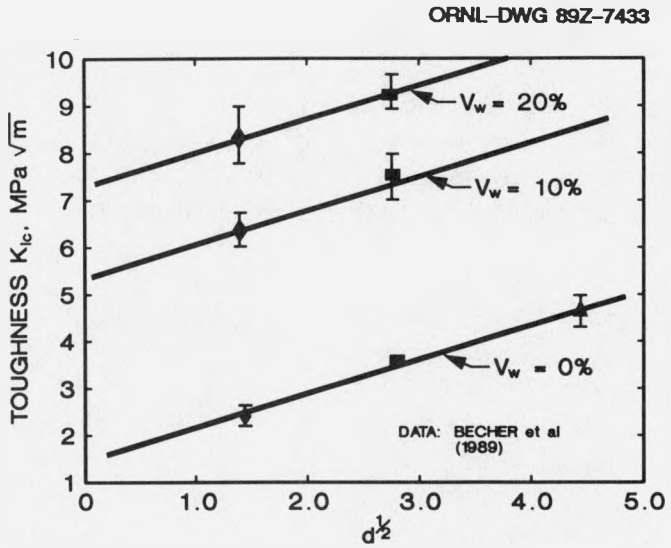

Fig. 3.1.4. Matrix microstructure can influence the toughness because of matrix grain bridging in alumina reinforced with SiC whiskers.

The mechanisms responsible for the toughening achieved by whisker reinforcement include both whisker bridging and whisker pullout within a zone immediately behind the crack tip.[10,11] Such processes are noted in fracture surface observations and scanning and transmission electron microscopy studies of cracks in these composites, Fig. 3.1.5.

The establishment of a whisker bridging zone in the crack-tip wake results in increased toughness ΔK^{wr}, which is defined as

$$\Delta K^{wr} = 2\sigma^c (2D_B/\pi)^{1/2} , \tag{11}$$

where σ^c is a closure stress imposed on the crack by the bridging whiskers over a zone of length D_B. In the case of aligned whiskers, the closure stress is the sum of the stress exerted by each whisker in the bridging zone (equal to the whisker tensile fracture strength of σ_f^w).[10]

When there is a strong toughening contribution from whisker reinforcement, the bridging zone length can be determined by analyzing the crack-opening displacement, which must equal the maximum tensile displacement in the debonded whisker at the far end of the bridging zone. From this and the analytical solutions for interface separation vs whisker fracture to define the debonded length of the whisker-matrix interface, we obtain

$$D_B = (\gamma^m E^c/\gamma^i E^w) [\pi\ r/48(1 - \nu^2)V_f] , \tag{12}$$

where γ is the fracture energy, E is the Young's modulus, r is the whisker radius, ν is the Poisson's ratio, V_f is the volume fraction of whiskers, and the superscripts m, c, i, and w refer, respectively, to the matrix, composite, interface, and whisker. The toughening contribution from whisker bridging ΔK^{wr} is then defined as

$$\Delta K^{wr} = \sigma_{fw} \{[V_f r/6(1 - \nu^2)](E^c/E^w)(\gamma^m/\gamma^i)\}^{1/2} , \tag{13}$$

for the case where whisker bridging imposes a uniform closure stress over the bridging zone.

These and companion analytical solutions[10] are found to accurately describe the experimentally observed toughening behavior in a variety of SiC-whisker-reinforced ceramics (e.g., alumina, mullite, and glasses) as shown in Fig. 3.1.6. First note that the toughness increases with increasing volume fraction of whiskers V_f as predicted by Eq. (13). Second, the toughening effects increase with increase in elastic properties of the composite for given whisker properties and whisker content V_f.

ORNL-PHOTO 4683-88R2

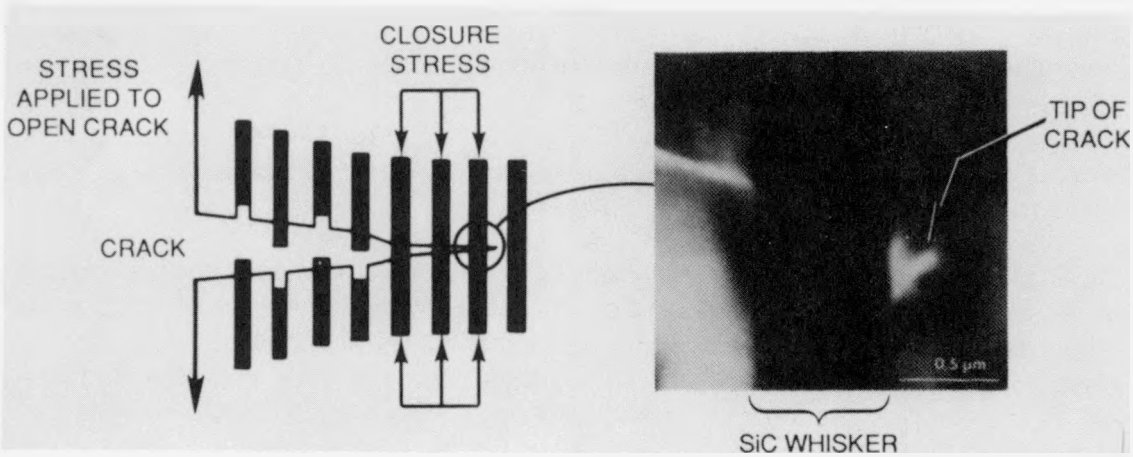

Fig. 3.1.5. The resistance to fracture is increased by reinforcing the ceramic with strong microscopic whiskers, which bridge the crack surfaces together.

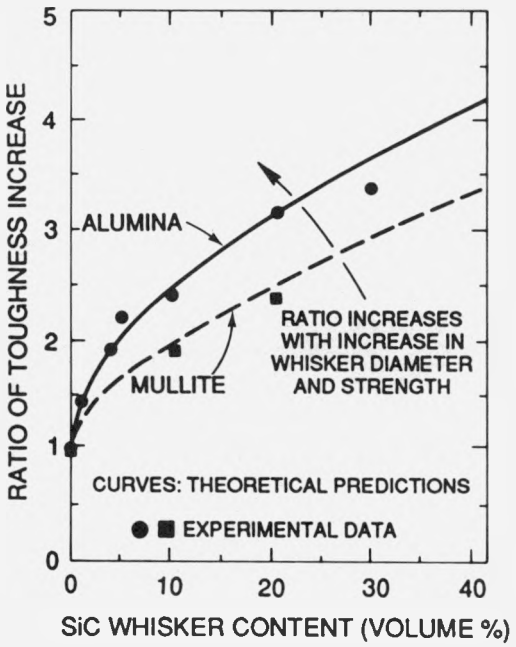

Fig. 3.1.6. The theoretical analysis of toughening behavior (curves):

$$\Delta K^{wr} = \sigma_f^{w}\left[\frac{V_f r}{6(1-\nu^2)}\,\frac{E^c\,\gamma^m}{E^w\,\gamma^i}\right]^{1/2},$$

(1) describes toughening effects observed in various ceramics (symbols) and (2) allows us to design new toughened ceramics based on material parameters.

Figure 3.1.6 illustrates this effect, where the value of E^c increases in order from the mullite to the alumina-based composites at any given value of V_f. Additional experiments also confirm the predicted dependence of the toughness on the radius of the whiskers and the ratio of the fracture energy of the matrix to that of the interface. Thus, the theoretical descriptions accurately predict which whisker, matrix, and interface properties must be controlled to obtain further increases in toughness by whisker reinforcement.

It became evident during the course of this work that the analytical solutions would also be affected by the form of the closure stress distribution within the bridging zone. Neither existing analytical descriptions nor experimental techniques were able to resolve the problem. Therefore, we derived additional analytical solutions that now allow us to determine the bridging stress distribution. The results can be incorporated into the toughening analysis.

In terms of the application of ceramics, the current results have considerable impact. First, they provide a rationale for designing whisker-reinforced ceramics. Second, because we have shown that the strength and size of the whiskers are critical features, research and development efforts have been stimulated to understand how to control these during whisker synthesis. Finally, our results allow us to focus on critical aspects of the toughening response of such composites. It is clear that the structure and properties of interfaces can substantially alter the toughness, and we have initiated studies to begin to define the structure-property relationships of the interfaces that are pertinent to ceramic composites.

3.1.5 Modelling of Interface and Related Behavior in Reinforced Ceramics – *C. H. Hsueh, P. Angelini, P. F. Becher, and M. C. Lu*[15]

Whisker- and fiber-reinforced ceramic composites have promising applications over a wide temperature range. Consequently, thermal properties and thermal stresses induced during temperature changes must be considered in the material design and various applications. The effects of (1) fibers on the thermal expansion coefficient[16] and (2) films at the fiber/matrix interface on the thermal stress of the composite have been revealed.[14] The first provides physical insights into the influence of internal stresses, induced by the thermomechanical mismatch between the fiber and the matrix, on the thermal expansion behavior of the composite. The second indicates characteristics resulting from the presence of the interfacial film and provides guidance regarding the minimization of the thermomechanical stresses in the composite.

Toughening of whisker- and fiber-reinforced ceramic composites results from bridging of the crack surfaces by whiskers or fibers when the composites are subjected to tension. Although the bridging stresses in fibers contribute to the toughening effect, the relative displacement in the loading direction between the fiber and the matrix at the crack surface is required to accommodate the crack-opening displacement. The bridging mechanisms for the composites have been studied.[12,13] From the crack tip to the end of the bridging zone, the characteristic behavior of the bridging stress for the typical example of toughening shows transition from elastic

bridging to friction bridging and to pullout bridging (Fig. 3.1.7). Immediately behind the crack tip, the bridging stress results from elastic stretching of the fiber while the interface remains intact. The bridging stress and the corresponding interfacial shear stress τ_i increase rapidly with the distance from the crack tip. When τ_i exceeds the interfacial shear strength τ_s, interfacial debonding followed by frictional bridging occurs. Within the frictional bridging zone, the bridging stress in the fiber σ_o, increases with the further increase in the distance from the crack tip until it reaches the fiber strength σ_s. At this point and beyond, fiber pullout occurs up to a distance behind the crack tip where the crack-opening displacement becomes greater than the fiber pullout length (Fig. 3.1.7).

Based on the above studies,[12,13] optimal conditions for toughening of the composites require debonding at the fiber/matrix interface by shear during fiber pullout and frictional sliding between the fiber and the matrix.[10,12,13,17,18] These conditions require studies of interfacial properties of composites: the interfacial shear strength and, after debonding, the interfacial frictional stress (IFS). Whereas studies of the interfacial shear strength elucidate the condition for interfacial debonding, studies of the IFS characterize the extent of the toughening effect.[12,13]

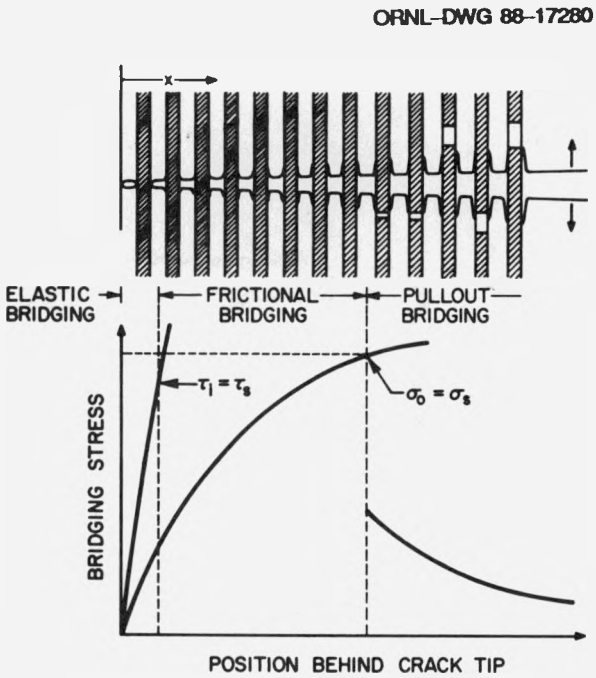

Fig. 3.1.7. Schematic diagram showing transitions from elastic to frictional to pullout bridging within the bridging zone for fiber–reinforced ceramics.

Stress transfer phenomena in which the interface remains bonded have been analyzed for the following systems: (1) from the matrix to the embedded fiber,[19,20] (2) from the partially embedded fiber to the matrix,[21] and (3) from the fiber to the coating.[22-24] The first system facilitates the understanding of toughening of the matrix by the presence of fibers. The effects of both the aspect ratio of the fiber and the Young's modulus ratio between the fiber and the matrix on the stress transfer are revealed.[19] The stress transfer phenomena are studied, respectively, when the ends of the fiber are bonded to and debonded from the matrix.[20] The second system is essential in understanding the toughening mechanism of elastic bridging and the criterion for the transition from elastic bridging to frictional bridging during cracking of the matrix. Interfacial debonding, and hence friction bridging, requires that the interfacial shear stress reaches the interfacial shear strength before the bridging stress in the fiber reaches the fiber strength. The strength requirements for the interface vs the fiber to achieve friction bridging and maximize the toughening effect for the composite are shown in Fig. 3.1.8.[13,21] The third system provides a methodology to evaluate an important parameter in controlling the toughness of the composite: the shear strength at the fiber/coating interface.[22-24]

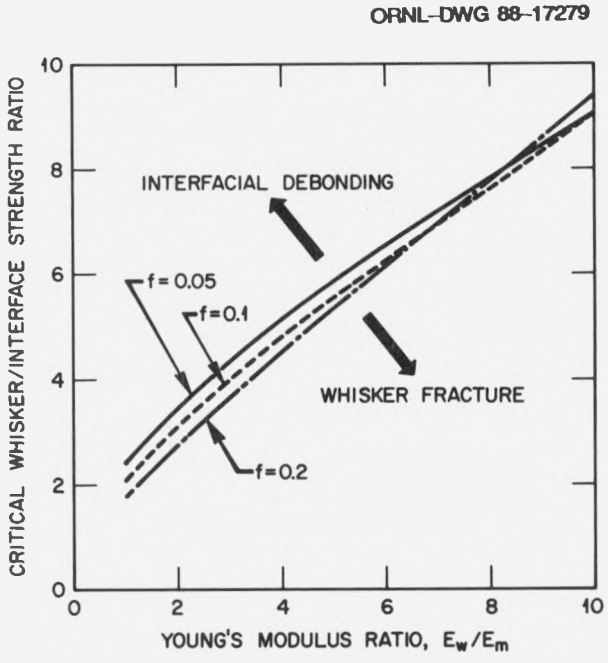

Fig. 3.1.8. Conditions of the whisker (or fiber) strength to the interfacial shear strength ratio for interfacial debonding and whisker fracture, where E_w and E_m are Young's moduli of the whisker and the matrix, respectively, f is the volume fraction of whiskers, and the Poisson's ratio of the matrix adopted in the figure is 0.25.

It has been recognized that high toughness achieved by extensive pullout requires an unbonded frictional fiber/matrix interface. The technique of indenting the end of an embedded fiber has been used extensively to evaluate the assumed constant value of the IFS, which is then used to predict toughening behavior during fiber pullout. Our study shows that the approach[25-27] must be modified. Theoretical analyses of the interfacial properties during fiber push-down (or indentation) show that the IFS is not constant but decreases along the fiber length with increasing distance from the surface as a result of Poisson's effect of the fiber. Also, the IFS increases as Poisson's ratio of the fiber, the coefficient of friction, or the residual clamping stress at the interface increases which, in turn, results in an increase in the stress transfer from the fiber to the matrix and a decrease in both the length of the sliding zone and the fiber displacement in the loading direction.[25] Furthermore, the average IFS along the sliding length is not an intrinsic property of the composite but is dependent on the loading condition.[25,26] Comparison of the interfacial properties of different composites based on the average IFS is not appropriate but must account for the effect of the loading condition.[26] Detailed analyses for both fiber push-down and fiber pullout have also been performed.[27] Comparisons of fiber push-down with pullout show substantial difference resulting from Poisson's effect of the fiber. Compared with fiber push-down, fiber pullout has lower IFS, longer sliding zone length, and greater fiber displacement in the loading direction.[27] Hence, the IFS measured from compressive loading cannot represent those appropriate to fiber pullout in tension during cracking.[26]

Composite samples having a variety of thicknesses have been used in the indentation technique such that partial sliding and push-out of the fiber occur, respectively, when the fiber is subjected to a compressive load. Based on these two indentation phenomena, two methodologies have been developed to evaluate various interfacial properties of composites including the interfacial shear strength, the residual clamping stress, and the coefficient of friction at the interface.

The solutions for both fiber push-down and fiber pullout have been derived.[25,27] Based on those solutions, a methodology of compressive loading and unloading on the exposed end of an embedded fiber is developed to evaluate the interfacial properties.[28,29] Theoretical analyses show that the loading curve (i.e., stress vs displacement relation) of the fiber is linear when the interface remains bonded.[29] The interfacial shear strength can be evaluated from the stress at which interfacial debonding initiates. In the absence of the interfacial bonding and Poisson's effect (i.e., when Poisson's ratio of the fiber is zero), the loading curve is parabolic, and after complete unloading, the residual fiber displacement equals half of the maximum fiber displacement at the peak load.[28] The residual clamping stress, the coefficient of friction, and the IFS can be evaluated from the loading and unloading curves and the residual fiber displacement after complete unloading by using the methodology developed in ref. 28.

In the fiber push-out test, the interfacial shear strength can be evaluated from the load at which debonding initiates and the corresponding stress analysis.[21,30] Interfacial sliding and fiber push-out occur after complete debonding. When Poisson's ratio of the fiber is zero, the IFS is constant and the relationship between the load required

to push out the fiber and the sample thickness is linear. On the other hand, the characteristic nonlinear relationship for a nonzero Poisson's ratio of the fiber now enables the residual clamping stress, the coefficient of friction at the interface, and, hence, the IFS to be evaluated.[30] When sample thicknesses are the same, the stress required for fiber push-out is higher compared with the stress required for fiber pullout because of Poisson's effect (Fig. 3.1.9).[31] Excellent agreement between the theoretical predictions[30,31] and the fiber push-out test of SiC-fiber-reinforced reaction bonded silicon nitride and the fiber pullout test of the steel-wire-reinforced epoxy resin are obtained.

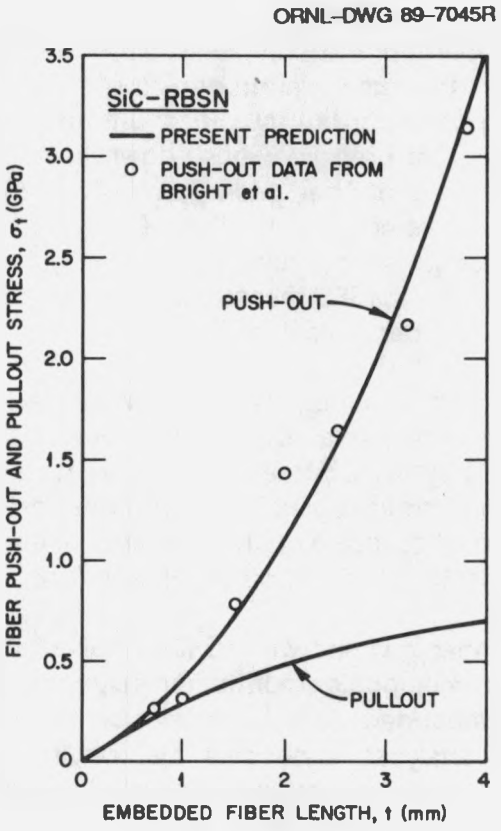

Fig. 3.1.9. The fiber push-out and the fiber pullout stresses as a function of the embedded fiber length for SiC–fiber–reinforced reaction bonded silicon nitride.

3.1.6 References

1. Materials Science and Technology Division, CSIRO, Melbourne, Australia.

2. Chemistry Division, ORNL, Oak Ridge, Tenn.

3. P. F. Becher, M. V. Swain, and G. M. Begun, "Grain Size Dependent Transformation Behavior in Polycrystalline Tetragonal Zirconia Ceramics," presented at The American Ceramic Society meeting, Indianapolis, Ind., May 1989; submitted for publication.

4. P. F. Becher, M. V. Swain, and M. K. Ferber, "Relation of Transformation Temperature to the Fracture Toughness of Transformation Toughened Ceramics," *J. Mater. Sci.* **22**(1), 76-84 (1987).

5. S. Schmander and H. Schubert, "Significance of Internal Stresses for the Martensitic Transformation in Yttria-Stabilized Tetragonal Zirconia Polycrystals During Degradation," *J. Am. Ceram. Soc.* 69(7), 534-40 (1986).

6. P. F. Becher and M. K. Ferber, "Grain-Size Dependence of the Slow-Crack Growth Behavior in Noncubic Ceramics," *Acta Metall.* **33**(7), 1217-21 (1985).

7. C. H. Hsueh and P. F. Becher, "Some Considerations of a Non-ideal Transformation Zone Profile," *J. Am. Ceram. Soc.* **71**(6), 490-93 (1988).

8. Summary of an invited paper to be published in *Micromechanics and Inhomogeneity,* G. J. Weng, M. Taya, and H. Abe, eds., Springer-Verlag.

9. Engineering Technology Division, ORNL, Oak Ridge, Tenn.

10. P. F. Becher, C. H. Hsueh, P, Angelini, and T. N. Tiegs, "Toughening Behavior in Whisker Reinforced Ceramic Matrix Composites," *J. Am. Ceram. Soc.* **71**(12), 1050-61 (1988).

11. P. Angelini, W. Mader, and P. F. Becher, "Strain and Fracture in Whisker Reinforced Ceramics," pp. 241-257 in *MRS Proceedings: Advanced Structural Ceramics*, Vol. 78, P. F. Becher, M. V. Swain, and S. Somiya, eds., Materials Research Society, Pittsburgh, Pa. (1987).

12. C. H. Hsueh and P. F. Becher, "Evaluation of Bridging Stress from R-Curve Behavior for Nontransforming Ceramics," *J. Am. Ceram. Soc.* **71**(5), C234-7 (1988).

13. C. H. Hsueh and P. F. Becher, "Some Considerations of Bridging Stresses for Whisker Reinforced Ceramics," submitted to *J. Am. Ceram. Soc.*

14. C. H. Hsueh, P. F. Becher, and P. Angelini, "Effect of Interfacial Films on Residual Thermal Stresses in Whisker Reinforced Ceramics," *J. Am. Ceram. Soc.* **71**(11), 929-33 (1988).

15. Mechanics and Materials Center, Texas A&M University, College Station, Tex.

16. C. H. Hsueh and P. F. Becher, "Thermal Expansion Coefficients of Unidirectional Fiber-Reinforced Ceramics," *J. Am. Ceram. Soc.* **71**(10), C438-441 (1988).

17. P. F. Becher, C. H. Hsueh, P. Angelini, and T. N. Tiegs, "Factors Influencing the Toughening Behavior of Whisker Reinforced Ceramics," pp. 109-12 in *Proc. Conference on Whisker- and Fiber-Toughened Ceramics*, American Society for Metals, Metals Park, Ohio (1988).

18. P. F. Becher, C. H. Hsueh, P. Angelini, and T. N. Tiegs, "Theoretical and Experimental Analysis of the Toughening Behavior of Whisker Reinforcement in Ceramic Matrix Composites," *Mater. Sci. Eng.* **A107**(1), 257-59 (1989).

19. C. H. Hsueh, "Effects of Aspect Ratios of Ellipsoidal Inclusions on Elastic Load Transfer of Ceramic Composites," *J. Am. Ceram. Soc.* **72**(2), 344-47 (1989).

20. C. H. Hsueh, "Analytical Analyses of Stress Transfer in Fiber-Reinforced Composites with Bonded and Debonded Fiber Ends," *J. Mater. Sci. Lett.*, in press.

21. C. H. Hsueh, "Elastic Load Transfer From Partially Embedded Axially Loaded Fiber To Matrix," *J. Mater. Sci. Lett.* **7**(5), 497-500 (1988).

22. C. H. Hsueh, "Analytical Evaluation of Interfacial Shear Strength for Fiber-Reinforced Ceramic Composites," *J. Am. Ceram. Soc.* **71**(6), 490-93 (1988).

23. C. H. Hsueh and M. C. Lu, "Elastic Stress Transfer from Fiber to Coating in Fiber/Coating System," *Mater. Sci. Eng.* **A117**(9), 115-23 (1989).

24. M. C. Lu and C. H. Hsueh, "Frictional Interaction in Ceramic Coating/Fiber Composites," *J. Comp. Mater.*, in press.

25. C. H. Hsueh, "Interfacial Friction Analysis for Fiber-Reinforced Composites During Fiber Push-Down (Indentation)," *J. Mater. Sci.*, in press.

26. C. H. Hsueh, "Some Considerations of Evaluation of Interfacial Frictional Stress from Indentation Technique for Fiber-Reinforced Ceramic Composites," *J. Mater. Sci. Lett.* 8(6), 739-42 (1989).

27. C. H. Hsueh, "Fiber Pullout Versus Push-Down for Fiber-Reinforced Composites," *J. Mater. Sci.*, in press.

28. C. H. Hsueh, M. K. Ferber and P. F. Becher, "Stress-Displacement Relation of Fiber for Fiber-Reinforced Ceramic Composites During (Indentation) Loading and Unloading," *J. Mater. Res.*, in press.

29. C. H. Hsueh, "Effects of Interfacial Bonding on Sliding Phenomena During Compressive Loading of an Embedded Fiber," submitted to *J. Mater. Sci.*

30. C. H. Hsueh, "Evaluation of Interfacial Shear Strength, Residual Clamping Stress and Coefficient of Friction for Fiber-Reinforced Ceramic Composites," *Acta Metall.*, in press.

31. C. H. Hsueh, "Interfacial Debonding and Fiber Pullout Stresses for Fiber-Reinforced Composites," *Mater. Sci. Eng.*, in press.

3.2 PROCESSING OF CERAMIC COMPOSITES – *A. Bleier*

The toughening behavior of composite ceramics is dictated by their composition and microstructure. The contribution of transformation toughening in zirconia-toughened alumina (ZTA) relative to that of other mechanisms, such as microcrack-derived toughening, depends on the alloy content, grain-size distribution, and spatial distribution of the zirconia.[1] Other types of toughened composites, such as those based on whisker reinforcement, also exhibit compositionally and microstructurally dependent mechanical behavior.[2]

The optimization of mechanical properties depends on our ability to reliably fabricate composites having controlled microstructural features prior to sintering or other high-temperature densification steps. In view that the precursory (green) microstructure largely dictates the microstructural evolution during high-temperature densification, powder processing is a critical component in the design of desirable microstructural and compositional characteristics of composites. These features can be reasonably adjusted using liquid suspensions containing desired precursory powders. However, most processing schemes do not specifically account for dissimilar surface chemistry and differences in particle size and material density, which can lead to clustering of particulates (agglomeration) and segregation of the two materials during the consolidation stage [Fig. 3.2.1(a)]. Our task has emphasized the colloidal and surface-chemical aspects of ceramic processing to control the microstructural design of binary oxide composites (e.g., the alumina-zirconia system). By using binary mixtures of well-characterized particles and by adjusting the chemistry of their suspensions to promote thermodynamically favorable forces, we generate densely packed particulate arrays having uniform pores prior to sintering. This approach allows us to densify composites at lower-than-normal temperatures and to achieve fine, uniform microstructures in systems for which dissimilar surface chemistry, particle size, and material density hinder our control of processing and, thereby, require unique conditions for each multicomponent system.

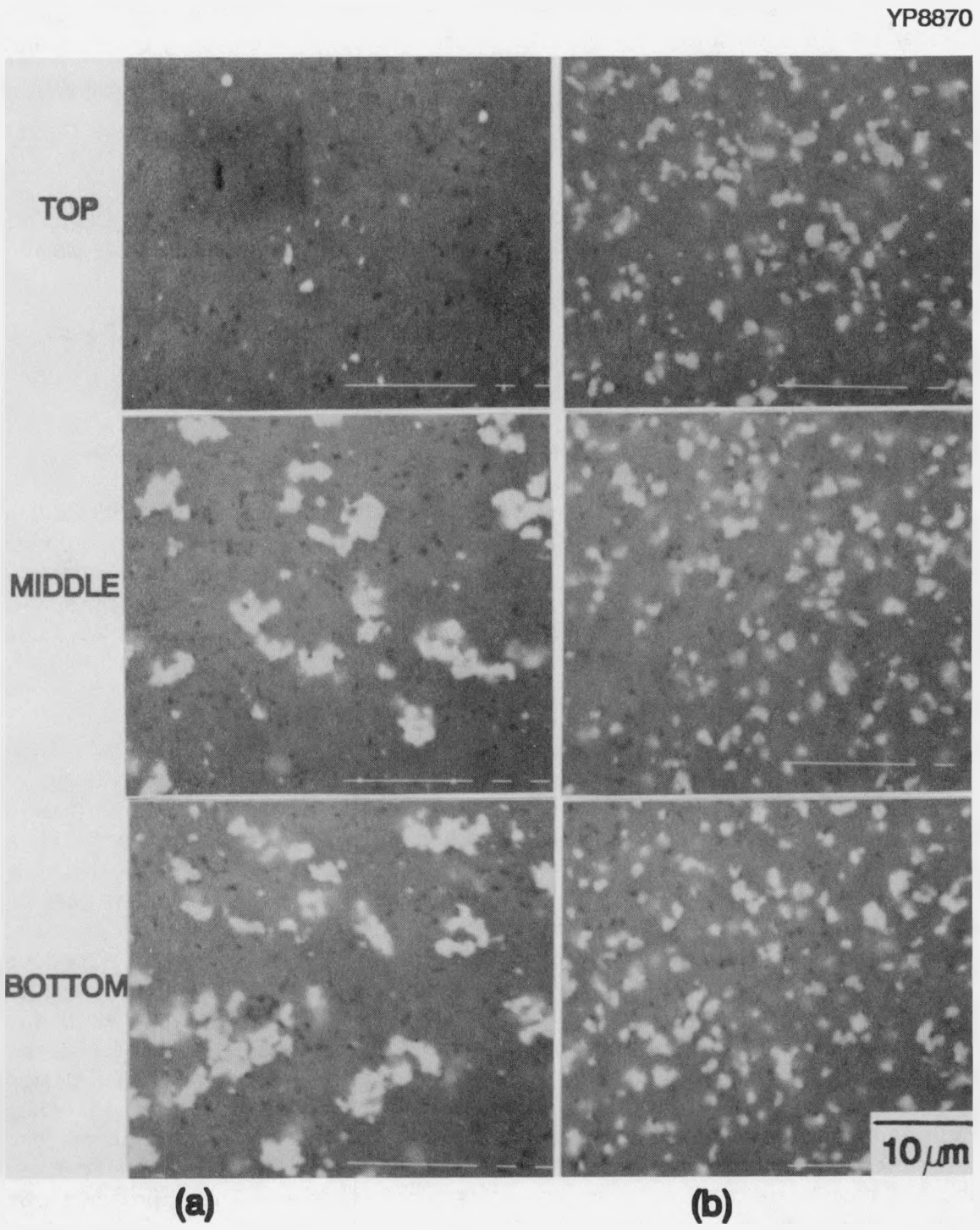

Fig. 3.2.1. Processing of positively charged powders: (*a*) SEM showing differential sedimentation in pressure-cast pellets using Al_2O_3 and ZrO_2 (bright grains); pH 3.9; (*b*) SEM showing uniform distribution; pH 5.6.

Specifically, we examine the interactions between dissimilar oxides in aqueous media [e.g., alumina (Al_2O_3) and zirconia (ZrO_2) under varied pH conditions] and form powder compacts in which particles of ZrO_2 are distributed throughout the matrix of Al_2O_3. By promoting weak, net attractive forces between these oxides, we can now generate desired microstructures in a controlled fashion for a wider variety of particle size ratios (3.5 to 0.7 for Al_2O_3:ZrO_2). The complication of differential sedimentation that commonly occurs in highly fluid, multicomponent slurries is circumvented by adjustment of the suspension pH [Fig. 3.2.1(*b*)].

Results obtained in this program demonstrate that (1) the best distribution of ZrO_2 in the Al_2O_3 matrix occurs when the two solids have the same sign of surface charge, usually positive; (2) the weak association between the two oxides which is responsible for the desirable microstructure in Fig. 3.2.1(*b*) is determined principally by the ratio of their electrostatic surface potentials; (3) this ratio needs to be critically high; and (4) it is optimal in the range pH 5 to 6. The exact pH value depends somewhat on the relative particle sizes of the two oxides. The optimal pH range is related to the isoelectric points of the two solids (i.e., the pH values at which either solid exhibits zero charge); the values for Al_2O_3 and ZrO_2 are 8 and 6, respectively, and provide for positively charged powders at pH <6, negatively charged powders at pH >8, and oppositely charged Al_2O_3 (+) and ZrO_2 (-) between these two values. Microstructures that demonstrate desirably uniform spatial distribution of the two oxides are reliably fabricated by pressure casting under conditions that avoid detrimental agglomeration, a direct consequence of the substantial, electrostatically charged surfaces characterizing the particulates. Systems with such uniform distribution of ZrO_2 also sinter more readily and predictably. Current efforts are elucidating the role of particle size ratio on densification rate and relative grain-size distribution.

Recent complementary adsorption experiments in which ZrO_2 particles were pretreated with soluble $AlCl_3$ to produce an Al_2O_3-like surface prior to mixing with those of solid Al_2O_3 constitute a critical test of points (1) to (4) in the previous paragraph and conclusively demonstrate[3] that the dissimilar chemical and electrostatic nature of the particulates underpins the association of alumina and zirconia. That is, as the magnitudes of the surface potential of the two oxides became more similar when each surface displays an alumina-like chemistry, the tendency to produce a nonuniform microstructure, as in Fig. 3.2.1(*a*), increases, even at pH ~5.6 (cf $AlCl_3$-free system in Fig. 3.2.1(*b*). Conversely, this work demonstrates that desirable microstructures form when the net surface charges on the two solids have the same sign but differ considerably in magnitude. This condition occurs near the isoelectric point of the more weakly charged solid surface, viz, ZrO_2 in the range pH 5 to 6.

Our surface-chemical approach enables us to process Al_2O_3-ZrO_2 composites, with or without typical polymeric additives,[4,5] while avoiding extensive formation of agglomerates that are difficult to densify during sintering. This feature is important because molecules adsorbed at the surface of either phase will alter the interactions of its particles among themselves and also those with particles of the second oxide. When ZTA suspensions are processed with polymeric additives, such as polyacrylic acid (PAA), to reduce viscosity in suspensions having a very high concentration of solids,

both types of particles may exhibit the same overall colloidal properties because these are now controlled by the adsorbed PAA.[5] For example, PAA possesses a negative electrostatic charge whose magnitude also depends on pH and may, then, impart each surface with nearly identical negative electrostatic properties. Thus, indiscriminate use of PAA to adjust rheological behavior of a slurry and to increase the limiting concentration of solid may generate processing conditions under which the electrostatics of each surface become virtually identical. As stated earlier, this relationship leads to differential sedimentation during consolidation and very undesirable microstructures [see Fig. 3.2.2(*a*)]. However, our research has demonstrated that PAA-containing ZTA systems can be properly processed [yielding structures resembling Fig. 3.2.2(*b*)] by maintaining a critical degree of surface coverage on each type of particle to yield a uniform distribution of ZrO_2 (i.e., without introducing problems of polymer redistribution resulting from competitive adsorption between the two oxide surfaces). Although the details differ from those describing successful processing of polymer-free suspensions, the overall guidelines itemized earlier still apply.

Our theoretical models[6] have been recently shown, for the range pH 3 to 12 and particle sizes between 0.2 and 0.7 μm, to apply equally well to binary slurries that significantly differ in detail, namely, to (1) additive-free ZTA suspensions, (2) those in which ZrO_2 was exposed to $AlCl_3$ prior to mixing with Al_2O_3, and (3) PAA-containing systems. Thus, these models provide a base from which detailed experimental advances in the Al_2O_3-ZrO_2 system are extended to other composites. This predictive element enables us to investigate the consequences of dissimilar particle shape and unequal density on the consolidation rate and the final fabricated microstructure for this and other oxide compositions, and even for nonoxides.[7-10] In addition, research to investigate the dynamic aspects of particle interaction during consolidation is planned.[11] Such issues on processing are then to be related to those operating during high-temperature densification (e.g., sintering) and to the subsequent microstructural features and mechanical properties of composites.

The work is also being extended to the processing of reaction-bonded silicon nitride (RBSN), particularly when whiskers of silicon carbide (SiC) are used to reinforce the matrix. For this system, pressure casting of silicon powder, a precursor to RBSN, and SiC whisker suspensions usually yields low green density as a result of the inefficient local packing of acicular particulates, attendant poor conversion of silicon to its nitride during nitridation because of premature closure of pore channels, and very poor distribution of whiskers because of their tendency to agglomerate.[12] The last point is critical because whiskers typically either agglomerate in bundles or settle faster than the matrix powder during casting. Consequently, an experimental program was undertaken, in collaboration with researchers at Rutgers University,[7-10] to investigate how green density and material distribution in this important system could be improved. Specifically, the use of a commercial dispersant, a polyethoxylated amine (KD-2), was studied because preliminary results suggested that green density and distribution of whiskers could be improved by the presence of KD-2 during processing.[12] Results[7,8,12] regarding the processing of silicon powder demonstrate the following:

YP8871

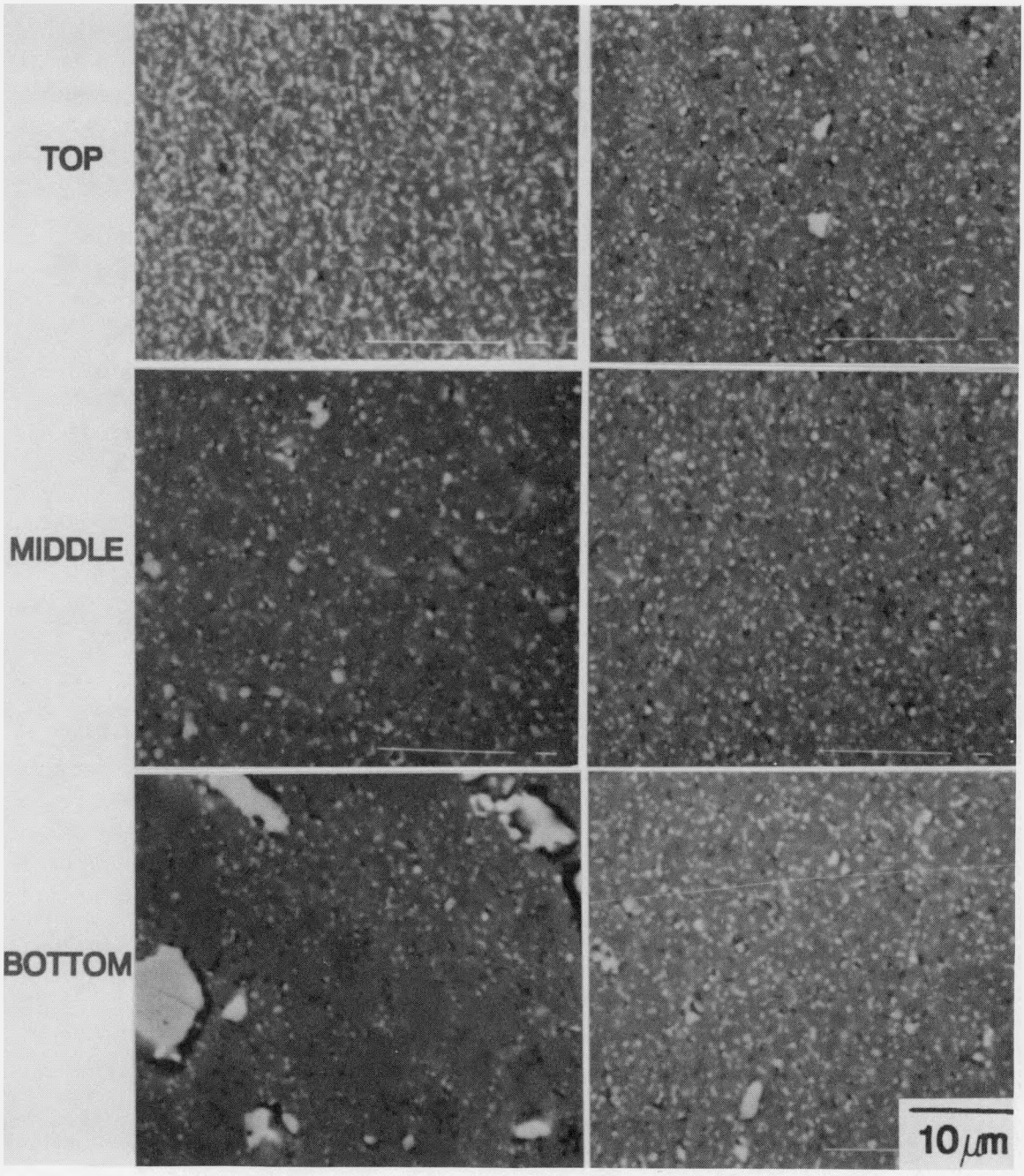

Fig. 3.2.2. Processing of negatively charged powders: (*a*) SEM showing differential sedimentation in pressure-cast pellets using PAA-coated Al_2O_3 and PAA-coated ZrO_2 (bright grains); pH 8.6; (*b*) SEM showing uniform distribution; pH 5.5.

1. Electrostatics also stabilize nonaqueous (ethanolic) suspensions.

2. Adsorption of KD-2 is governed by acid-base properties of the powder surface and additive, behavior which is comparable to that found for acidic, anionic polymer additions to basic alumina[4,5] and zirconia[5] aqueous suspensions. In the ethanolic case and contrary to the aqueous systems already described, the powder acts as an acid and the additive as a base; however, the net surface behavior of the solid remains acidic after adsorption of KD-2, indicating the dominance of the solid surface, even following adsorption.

3. An increased surface charge exists following adsorption which yields, in turn, less-dense green pellets that are more efficiently nitrided to RBSN.

Apparently, the overall effect of KD-2 is to favor a more open microstructure in the fabricated green state that allows for desirably high diffusion of nitrogen without detrimental closure of pore channels during nitridation. The generally low green density for this system seems to derive from the nonideal particle geometry, a situation which is made more complex by the chain-like structure of the silicon powder. Packing of such particulates is very difficult and is relatively insensitive to the presence of typical dispersing agents, including KD-2.

Extension of the nonaqueous processing study to include SiC whiskers[9,10] demonstrates that this solid acts as an acid in an ethanolic medium and, understandably, that KD-2 does not adsorb onto the SiC whiskers but, instead, removes acidic material inherent to the original surface. The resulting situation is that the SiC surface is made more basic in the presence of the additive, a condition that should increase the interaction of whiskers with the acidic matrix powder, especially because silicon exhibits an enhanced acidic character after exposure to KD-2, the reason for which is currently unclear. Nonetheless, recent observations in the SiC-reinforced RBSN system suggest that the bonding between the whiskers and the matrix is increased when polyethoxylated amine is incorporated in the processing of the silicon powder preform. Further work[13] is planned to elucidate better the detailed nature of these effects, their qualitative influence on toughening, and their role in modifying the details of fracture.

3.2.1 References

1. P. F. Becher, "Toughening Behavior in Ceramics Associated with the Transformation Toughening of Tetragonal ZrO_2: Overview No. 52," *Acta Metall.* **34**(10), 1885-91 (1986).

2. P. F. Becher, C. H. Hsueh, P. Angelini, and T. N. Tiegs, "Toughening Behavior in Whisker Reinforced Ceramic Matrix Composites," *J. Am. Ceram. Soc.* **71**(12), 1050-61 (1988).

3. A. Bleier and C. G. Westmoreland, "Chemical and Physical Principles of Processing That Affect Microstructure of Al_2O_3-ZrO_2 Composites," pp. 145-54 in *Better Ceramics through Chemistry III*, C. J. Brinker, D. E. Clark, and D. R. Ulrich, eds., Mater. Res. Soc. Symp. Proc., Vol. 121, Materials Research Society, Pittsburgh, Pa., 1988.

4. J. Cesarano, I. A. Aksay, and A. Bleier, "Relating Surface Chemistries to Adsorption and Stability of Polyelectrolyte Stabilized Suspensions," *J. Am. Ceram. Soc.* 71(4), 250-55 (1988).

5. A. Bleier and C. G. Westmoreland, "Effects of Adsorption of Polyacrylic Acid on the Stability of α-Al_2O_3, m-ZrO_2, and Their Binary Suspension Systems," pp. 217-36 in *Interfacial Phenomena in Biotechnology and Materials Processing*, Y. A. Attia, B. M. Moudgil, and S. Chandler, eds., Elsevier Science Publishers B.V., Amsterdam, 1988.

6. A. Bleier, "Secondary Minimum Interactions and Heterocoagulation Encountered in the Aqueous Processing of α-Al_2O_3:m-ZrO_2 Ceramic Composites," *Colloids and Surfaces*, submitted for publication, November 1988.

7. E. M. DeLiso and A. Bleier, "Colloidal Stability of Oxidized Silicon Particles in Ethanolic and Aqueous Media," pp. 171-86 in *Interfacial Phenomena in Biotechnology and Materials Processing*, Y. A. Attia, B. M. Moudgil, and S. Chandler, eds., Elsevier Science Publishers B.V., Amsterdam, 1988.

8. E. M. DeLiso and A. Bleier, "Nonaqueous Processing of Silicon for Reaction Bonded Silicon Nitride," in preparation, *J. Am. Ceram. Soc.*

9. P. Huber (Rutgers University), "Behavior of SiC Whiskers in Alcoholic LiCl and Aqueous NaCl Solutions," summer project at ORNL, 1988.

10. P. A. Huber, E. M. DeLiso, S. C. Danforth, and A. Bleier, "Processing Parameters for Whisker Reinforced Composites," in preparation, *J. Am. Ceram. Soc.*

11. Collaboration with Professor D. L. Feke, Case Western Reserve University, Cleveland, Ohio.

12. E. M. DeLiso, Rutgers University, Piscataway, N.J., private communication, June 1987.

13. Collaboration with Professor E. M. DeLiso, Rutgers University, Piscataway, N.J., since Summer 1987; present affiliation is Corning, Inc., Corning, N.Y.

4. RADIATION EFFECTS

L. K. Mansur

Research within this task covers the related areas of basic radiation effects studies and materials modification by ion beams. Benefit is also derived from research in surface modification by plasma techniques, which is supported within the group mainly by programs other than BES/DMS. Quantitative understanding of defect behavior and interactions underlying physical and mechanical properties is emphasized, leading to principles for the development of improved materials. Group efforts coordinate theoretical and experimental work to address major problems. Interactions and collaborations with other researchers include work with groups on materials for fusion reactors, applications of microstructural analysis, and surface-sensitive mechanical properties.

The radiation effects work emphasizes the evolution of microstructure and phase stability during irradiation and their relationship to properties. The aims are to explore the unique aspects of materials behavior made possible by irradiation and to develop principles for design of radiation-resistant alloys for fusion and fission reactors. Theoretical research covers original developments in the theory of radiation effects, together with modeling that both leads and supports the experimental program. Experimental studies are aimed at systematic understanding of mechanisms and processes achieved by means of critical experiments. The physical mechanisms underlying accelerated embrittlement observed in the pressure vessel of the High Flux Isotope Reactor (HFIR) have been the subject of one focus of work during this period. Numerous studies using fast neutrons or heavy ions have shown that, although cascades initiated by pka's in the keV range generate large quantities of point defects, only a few percent of them remain to participate in radiation effects. The remainder are lost to in-cascade recombination because of the high local density of vacancies and interstitials. Other studies with electrons in the MeV range and with light ions, which produce pka's measured in tenths of keV, show much higher point-defect availability, in the range 30-100%. These considerations suggest that in neutron irradiations the neutron energy spectrum will influence the point defect availability and may be a significant factor in the rate of development of radiation effects. Recent calculations at ORNL show that the thermal neutron flux at the HFIR pressure vessel is between 1 and 2 orders of magnitude larger than the fast neutron flux. Under these conditions, thermal and fast neutrons produce comparable numbers of displacements but with greatly different pka spectra. The fast neutrons produce displacements by elastic and nonelastic collisions, typically resulting in pka's of tens of keV. The thermal neutrons produce displacements by (n,γ) reactions with recoils (equivalent to pka's) of several hundred eV. These latter displacements are expected to be much more efficient in yielding available defects to form self-clusters, solute-point defect clusters, and

precipitates that give rise to embrittlement. Two predicted consequences follow: (1) embrittlement should be "accelerated" if plotted against only fast fluence, with respect to situations in which thermal neutrons are unimportant, and (2) embrittlement should correlate mainly with thermal fluence. Preliminary indications are that both expectations are fulfilled in embrittlement data from HFIR and ORR. However, the HFIR vessel and ORR in-core and near-core regions experience an overall difference in damage rate of 4 to 5 orders of magnitude which may affect the embrittlement. Experiments are being initiated to determine whether the spectral effect accounts for the observed results, or whether the difference in rate contributes.

In the area of materials modification by ion beams, a number of unique experiments have been carried out applying three beams on a specimen simultaneously. The first type of experiment was performed on Al_2O_3 with 2.0-MeV Al^+, 1.4-MeV O^+, and 0.2- to 0.4-MeV He^+ ions. The energies of the Al^+ and O^+ beams were selected so that the mean ion range was 1.2 μm for both species. The ion beam fluxes were controlled so that the Al^+:O^+ implantation ratio was close to the stoichiometric value for Al_2O_3. The helium simulates an important transmutation product in fission and fusion environments. The radiation effects were characterized using nanoindentation hardness and transmission electron microscopy (TEM). Other types of experiments centered on surface modification of metallic alloys for improving surface-sensitive mechanical properties. Beams of B, C, and N ions were applied both singly and simultaneously.

Recently developed techniques for manufacturing films of diamond and diamond-like materials have made it possible to create a wide variety of new materials in our laboratory. Nucleation and growth of diamond films grown by the hot-filament-assisted chemical vapor deposition method were studied on a variety of substrates under a wide range of conditions to provide a varied diamond microstructure. High-resolution scanning microscopy and TEM have been used to document and relate the topographic and internal features of diamond films to the film growth conditions. Growth features including twin pyramids, reentrant edges, ledges, growth spirals, and open lattice-work structures were related to growth conditions. The growth features can be rationalized in terms of hypothesized growth mechanisms, although much work remains before such mechanisms are fully understood. We have also correlated the physical and mechanical properties of the films to the growth processes through the characterization of the microstructure. Hardness, friction and wear, thermal conductivity, and infrared transmission/adsorption of selected films were measured for this purpose.

4.1 THEORY AND MODELING

4.1.1 Theory of Irradiation Creep by Glide-Induced Transient Absorption[1] – *A. D. Brailsford, W. A. Coghlan, and L. K. Mansur*

Generally accepted models for irradiation creep are based on either dislocation climb or climb-enabled glide. In the latter case, the requisite climb may be driven by a variety of processes including swelling, stress-induced preferred absorption of point

defects, or point-defect partitioning between dislocations and another type of sink, such as spatially correlated dislocation arrays or grain boundaries. The glide step in these models is assumed simply to follow when enough climb has been accumulated to permit the dislocation to escape from the pinning barrier. In particular, it is tacitly assumed that the dislocation continues to climb as before both during the glide step and when it is pinned at the next barrier. In examining this assumption, we found that the glide step is so rapid that the steady-state point-defect diffusion profiles about the dislocation are not maintained. When the dislocation arrives at the next barrier, it is as if the dislocation were suddenly created in a sink-free region that has the average uniform point-defect concentration of the bulk. There then follows a period when the point-defect concentrations experience a transient until new steady-state profiles are established near the dislocation. During this transient, excess vacancies are absorbed at the dislocation, producing an increment of climb that can sometimes result in escape from the barrier and subsequent glide. This transient is responsible for a previously unrecognized mechanism of irradiation creep.

The development of this idea into a theoretical model was carried out as follows: The diffusion solution[2] was evaluated for a unit length dislocation suddenly placed in a uniform concentration field of defects. The time-dependent absorption of these defects at the dislocation was then calculated. The irradiation conditions, the combined effects of interstitials and vacancies, the barrier heights, and the defect bias were found to be important features of the mechanism that determine barrier escape frequency and creep.

The transient diffusion problem considered was that of a small cylinder, representing the dislocation core, suddenly removed from a medium containing uniform defect concentration. The boundary condition at the inner boundary, the dislocation core, was the equilibrium vacancy concentration C_V^o; that for the outside boundary of a coaxial source-and sink-free region was assumed to remain equal to the steady-state defect concentration C_V. The solution was evaluated numerically using an available Bessel function solution. A typical set of transient concentration vs radius plots is shown in Fig. 4.1.1 for a dislocation density of $3.2 \times 10^{13} m^{-2}$.

When the gliding dislocation arrives at the barrier, the flow of vacancies begins rapidly because the vacancies diffuse initially from the region near the dislocation. As time passes the rate of vacancy arrival abates as steady state is approached. This initial high vacancy flux and the eventual approach to steady state can be seen in Fig. 4.1.1. Note that the transient flux is related to the difference per unit time between the concentration profiles.

The total climb, accounting for absorption of both vacancies and interstitials, gives the overall time behavior of a dislocation against a large barrier. This is shown in Fig. 4.1.2 as a function of Log (Dt), where D is the diffusion coefficient of the vacancy defect and t is time. The initial climb shown in the vacancy (positive) direction is the transient climb, and the slow climb in the interstitial (negative) direction at much longer times (notice the logarithmic scale) is the persistent bias-driven interstitial climb. If the positive climb is large enough to escape the barrier, the dislocation will advance to the next barrier and an increment of creep will result. If the climb is inadequate, the

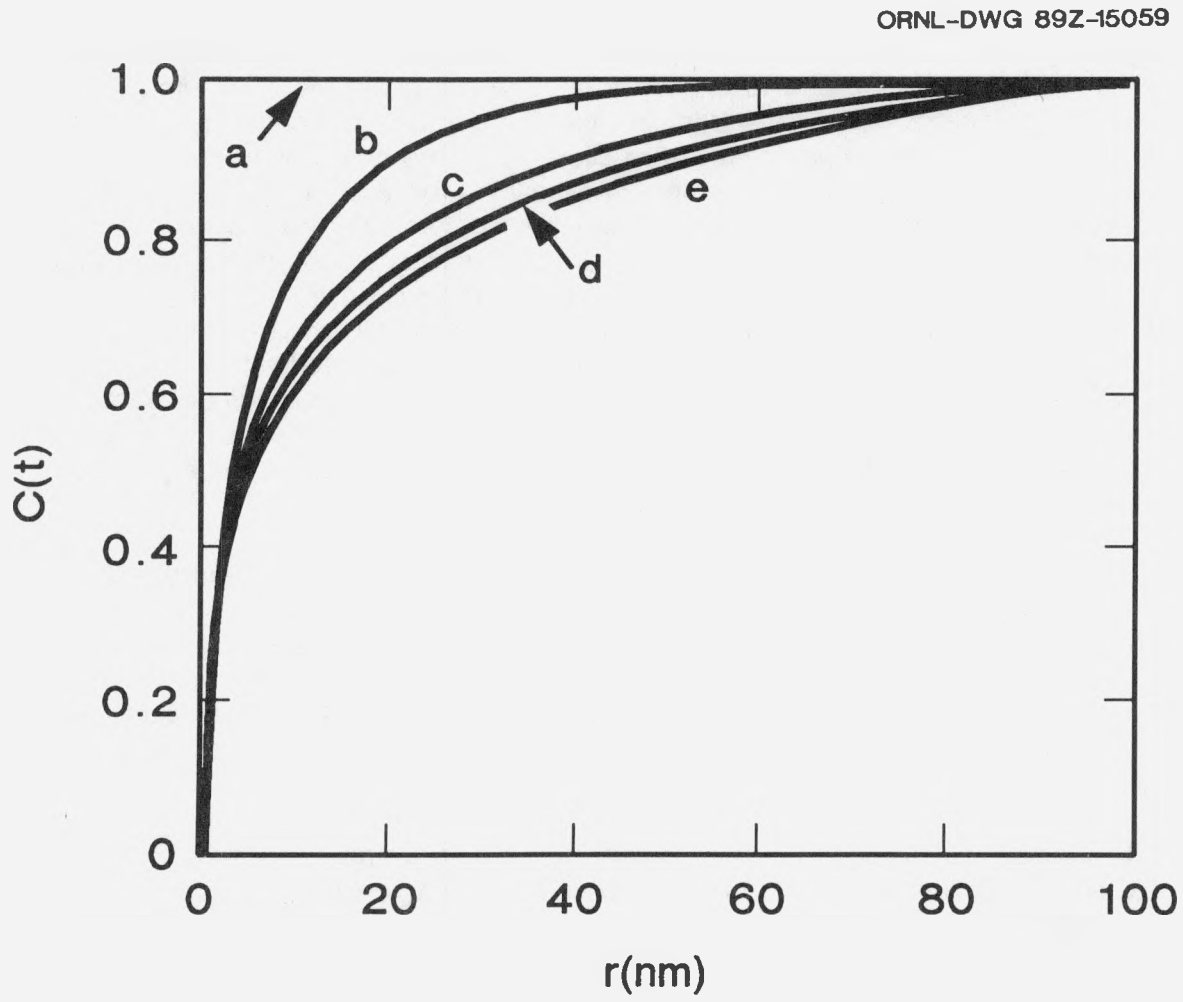

Fig. 4.1.1. The radius dependence of concentration plotted for several values of Dt from zero to infinity (steady state). The normalized time, Dt, is in units of nm^2. The plots are calculated for L = 3.2e13 m^{-2}. Dt values for curves a, b, c, d, and e are 0, 293, 1600, 3000 and infinity, respectively.

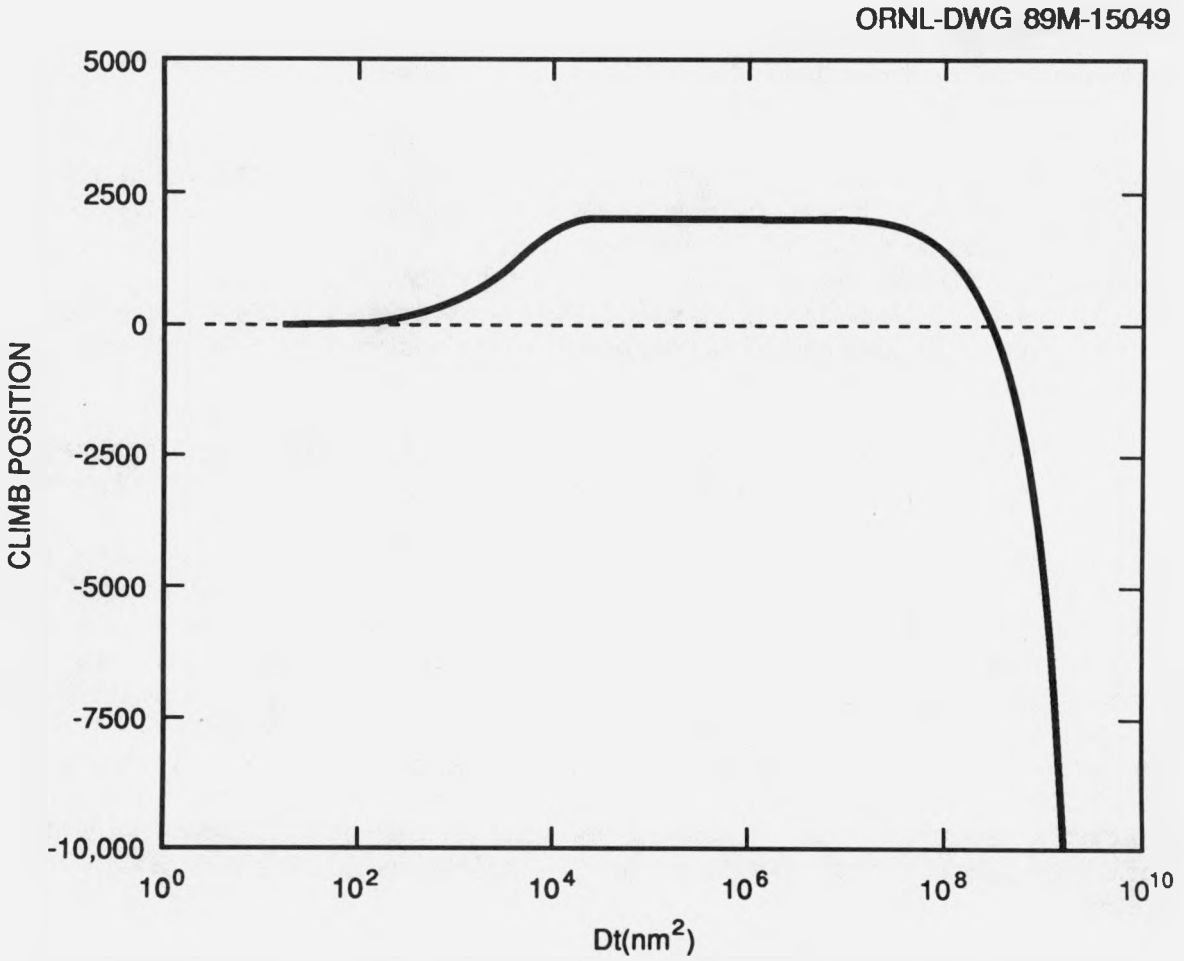

Fig. 4.1.2. Dislocation climb per unit length of dislocation in units normalized to the steady-state vacancy concentration divided by 1 x 10^{18}. The diffusion coefficient is in units of nm^2s^{-1}, and a steady-state climb rate of 0.01 of the total interstitial flux is assumed.

steady-state climb will eventually reverse the sense of the climb and the escape will eventually occur in the negative direction.

Analysis in light of this glide-induced transient mechanism shows that, in materials under irradiation at moderate temperatures, small barriers are ineffective in creep strengthening. The dislocations only stop for a short time, after which the climb excursion caused by the excessive transient vacancy influx promotes their escape. In a sense, these barriers become transparent to the dislocations. This conclusion is in agreement with experimental results such as those of Jung and Chilson,[3] who found that thorium oxide particles were ineffective in increasing the creep strength of a Ni–Cr alloy.

4.1.2 Transient Interstitial Absorption — A Mechanism for Enhanced Irradiation Creep at Low Temperatures — a. Mechanism* – *M. L. Grossbeck and L. K. Mansur*

Although irradiation creep is usually thought of as prevalent in the temperature regime of swelling where vacancies are mobile, there is no low-temperature cutoff. In fact, irradiation creep has been observed even at liquid nitrogen temperatures. However, such observations were made at low fluences and thought to be transient effects of limited duration. In the Oak Ridge Research Reactor (ORR), we have recently observed higher sustained creep rates at 60°C than in the range 330-600°C. These data, shown in Fig. 4.1.3, were acquired in a joint research program with the Japan Atomic Energy Research Institute.[4] Similarly high levels of irradiation creep were observed in laboratory heats of pure ternary austenitic stainless steels and in ferritic steels irradiated in the same experiment. The specimens consisted of pressurized tubes.

Currently accepted mechanisms of irradiation creep predict a reduction in creep of two to three orders of magnitude when temperature is reduced from 300 to 60°C. It was necessary to abandon existing steady-state models and to perform a more fundamental analysis based on point-defect kinetics to understand our new data.[5] Because the time for the vacancy population to reach steady state is longer than the duration of the experiment at 60°C, it is essential to consider transient defect behavior. To clarify terminology, here the transient we refer to envelopes the entire experiment and thus represents the behavior observed, rather than, for example, an unusual feature of short duration at the initiation of the experiment. Almost all of the climb produced by the arrival of interstitial atoms is balanced by vacancy absorption in steady state. It is the small imbalance induced by the presence of a stress that leads to the deformation in steady state. However, at temperatures as low as 60°C, of interest in the current experiments, the vacancies are essentially immobile. In this case, the climb produced by the arrival at dislocations of those interstitials that do not recombine with vacancies in the matrix is not balanced by arrival of vacancies. The result is a large climb rate. At regular intervals, a dislocation climbing in such a way will escape

---

*Research supported in part by the Office of Fusion Energy.

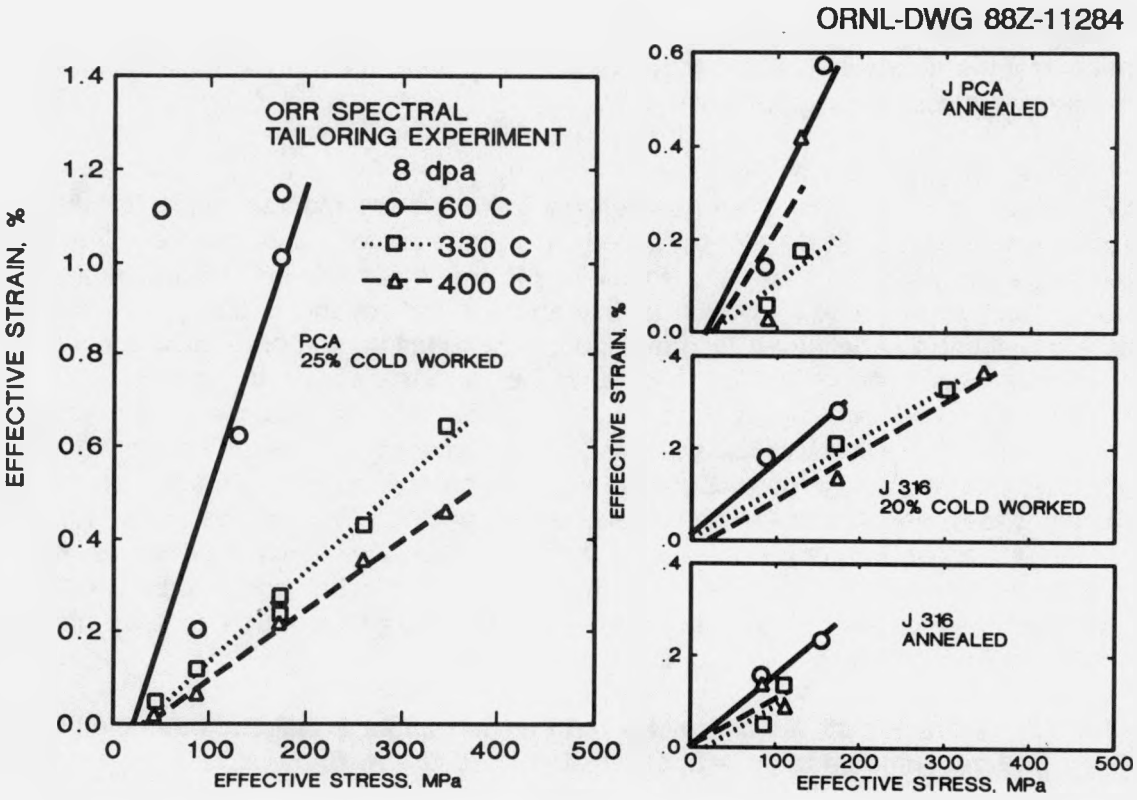

Fig. 4.1.3. Effective strain as a function of effective stress for PCA, Japanese PCA, and a Japanese heat of AISI type 316 stainless steel. The data are from pressurized tubes irradiated in the Oak Ridge Research Reactor.

an obstacle and slip, giving an increment of creep. The creep predicted by this new mechanism is larger than that occurring at steady state (i.e., at higher temperatures), in agreement with the experimental data.

This behavior can be described conceptually (see Fig. 4.1.4, a schematic of the concentrations of vacancies and interstitials following commencement of irradiation). Vacancies and interstitials are produced in equal numbers and increase linearly in concentration until the loss rate to sinks for the mobile interstitial balances their production. At this time (τ_i, which is only about a half-second at 60°C), a metastable state is reached for the interstitial population. The concentration of vacancies continues to increase until recombination begins to be significant. At this point (τ_{r1}), the concentration of interstitials begins to drop. The rate of increase in the vacancy concentration decreases simultaneously. The vacancy concentration continues to increase, and eventually the recombination rate increases to the level at which it is the dominant loss mechanism for interstitials and vacancies. Beyond this point (τ_{r2}), the concentrations of both point defects begin to approach the steady-state values, whose ratio is approximately the inverse of the ratio of interstitial and vacancy diffusion coefficients. This time (τ_v), as pointed out previously, is much longer than the irradiation time at low temperatures.

4.1.3 Transient Interstitial Absorption — A Mechanism for Enhanced Irradiation Creep at Low Temperatures — b. Calculated Results – *R. E. Stoller*

To explore this phenomenon further, fully time-dependent rate theory calculations were carried out in which the explicit dose dependencies of the point-defect concentrations were computed to obtain the creep strain as a function of dose. The calculated creep as a function of temperature and dose for an applied stress of 100 MPa is shown in Fig. 4.1.5 for doses up to 80 dpa. Experimental results for 25% cold-worked PCA at 8 dpa are also shown, and reasonable agreement is achieved. The contribution to irradiation creep by this new mechanism is important below about 250°C, where for low doses the predicted creep is higher than at higher temperatures. At higher doses, steady-state creep increases the predicted creep at the higher temperatures. The results of this work suggest that fission or fusion reactor components that operate at low temperatures may experience higher than expected levels of deformation resulting from startup-transient-induced interstitial absorption.

4.1.4 Theory of Amorphization – *D. F. Pedraza*

4.1.4.1 Radiation-Induced Microstructural Evolution[6]

Previously we developed a theoretical model to study the influence of radiation-induced microstructural evolution on the amorphization kinetics of intermetallic compounds.[7,8] In this model, the driving force for amorphization was assumed to be the buildup to a critical level of defect complexes. A complex consists of a coupled interstitial-vacancy pair, which is stable against recombination. In the current work, the process of amorphization under particle bombardment is shown to be obstructed in alloy systems in which interstitials exhibit a tendency to cluster. In these systems, interstitial clustering delays the buildup of complexes. Under electron irradiation, the

ORNL-DWG 89-14460

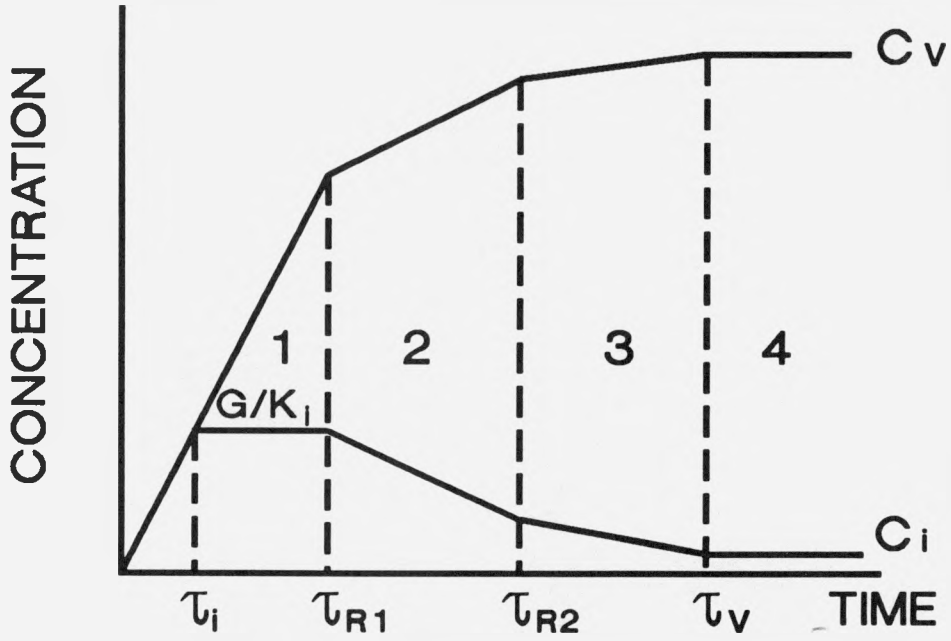

Fig. 4.1.4. A schematic representation of point defect concentration as a function of time for a strong sink density; C_v and C_i are concentrations of vacancies and interstitials, respectively.

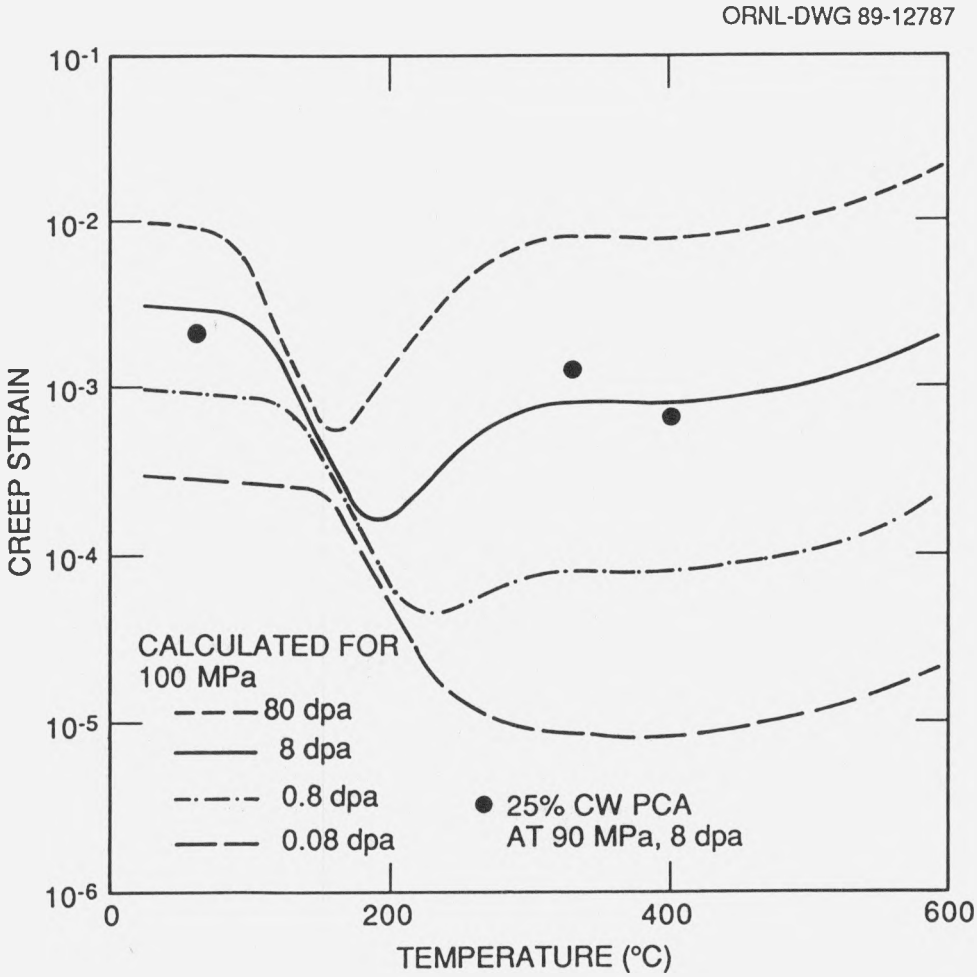

Fig. 4.1.5. Calculated and measured creep strain for 25% cold-worked PCA for an applied stress of 100 MPa.

complex concentration attains only low levels after high doses and the crystalline-to-amorphous transition is inhibited down to fairly low temperatures. During heavy ion bombardment, cascade damage increases complex formation and the transition takes place.

The current analysis highlights the profound difference between the effects of preexisting and radiation-induced microstructures on the process of amorphization. Whereas the existing microstructure may enhance the rate of complex buildup by absorbing point defects, as demonstrated in previous work,[9] the competition with radiation-induced microstructure is established at the nucleation level. Interstitial clusters, for example, are capable of destroying complexes in a process similar to that of indirect recombination with single interstitials.[7,10] The current analyses indicate that the kinetics of amorphization under ion bombardment depend on temperature at low temperatures, in which amorphization is mostly the result of accumulation of complexes. Direct in-cascade amorphization becomes more important as the bombardment temperature increases. Zr_3Al is used as a model system. Calculated amorphization kinetics are illustrated in Fig 4.1.6. These calculations yield good agreement with experimental results.[10]

4.1.4.2 Simultaneous Heavy-Ion and Electron Bombardment[11]

The theory of amorphization of ordered intermetallic compounds was applied to predict results for simultaneous irradiation by electrons and heavy ions. Our theory proposes that the local buildup of radiation-induced defects (interstitial-vacancy complexes) to a critical value in a small region destabilizes the crystalline lattice causing it to become amorphous. The rate of increase of the complex concentration results from a balance between complex formation by diffusional encounters, with a non-diffusional component representing direct production under ion bombardment, and complex annihilation by thermally activated processes. This mechanism predicts, in the case of electron irradiation, the existence of a cutoff temperature, T_e^C. Above this temperature no crystalline to amorphous transition occurs, because insufficient complex buildup. In the case of ion bombardment, a cutoff temperature, T_i^C, is also obtained above which no significant complex accumulation takes place, but T_i^C is higher than T_e^C. It is shown that simultaneous bombardment with ions and electrons leads to an acceleration of the transition up to temperatures around T_e^C and to a progressive delay and possible suppression of the transition at increasing irradiation temperatures between T_e^C and T_i^C. These results are illustrated in Fig. 4.1.7 for the case of irradiated NiTi.

4.1.4.3 Irradiation as a Tool for Studying Solid-State Amorphization Phenomena[12]

From theoretical analysis of the amorphization phenomenon under irradiation, it is proposed that a defective state characterized by localized anisotropic distortions of the crystalline lattice is the cause of destabilization. The hypothesis of a critical buildup of defect complexes affecting a region of several hundreds of atoms leads to a transition to the amorphous state with characteristics similar to nucleation phenomena, rather than to common first-order two-stage nucleation and growth processes. For two other cases of solid state amorphization phenomena, spontaneous vitrification, and interdiffusion-induced amorphization, some of the experimental evidence appears to support

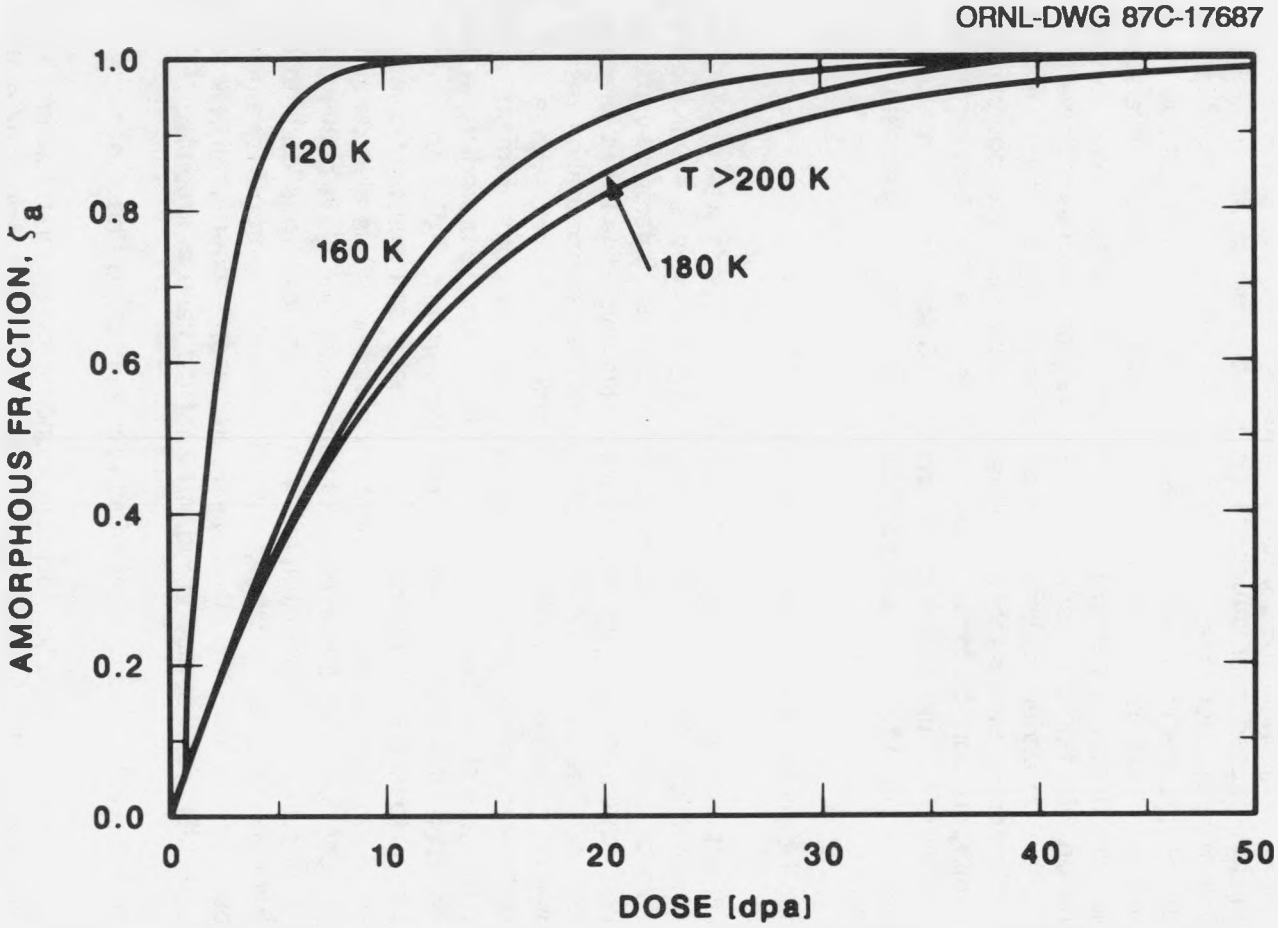

Fig. 4.1.6. Amorphization kinetics of ion-irradiated Zr_3Al at various temperatures, calculated assuming both enhanced complex production and direct amorphization events in the region of a displacement cascade.

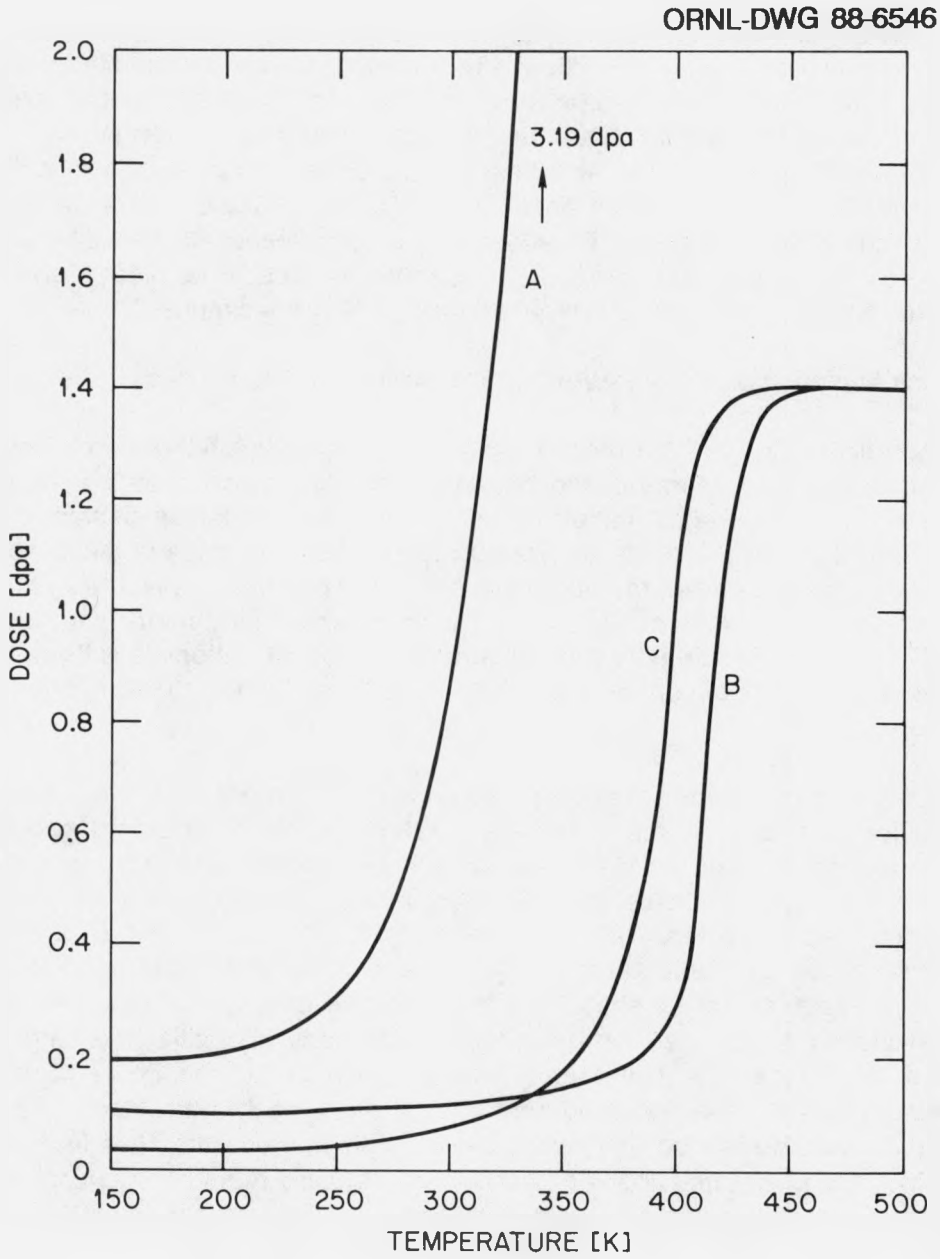

Fig. 4.1.7. Dose (the abscissa refers to the ion dose only) required to amorphize NiTi completely (97%), as a function of temperature, by irradiation with: (A) electrons ($K_e = 1.10^{-3}$ dpa/s); (B) ions ($K_i = 1.10^{-3}$ dpa/s); and (C) electrons ($K_e = 4.10^{-3}$ dpa/s); and ions ($K_i = 1.10^{-3}$ dpa/s), simultaneously.

mechanisms similar to those found during irradiation. For spontaneous vitrification, this evidence comes from X-ray diffraction and selected area electron-diffraction studies done before annealing. The patterns show that bcc (β-phase) metastable $Cr_{0.4}Ti_{0.6}$ specimens produced as thin films by laser quenching are strongly distorted and anisotropically strained.[13] These specimens experience spontaneous vitrification when solution annealed in the β-phase field. For diffusion couples, evidence is found of crystalline remnants left behind the advancing amorphous/crystalline interface during annealing of Zr-Cu diffusion couples.[14] Crystalline debris is also found in large amorphous regions produced by ion irradiation in NiTi specimens.

4.1.4.4 Ion-Implantation Induced Amorphization in Ceramic Oxides

A theoretical study of the mechanisms of ion-implantation-induced amorphization of ceramic oxides has been initiated based on the hypothesis that the production of highly localized and strongly anisotropic distortions causes lattice destabilization and the consequent transition to the amorphous state. Alpha-alumina is taken as a model system to develop a detailed mathematical approach capable of predicting the kinetics of amorphization. It is known from experimentation that many metallic and noble gas elements implanted at liquid nitrogen temperature to concentrations less than 3% induce amorphization. The effect of implantation first is being studied at these low temperatures.

Two aspects of the implantation process are considered: the site location of the implanted ion and displacement damage caused by the bombarding species. The oxygen sublattice is taken as the reference lattice. Irradiation is assumed to produce only vacancies and interstitials, of both oxygen and aluminum, and also to displace already implanted impurities from the sites on which they are located. It is assumed that aluminum can be displaced into any of the available interstitial positions but may not occupy oxygen sublattice sites. The implanted species is also assumed to occupy only interstitial sites. Oxygen can be displaced into any interstitial site, depending on the level of disorder of the aluminum sublattice. As a consequence, randomization of the aluminum sublattice is first produced. The atomic mechanism leading to localized distortions is assumed to be the accumulation of implanted impurities into tetrahedral interstices. It is postulated that once this accumulation reaches a critical value in a small region, amorphization of this region follows. Preliminary results show a fast amorphization rate, once the local impurity concentration reaches a certain level.

4.1.5 Radiation Damage in Binary Ceramic Oxides: A Preliminary Model*[15] – *R. E. Stoller*

The subject of radiation damage in ceramic materials has received increasing attention both because of ongoing ion-beam surface modification studies and the proposed use of ceramics in fusion reactors. The response of these materials to displacive irradiation has been shown experimentally to be complex. To improve our theoretical understanding of the irradiation response of ceramic oxides, a preliminary

---

*Research supported in part by the Office of Fusion Energy.

model of radiation damage in binary ceramic oxides has been developed based on an extension of the reaction rate theory that has been successfully applied to metallic alloys. The model accounts for some of the major differences between metallic alloys and ceramics that are believed to be responsible for the fact that ceramic materials behave differently than metallic alloys when exposed to displacive irradiation. To this end, the model considers the influence of a second lattice and the additional constraint of stoichiometric point-defect absorption by dislocation loops. The point-defect concentrations are then used to compute various measures of the sensitivity of these materials to the type of microstructural evolution that is observed in irradiated metals.

Initial results indicate that both the lattice and stoichiometry effects can help to mitigate radiation damage in ceramics. However, the effects are not necessarily large and, in agreement with recent data, the results indicate that at least some ceramic oxides may exhibit a sensitivity to displacement damage that is similar to metals.

One potentially significant difference between ceramics and metallic alloys that has been identified is illustrated in Fig. 4.1.8 in which the effective vacancy supersaturation on the metal lattice of the binary ceramic is plotted as a function of the net capture efficiency of the dislocation loops $(Z_i^{\ell} - Z_v^{\ell})$. The effective vacancy supersaturation, S, is defined as

$$S = \frac{Z_v^c D_v C_v - Z_i^c D_i C_i}{D_v^e C_v} ,$$

where the $Z_{i,v}^c$, $D_{i,v}$, and $C_{i,v}$ are the cavity capture efficiencies, diffusion coefficients and concentrations of interstitials and vacancies respectively, and C_v^e is the thermal equilibrium vacancy concentration. The tendency of an irradiated material toward void formation is a strong function of this effective supersaturation.[16] In the absence of any preferential attraction of one sink for either interstitials or vacancies (i.e., zero system bias in the conventional nomenclature), S = 1.0. In this case, no microstructural evolution would be observed under irradiation because all sinks would absorb both defect types at equal rates. This is not what is observed in metals, however, because dislocations preferentially absorb interstitials. In the case of a binary oxide, however, differences in either material or irradiation parameters between the two lattices give rise to what might be termed a different sort of "bias." The results shown in Fig. 4.1.8 were calculated using parameters appropriate for MgO, and all sink capture efficiencies were equal to unity except the dislocation loop capture efficiency for interstitials. As the net loop capture efficiency approaches zero, the effective supersaturation should approach unity. The solid curve in Fig. 4.1.8 shows that this is the case when all parameters on the metal lattice are the same as those on the oxygen lattice. However, there are parametric differences, the results are similar to those calculated if there were a small bias. This is shown by the dashed curve for the case in which the vacancy migration energy on the oxygen lattice is 0.1 eV greater than that on the metal lattice. Although

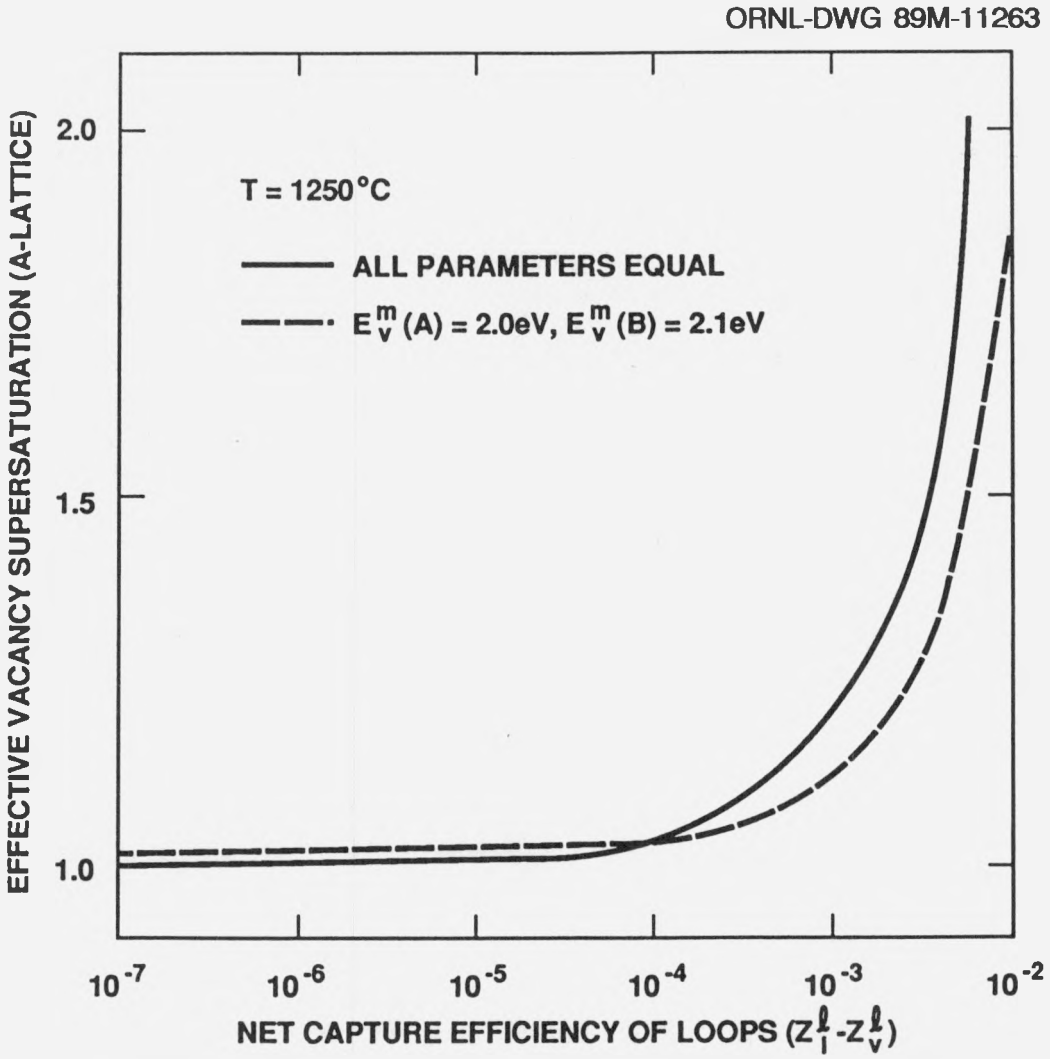

Fig. 4.1.8. Effective vacancy supersaturation on the metal (A) lattice as a function of the net capture efficiency of dislocation loops.

a small vacancy supersaturation persists on the metal lattice, a comparable subsaturation exists on the oxygen lattice.

4.1.6 Unified Theoretical Analysis of Experimental Swelling Data for Irradiated Austenitic and Ferritic/Martensitic Alloys[17] – *E. H. Lee and L. K. Mansur*

Austenitic and ferritic/martensitic alloys are the leading candidate materials for both fusion and fast-fission reactor applications. Radiation damage, swelling in particular, is known to be a life-limiting phenomenon for long-term service. During the past two decades, a large store of experimental data has been accumulated in international efforts to fully characterize the phenomenon and to provide the information necessary for the development of swelling-resistant alloys. This collection also serves as the largest source of information on which to develop and test mechanistic understanding of swelling.

An extensive theoretical framework has been developed to describe and predict swelling and other irradiation phenomena based on fundamental physical concepts. The ultimate goal is predictive accuracy under the widest possible variation in conditions. One of the important contributions of theory has been to reveal the sensitivity of cavity swelling to the point-defect sink microstructure. An important parameter is Q, the ratio of the dislocation to cavity sink strength. It is predicted that for $Q \sim 1$, cavity growth is maximum, whereas for $Q >> 1$ and $Q << 1$, cavity growth is lower.

Figure 4.1.9 plots the normalized swelling rates of alloys irradiated in various experiments against the sink strength ratio Q for various materials and irradiation conditions, such as alloy composition, damage rate, helium generation rate, and temperature. All high-swelling data points are clustered near the middle of the bell-shaped curves of Fig. 4.1.9. At the right and near the bottom center low cavity number density and low-dose data are included, and on the left are data for very low-swelling microstructures having high cavity number density. The broad trends seen here are explained well by theory. The analysis also reveals that the mechanisms by which some alloys nucleate lower cavity densities than others, rather than the relative cavity growth rates for different materials parameters, are the more important factors controlling swelling. This arises mainly from the physical consideration that sufficient defects are always produced during irradiation to effect a wide variety of responses and that the availability of defect sinks and their relative strengths for point-defect partitioning becomes a major factor in the response that is actually manifest.

When the sink strengths of dislocations and cavities are comparable, separation between interstitials and vacancies occurs most effectively, leading to maximum swelling rate. When the cavity number density is very low, most defects annihilate by mutual recombination in the lattice or recombine after absorption at dislocations, so that the growth rate of an individual cavity is low. More important, however, the void volume fraction is small because of the low cavity density, so that the total swelling is low. When the dislocation density is low or the cavity density is high, most defects recombine in the lattice or after absorption at cavities and cavity growth is again suppressed. In addition, for extremely high cavity number density, the required time for

ORNL-DWG 88M-14050AR

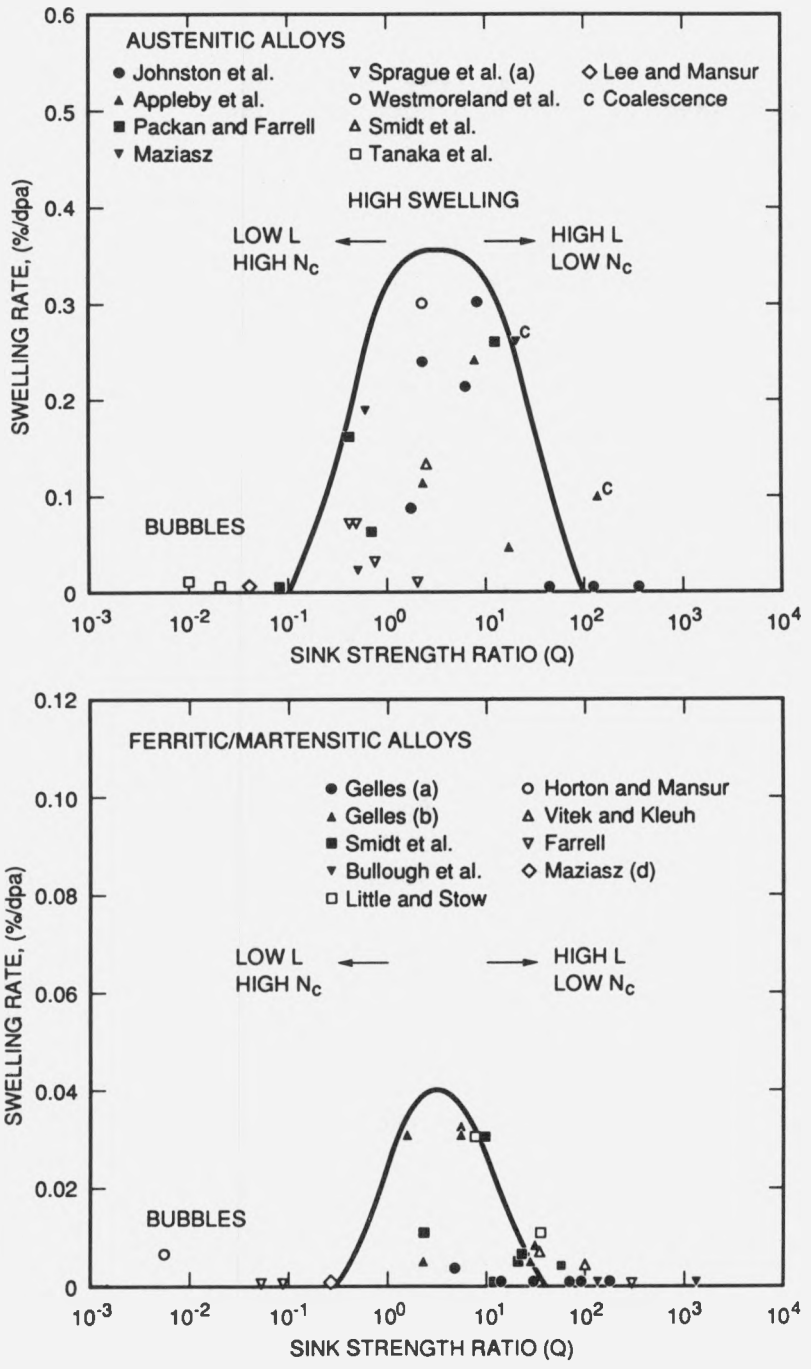

Fig. 4.1.9. Swelling rates as a function of Q-value for austenitic alloys (upper box) and ferritic/martensitic alloys (lower box). Swelling peaks are located around Q≈1.

individual bubbles to accumulate the critical number of gas atoms to convert to growing voids becomes large by simple dilution of helium over a large number of absorption sites.

The results call attention to the importance of the point-defect sink microstructure in determining swelling, over and above the parameters characterizing the intrinsic material properties and irradiation conditions. A wide array of experimental data now has been interpreted for the first time by means of these unifying concepts. Principles by which to design swelling-resistant alloys have been developed based on these results.

4.1.7 The Influence of Microstructure and Solutes on Void Growth in Irradiated Materials[18] – *R. E. Stoller and L. K. Mansur*

A comprehensive comparison was made of the relative importance of various mechanisms by which alloying and microstructural features can influence void swelling. One purpose of this work was to rank these mechanisms to add to the development of a strategy for reducing swelling. The model-based comparison was carried out using the reaction rate theory of radiation effects. This theory has established that the mechanism responsible for void formation under conditions of technological interest is the accumulation of a critical number of gas atoms by gas-stabilized bubbles.[19-21] The time required for void formation can be altered either by changing the gas accumulation rate or by changing the critical number of gas atoms required. The void growth rate can be altered by changing the partitioning of vacancies and interstitials to the voids and other microstructural sinks. Several of these mechanisms involve the presence of precipitates; they are helium collection at matrix-precipitate interfaces, point-defect collection at matrix-precipitate interfaces, an interfacial energy credit resulting from the coupled growth of a cavity-precipitate pair, and possible local bias effects resulting from matrix-precipitate interface strains. The influence of the total precipitate sink strength on the evolution of matrix cavities has also been examined. Other mechanisms included in this comparison were helium collection at network dislocations and solute trapping.

The results of the comparison indicate that an unfavorable microstructure can lead to large reductions in the void formation time and increases in the void growth rate. The influence of precipitates shown in this work is consistent with the experimental observation that the largest voids in irradiated alloys are frequently associated with these particles. Helium and point-defect collection were shown to be the most significant precipitate effects. Helium influences primarily the incubation time; point-defect collection, the swelling rate. Helium trapping at dislocations can also accelerate void formation to a great degree when some fraction of the trapped helium is distributed to bubbles. The results of this work support the proposal that one successful approach to limiting swelling in austenitic stainless steels would be to control the type and density of precipitates that form under irradiation by careful alloying and heat treatment.[22,23]

4.1.8 Analysis of ORR Irradiation Creep Results in Terms of a Phenomenonological Point-Defect and Helium Migration Model* – *C. Wassilew[24] and M. L. Grossbeck*

Irradiation creep results from a spectral tailoring experiment in the Oak Ridge Research Reactor (ORR) have been analyzed in terms of a phenomenonological model developed at the KfK.[25] Two austenitic stainless steels, AISI 316 and US PCA, were irradiated in the form of pressurized tubes with stresses from 20 to 470 MPa at temperatures of 330, 400, 500 and 600°C.[26] The neutron spectrum of the reactor was tailored by changing the core piece surrounding the irradiation vehicles as irradiation progressed to harden the spectrum and maintain a nearly constant production of helium with respect to displacement dose at the ratio characteristic of a fusion reactor. The diameters of the specimens were measured with a noncontacting laser profilometer at atomic displacement levels of 5 and 12 dpa and corresponding helium levels of 56 and 200 appm. The total strains accumulated during irradiation were nearly independent of temperature throughout the range investigated. This result is not in agreement with predictions of the KfK model that emphasizes the effects of creep-rupture. It is considered likely that some of the tubes that were loaded at the higher stresses ruptured. At 600°C, thermal creep might also have contributed significantly to the deformation.

The analyses were carried out using constitutive equations for time-to-rupture, irradiation-induced creep,[25-29] swelling, and creep-driven swelling.[25] The data from the ORR-irradiated specimens consisted of deformation values only. However, knowing the stresses, temperatures, irradiation times, helium concentrations, fluxes and fluences, rupture times resulting from growth and coalescence of grain boundary helium bubbles were calculated using the constitutive equation for in-reactor time-to-rupture,

$$t_m = t_{m,o}/\sigma^{2.5}\, \theta_{tm} ,$$

where σ is the applied stress and $t_{m,o}$ is the time to rupture for σ and θ_{tm} equal to unity, as determined from experimental data. The temperature dependence for the in-reactor damage-accumulating process is given by the function θ_{tm}, which represents the mobility of the helium atoms in terms of a sum of two Arrhenius functions. The values of the exponents are derived from a large data base.[25] We attribute them to the following: (1) the migration of substitutional helium atoms with an activation energy of 2.85 eV [for temperatures above $\sim 0.5\, T_m$ ($\sim$575°C)]; and (2) the migration of interstitial helium atoms with an activation energy of 0.127 eV (for temperatures below $\sim 0.5\, T_m$).

The calculated creep-rupture strengths, $R_{m\ t/\theta}$, for θ = 330 through 720°C are included in Fig. 4.1.10, which contains the in-reactor time-to-rupture data of the German austenitic steels 1.4981, 1.4988, 1.4970; the Ni-base alloy Hastelloy-X (refs. 25 and 29); and the US AISI 316 (refs. 27 and 28). The calculated creep-rupture strengths, $R_{m\ t/\theta}$, for temperatures greater than 480°C have been confirmed experimentally. Figure 4.1.11 shows the measured and the calculated strains vs stress for US PCAs irradiated in the

---

*Research supported in part by the Office of Fusion Energy.

ORNL-DWG 89Z-12512

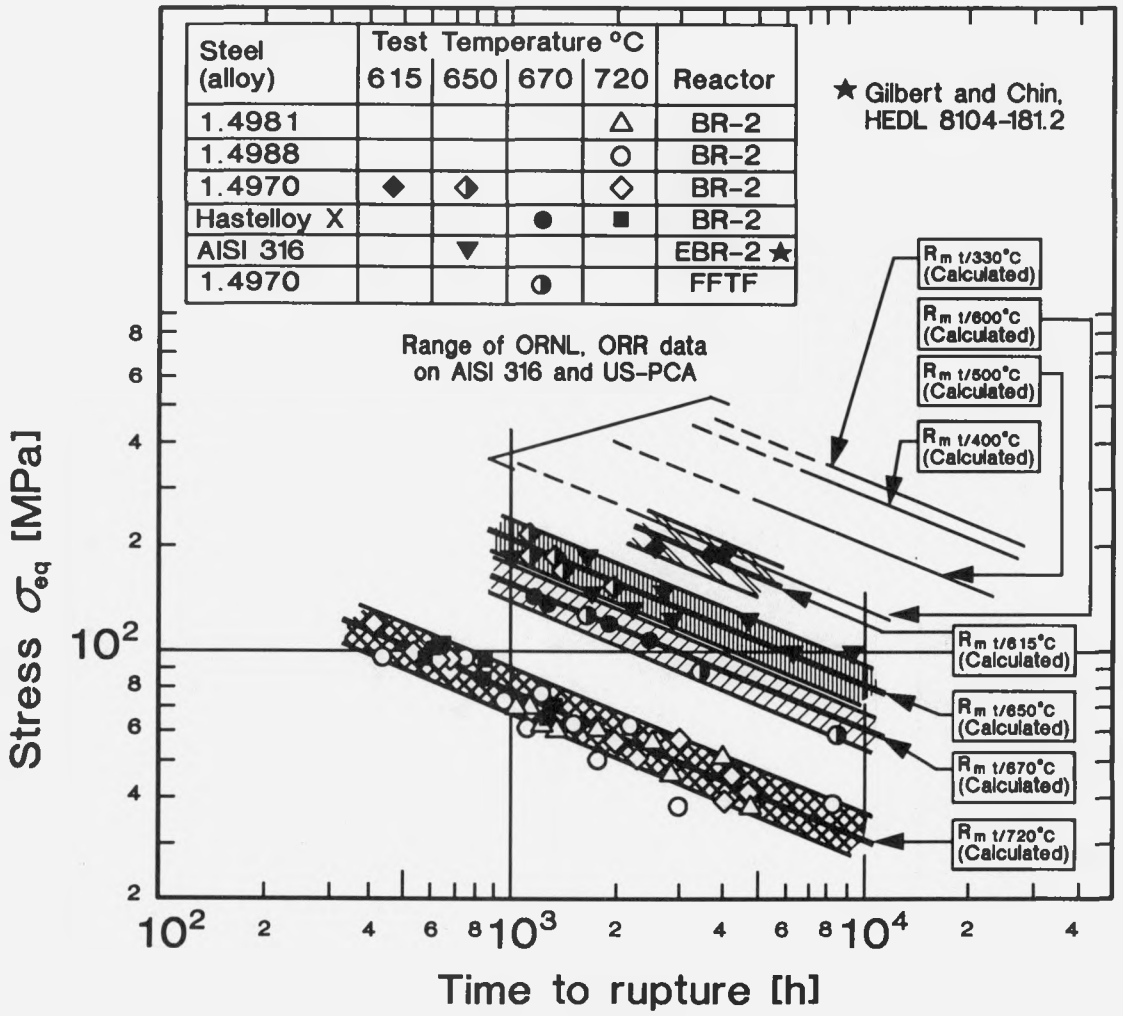

Fig. 4.1.10. Measured and calculated in-reactor time-to-rupture of austenitic alloys.

ORNL-DWG 89Z-12511

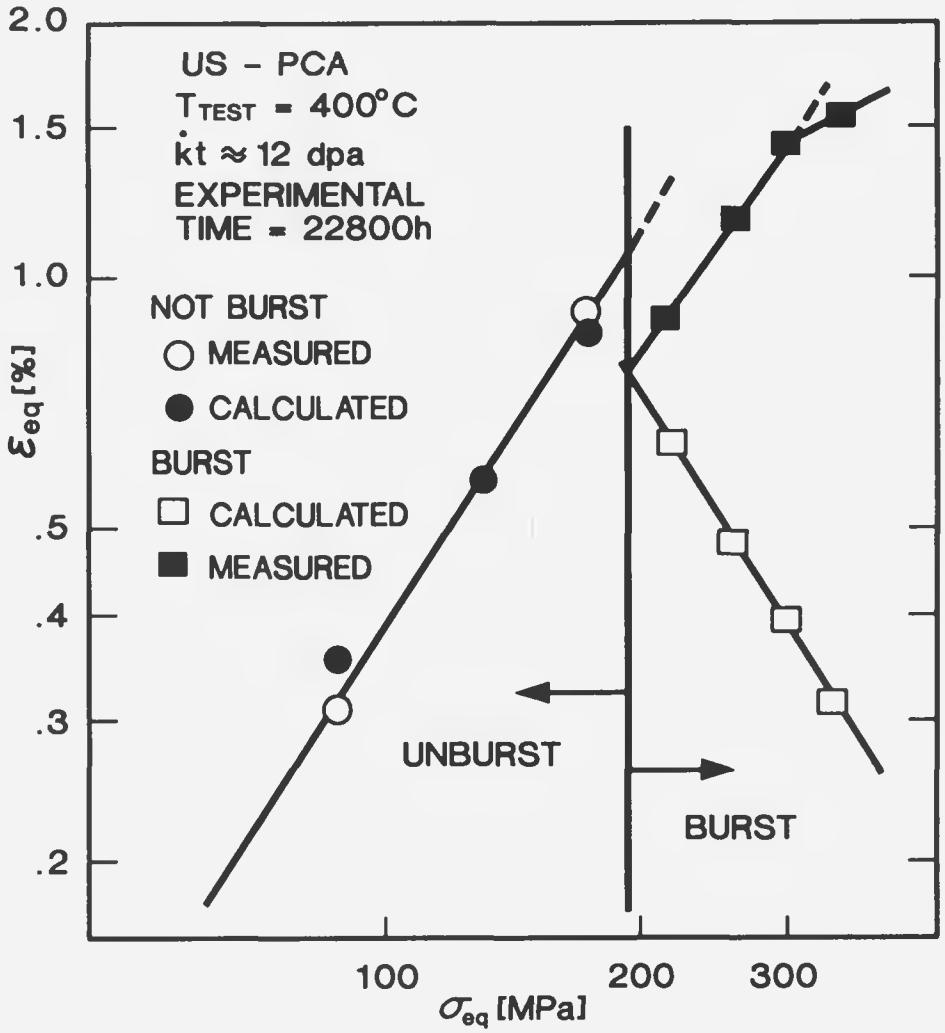

Fig. 4.1.11. Measured and calculated in-reactor creep strains of US-PCA.

ORR at 400°C for 22,800 h to 12 dpa. At a stress level of ~195 MPa the measured strain shows discontinuous behavior. This may represent tube rupture. All specimens loaded at stresses above this transition stress would be expected to have burst. The model also predicts failure at stresses of about 195 MPa. This predicted failure is indicated by the negative slope portion of the curve, representing the calculated strains. The large difference between this curve and the experimental data may be a result of tertiary creep contributions. Verification of tube failure by repressurizing and by doing further metallurgical analysis is planned.

An important result of these calculations and interpretation of experimental results is that irradiation creep is a damaging mechanism at temperatures below those at which thermally activated damage accumulation mechanisms are active.

4.1.9 On Mechanisms by Which a Soft Neutron Spectrum May Induce Accelerated Embrittlement[30] – *L. K. Mansur and K. Farrell*

Recent surveillance measurements on Charpy V-notch ferritic steel specimens irradiated at the inner surface of the High Flux Isotope Reactor (HFIR) pressure vessel showed that the materials were undergoing premature embrittlement. The embrittlement rate was about an order of magnitude greater than expected based on an existing body of test reactor irradiation measurements.[31,32] We have advanced two closely related mechanisms to explain the results on a physical basis. One mechanism, which can also be termed the *rate effect*, is based on *bulk recombination* and recognizes that different displacement rates will result in different relative fractions of bulk point–defect recombination. The displacement rates at the HFIR pressure vessel are up to five orders of magnitude lower than the displacement rates for the test reactor data. The second mechanism, which can also be termed the *spectral effect*, is based on *in-cascade recombination* and recognizes that not all point defects created in collision cascades produced by the irradiating particles escape the cascades. The ones that do not are not available to produce embrittlement. For small cascades produced by low-energy pka's, such as those produced profusely at the HFIR pressure vessel by (n,γ) recoils, the density of defects in a small volume is low and a large fraction avoid recombination. In the test reactor data, the effect of (n,γ) recoils is negligible. Most of these fast-neutron-produced defects are lost to in-cascade recombination and cannot cause embrittlement. Available evidence strongly suggests the spectral effect as the dominant mechanism for the early embrittlement.

In a neutron spectrum in which more than, for example, 10% of the atomic displacements are provided by (n,γ) reactions and which have an availability factor of 10 or more times that of fast neutrons, radiation effects, including embrittlement, should be dominated by the thermal fluence. Two consequences that follow under these conditions are:

1. Radiation effects should occur earlier in exposure by about an order of magnitude (i.e., the ratio of the availablity factors) with respect to neutron fluence or total dpa, when compared with neutron spectra in which the displacements produced by thermal neutrons are relatively unimportant.

2. Radiation effects should show a correlation mainly with thermal neutron fluence or with thermal neutron-produced displacements.

Continuing study of the HFIR vessel embrittlement situation suggests that both of these expectations are fulfilled. Calculations of the neutron spectra at the HFIR vessel and at test reactor-type sites in the ORR have confirmed that the HFIR vessel spectrum is considerably more thermalized. Figure 4.1.12 shows the calculated neutron spectrum at the HFIR pressure vessel. Results are displayed in terms of the percentage of total neutron flux in each decade of energy. Thermal neutrons comprise 96% of the total flux. The magnitudes of flux are 4.7 x 10^{12} n/m^2-s above 1 eV and 1.2 x 10^{14} n/m^2-s below this energy (0.4 eV). The corresponding calculated displacement production by neutrons in each energy range is also shown in Fig. 4.1.12. It can be seen that thermal neutrons below 1 eV account for about 30% of the displacements. For comparison, Fig. 4.1.13 shows the neutron spectrum and resulting displacement production for an out-of-core position of the ORR. About 10% of the atomic displacements are produced by thermal-neutron-induced reactions. Both these spectra satisfy our predicted conditions for establishment of "accelerated" embrittlement, evidence of which was documented elsewhere[31,32] and constituted the motivation for the current investigation.

This acceleration is illustrated for the A212B steel in Fig. 4.1.14(*a*), in which the increase in hardening is plotted as a function of fast-neutron fluence. Results for both the HFIR vessel position and the ORR out-of-core position are shown. The results do not superimpose on each other. Both these irradiations fulfill the conditions described above, where radiation effects should be dominated by thermal neutron fluence. Figure 4.1.14(*b*) shows the results of Fig. 4.1.4(*a*) plotted against thermal-neutron fluence. As expected, the points are along a single curve as anticipated in condition 2 above. We interpret this correspondence as preliminary evidence for the mechanism of accelerated embrittlement, based on the spectral effect we have described. Experiments (as described in 4.2.1) are now being undertaken to confirm these results by varying systematically the thermal to fast flux ratio in a series of ferritic alloys, some shielded by cadmium to control the thermal neutron exposure, as described in a separate entry in this report.

The analysis described may have implications for reactor pressure vessels and support structures remote from the core, where the neutron spectrum is highly thermalized. Wherever the displacement damage generated by thermal neutrons is within an order of magnitude of that generated by fast neutrons, it would be prudent to analyze components for accelerated radiation effects because of the higher efficiency of point-defect retention from low-energy cascades. Engineering solutions to the low-dose embrittlement problem are different if the *spectral effect* mechanism suggested here is the main contributor, rather than the *rate effect*. Low damage rates in components such as light-water reactor pressure vessel supports are hardly avoidable. However, it appears relatively less difficult to make design modifications to reduce the thermal component of the neutron spectrum in components remote from the core.

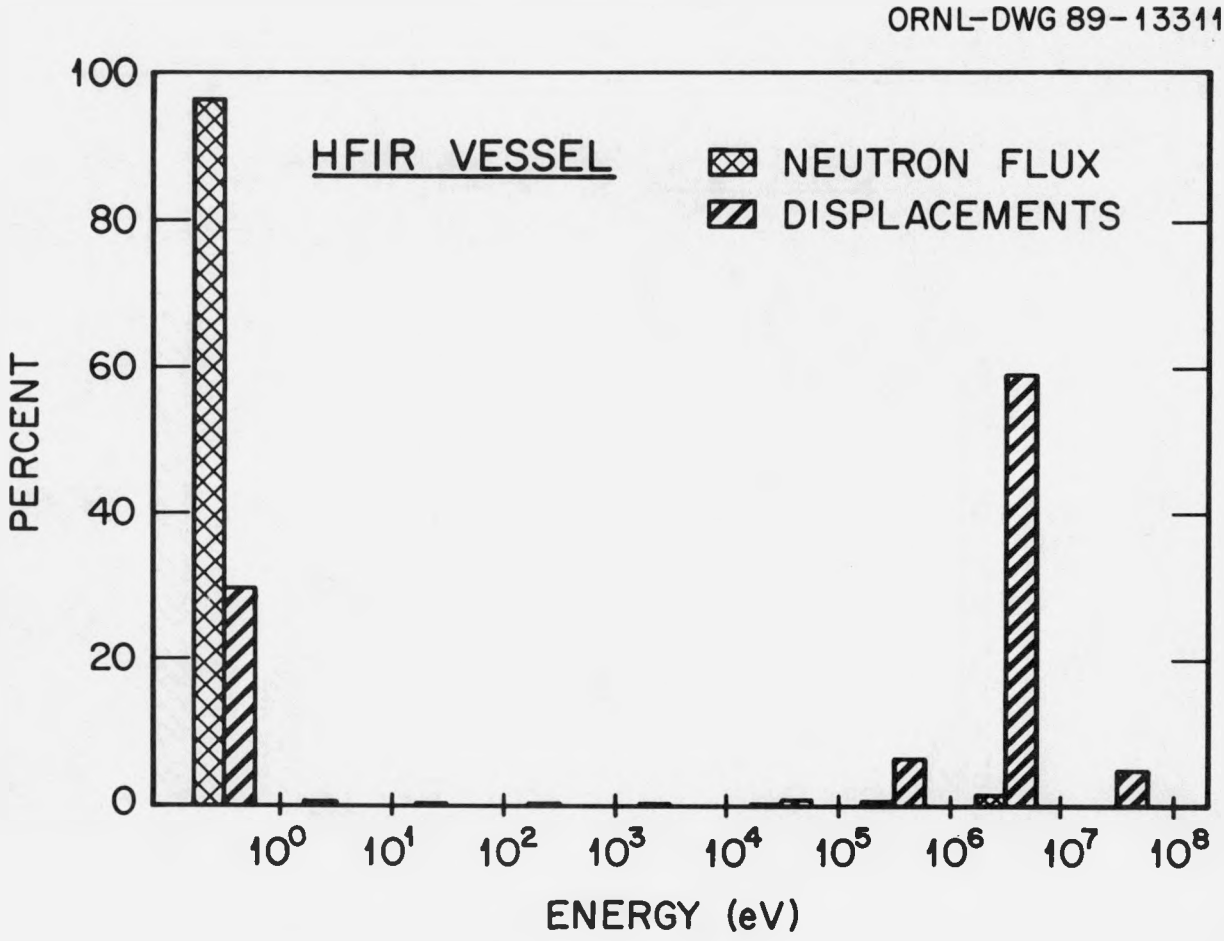

Fig. 4.1.12. Calculated distributions of neutron flux and corresponding displacement production at a typical location at the inner surface of the HFIR pressure vessel as a function of neutron energy. Contributions are shown for each decade of energy, with 0 on the abscissa corresponding to the energy range 0–10^0 eV, 1 corresponding to 10^0–10^1 eV, and so on.

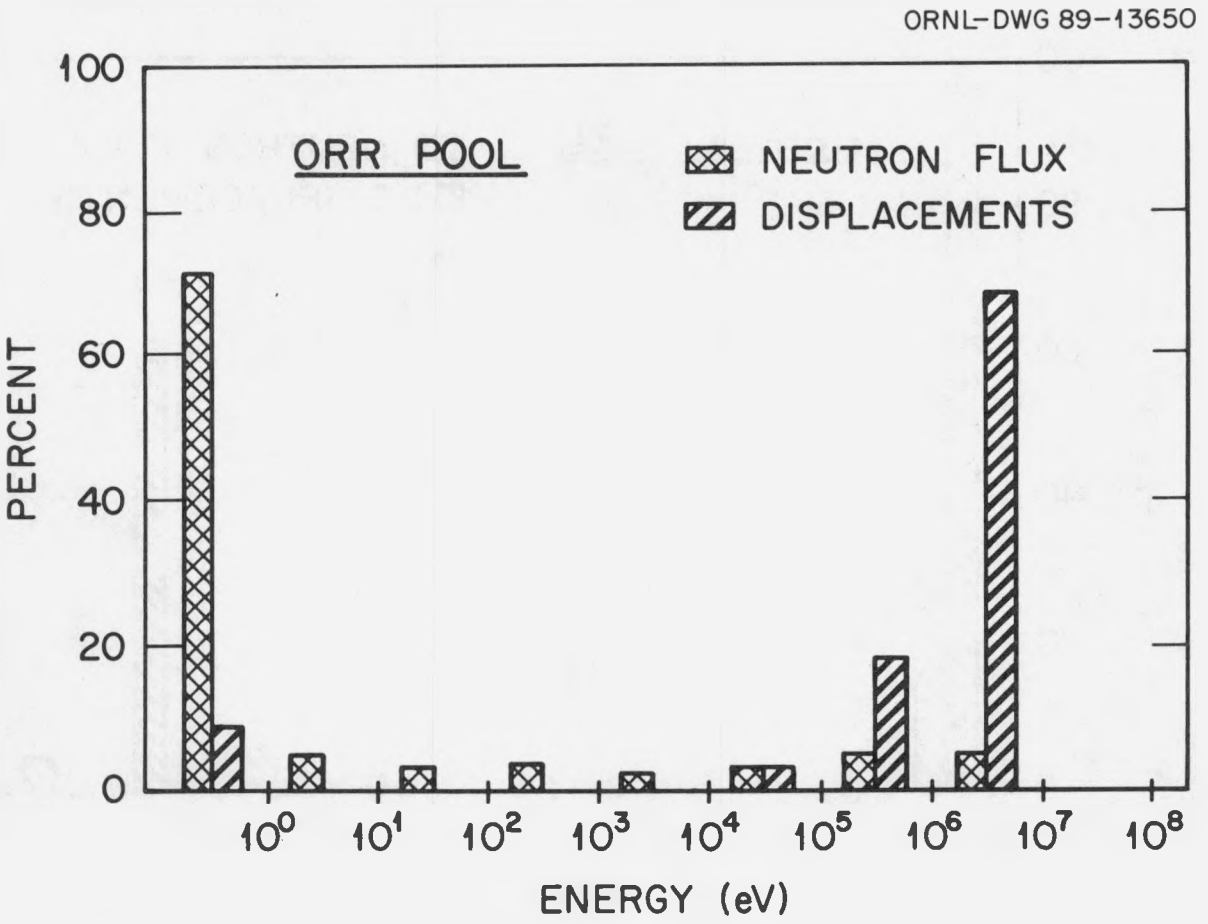

Fig. 4.1.13. Calculated distributions of neutron flux and corresponding displacement production at a location in an ORR out-of-core position.

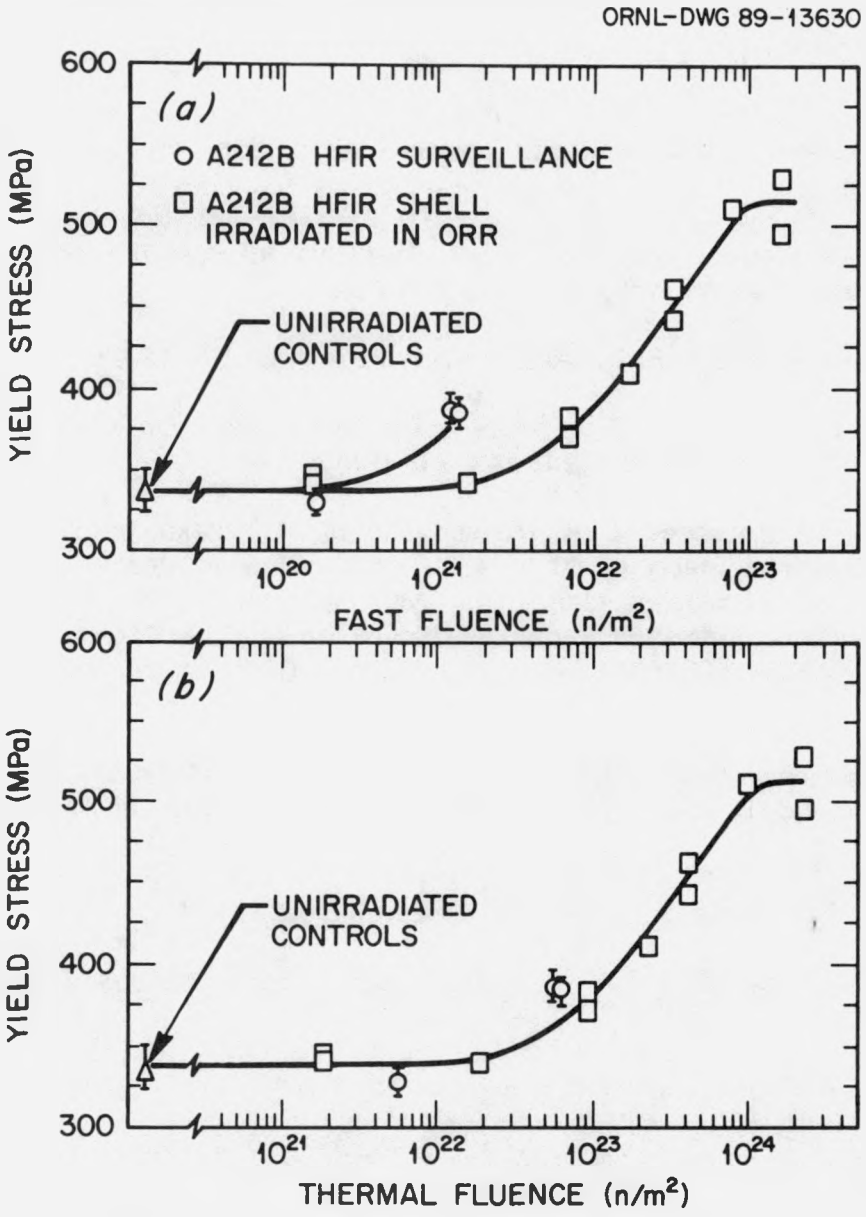

Fig. 4.1.14. Increase in yield strength as a function of neutron fluence for ferritic steels irradiated at the HFIR pressure vessel and in an ORR out-of-core position: (*a*) plotted against fluence with neutron energy greater than 1 MeV, and (*b*) plotted against fluence of thermal neutrons (<0.4 eV).

4.1.10 References

1. Summary of paper, A. D. Brailsford, W. A. Coghlan, and L. K. Mansur, "Irradiation Creep by Glide Induced Transient Absorption," to be submitted to the *J. Nucl. Mater.*

2. H. S. Carslaw and J. C. Jaeger, *Conduction of Heat in Solids, 2nd Edition*, Oxford at the Clarendon Press, 1959, pp. 189-205.

3. P. Jung and P. B. Chilson, *J. Nucl. Mater.* **149**, 1-6 (1987).

4. J. L. Scott et al., "Program of United States-Japan Collaborative Testing in HFIR and ORR," *J. Nucl. Mater.* **141-143**, 738 (1986).

5. M. L. Grossbeck, L. K. Mansur, and M. P. Tanaka, "Irradiation Creep In Austenitic Stainless Steels at 60 to 400°C with a Fusion Reactor He:dpa Ratio," presented at the Fourteenth International Symposium on the Effects of Radiation on Materials, Andover, June 1988, to be published by the American Society for Testing and Materials in ASTM STP 1046, ed. N. H. Packan, R. E. Stoller, and A. S. Kumar (in press).

6. Summary of paper, D. F. Pedraza, "Radiation-Induced Microstructural Evolution and Amorphization of Intermetallic Compounds," *Radiation Effects and Defects in Solids* (in press), 1989.

7. D. F. Pedraza, *J. Mater. Res.* **3**, 425-41 (1986).

8. D. F. Pedraza and L. K. Mansur, *Nucl. Instrum. Methods. Phys. Res.* B16, 203-11 (1986).

9. D. F. Pedraza, *Mater. Sci. Eng.* **90**, 69 (1987).

10. D. F. Pedraza, paper in *Radiation Effects and Defects in Solids* (in press), 1989.

11. Summary of paper, D. F. Pedraza, "Effect of Simultaneous Heavy-Ion and Electron Bombardment on the Amorphization Kinetics of Intermetallics," *Phys. Rev. B* **38**, 4803-09 (1989).

12. Summary of paper, D. F. Pedraza, "Irradiation as a Tool for Studying Solid-State Amorphization Phenomena," Proceedings of the 1988 TMS Fall Meeting Symposium on "Irradiation-Enhanced Materials Science and Engineering," Chicago, September 1988, to be published in *Metallurgical Transactions*.

13. A. Blatter, J. Gfeller, and M. vonAllmen, *J. Less Common Met.* **140**, 317 (1988).

14. K. Bhanamurthy, G. K. Dey, and S. Banerjee, *Scr. Metall.* **22**, 1395 (1988).

15. Summary of paper, R. E. Stoller, "Radiation Damage in Binary Ceramic Oxides: A Preliminary Model," to be published in *Fusion Reactor Materials Semiannual Progress Report for Period Ending March 31, 1989*, DOE/ER-0313/6, USDOE, in press.

16. R. E. Stoller and G. R. Odette, *J. Nucl. Mater.* **131**, 118-25 (1985).

17. Summary of paper, E. H. Lee and L. K. Mansur, "Unified Theoretical Analysis of Experimental Swelling Data for Irradiated Austenitic and Ferritic/Martensitic Alloys," Proceedings of 1988 Symposium "Irradiation-Enhanced Materials Science and Engineering," Chicago, September 1988, to be published in *Metallurgical Transactions*.

18. Summary of paper presented at the 14th International Symposium on the Effects of Radiation on Materials, Andover, Mass., June 1988, to be published in ASTM STP 1046.

19. R. E. Stoller and G. R. Odette, "Radiation-Induced Changes in Microstructure: 13th International Symposium," pp. 358-70 in ASTM STP 955, ed. F. A. Garner, N. H. Packan, and A. S. Kumar, American Society for Testing and Materials, Philadelphia, 1987.

20. R. E. Stoller and G. R. Odette, *J. Nucl. Mater.* **131**, 118-25 (1985).

21. L. K. Mansur, E. H. Lee, P. J. Maziasz, and A. F. Rowcliffe, *J. Nucl. Mater.* **141-143**, 633-46 (1986).

22. P. J. Maziasz, "Mi-con 86: Optimization of Processing, Properties and Service Performance Through Microstructural Control," pp. 116-61 in ASTM STP 979, ed. B. L. Bramfitt, R. L. Benn, C. R. Brinkman, and G. F. Vander Voort, American Society for Testing and Materials, Philadelphia, 1988.

23. E. H. Lee and L. K. Mansur, *J. Nucl. Mater.* **141-143**, 695-702 (1986).

24. On guest assignment from Kernforschungszentrum Karlsruhe, D7500 Karlsruhe - 1, Federal Republic of Germany.

25. C. Wassilew, "Phänomenologische Modelle, Mechanismen und Zustandsgleichungen der bestrahlungsinduzierten and thermischaktivierten Deformations – und Schadensakkumulationsprozsesse in Metallen," Ph.D. thesis, Fakultät für Bergbau, Hüttenwesen und Geowissenschaften der RWTH Aachen, 1988.

26. M. L. Grossbeck and J. A. Horak, "Irradiation Creep in Type 316 Stainless Steel and US PCA with Fusion Reactor He/dpa Levels," *J. Nucl. Mater.* **155-157**, 1001-05 (1988).

27. A. J. Lovell, B. A. Chin, and E. R. Gilbert, "In-Reactor Creep Rupture of 20% CW 316 Stainless Steel," *J. Mater. Sci.* **16**, 870-76 (1981).

28. R. J. Puigh and M. L. Hamilton, "In-Reactor Creep Rupture Behaviour of the D19 and 316 Alloys," pp. 22-29 in *Influence of Radiation on Material Properties: 13th International Symposium (Part II)*, F. A. Garner, C. H. Henager, Jr., and N. Igata, eds., ASTM STP 956, Philadelphia, 1987.

29. C. Wassilew, K. Ehrlich, and H. –J. Bergmann, "Analysis of the In-Reactor Creep and Rupture Life Behavior of Stabilized Austenitic Stainless Steels and the Nickel-Base Alloy Hastelloy-X," pp. 30-53 in *Influence of Radiation on Material Properties: 13th International Symposium (Part II)*, F. A. Garner, C. H. Henager, Jr., and N. Igata, eds., ASTM STP 956, Philadelphia, 1987.

30. Summary of paper, L. K. Mansur and K. Farrell, "On Mechanisms by Which a Soft Neutron Spectrum May Induce Accelerated Embrittlement," *J. Nucl. Mater.*, to be published.

31. R. D. Cheverton, J. G. Merkle, and R. K. Nanstad, *Evaluation of HFIR Pressure-Vessel Integrity Considering Radiation Embrittlement*, ORNL/TM-10444, April 1988.

32. R. K. Nanstad, K. Farrell, and D. N. Braski, *J. Nucl. Mater.* **158**, 1 (1988).

4.2 IRRADIATED STRUCTURE, COMPOSITION, AND PROPERTIES

4.2.1 Experiments to Elucidate the Early Embrittlement of the HFIR Pressure Vessel – *K. Farrell and L. K. Mansur*

To our knowledge there are no unambiguous experiments to delineate the contribution to embrittlement at low temperature of the very low rates and softened neutron spectrum described in Sect. 4.1.9. Accordingly, we have initiated experiments to address these factors. The experiments utilize both miniature tensile specimens to provide information on radiation hardening and embrittlement and needle-like specimens for atom probe-field ion microscopy microstructural characterizations. One experiment is a comprehensive investigation of displacement rate, damage level, neutron spectrum, and irradiation temperature to be carried out in the HFIR over a 3-year period. It requires building a gantry and access tube inside the reactor. This gantry will span the radial distance between the outer edge of the beryllium reflector and the inner face of the pressure vessel. It is estimated that over this distance the displacement rate falls by more than four orders of magnitude. The gantry will hold packages of test specimens at specified distances from the reactor core, corresponding to selected displacement rates. The access tube will allow removal and insertion of packages. Temperatures will be controlled by γ-heat. This experiment will require substantial resources and currently is in the conceptual stage, awaiting approval of funds.

The other experiment is simpler. It is intended to discriminate the effects of a soft neutron spectrum to confirm the ideas described in the summary above. Calculations indicate that the spectrum at the HFIR vessel has a thermal-to-fast flux ratio $>>10$. We have argued that a softened spectrum will allow more point defects per displaced atom to be available for producing embrittlement. To verify this concept, we are performing

experiments in two sites in the High Flux Beam Reactor (HFBR) at Brookhaven National Laboratory. One site is in the reactor core and has a thermal-to-fast flux ratio of <2. In this site about 65% of the atomic displacements are produced in large cascades by fast neutrons; 1% is produced by thermal neutrons; and about 34% are caused by neutrons of intermediate energies. The other site is outside the core in the heavy-water coolant, where the thermal-to-fast flux ratio is about 600. In this site about 90% of the displacements are produced by low-energy recoil events associated with iron (n,γ) reactions. Comparison of the degree of embrittlement per displaced atom measured at each site will give a measure of the relative embrittling efficiencies of thermal and fast neutrons. Further confirmation of the effectiveness of thermal neutrons in the soft spectrum site will be made by wrapping some of the specimens in cadmium to block the thermal neutrons. The first of these experiments, consisting of exploratory specimens and neutron dosimeters to gauge the exposure conditions prevailing at the two sites, was made in March 1989. Before we could continue with the main experiments, however, the HFBR was shut down unexpectedly in response to a safety inquiry. In case the shutdown is prolonged, we are investigating the possibilities of using another reactor to complete the experiments.

4.2.2 Helium Bubbles in α-Titanium and Titanium Tritide Arising from Tritium Decay: A TEM Study[1] – *T. Schober[2] and K. Farrell*

Hexagonal α-titanium in 1 atm of hydrogen gas at 600°C will absorb about 8 at. % hydrogen in solid solution; at room temperature, the solubility limit is less than 1 appm. On cooling from 600°C, the excess hydrogen is precipitated as the δ-hydride phase with an approximate stoichiometry of $TiH_{1.5}$. Hydrogen in the δ phase remains essentially immobile at room temperature but can be released by suitable heating. These features make titanium a useful material for storing and retrieving hydrogen. The behavior of the isotope tritium closely parallels that of hydrogen, and titanium is under consideration as a storage medium for tritium. However, tritium decays to ^3He via the reaction $T \rightarrow {}^3He + \beta^- + \nu^-$, forming helium bubbles.

Disks of high-purity, recrystallized titanium were exposed to low-pressure tritium at 600°C for 3 weeks to give a tritium concentration in the α-titanium of about 1 at. % and helium generation rates of about 10 appm per week. Most of the tritium was then removed by vacuum pumping, and the specimens were cooled to room temperature, where the remaining tritium formed discrete tritide platelets in the α-titanium matrix. They were then aged at room temperature for periods up to 3 years and their microstructures were examined by TEM. Bubbles of quite different nature were found in the α-titanium matrix and in the tritide platelets. Those in the α-titanium were of low concentration, about $5 \times 10^{18} m^{-3}$, with sizes in the range 7 to 35 nm. They were not correlated with any gross microstructural feature, and did not change during aging at room temperature. The bubbles in the tritide platelets were much smaller (~1.5–nm diam) and of much higher density ($\sim 5 \times 10^{23} m^{-3}$), and they displayed strong strain contrast. A large fraction of these bubbles were arranged in tight, irregular-shaped clusters and closely spaced in lines. On aging at room temperature, the concentration of bubbles in the tritide phase appeared to remain constant, but their mean diameter was found to increase with the cube root of time.

These two families of bubbles, those in the titanium matrix and those in the tritide platelets, fit descriptions of equilibrium helium bubbles and spontaneously generated nonequilibrium bubbles, respectively. The equilibrium helium bubbles in the α-titanium were created by coalescence of insoluble helium atoms and thermally produced vacancies during the soaking treatment at 600°C, when the concentration of tritium was about 1 at. %. The spontaneously generated, nonequilibrium bubbles in the tritide platelets were developed near room temperature after the formation of the tritide phase with its 60 at. % tritium. These nonequilibrium bubbles contain very high helium pressures, as indicated by their strain fields, and they grow athermally by ejecting metal atoms. Their volume growth rate is observed to be directly proportional to time, i.e., to the tritium decay rate, suggesting that growth is controlled by a steady influx of helium atoms that maintains the high gas pressures needed to drive athermal growth. It is suggested that growth and coalescence of aligned bubbles may develop channels for sudden helium release. These are the first reported observations of spontaneously generated ^{3}He bubbles in titanium tritide phase.

4.2.3 Helium Bubbles in Vanadium and Several Vanadium Alloys After High-Temperature Helium Ion Bombardment[3] – *T. Schober[2] and K. Farrell*

Vanadium-base alloys are under consideration for use as first-wall materials in prospective fusion reactors where they will be subjected to intense fluxes of neutrons, and helium, deuterium, and tritium ions at elevated temperatures. The hydrogen isotopes will probably diffuse out of the material, but the helium will be retained, most likely as bubbles that may trigger swelling and helium embrittlement. We have used TEM to examine such bubbles in vanadium alloys implanted with helium by ion bombardment.

The materials were pure vanadium and two commercial alloys, V-15Cr-5Ti-0.032C and 10Cr-3Fe-1Zr-0.064C (wt %). Helium ions at 200 keV were implanted at a flux of $\sim 1 \times 10^{20}$ m^{-2} ions during a 1-h period at temperatures of 600, 700, and 800°C using the ORNL 400 keV Van de Graaff accelerator. Peak helium concentrations of about 6000 appm were reached at a depth of about 0.7 μm, with a peak displacement damage level of about 0.2 dpa.

All of the specimens contained helium bubbles and dislocation loops or lines introduced during the ion implantations. The dislocation lines were developed by growth and coalescence of loops and were not present in the 600°C implants. In general, these microstructural features coarsened with increasing bombardment temperature, the loops giving way to dislocation lines at 800°C. Coarsening was slower in the alloys than in the pure vanadium. The spatial distribution of the bubbles was nonuniform. Although most of the bubbles were arranged randomly in the matrix, many were aggregated at inclusion-matrix interfaces, grain boundaries, and dislocations. Congregation at such regions was accompanied by denuded zones whose widths increased with irradiation temperature. In the pure vanadium irradiated at 600°C, the concentration of bubbles in the matrix was 3.3×10^{21}m^{-3} with a mean diameter of 46 nm. By comparison, the V-15Cr-5Ti alloy displayed more than 10 times as many bubbles, with a mean size 3.2 nm, and 40 times as many loops, with a mean size of 8 nm.

Two further conclusions deserve comment. One is that there is evidence that the bubbles did not reach equilibrium during these high-flux, short-term irradiations. In the V-15Cr-5Ti the bubbles produced at 800°C were not equiaxed, but were in the form of very thin plates similar to those seen in molybdenum after room temperature helium implantations. Also, the V-10Cr-3Fe-1Zr alloy at 800°C shows some cylindrical-type bubbles. Furthermore, in this alloy at 600 and 700°C matrix bubbles are positioned at the centers of dislocation loops. This latter correlation could arise if the loops were fueled by interstitial atoms punched out from vacancy-starved bubbles. The calculated amount of helium required to sustain the observed bubbles in equilibrium is only about one-tenth of the amount implanted.

The second conclusion is that the areal coverage of grain boundaries with helium bubbles is considerable, 2 to 15 % at 600°C increasing to as much as 42% at 800°C. This raises questions about the integrity of grain boundaries at high helium levels. It is usually considered that helium embrittlement, which classically occurs by stress-induced growth and linkage of grain boundary bubbles, will cause intergranular separation. Helium embrittlement tests of vanadium and its alloys containing up to several hundred appm helium have indicated seemingly good resistance to intergranular failure. The current observations, however, suggest that at high helium concentrations grain boundaries will be badly riddled with bubbles, even in the absence of stress-induced bubble growth, which might lead to penetration of the grain boundaries.

4.2.4 Void Swelling and Defect Cluster Formation in Reactor-Irradiated Copper[*4] – *S. J. Zinkle and K. Farrell*

There are proposed applications for copper and copper alloys in fusion reactors at temperatures of 100 to 400°C. Although there have been hundreds of studies of the effects of irradiation on copper over the past 30 years, relatively few of these have attempted to characterize the microstructure of neutron-irradiated copper over an extended temperature range at well-defined dose levels. The purpose of the current work was to provide a set of reference data at closely controlled temperature and damage levels.

Specimens of zone-refined copper in a fully annealed condition were sealed in helium-filled capsules and irradiated in the core of the Oak Ridge Research Reactor. Each capsule was housed in its own small, Nichrome-wound, electrically heated furnace. Thermocouples measured the temperature which was maintained within ±5°C of the nominal values. The lowest temperature was 182°C, and the highest was 500°C. Flux monitor wires provided a thorough map of the neutron environment. The fast neutron fluence (> 0.1 MeV) was 1.0 to 1.3 x 10^{25} nm^{-2}, resulting in a damage level of typically 1.3 dpa with a high of 1.5 dpa and a low of 1.3 dpa. The damage rate was 2 x 10^{-7} dpa s^{-1}. Postirradiation assessment was done with precision density measurements and TEM.

---

*Research supported in part by the Office of Fusion Energy.

The lower temperature limit for swelling was found to lie between 182 and 220°C, with a maximum swelling of about 0.5% at 300 to 350°C and no swelling at 500°C. The measured density changes are shown in Fig 4.2.1. TEM examination confirmed these results. At 182°C the microstructure consisted of black-spot-type damage, in which about half of the spots were resolvable as stacking fault tetrahedra (SFT). For temperatures of 220 to 450°C the damage structure comprised dislocation loops, SFT, and cavities. The mean cavity diameter increased with temperature from 19 nm at 220°C to 200 nm at 450°C; correspondingly, the cavity concentration fell from $\sim 1.5 \times 10^{20} m^{-3}$ to $< 1 \times 10^{16} m^{-3}$. The dislocation loops increased in size and decreased in concentration with increasing irradiation temperature. Zones on each side of grain boundaries and incoherent twin boundaries were denuded of damage structure. Voids reached their maximum sizes and concentrations at distances of a few micrometers from the rain boundaries.

These data substantially strengthen the data base for neutron-irradiated pure copper and establish unambiguously that the lower and upper temperatures for void formation lie in the narrow range of ~180 to 220°C and 450 to 500°C, respectively. Peak swelling occurs at 300 to 350°C for a damage rate of 2×10^{-7} dpa s^{-1}.

4.2.5 Effect of Oxygen on Vacancy Cluster Morphology in Metals[*5] – *S. J. Zinkle and E. H. Lee*

Numerous experimental studies have shown that the dominant vacancy cluster geometry for a given metal can be the SFT, the void, or the faulted or perfect loop, depending on minor changes in the experimental procedure. It has been recognized for many years that reactive gases such as oxygen can play an important role in void formation in metals during quenching or irradiation. However, a comprehensive quantitative assessment of the physical mechanisms associated with impurity-aided vacancy cluster formation has been lacking.

A thermodynamic model based on the adsorption equations of Gibbs and Langmuir has been developed to determine the relative stability of the void compared with the dislocation loop and SFT in the presence of oxygen. The physical basis for this model lies in the reduction in surface energy on chemisorption of oxygen. Representative calculations were performed for copper, nickel, and austenitic stainless steel (Fe-Cr-Ni). The thermodynamic model predicts that oxygen concentrations greater than 30 to 1000 appm will stabilize void formation in these metals, with SFT formation being energetically preferred for lower oxygen contents. To check the model predictions, foils of copper and several Fe-Cr-Ni alloys containing various amounts of oxygen were examined using TEM following ion irradiation. The presence of 30 to 1000 appm oxygen in the foils resulted in significant amounts of void formation, whereas no voids were observed in low-oxygen specimens. Oxygen introduced by ion implantation was found to be more effective in promoting void formation than was residual oxygen. Solutes such as phosphorus in the Fe-Cr-Ni alloys reduced the effectiveness of oxygen as a void-stabilizing agent.

---

*Research supported in part by the Office of Fusion Energy.

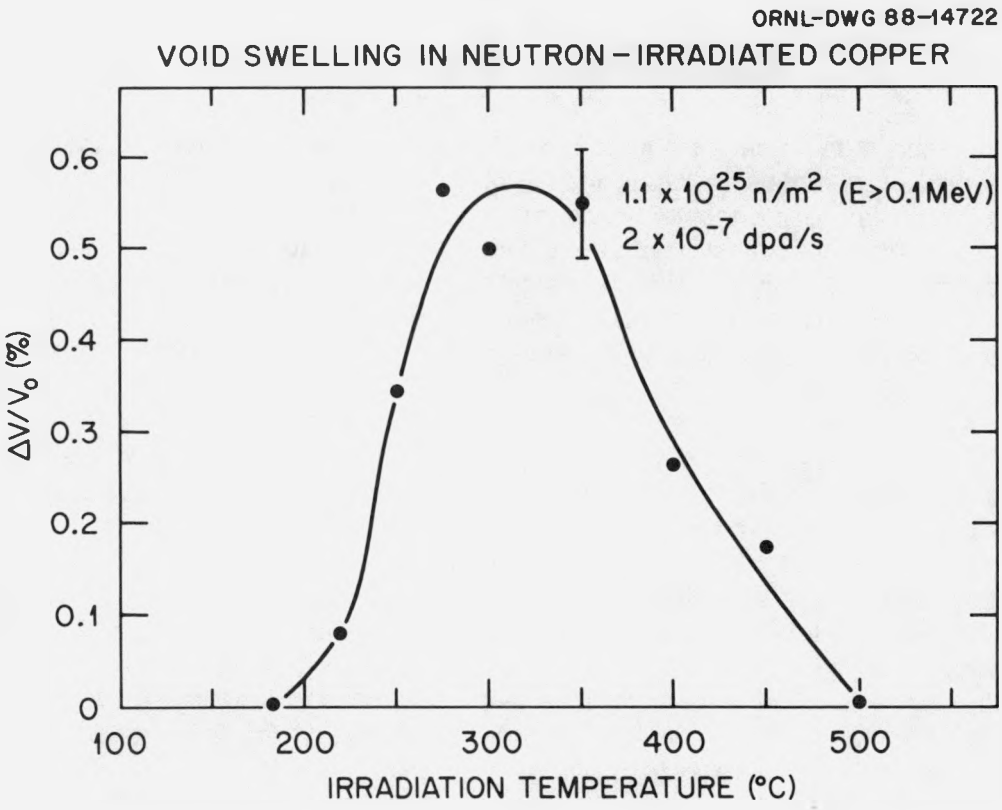

Fig. 4.2.1. Temperature dependence of swelling in neutron-irradiated pure copper, determined from changes in density.

The amount of oxygen required to stabilize void formation is comparable to the amount of impurity oxygen typically found in metals (~10 to 1000 appm). High-temperature annealing in inert gas or "poor" vacuum may introduce oxygen into metals as a result of the residual oxygen partial pressure that is often present in these environments. Nearly all of the published irradiation studies performed under conditions relevant for cavity formation have failed to list the oxygen content of the materials and have, therefore, apparently neglected to control what we now deem an important experimental parameter.

4.2.6 Ion Irradiation Studies of Oxide Ceramics* – *S. J. Zinkle*

Radiation effects in ceramics are of interest both because of the potential applications of ceramics in components of fusion reactors and because favorable surface properties for nonnuclear technological applications can be achieved through ion implantation. The objective of the current studies was to investigate microstructural changes that occur in three oxide ceramics as a result of ion irradiation. The materials were MgO, which has a simple cubic crystal structure; Al_2O_3, which has a close-packed hexagonal structure; and $MgAl_2O_4$ (spinel), which has cubic symmetry with 56 atoms in the unit cell.

The unique irradiation conditions attainable with the recently completed ORNL triple-ion-beam facility allowed a number of interesting experimental conditions to be investigated. The specimens were implanted with high-energy beams of Fe^+, Mg^+, Al^+, and O^+ ions at temperatures ranging from 300 to 923 K, and displacement damage doses of 5 to 100 dpa. The use of ion beams in the range 1.4 to 3.6 MeV produced implanted ion profiles that were localized in the depth regions of 1 to 2 μm. Comparison of the microstructures in these implanted ion regions with the microstructures at shallower depths, where displacement damage occurred in the absence of implanted ions, provided useful information on the importance of injected ions on the irradiation response.

Alumina was selected for the first simultaneous triple beam irradiation, using 1.4 MeV O^+, 2 MeV Al^+, and 200-400 keV He^+ ion beams. The O^+ and Al^+ ion energies were chosen to give similar implantation depth for both ions (1.2 μm), and the fluxes of the two beams were controlled to produce nearly stoichiometric implantation of the ions. The helium beam was used to study the effects of inert-gas implantation on cavity formation at fusion-relevant gas production rates.

Initial results obtained on the implanted ceramic specimens can be summarized as follows: Amorphization was not observed for any of the irradiation conditions; instead, dislocation loops and tangled dislocations were created.

This suggests that displacement damage processes alone cannot produce amorphization in these materials during room temperature irradiation -- the

---

*Research sponsored in part by the Office of Fusion Energy.

microstructure can accommodate point defects by creating extended defect clusters that evolve into network dislocations, which can absorb defects by undergoing dislocation climb. Figure 4.2.2 shows the cross-section microstructure of spinel irradiated at 923 K with 1.5 x 10^{21} $Mg^{+}m^{-2}$ (40 dpa peak damage). A network of dislocations is present in the region, coinciding with the peaks in the displacement damage and implanted ion profiles (1.5 to 2.0 μm), and isolated loops are visible at intermediate depths. The dislocation loops in the irradiated spinel specimens were identified to be interstitial in nature, lying on (110) and (111) planes with Burgers vectors of a/4<110>. The <110>(111) loops were unfaulted on the anion sublattice but still contained a cation fault. The <110>(110) loops were faulted on both sublattices. Spinel specimens irradiated at 923 K exhibited surface and grain boundary denuded zones (Fig. 4.2.2), whereas specimens irradiated at room temperature contained dislocation loops in these regions. The formation of dislocation tangles appeared to be somewhat aided by the implanted ions.

The microstructural features in the irradiated Al_2O_3 and MgO specimens were of smaller size than in the spinel specimens. Four types of irradiation-produced defects were observed in the Al_2O_3 specimens exposed to the triple-beam implantations, namely dislocation loops, network dislocations, cavities, and unidentified clusters that may be aluminum metal precipitates (colloids).

4.2.7 Suppression of Swelling in Phosphorous-Modified Fe-Cr-Ni Alloys During Neutron Irradiation[6] – *E. H. Lee and N. H. Packan*

The swelling behavior of an alloy is a complex phenomenon that depends strongly on the alloy composition and precipitate phases, both in the preirradiated state and during evolution under irradiation. Because of low swelling behavior of certain alloy compositions, interest was recently developed in phosphorous-containing stainless steels for application in the fusion- and fast-reactor environments.

Phosphorous-containing austenitic alloys in the solution annealed condition were irradiated at 745-760 K (470-485°C) in the Fast Flux Test Facility (FFTF) to doses ranging from 0.1 to 10 dpa (Fig. 4.2.3). The alloys were variations on Fe-13Cr-15Ni-0.05P, with respective additions of 0.8 Si, 0.2 Ti, or 0.8 Si + 0.2 Ti; also included were 0.01 and "zero" P compositions (all values in wt %). This alloy set was studied previously using heavy-ion irradiations.[7]

The reference ternary and the two phosphorous-only variations contained few precipitates and numerous voids and swelled rapidly, while the three variants containing P with Si and/or Ti showed little or no void formation and profuse phosphide precipitation. Phosphorous caused rapid loop nucleation initially, and a high density of phosphide precipitates formed at these defects. Loop growth was, however, delayed until the phosphide precipitates were well established. New loops subsequently nucleated, grew, unfaulted, and developed into line dislocations. Helium atoms were trapped at such defects (dislocation loops, lines, and precipitates) producing a high cavity density microstructure. The alloy with phosphorous only contained only a few unstable precipitates and swelled readily.

ORNL–PHOTO 0374–88R

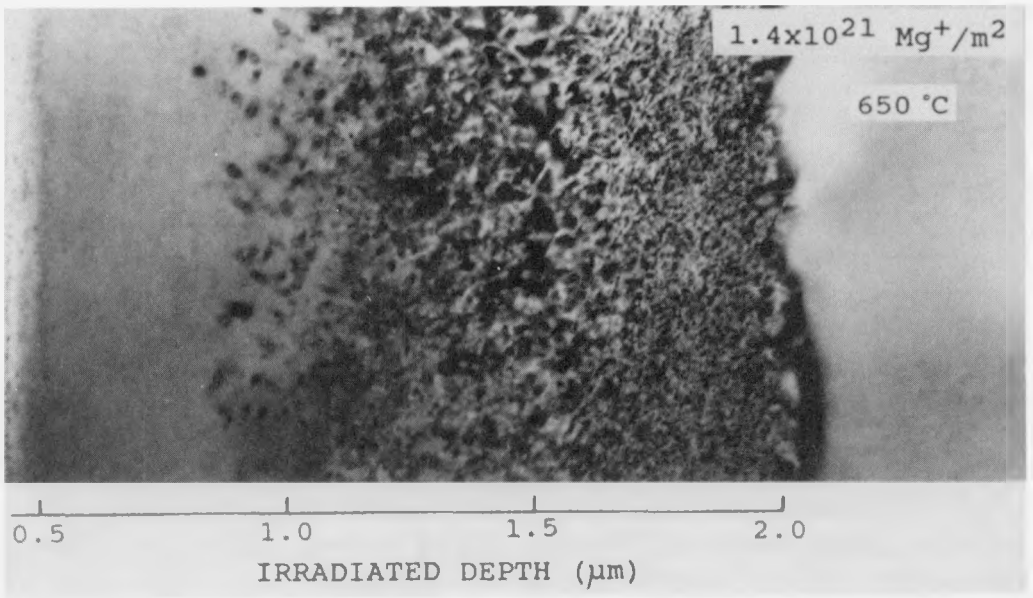

Fig. 4.2.2. Depth-dependent microstructure of ion-irradiated spinel.

ORNL–PHOTO 00315–88

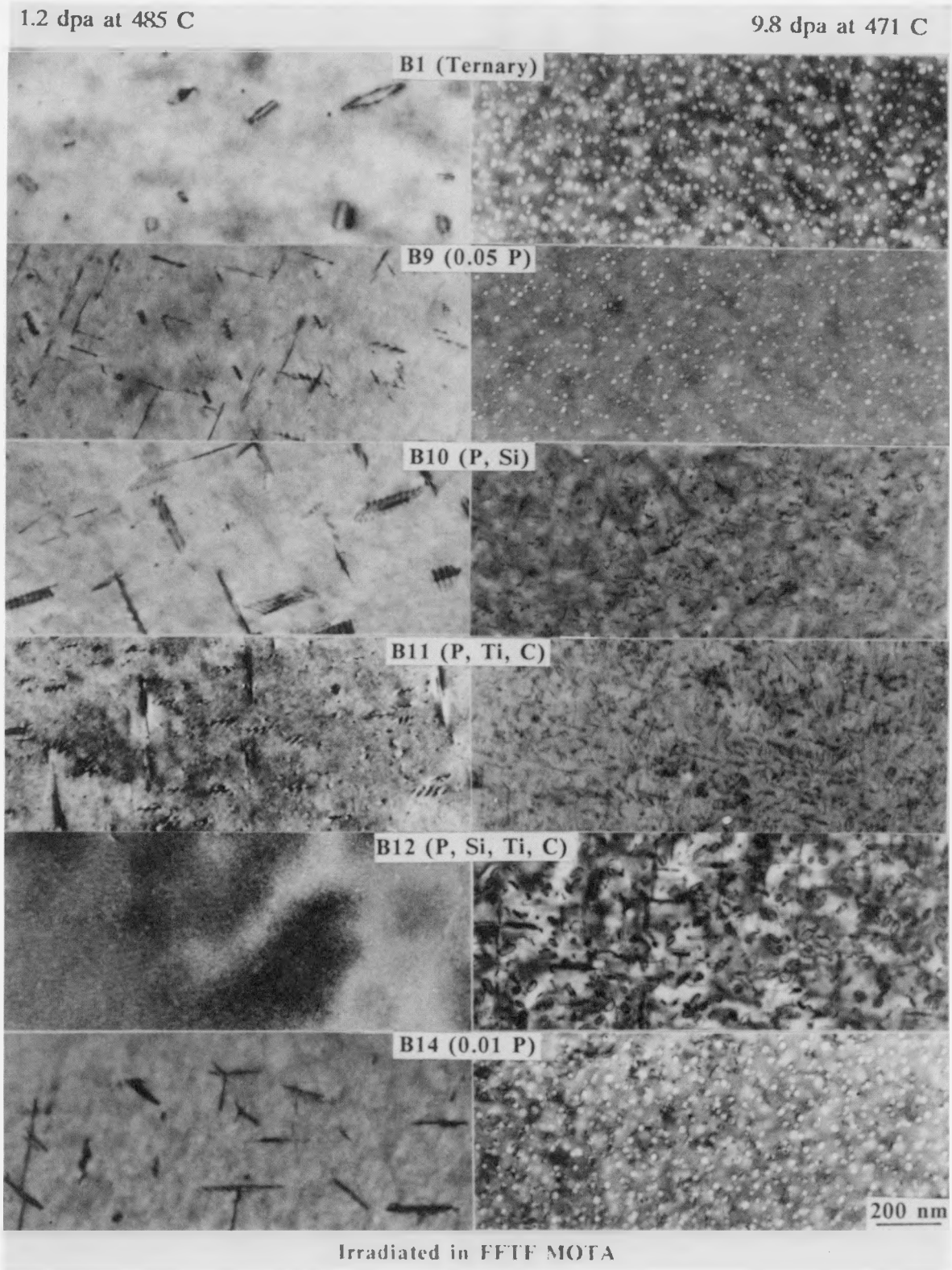

Fig. 4.2.3. Damage microstructure of B-series alloys irradiated to 1.2 dpa at 758 K (left column) and 9.8 dpa at 744 K (right column) in FFTF MOTA.

These results confirmed those of our earlier study, which showed that phosphorous in solution alone did not have a major influence on void swelling, whereas fine-scale phosphide precipitation was quite effective in suppressing void formation.[7] The possible contributing role of impurity oxygen to void formation was considered, but this was found to be secondary to the principal mechanism restricting swelling, the effect of the dense precipitate microstructure. These precipitates foster profuse cavity nucleation, which in turn reduces by dilution the helium accumulation in any given cavity. The cavities thereby require more total helium atoms and much higher dose for individual cavities to exceed the critical number of gas atoms necessary for growth as voids.

4.2.8 Helium Effects on the Microstructural Evolution of Reactor-Irradiated Ferritic and Austenitic Steels[*8] – *D. F. Pedraza, P. J. Maziasz, and R. L. Klueh*

Our review of experimental observations in neutron irradiated austenitic stainless steels and Cr-Mo ferritic steels highlighted several important features of microstructural evolution during irradiation: (1) strong correlation exists between precipitation and void evolution in austenitic steels; (2) helium affects precipitate evolution in austenitic steels, but observations indicate no effect on precipitation in ferritic steels; and (3) helium has a pronounced effect on the cavity evolution in both steel types. Helium effects are explained in terms of the interrelationship between microstructural evolution and point-defect annihilation processes. In stainless steel, three regimes of microstructural behavior for different helium generation rate-displacement rate ratios are recognized: (1) "low" He/dpa ratio, where helium effects on the radiation-induced microstructural evolution are negligible or develop slowly; (2) "medium" He/dpa ratio, where helium effects strongly enhance the micro-structural changes; and (3) "high" He/dpa ratio, where helium effects are limited to the early development of a high density of fine bubbles which interfere with other radiation-induced microstructural changes but allow enhanced thermal microstructural evolution to take place. The extensive data on austenitic steels fall within these regimes. Ferritic steels are known to be highly resistant to void swelling without helium. It is suggested that enhanced cavity formation caused by helium in ferritic steels makes higher swelling a potential concern for fusion reactor applications.

---

[*]Research supported in part by the Office of Fusion Energy.

4.2.9 References

1. Summary of paper, T. Schober and K. Farrell, "Helium Bubbles in α-Ti and Ti Tritide Arising from Tritium Decay: A TEM Study," to be published in the *J. Nucl. Mater.*

2. Visiting Scientist from IFF, KFA Jülich, Federal Republic of Germany.

3. Summary of paper, T. Schober and K. Farrell, "Helium Bubbles in Vanadium and Vanadium Alloys after High Temperature Helium Ion Bombardment," in preparation.

4. Summary of paper, S. J. Zinkle and K. Farrell, "Void Swelling and Defect Cluster Formation in Reactor-Irradiated Copper," *J. Nucl. Mater.*, in press.

5. Summary of paper, S. J. Zinkle and E. H. Lee, "Effect of Oxygen on Vacancy Cluster Morphology in Metals," to be published in the proceedings of the TMS-AIME Fall Symposium on "Irradiation-Enhanced Materials Science and Engineering," Chicago, September 1988, to be published in *Metallurgical Transactions*.

6. Summary of paper, E. H. Lee and N. H. Packan, "Swelling Suppression in Phosphorous-Modified Fe-Cr-Ni Alloys During Neutron Irradiation," to be published in the Proceedings of the 14th ASTM International Symposium on the Effects of Radiation on Materials, Andover, Massachusetts, 1988.

7. E. H. Lee and L. K. Mansur, to be published in *Phil. Mag.*

8. Summary of paper, D. F. Pedraza, P. J. Maziasz, and R. L. Klueh, "Helium Effects on the Microstructural Evolution of Reactor-Irradiated Ferritic and Austenitic Steels," presented at the Workshop on the Effects of Recoil Energy Spectrum and Nuclear Transmutations on the Evolution of the Microstructure, Lugano, Switzerland, March 1988, to be published in *Radiation Effects and Defects in Solids*.

4.3 MATERIALS MODIFICATION AND CHARACTERIZATION

4.3.1 Diamond and Diamond-Like Materials* – *R. E. Clausing, L. Heatherly, K. L. More, and G. M. Begun*[1]

Recently developed techniques for manufacturing films of diamond and diamond-like materials make it possible to create a wide variety of new materials. There are many opportunities to make use of the superlative properties of diamonds if the material can be incorporated into extended surfaces and/or thin layers. We have been fabricating, characterizing, and determining the properties of both hard-carbon diamond-like coatings and polycrystalline diamond films.

Nucleation and growth of the diamond films were carried out by the hot-filament-assisted chemical vapor deposition method under a variety of conditions to provide the basis for a systematic study of diamond microstructures. High-resolution scanning and transmission electron microscopy (SEM and TEM) were used to document and relate the topographic and internal features of diamond films to the film growth conditions. Growth features including twin pyramids, reentrant edges, ledges, growth spirals, and open-lattice-work structures were observed. The growth features can be rationalized in terms of growth mechanisms, although much work remains before the mechanisms are fully understood. We are also correlating the crystal defect density and structure to both the growth conditions and to selected properties of the resulting films. Many of the outstanding chemical, physical, and mechanical properties of diamond are strongly dependent on the impurities, the microstructure of polycrystaline films, and the degree of crystal perfection of the diamond crystal lattice. These factors in turn are dictated by film growth conditions. The hot-filament-assisted chemically vapor-deposited method provides simple, easily characterized and reproducible growth environments. Our goal is to characterize and understand the relations between physical and mechanical properties of the films and the plasma processing parameters through their dependance on microstructure and crystal defects.

Three types of films, each with its own distinctively different morphology, have been grown under controlled closely related conditions. In each case, the growth mechanism

---

*This research was jointly sponsored by: (1) the U.S. Army Strategic Defense Command under MIPR No. W331RPD-8-P4030 with the U.S. Department of Energy and Martin Marietta Energy Systems, Inc.; (2) the U.S. Department of Energy, Division of Materials Sciences, Office of Basic Energy Sciences; (3) the Oak Ridge National Laboratory Seed Money Program; and (4) the U.S. Department of Energy, Assistant Secretary for Conservation and Renewable Energy, Office of Transportation Systems, as part of the High Temperature Materials Laboratory Program.

appears to be dominated by different factors. In the case of the films that have (111) faces exposed, the evidence is that growth often occurs as the result of twin formation on (111) facets or in layers parallel to (111) planes, which originate at the intersection of the plane with another surface. Nucleation of a new layer on a (111) plane is difficult because it requires the addition of two- or three-carbon-atom species. It can be shown that the formation of a new layer is much easier under special circumstances such as those found when twin planes intersect at reentrant angles. This would explain the apparently rapid growth observed at these locations because layers could nucleate and propagate from the junction of the reentrant twin planes by the addition of single-carbon-atom species. The observed proliferation of microtwins, as observed by TEM, is also a likely result of growth on (111) planes. Because these are the dominant twin planes, it is easy to build in stacking faults and/or propagate twins as the microstructure grows by step motion along the (111) plane. The height and width of stepped layers can be analyzed to give insights into the relative importance of surface diffusion and the capture rate of feed material.

Films with (100) faces exposed and nearly parallel to the substrate imply that the crystallites grow more rapidly in <100> directions than in any other direction. Under the growth conditions used the (100) facets remain flat (i.e., the SEM images do not reveal growth spirals or steps). Molecular models show that it is possible to add single carbon atom species to flat (100) faces. One would expect that growth in this manner could lead not only to freedom from growth twins and stacking faults but also perhaps to an increase in the point defects present. This appears to be the case, as evidenced by the TEM studies and by the luminescence in the Raman spectra.

In summary, we are working to understand the relationship among the properties of the films, their structures, and growth conditions to be able to design and grow better films for specific applications. The ORNL M&C Division is uniquely positioned to exploit existing capabilities to develop understanding and applications of this new materials technology.

4.3.2 Effect of Simultaneous B^+ and N_2^+ Implantation on Microhardness, Fatigue Life, and Microstructure[2] – *E. H. Lee and L. K. Mansur*

Ion beam modification of surfaces is a rapidly expanding technology that has been applied to many engineering materials to improve properties ranging from mechanical, electrical, magnetic, and optical to corrosion and biocompatibility. Of interest in the current work are surface-sensitive mechanical properties, in particular hardness, wear and fatigue. Previous studies have shown that ion implantation can have beneficial effects on tribological properties and fatigue life of materials and that the improvement is highly dependent on implantation parameters as well as the bulk material composition. The current work is part of our program to examine the effects of multiple-ion-beam treatment on surface-sensitive properties of Fe-Ni-Cr alloys.

Microhardness and cantilever beam fatigue measurements were conducted on Fe-13Cr-15Ni base austenitic alloys that were implanted with boron and nitrogen ions

either singly or simultaneously. Experimental data show that both hardness and fatigue life were improved by ion implantation. The similar trend of these two properties with ion beam treatment may have similar microstructural origins including damage-induced defect hardening, solution strengthening, and/or precipitate pinning, which restrict dislocation motion and slip distance. Fatigue life was, however, more dependent on both alloy composition and implanted-ion species. Changes in stacking fault energy and the nature of precipitate formation appeared to play important roles. A clear change of slip mode with implantation from wavy to planar glide suggests that stacking fault energy is reduced by implantation, as demonstrated in Fig. 4.3.1, and that crack initiation and, consequently, fatigue failure are delayed.

The degree of fatigue improvement varied with minor changes in the base-alloying compositions and the concentration of implanted species. Nitrogen was detrimental or ineffective in the presence of titanium, and boron was much more effective in the presence of molybdenum. Implanted concentrations in excess of 2 at. % appear to have no beneficial effect. Although precipitate formation was not observed in the implanted specimens, the size and concentration of the observed but unidentified ion-beam-induced clusters may play a crucial role in determining fatigue life.

4.3.3 Diffusion of Ion-Implanted Helium in Vanadium and Niobium[3] – *M. B. Lewis*

In our previous investigations of the migration of helium in metals,[4-7] we show that helium migrated by trapping and detrapping, which retarded the effective diffusion rate by many orders of magnitude below that expected for interstitial diffusion. Helium diffusion in fcc nickel and stainless steel was shown to be low compared with hcp titanium and zirconium. The one bcc material investigated, iron, showed characteristics intermediate between the two. In the current work, bcc vanadium and niobium were investigated.

The materials were implanted with ^{3}He at an energy of 200 keV and a flux of 3×10^{16} He m^{-2} s^{-1} for a period of 1 h; this would have produced a calculated peak helium density of a few tenths of an atomic percent if no diffusion took place during the implantation. Helium concentration versus depth profiles for implantations into vanadium targets are shown in Fig. 4.3.2. The target temperatures chosen for the implantation were 300, 880, and 1064 K. A statistical analysis of the shape of the 300 K data indicated a mean range of 0.59 μm and a range width of 0.10 μm. These mean range and range width values are similar to those given by theoretical range calculations. At the implantation temperature of 880 K, however, significant helium diffusion is indicated in Fig. 4.3.2. At 1064 K even more diffusion is indicated. In particular, the peak concentration has decreased by nearly a factor of 2 and a noticeable amount of helium has collected at the target surface. Approximately 80% of the implanted helium is accounted for by integrating the region from the surface to 1.0-μm depth. The helium concentration versus depth profiles for implantations into the niobium targets are qualitatively similar to those for vanadium.

YP 8898

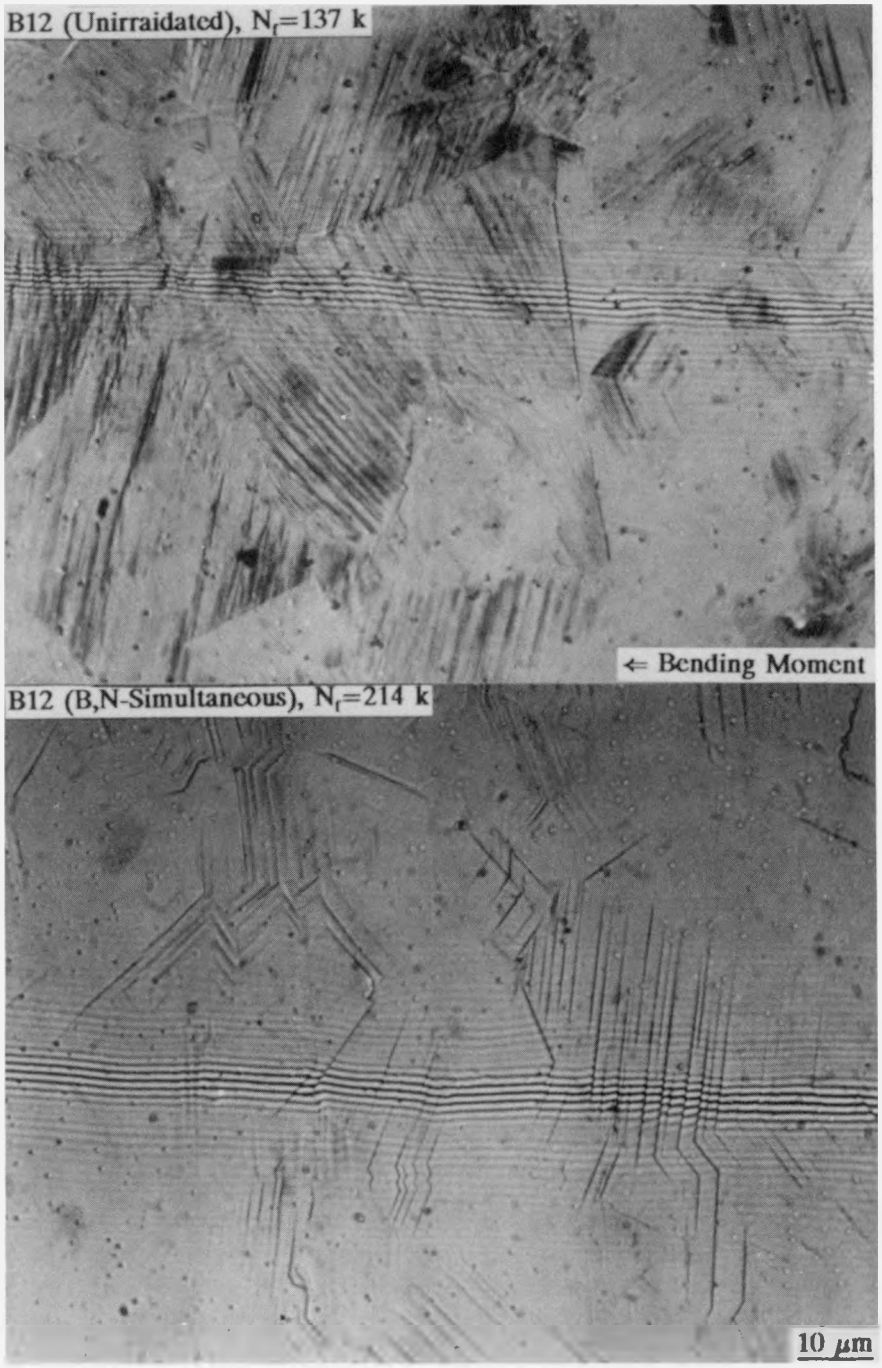

Fig. 4.3.1. Unirradiated B12(Fe-Cr-Ni-Si,P,Ti,C) alloy shows shorter fatigue-life, wavy slip deformation, and cracks mostly at twin or grain boundaries, whereas B,N-implanted specimen shows longer fatigue-life, planar slip deformation and cracks mostly at persistent slip bands. Slip deformation occurs much slower and is confined locally near the maximum stress area in B,N-implanted specimen. Optical interference fringes delineate the surface roughness.

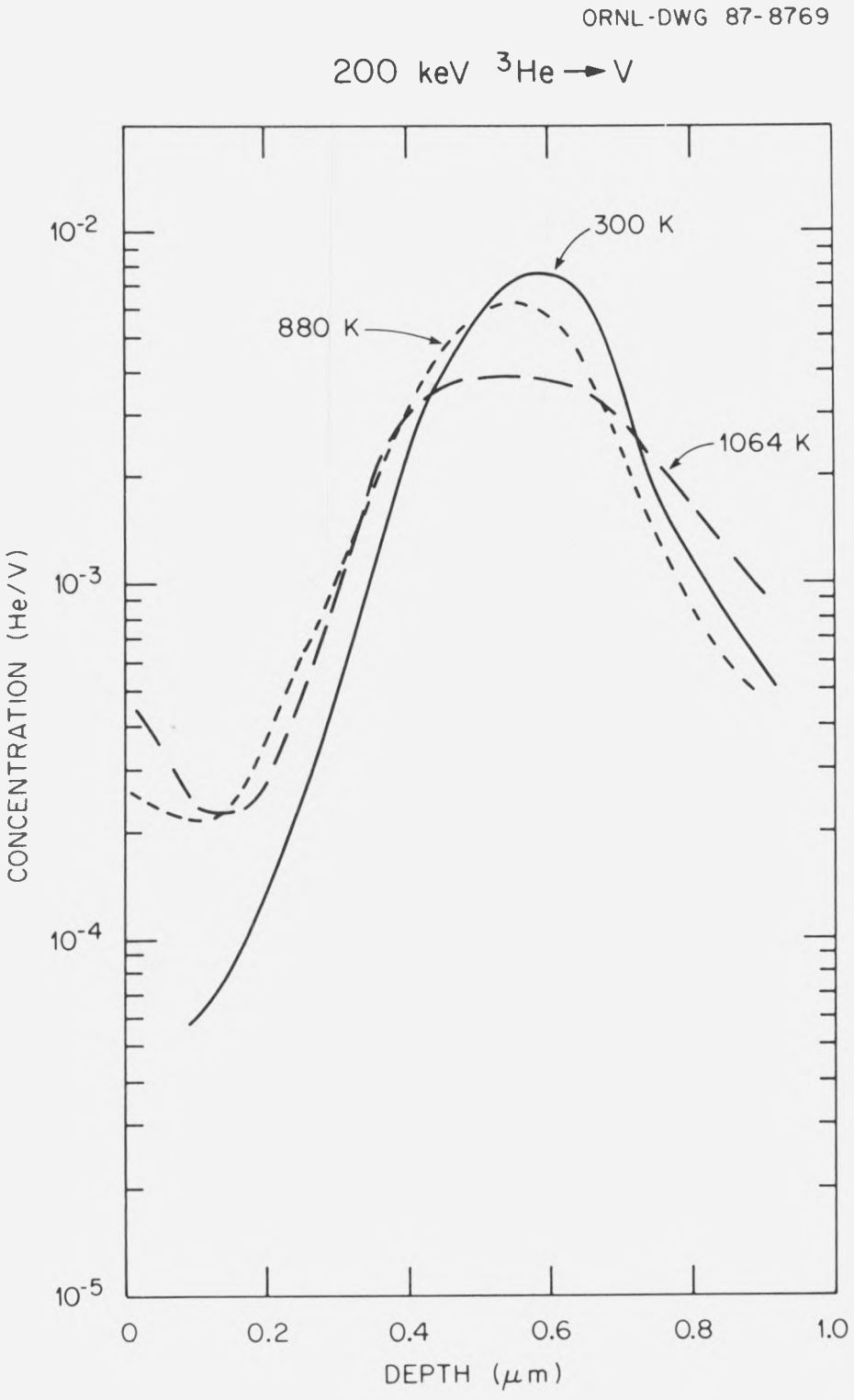

Fig. 4.3.2. Measured concentration versus depth profiles for 200-keV helium-implanted vanadium at the indicated temperatures.

To derive quantitative information for the helium concentration versus depth profiles, two types of diffusion models were tested.[4,6,8] Both models assume that the ion-implanted helium, after reaching its end of range, becomes trapped in a vacancy. In the first model, the substitutional or S-model, the binding energy of the helium to the vacancy is very strong such that it cannot escape the vacancy unless another lattice vacancy becomes a nearest neighbor and the helium hops into it. This mechanism is the same as that for substitutional diffusion. In the second model, the dissociative or D-model, helium can detrap from the vacancy and migrate as an interstitial until it is trapped elsewhere. A comparison of S-model and D-model calculations is shown in Fig. 4.3.3 for a profile of helium in vanadium. These curves for the highest temperature implantation are compared with the measured profile. The agreement between calculated and measured curves is good.

The current results, together with those from our previous work[4-7] and some of our unpublished measurements, show a trend in the relationship between helium diffusion and radiation induced swelling, namely that lower-swelling materials exhibit higher helium diffusion rates. A qualitative summary is given in Table 4.3.1.

Table 4.3.1. Qualitative trends of helium diffusion and swelling

fcc	bcc	hcp
Al[a]	V	
Ni	Fe	Ti
SS[b]	Nb	Zr
High swelling	Moderate swelling	Low swelling
Low diffusivity	Moderate diffusivity	High diffusivity
No surface trapping	Moderate surface trapping	Large surface trapping

[a]Tentative and unpublished data.

[b]Stainless steel type 316.

4.3.4 Lattice Site Occupation of Helium in Magnesium Oxide and Aluminum Oxide – *W. R. Allen[9] and M. B. Lewis*

Radiation damage and transmutation-produced helium contribute to dimensional instability and mechanical property degradation in metals and alloys under neutron irradiation. Swelling, phase transformations, and embrittlement strongly depend on helium mobility. The large (n,α) cross section of oxygen for fast neutrons implies abundant helium production for ceramic oxides in a fusion reactor environment. Yet there is little information on the behavior of helium in ceramics. To investigate the

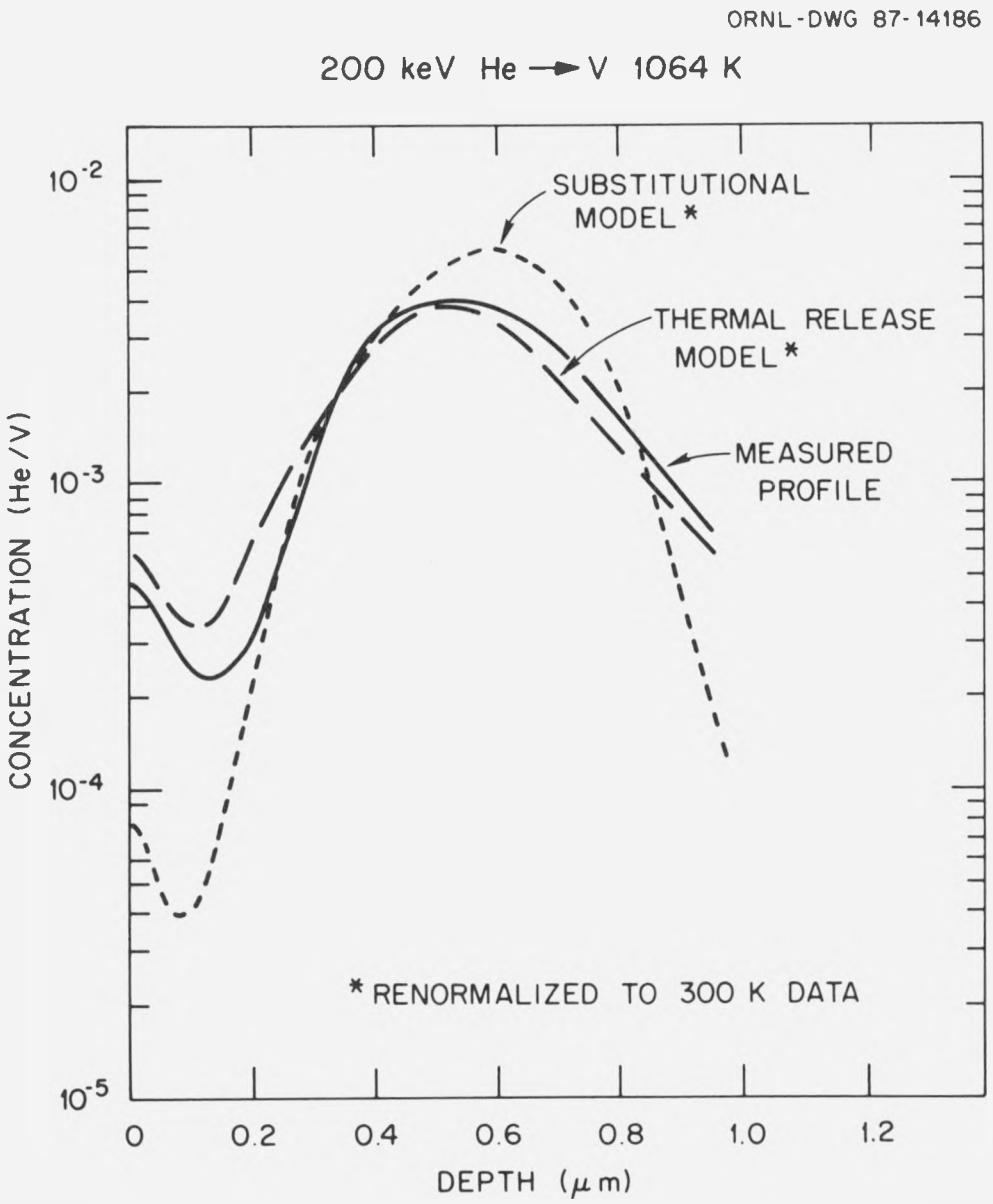

Fig. 4.3.3. Measured and calculated profiles for helium-implanted vanadium.

lattice site occupation and mobility of helium in ceramic oxides, we used helium ion implantation and nuclear-scattering techniques.

Helium was implanted at an energy of 200 keV to a fluence of 10^{20} m^{-2} into single-crystal MgO and Al_2O_3. Targets were held at temperatures ranging from room temperature to 800°C. Depth profiling with the $^3He(d, \alpha)^1H$ reaction revealed that the helium was trapped in a well-defined profile for all implant temperatures in both materials. Ion channeling with deuterons along the <0001> axis of aluminum oxide implanted at room temperature indicated that the helium was shielded from the analysis ion beam. Angular yield profiles are presented in Fig. 4.3.4. However, the helium was highly visible as randomly oriented to the ion beam along the [001] axial direction of magnesium oxide implanted at room temperature. Angular yield profiles are presented in Fig. 4.3.5.

The contrasting ion-channeling behavior between the two materials may be explained if the helium occupies individual lattice sites in aluminum oxide and is distributed randomly within the lattice structure of magnesium oxide. Multiple helium-vacancy complexes would present the helium to the analysis ion beam as being randomly positioned. The implantation process produces some vacancies (<0.04 dpa), but probably not enough to promote significant occupation of lattice sites through replacement collisions. Helium atoms may reside in the intrinsic "structural" vacancies present in aluminum oxide.

Magnesium oxide and aluminum oxide have polyatomic lattice structures. Aluminum oxide possesses the corundum structure and magnesium oxide the sodium-chloride structure. Within a corundum lattice structure, cations occupy only two-thirds of the octahedral interstices within the hexagonal oxygen sublattice. The unique empty octahedral interstices may contribute to the placement of helium on regular lattice sites within the corundum lattice structure. Measurements along other major axes and planes of aluminum oxide are under way to confirm a unique lattice site.

The degree of lattice-site occupation by the implanted helium in aluminum oxide is sensitive to the implant temperature. As the implant temperature is raised, the degree of apparent substitutionality and the channeling half-angle decrease for measurements along the [0001] axis. This may indicate that the helium atoms are gathering in multiple helium-vacancy clusters. Such distorted sites would be more visible to the analysis ion beam.

4.3.5 Range Distributions of 200 keV Helium in Selected Metals and Ceramics[10] – *M. B. Lewis and W. R. Allen*[11]

Helium range data are important for purposes of designing the first walls of future fusion reactors and for basic research studies. Ion-implantation and ion-beam characterization techniques offer powerful methods to obtain basic profile and diffusion information. Helium profiles were measured for 30-300 keV implantations using the

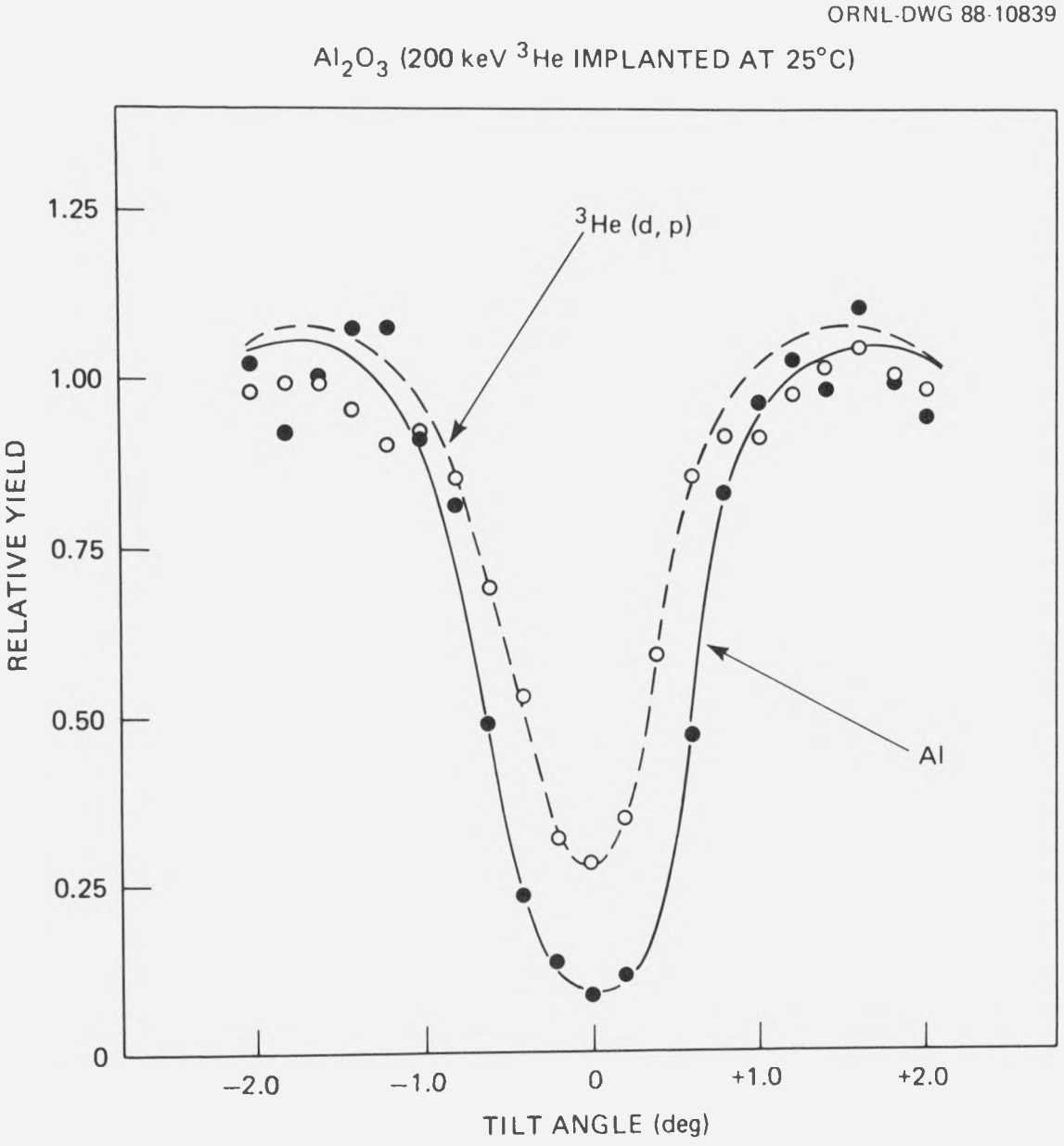

Fig. 4.3.4. Angular yield profiles generated by an analysis ion beam of 500-keV deuterons as the helium-implanted aluminum oxide crystal is rocked near the <0001> axial symmetry direction. The Al curve denotes elastic scattering of deuterons from aluminum, and the second curve denotes protons from the $^3He(d,p)He$ reaction.

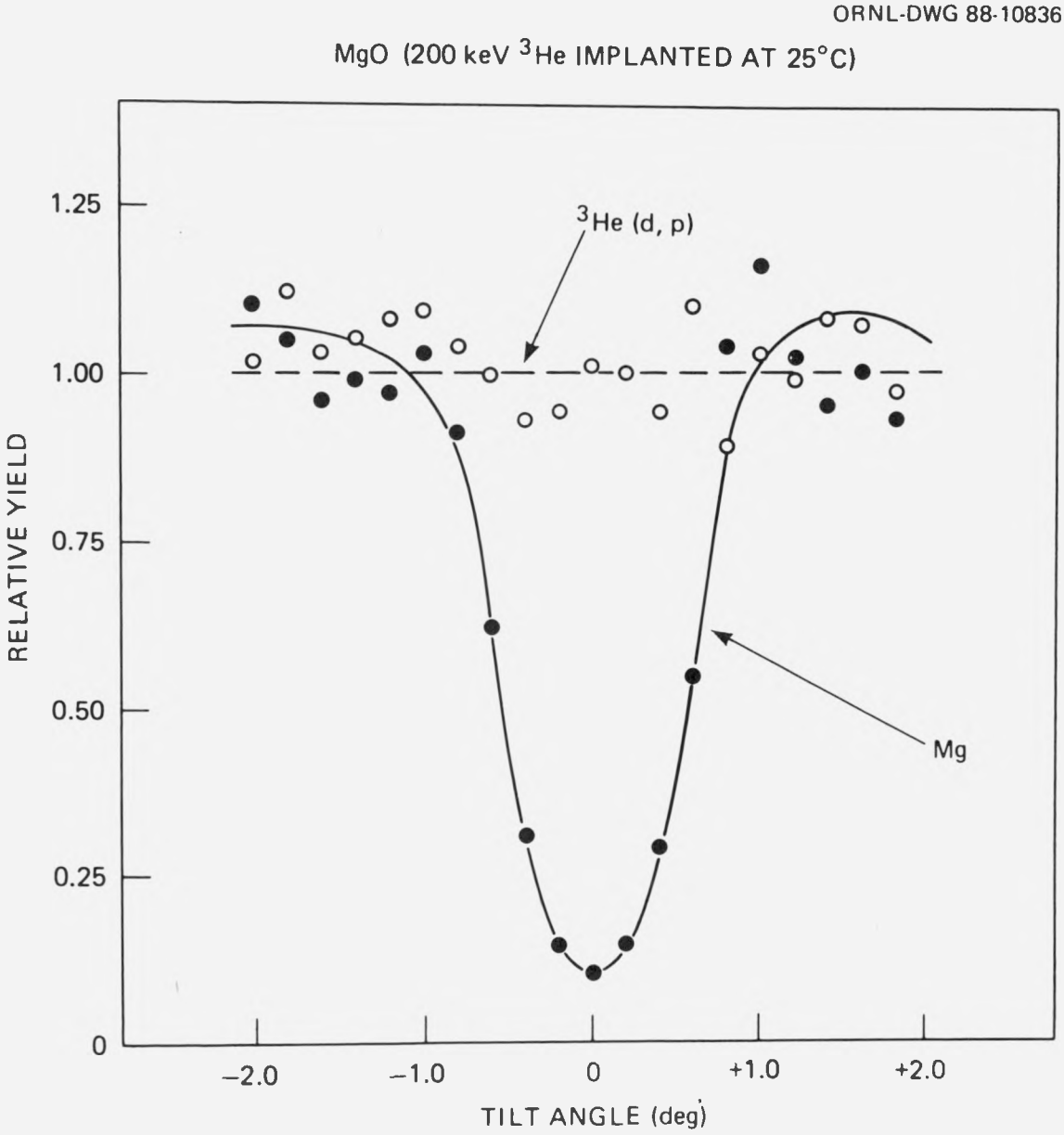

Fig. 4.3.5. Angular yield profiles generated by an analysis ion beam of 500-keV deuterons as the helium-implanted magnesium oxide crystal is rocked near the <001> axial symmetry direction. The Mg curve denotes elastic scattering of deuterons from magnesium, and the second curve denotes protons from the ^{3}He(d,p) He reaction.

$^{3}He(n,p)^{3}H$, $^{4}He(p,p)^{4}He$, and $^{3}He(d,\alpha)^{1}H$ nuclear reaction methods. A typical nuclear reaction product energy spectrum for 500 keV deuterium incident on Al_2O_3 is displayed in Fig. 4.3.6. Various reaction products from inelastic deuteron interactions with oxygen nuclei are noted in the spectrum. The 4.52-MeV alphas from the $^{3}He(d,\alpha)^{1}H$ reaction appear in the spectrum near an energy of 3 MeV.

When 200-keV helium ions were implanted at room temperature in the metals Mg, Al, Ti, V, Fe, Ni, Zr, and Nb, and in the ceramics MgO and Al_2O_3, they became trapped near the end of the ion range. Assuming no appreciable diffusion took place during or after the implantation, the measured helium concentration profiles may be compared with corresponding profiles calculated by a range code such as TRIM. When we made such comparisons, it was apparent that most mean ranges were similar to and range widths were slightly larger than the calculated values. The measured skewness was negative and the kurtosis was usually larger than 3. The third and fourth moments were in some cases more Gaussian-like than theoretical estimates.

The fact that the measured values of range straggling were larger than theoretical values could be evidence for some interstitial diffusion of helium during the implantation. Such diffusion is expected to manifest itself by making the range distributions more Gaussian. The discrepancy might also be resolved by lowering slightly the repulsive interatomic potential used in the TRIM code. This should lead to somewhat more Gaussian-like range distributions. Finally, the structure of crystalline targets may affect the distribution of implanted ions via unintentional channeling. In this case, measured range parameters may deviate from predictions of range codes that consider the target to be structureless.

4.3.6 Range Study of Oxygen Implanted in Selected Materials[12] – *W. R. Allen[13] and M. B. Lewis*

A recent study of oxygen implanted into single-crystal magnesium oxide[14] has reported an anomalous range for the damage peak that differs from the forecasts of popular range codes by a factor of 2. We performed experiments to clarify this discrepancy in MgO and add to the existing data base of ion implantation range profile measurements in a number of other materials.

Oxygen in the form of the isotope ^{18}O was implanted into MgO, Al_2O_3, $MgAl_2O_4$, silicon, aluminum, and magnesium at energies of 0.25, 0.90, and 2.00 MeV. Concentration profiles of oxygen were characterized with the $^{18}O(p,\alpha)^{15}N$ nuclear reaction. The projected range and range straggling of each profile were compared with the predictions of the range simulation codes TRIM (ref. 15) and EDEP-1 (ref. 16). General agreement between the experimental and the calculated values was obtained.

The position of the damage peak found in ref. 14 is inconsistent with both the measured and calculated values of projected range found in the current work. Because the previous study was based on the range of microstructural change, this implies that the observed microstructural damage extends well beyond the ion-implantation range.

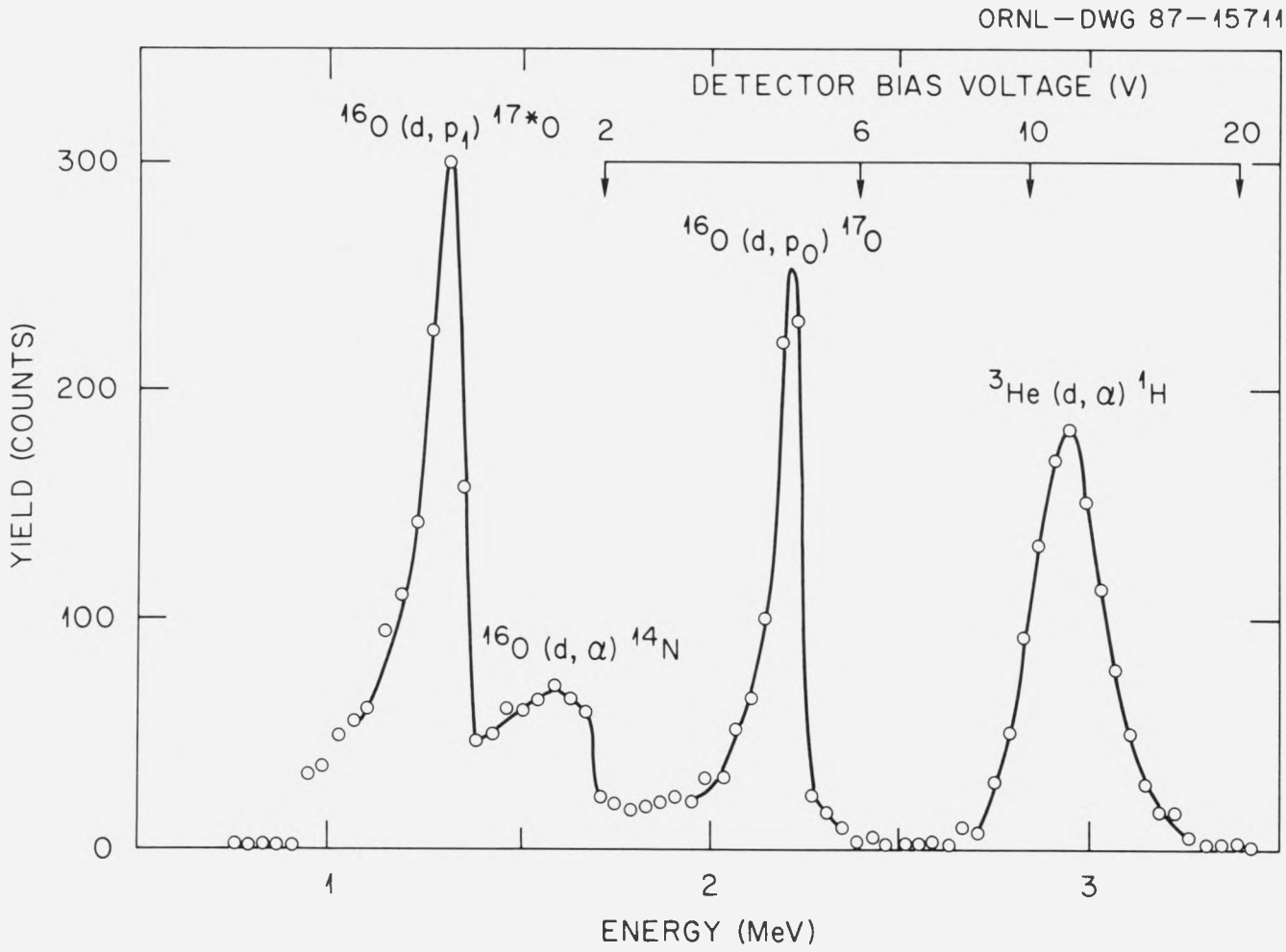

Fig. 4.3.6. Typical nuclear reaction product spectrum for 500-keV deuterium incident on a ^{3}He-implanted sample of Al_2O_3. The primary peaks are identified by their reaction type. The location of reaction protons in the spectrum is dependent on the detector bias.

4.3.7 In Situ Study of Crystallization and Recovery of Partly Amorphous NiTi[17] – *P. J. Maziasz and D. F. Pedraza*

During ion irradiation of NiTi at temperatures of 150 to 250°C, it was found that amorphization proceeded inhomogeneously throughout a volume that had been irradiated to a given displacement dose. Amorphous regions, immersed in a heavily damaged B2 crystalline matrix, were fairly large and exhibited a morphology that very closely resembled the martensitic structure that existed prior to heating to the irradiation temperature, as shown in Fig. 4.3.7. Because the irradiations began shortly after the specimens reached the desired temperature, it is considered likely that any defect microstructure remaining after the reversion of martensite to B2 did not anneal away. The presence of such defects could accelerate the amorphization kinetics. The particular morphology that we obtained in partly amorphous specimens allowed us to study some relevant aspects of post-irradiation annealing of the microstructural changes induced by irradition.

A specimen that had been partly amorphized by Ni-ion irradiation at 200°C to a dose of 0.5 dpa was subjected to a series of thermal anneals at temperatures that were increased stepwise between 200 and 425°C. When the temperature of 425°C was reached, the microstructure started to change. Crystallization began in the bulk of the amorphous regions, unrelated to the existing crystalline/amorphous interface. Nucleation and growth of grains took place, while the initially crystalline regions remained unchanged. A time sequence showing various stages in the crystallization of a single amorphous region can be seen in Fig. 4.3.8. When crystallization of the amorphous regions was quite advanced, changes began to be detected in the crystalline regions as damage recovered, interspersed amorphous pockets crystallized, and possibly some grain growth occurred.

4.3.8 Temperature Dependence of the Amorphization of NiTi Irradiated With Ni Ions[18] – *P. J. Maziasz, D. F. Pedraza, J. P. Simmons,[19] and N. H. Packan*

NiTi was irradiated with Ni ions at various temperatures to study the temperature dependence of the irradiation-induced crystalline-to-amorphous transition. The irradiations were conducted above the Af temperature, and thus the specimens contained only the ordered B2 (CsCl) phase. Irradiations to similar doses at 150, 200, and 250°C showed that the amorphization kinetics slowed down appreciably as the temperature was increased in this range. No amorphization was detected at irradiation temperatures of 350°C or higher, up to doses of 4 dpa. The small volume fraction of amorphous material observed after irradiation to 0.67 dpa at 250°C indicated that the cutoff temperature for amorphization was in the vicinity of this temperature. The amorphous regions of partly amorphous samples were distributed nonuniformly, and exhibited a morphology similar to the martensitic microstructure that existed in the specimens before heating to the irradiation temperature. Large amorphous regions in these specimens exhibited some very fine crystalline debris that tended to disappear with increasing irradiation dose. Postirradiation annealing experiments indicated that no thermally activated crystallization occurred during irradiation at temperatures up to 250°C.

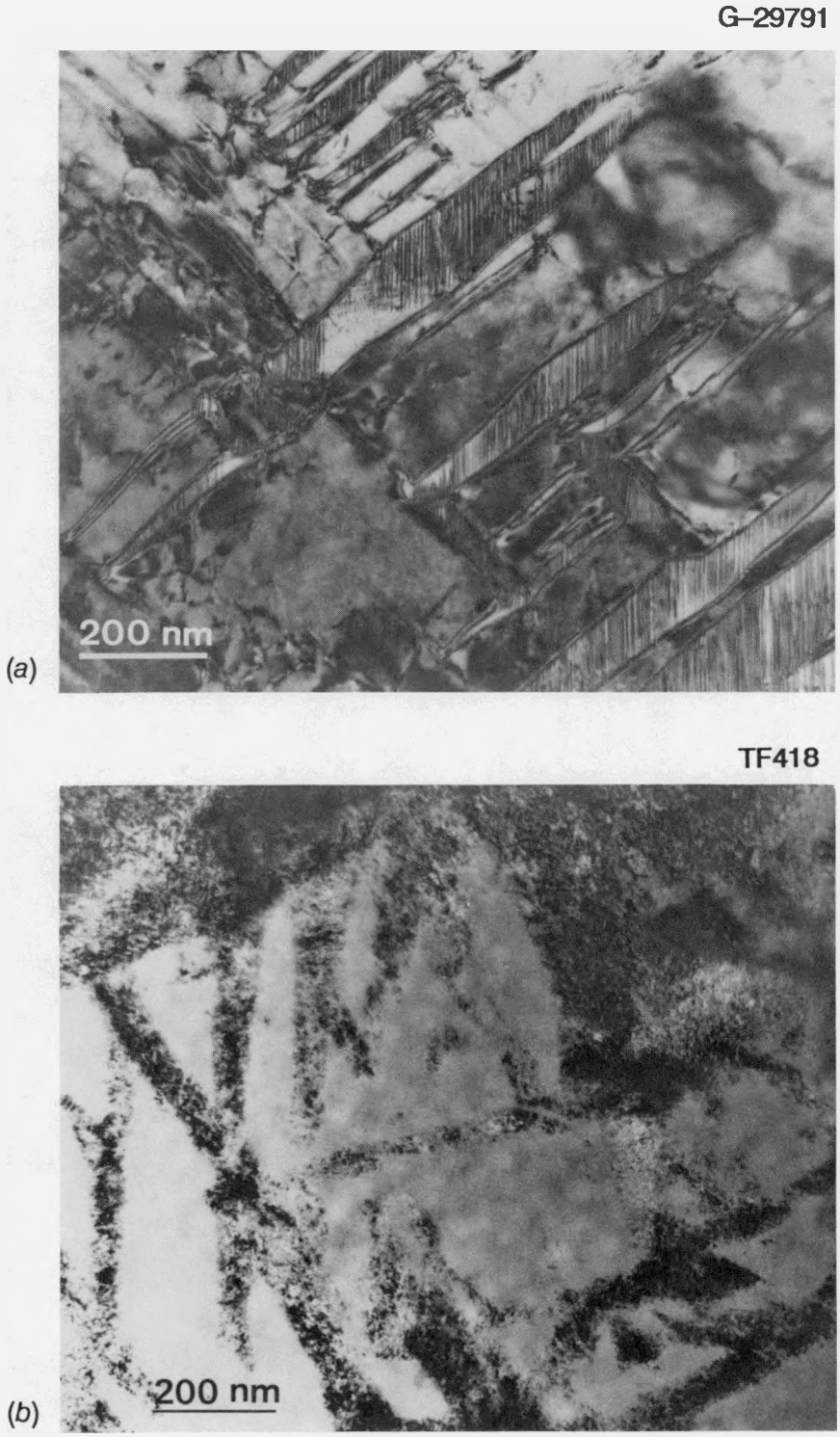

Fig. 4.3.7. Microstructure of NiTi; (*a*) prior to heating and irradiation showing martensitic plates immersed in an austenitic (B2) matrix and (*b*) irradiated at 200°C to a dose at 0.5 dpa.

ORNL PHOTO 4028–89

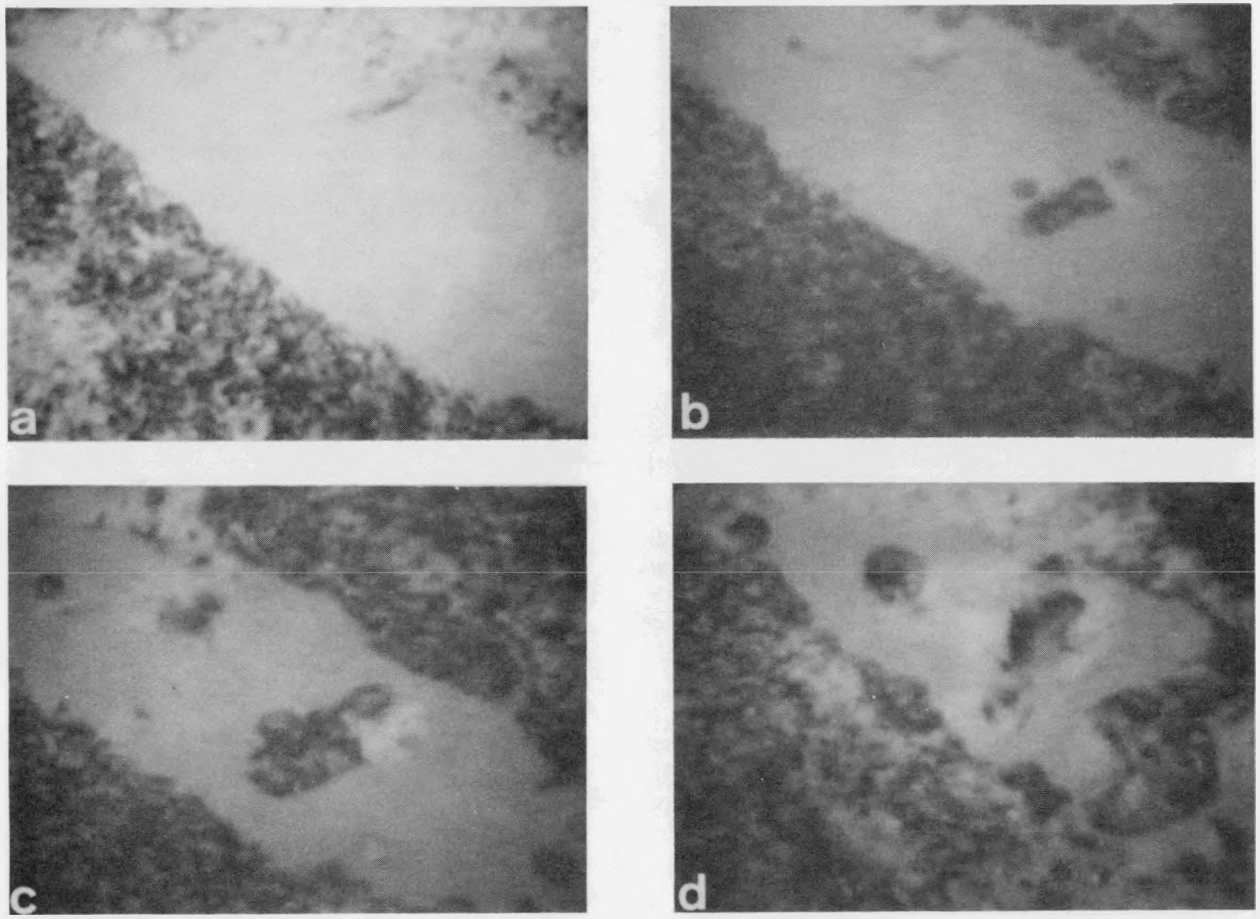

Fig. 4.3.8. The progress of crystallization in a single area during postirradiation annealing at 425°C; (*a*) amorphous region surrounded by damaged crystalline matrix; (*b*) small crystals are seen to have nucleated homogeneously; (*c*) later stage showing a larger number of grains; and (*d*) advanced crystallization stage showing impingement of internally nucleated grains into the surrounding damaged crystalline region.

4.3.9 Nucleation and Amorphization of Radiation-Induced Phases in a Modified Austenitic Stainless Steel During Ni-Ion Irradiation[20] – *E. H. Lee and E. A. Kenik*

The formation of radiation-induced (G) and radiation-enhanced (η) phases in a silicon- and titanium-modified austenitic stainless steel have posed particular problems. These precipitates often aid cavity growth by collecting gas atoms and point defects at the precipitate-matrix interfaces during irradiation. It is, therefore, important to understand the nature and origin of these precipitate phases to avoid such detrimental effects.

The Si- and Ni-enriched intermetallic G and n phases form under high temperature (950 K) irradiation as the result of radiation-induced segregation to interstitial dislocation loops. Availability of carbon promotes the formation of n phase relative to G phase. Under lower-temperature (450 K) irradiation, G and n phases are amorphized without significant change in composition of metallic elements. Two carbide phases (MC and $M_{23}C_6$) remain crystalline for the same irradiation conditions. This difference in propensity for amorphization may be related to the fact that the latter phases have a higher degree of nonmetallic bonding. Alternatively, the more mobile carbon may allow faster repair of the damaged carbides than the lower mobility silicon allows for the silicides. The amorphization is believed to result from point-defect buildup increasing the free energy of these crystalline phases above that of the amorphous state. The control of these phases may be achieved by optimizing silicon additions and by minimizing radiation-induced defect fluxes by cold-working of the material.

4.3.10 References

1. Chemistry Division.

2. Summary of paper, E. H. Lee and L. K. Mansur, "Effect of Simultaneous B^+ and N_2^+ Implantation on Microhardness, Fatigue Life, and Microstructure," to be published in the *Journal of Materials Research*, Nov./Dec. 1989.

3. Summary of paper, M. B. Lewis, "Diffusion of Ion Implanted Helium in Vanadium and Niobium," *J. Nucl. Mater.* **152**, 114-22 (1988).

4. M. B. Lewis and K. Farrell, *Nucl. Instrum. Methods* **B16**, 163 (1986).

5. M. B. Lewis, *J. Nucl. Mater.* **148**, 175 (1987).

6. M. B. Lewis, *Nucl. Instrum. Methods* **B22**, 499 (1987).

7. M. B. Lewis, *J. Nucl. Mater.* **149**, 143 (1987).

8. L. K. Mansur, E. H. Lee, P. J. Maziasz, and A. F. Rowcliffe, *J. Nucl. Mater.* 141-43, 633 (1986).

9. University of Tennessee, Knoxville.

10. Summary of paper, M. B. Lewis and W. R. Allen, "Range Distributions of 200 keV Helium in Selected Metals and Ceramics," *Nucl. Instrum. Methods* B35, 10 (1988).

11. University of Tennessee, Knoxville.

12. Summary of the paper (in preparation).

13. University of Tennessee, Knoxville.

14. L. L. Horton, J. Bentley, and M. B. Lewis, *Nucl. Instrum. Methods* B16, 221 (1986).

15. J. P. Biersack and L. G. Haggmark, *Nucl. Instrum. Methods* 174, 257 (1980).

16. I. Manning and G. P. Mueller, *Comput. Phys. Commun.* 7, 85 (1974).

17. Summary of paper P. J. Maziasz and D. F. Pedraza, "In Situ Study of Crystallization and Recovery of Partly Amorphous NiTi," *Scr. Metall.*, to be published.

18. Summary of the paper, P. J. Maziasz, D. F. Pedraza, J. P. Simmons and N. H. Packan, "Temperature Dependence of The Amorphization of NiTi Irradiated with Ni Ions," *J. Mater. Res.*, in press.

19. Carnegie-Mellon University, Pittsburgh, Pa.

20. Summary of paper, E. H. Lee and E. A. Kenik, "Nucleation and Amorphization of Radiation-Induced Phases in a Modified Austenitic Stainless Steel During Ni-Ion Irradiation," *J. Mater. Res.* 3(5), 840 (Sept./Oct. 1988).

4.4 FACILITY AND TECHNIQUE DEVELOPMENT

4.4.1 Progress in the Development of the Triple-Ion Laboratory – *M. B. Lewis, W. R. Allen, R. A. Buhl, N. H. Packan and S. W. Cook*

In the spring of 1987 a 2.5-MV Van de Graaff ion accelerator was added to the M&C dual-ion-beam laboratory, comprised of 5-MV and 400-kV Van de Graaff accelerators. Experimental work with this new "Triple Ion Laboratory" was initiated immediately. One of the first uses of the new accelerator was to perform irradiations simultaneously with the 5-MV accelerator. An oxygen beam from the 2.5-MV machine and a magnesium beam from the 5-MV machine were used to irradiate MgO targets for microstructural studies.

In the fall of 1987, a duoplasmatron source was installed on the 5-MV machine. Proton intensities of about 40 microamps/cm^2 were used to irradiate tensile specimens of about 100-μm thickness. The specimens were mounted in a special stressed-specimen chamber to study stress effects on microstructural development. Meanwhile, a new scattering chamber was being set up on the 2.5-MV beam line. This chamber had instrumentation that enabled us to characterize materials using nuclear analysis techniques including Rutherford backscattering/channeling and nuclear-reaction analyses. Two special target asssemblies were tested, one for ion channeling and one for high- and low-temperature ion implantation.

During the winter of 1987-88, development work with the ion source for the 400–kV machine led to two new and useful ion beams, carbon and boron. Carbon beams of several microamps were produced in the form of CH^+, starting with methane source gas. Boron beams of several microamps were produced with boron triflouride gas. Both these gases reduced the life-time of the source bottle to about 200 h of continuous service but so far have caused no destructive effects on other components of the accelerator. The carbon beam was used to irradiate organic films. The boron beam was used along with a nitrogen beam from the 2.5-MV machine for simultaneous implantation to form subsurface boron nitride precipitates in steel.

In February 1988, the first triple-beam irradiation was carried out. A 2-MeV Al^+ beam, a 1.4-MeV O^+ beam, and a 0.2-MeV He^+ beam were used simultaneously to irradiate an $MgAl_2O_4$ spinel. Software for beam profile analysis was upgraded to track the fluence of all three beams. During the spring of 1988, isotopic ^{18}O was implanted into Al_2O_3 and the depth profile was measured with the (p,α) nuclear reaction. Both implant and characterization were carried out with the new 2.5-MV accelerator. In addition, the new accelerator was used to perform several ion-channelling studies on helium-implanted Al_2O_3 and MgO. This led to the discovery that helium in Al_2O_3 can be implanted above room temperature on individual lattice sites without precipitation into larger clusters. During 1988, the primary documents for radiation safety were completed, viz, the "Safety Study" and "Operational Safety Requirements."

In late 1988 and early 1989 a second type of triple-ion irradiation was performed. Carbon ions were extracted from the 5-MV accelerator by stripping CO ions, nitrogen

ions were accelerated by the 2.5 MV machine and boron ions were again produced by the 400-kV Van de Graaff. These ions were used to irradiate Fe-Ni-Cr alloys. These unique experiments will investigate the effects of multiple-ion beams on surface-sensitive mechanical properties and the relation to microstructure and composition. Recently, the first implantations were completed using the new high temperature target goniometer. Helium was implanted into Al_2O_3 and MgO targets, which were held at temperatures up to 1000°C as part of our program to study diffusion of helium in ceramics. During the past two years, development of a more sophisticated triple ion irradiation chamber has been under way, and is described in Sect. 4.4.2.

4.4.2 Multiple-Ion-Beam Target Chamber – *R. A. Buhl*

A unique multiple-chamber system to facilitate experiments at the Triple Ion Laboratory is nearing completion. The system consists of three chambers, linked by ultrahigh-vacuum valves through which specimens are transferred via a track-type shuttle system. Only one chamber need be vented to the atmosphere during the specimen loading procedure. The three principal modules are a loading/evaporation dual-purpose chamber, a bombardment chamber, and an Auger chamber. Under normal operating conditions, the bombardment chamber resides at the intersection of three beam lines from the three Van De Graaff accelerators, allowing simultaneous triple ion bombardments on a single target. However, the chambers are mounted on a frame with "airfloat" pads beneath the feet, so that lateral translation permits ion bombardments within either of the other two chambers in the system. In the loading/evaporation chamber, simultaneous film evaporation and ion-beam-implantation/mixing experiments can be carried out.

Figure 4.4.1 shows the modular target chamber from the downstream side. The airfloat pads can be seen at the floor. Vacuum pumps include a Balzers TPU 510 turbopump for the loading/evaporation chamber, an Air Products AP-8 cryopump for the main damage chamber, and a combination of a Varian 4001/s model 912-7022 Vaclon pump and LN shrouded titanium sublimation pump for the Auger chamber. The electronic equipment rack contains an Icon evaporation rate controller, a Hewlett-Packard 3853 data-acquisition/controller extender crate, Granville Phillips TC and ion gauge controllers, a stepping motor controller, a 2.5-kV electron gun evaporation power supply and controller, a titanium sublimation pump controller, and the Vaclon pump controller.

A dispenser cathode triode-type electron gun assembly is used to heat the specimen holder from the back side. This electron beam heater is mounted on a water cooled, spring loaded, pneumatic positioner attached to the top flange of the bombardment chamber. Specimens are mounted in a 3 x 3 array in the specimen holder with a 0.005–in. surface thermocouple,as shown in Fig. 4.4.2. The surface thermocouple is used to set the emissivity value in the infrared pyrometer that measures the specimen temperatures. Two 0.040–in. sheathed, spring-loaded thermocouples are positioned in the midplane of the specimen holder to control the output of the electron beam heater. The trolley assembly contains bearings that suspend the trolley as it

YP 6663

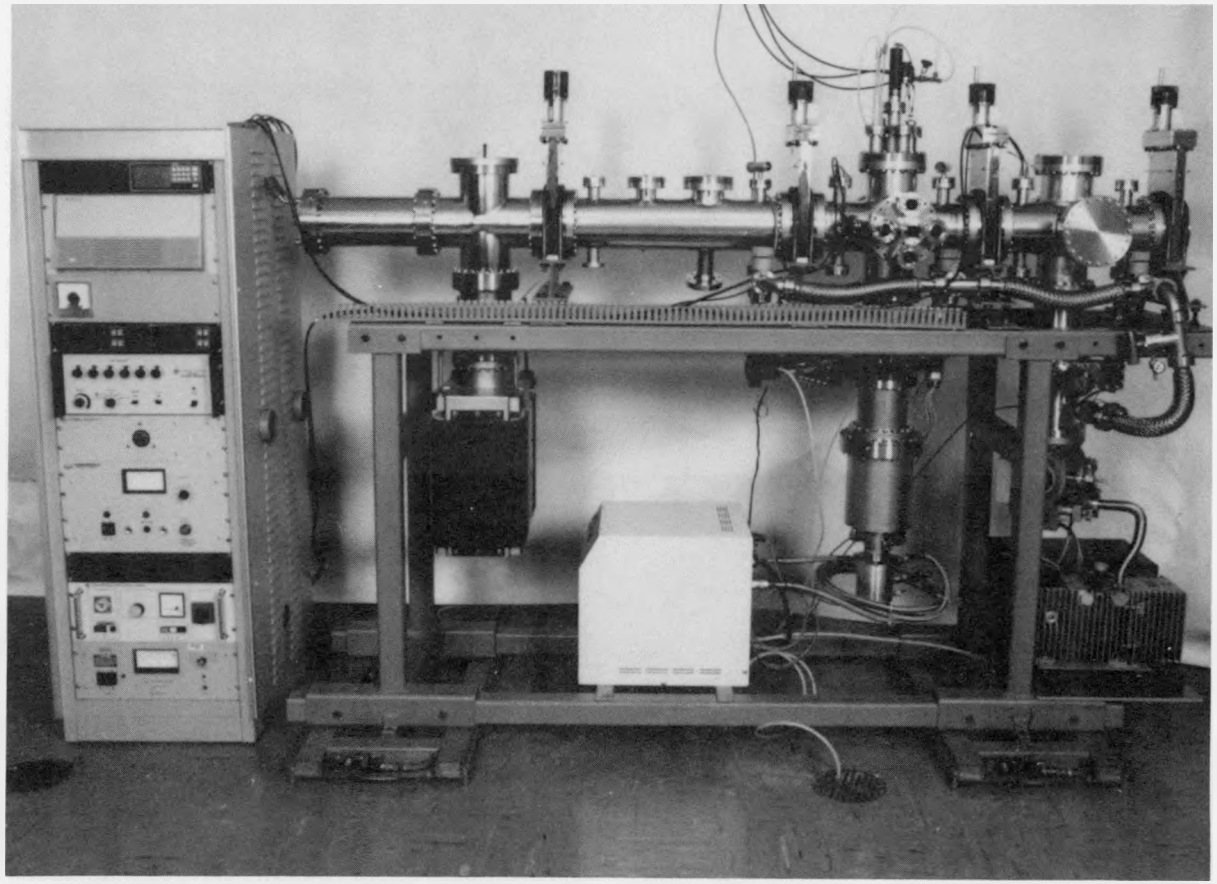

Fig. 4.4.1. Modular target chamber as viewed from downstream side.

YP 6667

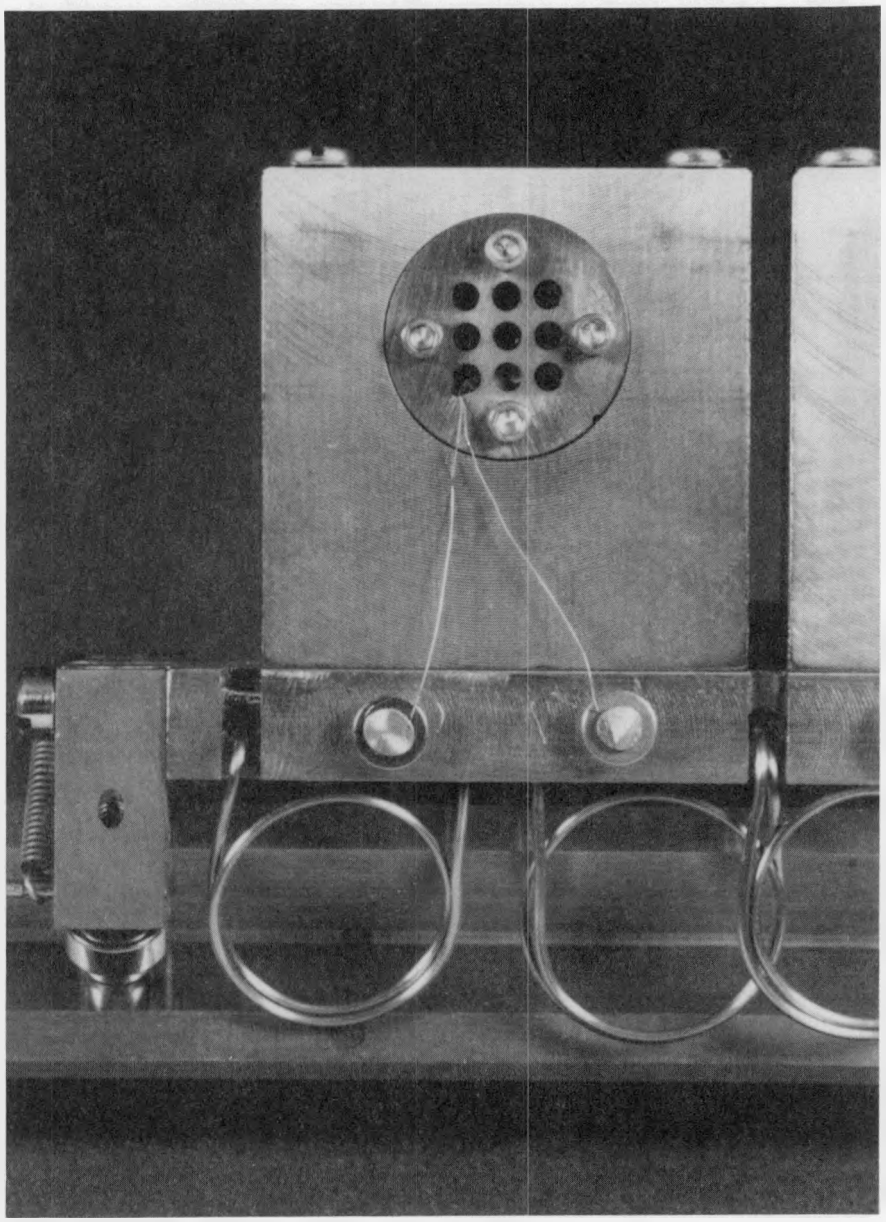

Fig. 4.4.2. Specimen holder. Specimens are mounted in 3 x 3 array on a trolley transfer system.

moves along the tracks. A set of bearings at the trolley's centerline serves to cantilever the end that passes through an open valve into the next chamber. Locomotion is accomplished by a rack, located at the lower backside of the trolley and pinion gears located along the side of the tracks. The pinion is linked to stepping motors through an ultrahigh-vacuum rotary feed-through.

The system is controlled by a Hewlett-Packard personal computer. A HP 3852A controller located in the control room communicates with a HP 3853 extender in the target room. These are interconnected via an IEEE488 bus to the personal computer and have numerous data input/output and control functions. A touch-screen input device allows manual operation of parts of the system and is used in the run initiation process. A voice synthesizer incorporated into the personal computer allows verbal readouts of instruments and is capable of alerting the accelerator operator when the machine is malfunctioning or is operating outside preset limits. A new algorithm for integrating the beam currents has been developed. Continuous monitoring of the accumulated dose and its statistical distribution on the specimen can be performed by integrating the relative current observed on the beam profilometer. Calibrations are performed at preset intervals using a multiple deep-cup array.

5. STRUCTURE AND PROPERTIES OF SURFACES AND INTERFACES

C. J. McHargue

Two principal lines of research are being followed: study of ion-beam modification of ceramic surfaces and investigation of the structure and properties of molecular beam epitaxy (MBE) grown multilayer and thin-film materials.

Ion-implantation doping is a major processing technique in current semiconductor technology, and it is widely used to improve the wear resistance of metallic alloys. Until recently, there was little research on the use of ion beams to systematically alter the structure and properties of ceramic materials.

Implantation for metallurgical purposes requires implanted ion concentrations of a few to several atomic percent (fluences of 10^{18} to 10^{17} ions/cm^2) whereas the doping of semiconductors is to a level of a few parts per billion. At these high fluences, effects such as sputtering and composition-dependent phase stability become important considerations. Additionally, the radiation-induced defect structure is more complex. Similar concentrations of implanted ions are required to alter the surface mechanical properties of ceramics.

Implantation and radiation damage in ceramics are more complex and have been less studied than in semiconductors or metals. In the displacement cascade, one must deal with at least two sublattices whose atoms (ions) may have different displacement energies. The types of defects that can be produced are strongly influenced by the requirements of local electrical charge neutrality, the local stoichiometry, and the nature of the chemical bonding of the particular structure. The local structure is also sensitive to the chemical nature of the impurity or dopant introduced by implantation.

We are studying the structural and mechanical properties changes associated with ion beam treatments of a variety of ceramics in collaboration with members of the ORNL Solid State Division.

An MBE facility has been developed in our group. It consists of an introduction and transfer chamber assembly, which facilitates the manipulation of substrates up to 9 cm diameter; a growth chamber in which four metal sources can operate to control the vapor pressure/temperature to 2000°C, with a separate molecular source for oxygen; an analysis chamber with spot Auger, low energy electron diffraction (LEED), and ellipsometry capability; and a separate chamber for electron spectroscopy for chemical analysis (ESCA). This system allows us to synthesize and control the microstructure of a variety of ceramic and metallic materials. This system is truly a unique research facility for ORNL in that it has advanced the state-of-the-art in MBE synthesis of

materials with its effusion cell design. Current technology in commercial MBE systems uses effusion cells that are limited to continued operation at temperatures below 1200°C; however, the ORNL effusion cell will operate efficiently to 2000°C under ultrahigh vacuum (UHV) conditions. This operational capability allows us to grow thin films and multilayer structures of materials such as Ti, Ni, Cu, Y, and their oxides with the complete control over growth rate and epitaxial development that is normally associated with MBE processing. No commercially available system has this capability.

We have been using our MBE facility primarily to study metal/oxide interfaces and layered structures and Ti and Al oxides. The metal thin-film work is concentrating on the fundamentals of metal-insulator and metal-semiconductor epitaxial structure development at the monolayer level. The initial growth structure controls single-crystal layered structure growth, and this is proving to be very useful to us in our multilayered oxide work. The ceramics research is an attempt to develop a new class of ceramics whose properties are sensitively controlled by a two-dimensional structuring concept. We synthesize the ceramics (Al_2O_3 and titanium oxides) from their constituents Al, Ti, and O and grow them in a multilayer structure in which the individual layers are as small as 1 nm. This structuring concept is producing materials that can be harder than their monolithic counterparts or, depending on the wavelength of the modulation, softer. This control over the ceramic property is a unique result of the microstructural development.

5.1 ION-BEAM MODIFICATION OF CERAMIC SURFACES

5.1.1 Structure of Ion-Implanted Ceramics – *C. J. McHargue, P. S. Sklad, C. W. White,[1] G. C. Farlow,[2] J. C. McCallum,[3] A. Perez,[4] and G. Marest[4]*

Much of our work on the structure of ion-implanted ceramics has been reported in three review papers[5-7] that will be summarized below.

Sapphire, Al_2O_3, may remain crystalline or become amorphous during implantation, depending on the implantation parameters of fluence, ion species, substrate temperature, and orientation of the ion beam relative to the crystallographic axes. First, the observations for crystalline implanted sapphire will be discussed; then, those for amorphous sapphire.

Rutherford backscattering measurements indicate that the stoichiometry of Al_2O_3 does not change during implantation (i.e., there is no indication of preferential sputtering). Measurements of the channeling yields lead to the conclusion that the displaced aluminum and oxygen ions that remain in the crystals also occur in the stoichiometric ratio. Thus, regardless of how the defects are produced, those that survive the postcascade cooling period maintain the stoichiometry of the crystal.

The type of damage remaining after ion implantation has been studied by optical absorption measurements and transmission electron microscopic (TEM) observations. Samples implanted with cations at room temperature have a characteristic gray-brown color to the unaided eye. Optical absorption measurements confirm the presence of F-centers and F^+-centers. TEM micrographs contain a high density of "black spots" typical of point defect clusters that probably are stoichiometric, interstitial dislocation loops. Dense arrays of tangled dislocations are also observed. The loops lie on {0001} and $\{10\bar{1}0\}$ habit planes. Burgers vector analyses give b = $1/3\langle 01\bar{1}1\rangle$ for many of the dislocations.

The amount or degree of disorder introduced by implantation may be determined from channeling measurements in Rutherford backscattering spectrometry (RBS). The ratio of the backscattered yield of the aligned crystal/yield from the "random" sample, X, indicates the disorder in a given sublattice. Disorder in the Al-sublattice increases with damage-energy (fluence) to a value of $X \approx 0.67$ at DE ≈ 0.8 keV/atom and remains at this value for damage energy densities as high as 9 keV/atom for implantation of Cr, Fe, Ti, or Nb. Dynamic recovery processes apparently prevent further defect accumulation.

As might be expected, the higher the substrate temperature during implantation, the lower the residual disorder or damage. The amount of residual disorder for a given deposited damage energy is strongly dependent on the orientation of the ion beam relative to the crystallographic axes. The RBS spectra for specimens of sapphire implanted with various fluences of chromium or aluminum plus oxygen in the stoichiometric ratio with the direction of the beam ≈7° from (a) the c-axis or (b) the a-axis show that the increase in disorder with fluence is much faster for the c-axis orientation.

Until recently, most of the information about the final disposition of the implanted ions was limited to RBS-channeling measurements of the lattice location of a few species.

An indication of the degree of "substitutionality" in the sublattices may be obtained for a given crystallographic direction from the backscattered yields from the impurity in an aligned and a randomly oriented crystal. Such measurements for room-temperature implantation of Cr, Ti, Fe, W, Ga, Mn, Ni, Cu, and Nb fail to show any simple correlation between the fraction of implanted ions that have substituted for Al, as viewed along the c-axis, and ionic size, valence, or electronegativity of the implanted species. The fraction substitutional varied from ≈0.04 to >0.9. There is no detectable substitution of Zr, Si, or Zn.

A combined RBS, TEM, and conversion electron Mössbauer spectroscopy (CEMS) study has determined the residual charge state on iron ions implanted into Al_2O_3 at room temperature at fluences of 10^{16} to 10^{17} $^{57}Fe/cm^2$. The matrix remains crystalline for these implantation conditions. The following components were identified in the CEMS

spectra: three quadrupole split doublets and one single line. These components were assigned to a ferric ion (Fe^{3+}), two forms of ferrous iron (Fe^{2+}_{I} and Fe^{2+}_{II}) , and metallic iron clusters (Fe^{0}).

TEM micrographs have been obtained that show second-phase particles having a size of ≈2 nm (ref. 8). Electron diffraction patterns suggest that the precipitate is α–Fe, and the isomer shift in the CEMS spectra indicate that the particles are under very high hydrostatic pressure.

From the earliest studies of ion implantation into Al_2O_3 there have been conflicting reports on the amorphorization of this material. An understanding of the phenomenon is beginning to emerge from current studies of metal ion implantation to various fluences and at various substrate temperatures and the use of several techniques to characterize the resulting structures. It now appears that displacement damage alone will produce the amorphous state if the temperature is low enough to suppress dynamic recovery and that "chemical" or "impurity" effects are important for many implanted species.

Implantation at low substrate temperatures (<100 K) will produce the amorphous state by damage accumulation alone at relatively low values of deposited damage energy, ≈0.3 keV for 260 keV Cr^{+}-implantation at 77 K (c-axis orientation).

In other instances, amorphization at room temperature appears to be due to unidentified "chemical effects." Implanting ^{90}Zr and ^{93}Nb to the same fluence at similar ion beam energies gives different amounts of disorder; the Zr-implanted specimens are amorphous, whereas the Nb-implanted ones are crystalline. Because these elements differ by only 3 amu, the details of the cascade formation should be similar; hence, the difference in the disorder must originate in some chemical effect during the cool-down period.

The existence of a critical concentration (of Zr) for amorphization is indicated by an analytical electron microscopy (AEM) study. Measurements of the Zr-concentration profile were made in a series of cross-sectioned specimens that had been implanted to give buried amorphous layers of different widths. The amorphous region was centered on the peak of the zirconium depth profile, and the boundaries of the amorphous layer corresponded to a Zr/Al atomic fraction of ≈0.065. The position of the boundaries exhibited no correlation with the rate of damage energy deposition (i.e., defect production).

Information on the structure of the amorphous phases has been obtained. The radial distribution function that gives the Al-O nearest-neighbor distances has been obtained from an anaylsis of the fine structure of the electron energy loss spectra.[9] The amorphous material contains short-range order that depends on the ion species that produces the amorphous state. The Al-O first near-neighbor distance in an amorphous stoichiometric implanted sample is that of γ-Al_2O_3, whereas that in an amorphous Fe-implanted sample is α-Al_2O_3.

CEMS measurements have been made for a series of samples implanted with iron at 77 K (ref. 10). These samples were amorphous. The iron in the amorphous matrix resides in two Fe^{2+}, two Fe^{4+}, and one Fe^{0} states, whereas that in the crystalline matrix was present as two Fe^{2+}, Fe^{3+}, and Fe^{0}. There are significant differences in the Mössbauer parameters for the two 2^{+} components in the amorphous matrix and in the crystalline matrix. The unusual charge state of Fe^{4+} is consistent with the iron residing in tetragonally distorted octrahedra that contain oxygen vacancies or nonbridging oxygen ions.

Room-temperature implantation of tin also produces an amorphous layer and it is believed that this is another example of a chemical effect. The CEMS spectra show the presence of Sn(II) and Sn(IV).[11]

Silicon carbide is easily amorphized by ion implantation at room temperature. Random RBS spectra are obtained at relatively low (compared with Al_2O_3) fluences of all ions studied. Within the accuracy of the measurements, the rates of damage accumulation for nitrogen and chromium implantation fall on the same curve. The critical damage energy for amorphization is about 0.02 keV/atom. That the random scattering is indicative of an amorphous surface has been confirmed by TEM and selected area diffraction (SAD).

The analysis of ion channeling yield indicates that the implanted zone maintains its stoichiometry. Results from Raman spectroscopy also indicate that there is no decomposition or preferential sputtering.

5.1.2 Residual Stresses in Ion-Implanted Sapphire[12] – *C. J. McHargue, M. E. O'Hern, C. W. White,[1] G. C. Farlow,[2] and M. B. Lewis*

Average and integrated stresses have been measured by an indentation technique for a series of Al_2O_3 single crystals implanted with chromium or iron using a wide range of ion beam energy and fluences. The stress is compressive in nature, and the average residual stress is in the range of 1100 MPa (i.e., about the value of the bulk rupture strength of defect-free single-crystalline sapphire). Data for specimens implanted with iron indicate that a saturation value for average stress is reached at 10^{16} Fe/cm^2 (160 keV), but a saturation for chromium is not apparent for fluences up to 10^{17} Cr/cm^2 (150 to 180 keV).

The effect of the orientation of the ion beam relative to the crystallographic axes on the residual stress was investigated for Al_2O_3 single crystals having the c-axis or the a-axis approximately parallel to the incident beam of 180 keV Cr^{+}. For a fluence of 10^{17} ions/cm^2, the average compressive stress in the c-axis crystal was 1.75 times that in the a-axis crystal (1313 and 752 MPa, respectively). It was noted in Sect. 5.1.1, Structure of Ion Implanted Ceramics, that disorder accumulation is likewise much faster for the c-axis orientation.

The residual compressive stress has a marked influence on the apparent fracture toughness as measured by the indentation technique and the fracture strength measured in bend tests.

5.1.3 Mechanical Properties of Ion-Implanted Ceramics – *C. J. McHargue, M. E. O'Hern, C. W. White,[1] J. C. McCallum,[3] W. C. Oliver, and D. L. Joslin*[13]

Much of our work on the effects of ion implantation on the mechanical properties of ceramics are summarized in review papers.[5,6,14,15] The general observation can be made that ceramics that remain crystalline during implantation will be hardened, the apparent fracture toughness will increase, and the rupture strength in four-point bend tests will increase. Materials that become amorphous during implantation will exhibit lower hardnesses, but their apparent fracture toughness and rupture strengths may increase.

Development of testing techniques for using the ultralow load microindentation tester [mechanical property microprobe (mpm)] for ceramic materials has continued.[16-18] Implantation of Al_2O_3 with chromium at room temperature produces an increase in hardness of 31% but no change in elastic modulus for fluences as high as 10^{17} ions/cm^2 (ref. 12).

Implantation of SiC with chromium to fluences less than that required for amorphization causes a slight (≈10%) increase in hardness. The hardness of the fully amorphous surface is ≈40% that of the unimplanted single crystal. However, implantation caused the elastic modulus to decrease both for specimens that remained crystalline and those that became amorphous.[19]

5.1.4 Studies on Ion Beam Mixing – *C. J. McHargue and J. E. Pawel*[20]

A critical review has been made of the factors involved in ion-beam mixing process in which at least one component is a ceramic.[21] The "enthalpy rule" has manifest failings when applied to metal/ceramic couples. Ternary phase diagrams are better for predicting whether or not mixing will occur; however, kinetics may be the dominating factor. There is some evidence that radiation-enhanced diffusion has only a small effect in the case of metal/sapphire couples.

An analysis of the variables involved in tests of the strength of the bond between a metal film and a ceramic substrate shows that the effect of the ion beam on thickness (resulting from sputtering), film hardness, substrate hardness, and friction significantly affect the measurements.[22] We found that after correction for these effects, the measured strength of the bond between a chromium thin film and an Al_2O_3 substrate was increased by more than 1800% by ion bombardment.[23]

5.1.5 References

1. Solid State Division.

2. Guest from Wright State University, Dayton, Ohio.

3. ORAU postdoctoral fellow.

4. University Claude Bernard Lyon I, Villeurbanne Cedex, France.

5. C. J. McHargue, "The Structure and Properties of Ion Implanted Ceramics," *Nucl. Instrum. Methods Phys. Res. B.* **B19/20,** 797-808 (1987).

6. C. W. White, C. J. McHargue, P. S. Sklad, L. A. Boatner, and G. C. Farlow, "Ion Implantation and Annealing of Insulating Materials," *Mater. Sci. Rep.* **4**, 41 (1989).

7. C. J. McHargue, P. S. Sklad, and C. W. White, "The Structure of Ion Implanted Ceramics," to be published in *Nucl. Instrum. Methods Phys. Res. B.*

8. P. S. Sklad, J. D. McCallum, S. J. Pennycook, C. J. McHargue, C. W. White, and A. Perez, "Microstructural Characterization of α-Al_2O_3 Implanted with Iron," in *Characterization of the Structure and Chemistry of Defects in Materials*, B. C. Larson, M. Ruhle, and D. N. Seidman, eds., MRS, Pittsburgh, Pa., to be published.

9. P. S. Sklad, P. Angelini, C. J. McHargue, and C. W. White, "An Analytical Electron Microscopy Investigation of Amorphous Structures in Ion Implanted Al_2O_3," pp. 45-48 in *Analytical Electron Microscopy - 1987*, D. C. Joy, ed., San Francisco Press, San Francisco, 1987.

10. Summary of (a) G. Marest, C. J. McHargue, and A. Perez, "Caracterisation de α-Al_2O_3 apres Implantation Ionique," to be published in *Surfaces-Materiaux-Technologie-1988*, Societe Francaise de Vide, France, and (b) C. J. McHargue, P. S. Sklad, J. C. McCallum, C. W. White, A. Perez, and G. Marest, "The Structure of Al_2O_3 Implanted with Iron at 77K," to be published in *Nucl. Instrum. Methods Phys. Res. B.*

11. C. J. McHargue, P. S. Sklad, J. C. McCallum, C. W. White, E. Abonneau, A. Perez, and G. Marest, "The Residual Charge of Tin Implanted into Sapphire," to be published in *Nucl. Instrum. Methods Phys. Res. B.*

12. Summary of (a) C. J. McHargue, M. E. O'Hern, C. W. White, and M. B. Lewis, "Ion Implantation in Ceramics—Residual Stresses and Properties," *Mater. Sci. Engr. A*, **A115**, 361 (1989), and (b) M. E. O'Hern, C. J. McHargue, and C. W. White, "The Effect of Chromium Implantation on the Hardness, Elastic Modulus, and Residual Stress of Al_2O_3," to be published in *Nucl. Instrum. Methods Phys. Res. B.*

13. Guest from the University of Tennessee, Knoxville, Tenn.

14. C. J. McHargue, "The Mechanical Properties of Ion-Implanted Ceramics–A Review", pp. 359-80 in *Ion Implantation-88*, F. H. Wohlbier, ed., Trans. Tech Publications, Aedermannsdorf, Switzerland, 1988.

15. C. J. McHargue, "The Mechanical Propweries of Ion Implanted Ceramics," pp. 248-68 in *Structure-Property Relationships in Surface-Modified Ceramics*, C. J. McHargue, R. Kossowsky, and W. O. Hofer, eds., Kluwer Academic Publishers, Dordrecht, 1989.

16. W. C. Oliver and C. J. McHargue, "Thin Film and Near-Surface Characterization Using a Mechanical Properties Microprobe," pp. 157-61 in *Ion Implantation and Plasma Assisted Processes*, R. F. Hochman, H. Solnick-Legg, and K. O. Legg, eds., ASM, 1988.

17. W. C. Oliver and C. J. McHargue, "Characterizing the Hardness and Modulus of Thin Films Using a Mechanical Properties Microprobe," *Thin Solid Films* **161**, 117 (1988).

18. D. L. Joslin, C. J. McHargue, and W. C. Oliver, "Thin Film and Near-Surface Characterization Using a Mechanical Properties Microprobe," pp. 289-96 in *Structure-Property Relationships in Surface-Modified Ceramics*, C. J. McHargue, R. Kossowsky, and W. O. Hofer, eds., Kluwer Academic Publishers, Dordrecht, 1989.

19. C. J. McHargue, D. L. Joslin, and J. M. Williams, "The Hardness and Elastic Modulus of Chromium-Implanted Silicon Carbide," to be published in *Nucl. Instrum. Methods Phys. Res. B.*

20. Guest from Vanderbilt University, Nashville, Tenn.

21. C. J. McHargue, "Ion Beam Mixing of Metals with Ceramics—Material Considerations," pp. 115-32 in *Structure-Property Relationships in Surface-Modified Ceramics*, C. J. McHargue, R. Kossowsky, and W. O. Hofer, eds., Kluwer Academic Publishers, Dordrecht, 1989.

22. J. E. Pawel and C. J. McHargue, "Use of the Scratch Test to Measure Changes in Adhesion of Cr/Al_2O_3 Due to Ion Beam Mixing," *J. Adhesion Sci. Technol.* **2**, 385 (1988).

23. J. E. Pawel and C. J. McHargue, "Testing of the Adhesion of Thin Films to Substrates," *J. Adhesion Sci. Technol.* **2**, 369 (1988).

5.2 MOLECULAR BEAM EPITAXY – GROWTH AND STRUCTURE CHARACTERIZATION OF OXIDES AND METAL OXIDE SUPERLATTICES – *R. A. McKee, F. A. List, F. J. Walker, and J. R. Conner*

We are using ultrahigh vacuum techniques of molecular beam epitaxy (MBE) processing for thin-film and multilayer oxide growth. The objectives of the research are (1) to develop experimental techniques for thin-film oxide growth and to provide a fundamental understanding of the atom-by-atom interactions that occur when metal oxides grow as thin-film structures and (2) to use such MBE processing methods to grow a new class of oxide or ceramic structures using superlattice concepts. Multilayering oxides will allow us to manipulate mechanical properties that are interface-related and to develop novel physical properties associated with superlattice influences on electronic structures.

During this period, we have reached several significant goals in our program and are in the process of publishing some of our work. Primarily, we have been working on Ti and its oxides, and already, we have a unique and technologically promising new result: Ti_2O_3, which has never been grown as a single-crystal thin film, has been grown epitaxially on sapphire. It is an antiferromagnetic oxide with a metal/semiconductor transition at 180°C. We summarize our work in the following abstracts of papers and talks.

5.2.1 The Growth and Epitaxy of Ti_2O_3 on Sapphire[1] – *R. A. McKee*

An MBE technique has been used to grow Ti_2O_3 on the basal plane of sapphire. High-temperature effusion cell, ultrahigh vacuum techniques have permitted a Ti metal source to be precisely shuttered to control the stoichiometry of the growing oxide, thereby avoiding the higher oxide, TiO_2; a molecular source has been used to supply oxygen to the substrate surface at approximately 1 monolayer/s. The epitaxy is specified by (0001) Ti_2O_3 parallel to (0001) Al_2O_3 with film growth along [0001]; [11$\bar{2}$0] is parallel in both substrate and film. The Ti_2O_3 has been grown at 800°C and is then stable to room temperature. Reflection high-energy electron diffraction (RHEED) during growth confirms the orientational relationship, and film growth is atomically flat. Ex situ X-ray measurements have provided lattice parameters consistent with Ti_2O_3, and in situ electron spectroscopics for chemical analyses (ESCA) characterization has been used to confirm the oxide stoichiometry. This is the first time that Ti_2O_3 has ever been grown as an epitaxial thin film.

5.2.2 Characterization of Titanium/Titanium Oxide Multilayers by X-ray Photoemission Spectroscopy[2] – *F. A. List and R. A. McKee*

X-ray photoelectron spectroscopy has been used to investigate the chemistry of a multilayer film of titanium/titanium oxide grown on sapphire (0001) at ≈800°C. The film was grown epitaxially with a composition modulation wavelength of ≈5.5 nm. Both photoelectron and X-ray induced Auger spectra of the as-grown film suggest the presence of a titanium suboxide (TiO or Ti_2O_3) at the surface of the film. The

dependence of the Ti(LMV) Auger transition on the detection angle is consistent with metallic Ti underlying the surface suboxide. Photoemission from a single monolayer of titanium on sapphire (0001) indicates a strong initial film-substrate interaction. Results of exposure of the as-grown multilayer film to air will be discussed.

5.2.3 The Influence of Thickness and Wavelength on the Mechanical Properties of a Compositionally Modulated Ceramic Thin Film[3] – *W. C. Oliver, F. A. List, and R. A. McKee*

The hardness and modulus of thin (<1 μm) ceramic films have been investigated using the differential mechanical properties microprobe (DMPM). The DMPM consists of a computer-controlled ultralow-load indentation system with a special system that allows the elastic stiffness of the contact to be determined continuously during the indentation process. The films were deposited in a MBE system utilizing unique high-temperature effusion cells. Two specimens have been studied. The first is a wedge-shaped layer of amorphous Al_2O_3 on a silicon substrate. The thickness of the layer varies from 0 to 990 nm at the two extreme sides of a 7.6-cm (3-in.) silicon wafer. The effect of layer thickness on the hardness and modulus as measured with the DMPM has been quantified for this system. The second specimen is made up of 38 repetitions of alternating layers of crystalline TiO_2 and amorphous Al_2O_3. The wavelength of the composition modulation and the thickness of the film varies uniformly from 0 to 38 nm and from 0 to 1460 nm, respectively, across the 7.6-cm (3-in.) diameter of the silicon substrate.

5.2.4 Transmission Electron Microscopy of Ti/Ti_2O_3 Superlattices[4] – *J. R. Conner*

A superlattice of Ti/Ti_2O_3 grown on the (0001) face of Al_2O_3 has been examined using high-resolution TEM. Observations along both the $[11\bar{2}0]$ and $[10\bar{1}0]$ zone axes of Al_2O_3 show that a sharp interface exists between the Al_2O_3 substrate and Ti_2O_3. Long-range periodic contrast near this interface suggests a regular dislocation structure between the epitaxial oxide and the substrate. The superlattice, with dimensions of approximately Ti_2O_3 3.5 nm and Ti 2.0 nm, has retained interfaces sharp to within one to two atomic layers despite a growth temperature of 800°C. The epitaxial relationships between Ti_2O_3/Al_2O_3 and Ti/Ti_2O_3 have been determined by selected area diffraction. The epitaxy of Ti on Al_2O_3 (0001) has also been investigated.

5.2.5 Epitaxy of Ti and Ti Oxides on Sapphire[5] – *F. J. Walker*

An MBE technique has been used to grow Ti_2O_3 and Ti on the basal plane of sapphire. High-temperature effusion cell, ultrahigh vacuum techniques have permitted a Ti metal source to be precisely shuttered so that the stoichiometry of the growing oxide is controlled, thereby avoiding production of the higher oxide, TiO_2; a molecular source has been used to supply oxygen to the substrate surface at ~1 monolayer/s. The epitaxy is specified by (0001) Ti_2O_3 parallel to (0001) Al_2O_3 with film growth along [0001]; $[11\bar{2}0]$ is parallel in both substrate and film. Titanium grows with the (0001) parallel to the (0001) of Al_2O_3 as well, but the $[11\bar{2}0]$ Ti is parallel to the $[10\bar{1}0]$ of Al_2O_3.

This epitaxial relationship of Ti on sapphire suggests that the Ti occupies the next sites normally occupied by Al in the sapphire structure. When the Ti in these sites is oxidized at a certain rate, the Ti_2O_3 structure is grown.

5.2.6 In Situ ESCA Characterization of Ti_2O_3 Thin Films[6] – *F. A. List*

X-ray photoelectron spectroscopy has been used to investigate the chemistry of a multilayer film of titanium/titanium oxide grown on sapphire (0001) at ≈800°C. The film was grown epitaxially with a composition modulation wavelength of ≈5.5 nm. Both photoelectron and X-ray induced Auger spectra of the as-grown film suggest the presence of Ti_2O_3 at the surface of the film. The dependence of the Ti(LMV) Auger transition on the detection angle is consistent with metallic Ti underlying the surface oxide. Results of exposure of the as-grown film to air will be discussed.

5.2.7 Multilayer Ceramic Films[7] – *K. B. Alexander, F. J. Walker, R. A. McKee, and F. A. List*

Titanium oxide/aluminum oxide films have been deposited using MBE methods and characterized by reflection high-energy electron diffraction and TEM techniques. Growth on silicon substrates below 973 K resulted in primarily amorphous multilayers. At 1323 K, the deposition of titanium in an oxygen atmosphere on (0001) Al_2O_3 substrates resulted in films of Ti_2O_3. These films consisted of small domains, up to 60 nm, slightly misoriented from a $[11\bar{2}0]$ $[11\bar{2}0]$ orientation relationship. Two variants of Ti_2O_3 were observed as a result of multiple positioning during growth. Closing the titanium shutter during growth resulted in an oriented TiO_2 film.

5.2.8 The Growth and Epitaxy of Copper on Silicon[8] – *F. J. Walker, J. R. Conner, and R. A. McKee*

The progression of the epitaxy of (111) copper on (111) silicon has been studied using surface-sensitive techniques and the as-grown film studied using X-ray diffraction and TEM. An MBE system has been used to deposit films on 7.6-cm-diam (3-in.) silicon substrates. Across this large surface area, a graded thickness of 0 to 50-Å copper was deposited and scanned using Auger and low-energy electron diffraction (LEED). For films grown at 100°C, Si alloys were deposited with copper up to a thickness of 25 Å, consistent with previous studies. LEED, however, indicates an ordered root 3 Cu surface at thicknesses of 10 to 25 Å, possibly as a result of the ordering of Si on the growing Cu surface. Films as thick as 1000 Å scatter X rays coherently across the whole thickness and have an out-of-plane rocking curve of 0.06° and in-plane of 0.5°.

5.2.9 The Structure of the Copper/Silicon Interface[9] – *F. J. Walker, E. D. Specht, and R. A. McKee*

The structure of the interface between an epitaxial Cu film on Si (111) has been studied by measuring the intensity along Si crystal truncation rods. A 1000-Å Cu film was deposited at 100°C on well-oriented Si (111) wafers. The scattering near the Bragg

reflections indicates an ordered Si lattice right up to the interface. An analysis of the intensity along the rod in between Bragg reflections is consistent with Cu atoms sitting in three inequivalent surface sites of a double-layer truncated silicon (111) surface. These surface sites define the close-packed planes that make up the face-centered cubic (FCC) Cu lattice and thus determine the epitaxial relationship of the growing Cu film. This first Cu layer is about 0.8 Å above the Si surface. Anomalous X-ray scattering close to the Cu edge indicates a Cu layer commensurate to the Si surface. This conclusion is model independent. The first layer of Cu, though comensurate on the average, is strongly disordered. This disorder could arise from the next layers of Cu which are strained relative to the Si by as much as 15%.

5.2.10 References

1. R. A. McKee, "The Growth and Epitaxy of Ti_2O_3 on Sapphire," invited talk at IBM, San Jose, May 2, 1989.

2. F. A. List and R. A. McKee, "Characterization of Titanium/Titanium Oxide Multilayers by X-ray Photoemission Spectroscopy," paper in preparation for submission to *J. Vac. Sci. Technol.*

3. W. C. Oliver, F. A. List, and R. A. McKee, "The Influence of Thickness and Wavelength on the Mechanical Properties of a Compositionally Modulated Ceramic Thin Film," *Mater. Res. Soc. Proc.* **130**, 99 (1989).

4. J. R. Conner, "Transmission Electron Microscopy of Ti/Ti_2O_3 Superlattices," presented at 9th TVC-AVS Meeting, Oak Ridge, Tenn., May 15-18, 1989.

5. J. F. Walker, "Epitaxy of Ti and Ti Oxides on Sapphire," presented at 9th TVC-AVS Meeting, Oak Ridge, Tenn., May 15-18, 1989.

6. F. A. List, "In Situ ESCA Characterization of Ti_2O_3 Thin Films," presented at 9th TVC-AVS Meeting, Oak Ridge, Tenn., May 15-18, 1989.

7. K. B. Alexander, F. J. Walker, R. A. McKee, and F. A. List, "Multilayer Ceramic Films," submitted to *J. Am. Ceram. Soc.*

8. F. J. Walker, J. R. Conner, and R. A. McKee, "The Growth and Epitaxy of Copper on Silicon," paper in preparation for submission to *Phys. Rev. B.*

9. F. J. Walker, E. D. Specht, and R. A. McKee, "The Structure of the Copper/Silicon Interface," paper in preparation for submission to *Phys. Rev. B.*

6. COOPERATIVE RESEARCH CENTERS

6.1 SHARED RESEARCH EQUIPMENT PROGRAM (SHaRE) – *E. A. Kenik and N. D. Evans*

The past 22 months have been a productive period for the SHaRE program. The program, which allows participants from universities, industrial research, and other national laboratories access to the wide range of often unique microanalytical facilities, is aimed at cooperative research in materials science in areas pertinent to the DOE-ORNL mission and emphasizes areas under current investigation in the Metals and Ceramics Division. Facilities and techniques included under the SHaRE program are analytical and high-voltage electron microscopy, Auger electron spectroscopy, nuclear microanalysis, X-ray diffraction, and rapid solidification facilities. The atom probe field ion microscope and mechanical properties microprobe (nanoindenter) have each attracted several new external participants. A number of SHaRE projects are in support of advanced materials development programs in the Metals and Ceramics Division, such as nickel-based aluminides, welding of irradiated austenitic alloys, and high-performance ceramics.

During this period, the Division of Materials Sciences, Office of Basic Energy Sciences, provided funds through Oak Ridge Associated Universities (ORAU) to support the SHaRE activity. Program funds are used for travel and living expenses for SHaRE participants while at ORNL and for the support of an electron microscopist. However, this position was vacant until Neal Evans was hired in the second quarter of FY 1989. It is the responsibility of the SHaRE microscopist to familiarize SHaRE participants with the electron microscope and computer facilities and to participate in SHaRE research when appropriate. The presence of such an individual has allowed the high level of SHaRE participation with minimal interference with in-house programs.

A steering committee reviews all proposed SHaRE projects and defines SHaRE program policy. The members in FY 1988 were:

E. A. Kenik, ORNL	P. S. Sklad, ORNL
C. B. Carter, Cornell University	I. A. Baker, Dartmouth College
K. L. More, ORAU	K. Newport, ORAU

In FY 1989, two changes were made in the steering committee: J. E. Wittig, Vanderbilt University, replaced C. B. Carter, and N. D. Evans of ORAU replaced Karren L. More.

In the past 22 months, 32 SHaRE projects have been active, involving approximately 50 participants. These projects follow.

C. Allison, Oklahoma State University, with R. Stoller: "Study of Electron Irradiation Defects in Transition Metal Carbides by Electron Microscopy."

I. Baker and E. Schulson, Dartmouth College, with J. Horton: "In-situ Straining of Ni_3Al in the Electron Microscope at Elevated Temperature."

I. Baker, Dartmouth College, with J. Horton, P. Camus, and M. K. Miller: "Grain Boundary Structure and Chemistry in B2-Ordered Alloys."

R. J. Bayuzick, Vanderbilt University, with E. A. Kenik: "Studies of Microstructures of Nb Alloys Resulting from Large Degrees of Supercooling."

R. B. Benson, North Carolina State University, with P. F. Becher: "Stress Induced Transformation and Fracture in Transformation Toughened Zirconia."

M. G. Burke, University of Pittsburgh, with M. K. Miller: "Advanced Microstructural Analysis: Morphological Interpretation and Characterization."

M. G. Burke, Westinghouse Research and Development Center, with M. K. Miller: "Advanced Microstructural Analysis of PWR and BWR Materials."

C. B. Carter, Cornell University, with P. S. Sklad: "The Chemical Analysis of Interfaces in Ceramic Oxides."

Bryan Chin, Auburn University, with A. Rowcliffe: "Weldability of Low Activation Ferritic Steels for Fusion Reactor Applications."

Bryan Chin, Auburn University, with E. A. Lee: "Bending Fatigue of Ion-Beam Surface Modified Ferrous Alloys."

D. L. Cocke, Texas A&M University, with M. K. Miller: "Characterization of Ni/Zr Intermetallic Compounds by APFIM."

R. F. Davis, North Carolina State University, with J. Bentley: "Transmission Electron Microscopy Studies of Ceramic-Ceramic Composites and the Beta to Alpha Phase Transformation in Silicon Carbide."

F. Ebrahimi, University of Florida, with M. K. Miller: "Effect of Composition on Irradiation Embrittlement of Pressure Vessel Steels."

B. D. Fabes, University of Arizona, with W. C. Oliver: "Mechanical Properties of Sol–Gel Coatings."

J. F. Glass, North Carolina State University, with J. Bentley: "TEM Studies of MPCVD Diamond and Diamond-Substrate Interfaces."

R. Herring, Martin Marietta Laboratories, with J. Bentley: "Characterization of Damage Regions Formed in Silicon by Implantation of S, Mg, and As."

J. J. Hren and R. Jayaram, North Carolina State University, with M. K. Miller: "APFIM of Ni-Al-Mo-Ta Alloys."

C. C. Koch, North Carolina State University, with J. Horton: "Analytical Electron Microscopy of Rapidly Solidified or Undercooled Nickel or Iron Aluminides."

D. B. Marshall, Rockwell International Science Center, with W. Oliver: "Interface Properties in Ceramic Composites."

M. Mecartney, University of Minnesota, with P. Angelini: "Analytical Electron Microscopy Investigation of Grain Boundary Phases in Y_2O_3-ZrO_2 Ceramics."

J. Newkirk, University of Missouri — Rolla, with M. K. Miller: "An Atom Probe Study of Nanocrystalline Iron Filaments Grown by CVD."

G. B. Olson and M. G. Hetherington, Massachusetts Institute of Technology, with M. K. Miller: "The Ultimate Resolution of the Atom Probe."

G. Pharr, Rice University, with W. Oliver: "Relations Between Microhardness and Dislocation Substructure in Single Crystals of Silver."

G. Pharr, Rice University, with W. Oliver: "The Unloading Displacement Discontinuity During Nanoindentation of Silicon."

G. Pharr, Rice University, with W. Oliver: "Determination of Elastic Moduli in Hard Materials Using Nanoindentation Techniques."

P. J. Reucroft, University of Kentucky, with J. Bentley: "Chemical and Physical Characterization of Dispersed Metal Particles in Porous Media."

S. L. Sass, Cornell University, with E. A. Kenik: "A Study of the Spatial Distribution of Au Segregated to Grain Boundaries in Fe Alloys by AEM."

J. Todd, University of Southern California, with P. Maziasz: "Microstructural Studies of Advanced Austenitic Stainless Steels."

V. K. Vasudevan, University of Cincinnati, with J. A. Horton, "Behavior of Elevated Temperature Intermetallic Compounds Based on Ti-Al."

S. Walck, University of Alabama at Birmingham, with M. K. Miller: "A Study of Trapping of Deuterium to Ion-Induced Traps Using the Atom Probe."

J. Wert, Vanderbilt University, with P. S. Sklad: "The Role of Microstructure in Tribology."

J. E. Wittig, Vanderbilt University, with E. A. Kenik: "Investigation of Metastable Microstructures Produced by Deep Undercooling and Rapid Solidification."

Some 70 papers based on SHaRE research have been published in the past 22 months, and approximately 54 presentations have been made at technical meetings. Eleven theses have been completed by students working on SHaRE-related projects. This brings the totals for SHaRE-related research to approximately 206 publications, 201 presentations, and 38 completed theses. Results from research on some of the current SHaRE projects listed above are described elsewhere in this report.

6.2 OAK RIDGE SYNCHROTRON ORGANIZATION FOR ADVANCED RESEARCH (ORSOAR) – *C. J. Sparks*

Our beamline on the National Synchrotron Light Source (NSLS) is one of the most desirable among users of X-ray diffraction because our facility uses sagittal-crystal focusing optics to focus up to 5 mrad from 3 to 40 keV. The flux focused in an approximately 1-mm^2 spot at 8.3 keV is near theoretical predictions when corrected for crystal reflectivity and absorption from beamline windows. The vertically focusing mirror was repolished to obtain a reflectivity of 80% at 8.3 keV and a 6-mrad glancing angle. The focused-beam size of approximately 1 mm^2 is near that expected from pinhole images of the electron source size. To date, we have achieved the highest flux of focused radiation between 4 and 20 keV of any bending magnet beamline.

The NSLS shutdown for Phase II installation of high-intensity insertion devices in late March 1987 was not completed until June 1988. This interval was used to upgrade our facility with a faster computer, better mirror, and a four-circle goniometer with extended angular range.

From June 1988 through April 1989, about 20 experiments were performed. In general, these experiments were chosen because of programmatic interest or because they were "good science" and were selected by the NSLS review panel for our beamline because it offered some unique advantages over others in terms of flux, energy resolution, and/or Q-space resolution.

Among the research highlights of this reporting period are the following: We have advanced the technique for depth-profiling strain distributions in materials. We continued our studies of depth-profiling of polished and severely grounded, fully stabilized zirconia using long-wavelength X rays and shallow glancing angles; strain gradients near the surface approached maximum compressive strains of 4% but dropped rapidly as a function of depth. Although the maximum strains are large, they are reasonable for ceramic materials in compression. Means to reduce crack initiation can result from this better understanding of surface strains.

Strain profiles in thin (~900-Å) films of GaAs grown on Si(001) substrates have shown that about 90% of the strain from lattice mismatch is dissipated in a few GaAs planes (~10 Å) at the Si interface. The other 10% of the strain is distributed uniformly throughout the bulk of the GaAs film. Means to reduce the deleterious effects of strain in semiconductor heterostructure technology are more likely to be found with this better understanding of the strain distribution.

An exciting discovery of a huge X-ray magnetic resonance scattering effect in UAs opens the door for mapping the magnetic structure of materials by tuning the X-ray energy near an absorption edge. Enhancements of 10^7 in magnetic X-ray scattering arise from strong electric multipole transitions between atomic core states and exchange-split Fermi edge states. Heavy fermion systems such as UBe_3 may now be studied with new insight to understand the coexistence of magnetism and coexistence superconductivity.

6.2.1 Recent Publications

The publications resulting from this facility in a users mode are listed below. Further details can be obtained by writing to the principal authors listed, or you may find some abstracted under the heading X-Ray Diffraction Research, Sect. 1.3 of this report.

1. A. S. Bommannavar, C. J. Sparks, A. Habenschuss, G. E. Ice, A. Dhere, H. Morkoc, and H. Zabel, "X-Ray Diffraction Study of a Thin GaAs Film on Si(100)," pp. 223-27 in *Mater. Res. Soc. Symp. Proc.* **102**, 223-27 (1988).

2. J. Z. Tischler, J. D. Budai, G. E. Ice, and A. Habenschuss, "Multiple Scattering and the (200) Reflection in Silicon and Germanium," *Acta Crystallogr.* **A44**, 22 (1988).

3. A. Habenschuss, G. E. Ice, C. J. Sparks, and R. A. Neiser, Jr., "The ORNL Beamline at the National Synchrotron Light Source," *Nucl. Instrum. Meth.* **A266**, 215 (1988).

4. C. J. Sparks, M. Hasaka, D. S. Easton, S. Baik, A. Habenschuss, and G. E. Ice, "Structural Studies of Nickel Films and Their Interface with Sapphire Substrates," *Mater. Res. Soc. Symp. Proc. Interfaces, Superlattices, Thin Films* **77**, 495 (1987).

5. Bing Hwang, C. R. Houska, G. E. Ice, and A. Habenschuss, "Residual Strain Gradients in a Fully Stabilized Zirconia Sample," *J. Appl. Phys.* **63**, 11 (1988).

6. Bing Hwang, C. R. Houska, G. E. Ice, and A. Habenschuss, "X-Ray Analysis of the Near Surface Phase Distribution Applied to Wear on a PSZ Disk," *Adv. Ceram. Mater.* **3**, 180 (1988).

7. E. D. Isaacs, D. B. McWhan, C. Peters, G. E. Ice, D. P. Siddons, J. P. Hastings, C. Vettier, and O. Vogt, "Resonant Magnetic X-Ray Scattering in UAs," submitted to *Phys. Rev. Lett.*, 1989.

8. H. Zabel, N. Lucas, H. Morkoc, and C. J. Sparks, "X-Ray Characterization of Heteroepitaxial GaAs on Si(001)," submitted to *J. Electrochem. Soc.* (1989).

9. B. C. Larson, S. Iida, J. Z. Tischler, J. D. Lewis, G. E. Ice, and A. Habenschuss, "X-Ray Diffuse Scattering from Cobalt Precipitates in Copper," *Mater. Res. Soc. Symp. Proc.* **82**, 73 (1987).

10. S. Amador, P. S. Pershan, H. Stragier, B. D. Swanson, D. J. Tweet, L. B. Sorensen, E. B. Sirota, G. E. Ice, and A. Habenschusss, *Phys. Rev. A* **39**(5), 2703 (1989).

11. S. I. Rao, C. R. Houska, R. A. Neiser, G. E. Ice, T. A. Habenschuss, K. Grabowski, S. Wolf, and J. Claassen, "X-Ray Diffraction Study of N Implanted Nb Films," (submitted for publication).

12. R. J. DeAngelis, A. G. Dhere, M. A. Maginnis, P. J. Reucroft, G. E. Ice, and A. Habenschuss, "Synchrotron X-Ray Scattering for the Structural Characterization of Catalysts," *Adv. X-Ray Anal.* **30**, 389-94 (1987).

Appendix A

PRESENTATIONS AT TECHNICAL MEETINGS

Compiled by Jamie Bain

Department of Metallurgy and Science of Materials, University of Oxford, Oxford, England, July 2, 1987:

M. K. MILLER, "APFIM Characterization of Irradiated A533B and Model Pressure Vessel Steel and Boron Segregation in Ni_3Al"

2nd International Conference on Solid-Solid Phase Transformations, Cambridge, Great Britain, July 6–10, 1987:

M. K. MILLER, "The Morphology of Low Temperature Phase Transformations in the Iron-Chromium System"

M. K. MILLER* AND M. G. BURKE, "Characterization of Low Temperature Phase Transformations in the Iron-Beryllium System"

Radiation Effects in Insulators-4, Lyon, France, July 6–10, 1987:

T. F. PAGE, C. J. MCHARGUE,* AND C. W. WHITE, "Ion-Implantation-Induced Changes in the Electron Channelling Behavior of (0001) Sapphire: ECP as a Damage Characterizing Technique"

Pacific Workshop on Analytical Electron Microscopy - Analysis '87, Kona, Hawaii, July 13–17, 1987:

K. B. ALEXANDER* AND D. E. LAUGHLIN, "AEM Determination of Composition Profiles Formed During Cellular Precipitation in Ni-In Alloys"

P. ANGELINI,* J. SEVELY, K. HSSEIN, AND G. ZANCHI, "EXELFS of Amorphous and Crystalline SiC"

*Speaker

J. BENTLEY, "Ionization Delocalization Effects in ALCHEMI"

J. BENTLEY* AND M. K. MILLER, "Phase Transformations in Aged CF 8 and CF 8M Stainless Steels"

E. A. KENIK,* M. J. GODBOLE, D. H. LOWNDES, A. J. PEDRAZA, AND D. F. PEDRAZA, "Structure of Rapidly Solidified NiTi"

K. L. MORE,* J. BENTLEY, C. H. CARTER, JR., AND R. F. DAVIS, "Analytical Electron Microscopy Characterization of Boron in Sintered α-SiC"

J. SEVELY, P. ANGELINI,* K. HSSEIN, AND G. ZANCHI, "EXELFS Analyses at 300 kV and 1 MV"

P. S. SKLAD,* P. ANGELINI, C. J. MCHARGUE, AND C. W. WHITE, "An Analytical Electron Microscopy Investigation of Amorphous Structures in Ion-Implanted Al_2O_3"

J. M. VITEK* AND S. A. DAVID, "Time-Dependent Composition Behavior of Precipitates in Aged Stainless Steels"

34th International Field Emission Symposium, Osaka, Japan, July 13–18, 1987:

P. P. CAMUS, "Solute Clustering Above a Miscibility Gap"

M. G. HETHERINGTON AND M. K. MILLER,* "On the Statistical Analysis of Atom Probe Data"

M. K. MILLER, "The Effects of Local Magnification and Trajectory Aberrations on Atom Probe Analysis"

M. K. MILLER* AND M. G. BURKE, "Characterization of Irradiated A533B Pressure Vessel Steel Weld"

M. K. MILLER,* D. T. HOELZER, F. EBRAHIMI, AND M. G. BURKE, "Characterization of Irradiated Model Pressure Vessel Steels"

M. K. MILLER* AND J. A. HORTON, "Boron Segregation in Ni_3Al"

M. K. MILLER,* E. A. KENIK, AND T. A. ZAGULA, "Ordering in Ni_4Mo: An APFIM/TEM/HVEM Study"

1987 Gordon Research Conference on Physical Metallurgy/Intermetallic Compounds, Tilton, New Hampshire, July 20–24, 1987:

C. T. Liu, "Ductile Nickel-Aluminide Alloys"

45th Annual Meeting of the Electron Microscopy Society of America, Baltimore, Maryland, August 2–7, 1987:

P. ANGELINI* AND P. F. BECHER, "In Situ Fracture of SiC-Whisker-Reinforced Al_2O_3"

J. BENTLEY,* A. T. FISHER, C. P. HALTOM, J. BRYNESTAD, R. J. LAUF, R. K. WILLIAMS, AND D. M. KROEGER, "Electron Microscopy of High-Temperature Oxide Superconductors"

E. A. KENIK,* T. A. ZAGULA, M. K. MILLER, AND J. BENTLEY, "Ordering in Ni_4Mo by TEM and APFIM"

P. J. MAZIASZ,* N. H. PACKAN, D. F. PEDRAZA, AND E. H. LEE, "A TEM Study of Amorphization in NiTi Irradiated with Ni^{2+} Ions at Room Temperature"

M. L. MECARTNEY* AND P. ANGELINI, "Analytical TEM of Grain Boundary Phases in Yttria-Zirconia Ceramics"

K. L. MORE,* J. BENTLEY, AND R. F. DAVIS, "Antiphase Boundaries in Beta-SiC Thin Films"

P. S. SKLAD, "Analytical Electron Microscopy of Alpha-Al_2O_3 Implanted with Iron"

J. M. VITEK, "Diffraction Effects from Interfaces"

6th International Conference on Rapidly Quenched Metals, Montreal, Canada, August 3–7, 1987:

P. LAMPARTER,* S. STEEB, D. M. KROEGER, AND S. SPOONER, "Neutron- and X-Ray Small Angle Scattering with Fe-Base Metallic Glasses"

Symposium on Interfacial Phenomena in Biotechnology and Materials Processing, 18th Annual Meeting of the Fine Particle Society, Boston, Massachusetts, August 3–7, 1987:

A. BLEIER* AND C. G. WESTMORELAND, "Effects of Adsorption of Polyacrylic Acid on the Stability of α-Al_2O_3, m-ZrO_2, and Their Binary Suspension Systems"

E. M. DELISO* AND A. BLEIER, "Role of Acid-Base Equilibria on the Stabilization of Oxidized Silicon Particles in Ethanolic and Aqueous Media"

Durham University, Durham, England, August 4, 1987:

C. J. MCHARGUE, "The Effects of Ion Implantation on the Mechanical Properties of Ceramics"

Seminar, Department of Metallurgy and Engineering Materials, The University of Newcastle, Newcastle Upon Tyne, England, August 5, 1987:

C. J. MCHARGUE,* P. S. SKLAD, C. W. WHITE, G. C. FARLOW, A. PEREZ, N. KORNILIOS, AND G. MAREST, "The Charge State of Iron Ions Implanted into Sapphire"

Materials Sciences Subcommittee of the Basic Energy Sciences Advisory Committee, Argonne National Laboratory, Argonne, Illinois, August 6–7, 1987:

E. E. BLOOM, "Basic Energy Sciences Research in the Metals and Ceramics Division of Oak Ridge National Laboratory"

C. J. SPARKS, "X-Ray Scattering Research at the NSLS"

Conference on Solid State Amorphizing Transformations, Los Alamos National Laboratory, Los Alamos, New Mexico, August 10–13, 1987:

D. F. PEDRAZA, "Radiation-Induced Collapse of the Crystalline Structure of Ordered Intermetallic Alloys"

National Bureau of Standards, Washington, D.C., August 12, 1987:

M. H. YOO, "Strengthening Mechanisms in Ordered Intermetallic Compounds"

Naval Research Laboratory, Washington, D.C., August 13, 1987:

M. H. YOO, "Strengthening Mechanisms in Ordered Intermetallic Compounds"

Columbia University, New York, New York, August 17, 1987:

M. H. YOO, "Strengthening Mechanisms in Ordered Intermetallic Compounds"

NATO-ASI Materials Modification by High-Fluence Ion Beams, Viana Do Castelo, Portugal, August 24–September 4, 1987:

C. J. MCHARGUE, "Charge State of Iron Ions Implanted into Sapphire"

Seminar, Oxford University, Oxford, England, August 25, 1987:

C. J. MCHARGUE,* P. S. SKLAD, C. W. WHITE, G. C. FARLOW, A. PEREZ, N. KORNILIOS, AND G. MAREST, "The Charge State of Iron Ions Implanted into Sapphire"

Newcastle University, Newcastle Upon Tyne, England, August 30, 1987:

C. J. MCHARGUE, "The Effects of Ion Implantation on the Mechanical Properties of Ceramics"

3rd International Symposium on Environmental Degradation of Materials in Nuclear Power Systems - Water Reactors, Traverse City, Michigan, August 30–September 3, 1987:

F. EBRAHIMI, D. VENABLES, D. T. HOELZER, V. KRISHNAMOORTHY, AND M. K. MILLER,* "A Study of the Mechanisms of Radiation-Hardening Enhancement by Phosphorus in Iron and Steel Alloys"

D. T. HOELZER, F. EBRAHIMI, AND M. K. MILLER,* "Analysis of Copper and Nickel in Irradiated Iron Based Alloys Using FIM/Atom Probe"

M. K. MILLER* AND J. BENTLEY, "Characterization of Fine-Scale Microstructures in Aged Primary Coolant Pipe Stainless Steel"

M. K. MILLER* AND M. G. BURKE, "Microstructural Characterization of PWR Steels Using the Atom Probe Field-Ion Microscope"

7th International Conference on Erosion by Liquid and Solid Impact, Cambridge, United Kingdom, September 7, 1987:

R. H. PARRISH,* J. J. WERT, W. C. OLIVER, AND P. S. SKLAD, "The Effect of Varying Sputtering Parameters on the Microstructure and Mechanical Properties of 10%Ni+TiB_2 Thin Films"

American Society of Metals European Technical Conference: Advanced Materials and Processing Techniques for Structural Applications, Paris, France, September 7–9, 1987:

V. K. SIKKA, "Advances in Processing Techniques for Nickel Aluminides"

Sandia National Laboratories, Albuquerque, New Mexico, September 8, 1987:

M. H. YOO, "Strengthening Mechanisms in Ordered Intermetallic Compounds"

U.S./China Symposium on Advanced Ceramics at National Bureau of Standards, Gaithersburg, Maryland, September 8–10, 1987:

P. F. BECHER, "Whisker Reinforced Ceramics"

University of California, Berkeley, California, September 10, 1987:

M. H. YOO, "Strengthening Mechanisms in Ordered Intermetallic Compounds"

Stanford University, Palo Alto, California, September 11, 1987:

M. H. YOO, "Strengthening Mechanisms in Ordered Intermetallic Compounds"

American Society for Metals International Meeting, Baton Rouge, Louisiana, September 16, 1987:

P. P. CAMUS, "Field-Ion Microscopy and Atom Probe Analysis: Techniques and Applications"

American Society for Metals International Meeting on Toughening and Strengthening Process in Ceramics, Raleigh, North Carolina, September 17, 1987:

P. F. BECHER, "Toughening and Strengthening Processes in Ceramic Systems"

North American Welding Research Seminar, Ohio State University, Columbus, Ohio, September 28–30, 1987:

S. A. DAVID, "Welding of Ductile Intermetallic Alloys"

S. A. DAVID,* M. L. SANTELLA, AND G. M. GOODWIN, "Welding and Weldability of Ductile Intermetallic Alloys"

Symposium on Accuracy in Trace Analysis - Accomplishments, Goals, Challenges, Gaithersburg, Maryland, September 28–October 1, 1987:

M. K. MILLER, "Analysis at the Atomic Level: The Atom Probe Field-Ion Microscope"

Third International Conference on Fusion Reactor Materials (ICFRM-3), Karlsruhe, West Germany, October 4–8, 1987:

L. K. MANSUR* AND M. L. GROSSBECK, "Mechanical Property Changes Induced in Structural Alloys by Neutron Irradiation with Different Helium to Displacement Ratios"

ASM Joining of Advanced Materials Program, Cincinnati, Ohio, October 10–15, 1987:

S. A. DAVID, "Welding of Ductile Intermetallic Alloys"

Materials Week '87, sponsored by ASM International, Cincinnati, Ohio, October 10–15, 1987:

R. A. MCKEE, "Elastic Properties and Adherence of Thin Films Using Dynamic Resonance Methods"

W. C. OLIVER* AND J. B. PETHICA, "Continuous Measurements of Contact Stiffness During Indentation Experiments"

International Symposium on Strain Hardening/Annealing and Recovery of Intermetallic Compounds, Cincinnati, Ohio, October 10–16, 1987:

C. T. LIU,* J. A. HORTON, AND E. H. LEE, "Grain Growth and Work Hardening in Boron-Doped Ni_3Al Alloys"

V. K. SIKKA, "Mechanical Properties of Nickel Aluminide"

1987 TMS-AIME Fall Meeting, Cincinnati, Ohio, October 12–16, 1987:

J. BRYNESTAD,* E. D. SPECHT, C. J. SPARKS, A. G. DHERE, O. B. CAVIN, D. M. KROEGER, R. K. WILLIAMS, H. A. OYE, AND F. J. SEILER, "Effect of Oxygen Pressure on the Oxygen Content and the Orthorhombic-Tetragonal Transition in $YBa_2Cu_3O_x$"

W. H. BUTLER,* C. J. SPARKS, G. M. STOCKS, D. M. KROEGER, R. K. WILLIAMS, AND N. F. WRIGHT, "Overview of Experimental and Theoretical Studies on High-T_c Superconductivity in the Metals and Ceramics Division at ORNL"

D. M. KROEGER,* A. CHOUDHURY, J. BRYNESTAD, R. K. WILLIAMS, AND R. A. PADGETT, "Auger Spectroscopy of Fracture Surfaces in $YBa_2Cu_3O_7$"

M. B. LEWIS* AND W. R. ALLEN, "Diffusion and Trapping of Ion Implanted Helium: Nb, V, Al, Mg, MgO"

M. B. LEWIS,* W. R. ALLEN, R. A. BUHL, S. W. COOK, N. H. PACKAN, AND L. K. MANSUR, "Triple Ion Beam Facility for Materials Research"

G. S. PAINTER, "Density Functional Atomic Cluster Models of Localized Chemical Bonding of Impurities at Grain Boundaries"

J. H. SCHNEIBEL* AND L. MARTINEZ, "The Limitations of the Chen & Argon and Martinez & Nix Models for Intergranular Cavity Growth"

G. M. STOCKS, D. M. NICHOLSON, F. J. PINSKI,* D. D. JOHNSON, B. L. GYORFFY, AND J. B. STAUNTON, "On the Theory of Ordering Processes in Alloys"

J. M. VITEK,* S. A. DAVID, AND V. K. SIKKA, "The Basis for Improved Creep Properties in Titanium-Modified Type 308 Stainless Steel Weld Filler Metal"

Clemson University, Clemson, South Carolina, October 19, 1987:

P. F. BECHER, "Whisker Reinforced Ceramics"

AERE, Harwell, England, October 20, 1987:

J. BENTLEY, "Site Occupations of Ternary Elements in Ni_3Al by ALCHEMI and Atom Probe"

High Temperature Materials Workshop, Wright-Patterson Air Force Base, Dayton, Ohio, October 22–23, 1987:

M. H. YOO, "Strengthening Mechanisms in Ordered Intermetallic Compounds"

Materials for Nuclear Applications, University of Missouri, Rolla, Missouri, October 26–27, 1987:

N. H. PACKAN, "Accelerator Irradiations for Radiation Effects Studies of Future Nuclear Systems"

PM Aerospace Materials Conference, Luzern, Switzerland, November 2–4, 1987:

W. D. PORTER* AND J. H. SCHNEIBEL, "Coble Creep and Cavitation in a Powder Metallurgical (PM) Nickel Aluminide of Composition Ni-22.8Al-0.6 Hf-0.1B (at.%)"

Research Facilities for Materials Characterization, Argonne National Laboratory, Argonne, Illinois, November 3–5, 1987:

J. BENTLEY, "Analytical Electron Microscopy"

J. BENTLEY, "SHaRE: A Collaborative Users Program for Microanalysis in Materials Science"

32nd Annual Conference on Magnetism and Magnetic Materials, Chicago, Illinois, November 9–12, 1987:

D. D. JOHNSON,* F. J. PINSKI, AND G. M. STOCKS, "Electronic Structure and the Magnetic State of Disordered $Fe_{50}Mn_{50}$"

3rd International Conference on Science of Hard Materials, Nassau, The Bahamas, November 9–13, 1987:

C. J. MCHARGUE AND C. S. YUST,* "The Friction and Wear of Ion Implanted TiB_2"

Cornell University, Ithaca, New York, November 12, 1987:

C. T. LIU, "Alloy Stoichiometry and Intergranular Fracture in B-Doped Ni_3Al"

American Nuclear Society's 1987 Fall Meeting, Los Angeles, California, November 16–18, 1987:

C. J. MCHARGUE, "The Effects of Ion Implantation on the Mechanical Properties of Ceramics"

Local Chapter Meeting, Northeast Tennessee Section, American Welding Society, Oak Ridge, Tennessee, November 17, 1987:

R. K. NANSTAD, "Evaluation of the Irradiation-Embrittled High-Flux Isotope Reactor Pressure Vessel"

Tenth Annual DOE Workshop on Glass and Ceramic Processing, Los Alamos National Laboratory, Los Alamos, New Mexico, November 17–19, 1987:

D. S. EASTON, "Melt Spinning of Lithium Hydride"

Seminar, Indiana University, Bloomington, Indiana, November 20, 1987:

D. M. NICHOLSON, "Short-Range Order in Alloys"

Seminar, Westinghouse R&D Center, Pittsburgh, Pennsylvania, November 25, 1987:

M. K. MILLER, "Atomic Scale Analysis"

1987 Materials Research Society Fall Meeting, Boston, Massachusetts, November 30–December 5, 1987:

A. S. BOMMANNAVAR,* A. HABENSCHUSS, G. E. ICE, AND C. J. SPARKS, "X-Ray Diffraction Study of a Thin GaAs Film on Si(100)"

L. A. HARRIS, "Materials Characterization in Coal"

C. J. MCHARGUE,* P. S. SKLAD, C. W. WHITE, G. C. FARLOW, A. PEREZ, N. KORNILIOS, AND G. MAREST, "The Charge State of Iron Ions Implanted Into Sapphire"

M. K. MILLER* AND G. D. W. SMITH, "Atom Probe Microanalysis: Principles and Materials Applications"

P. S. SKLAD, "The Preparation of TEM Specimens from Hazardous or Difficult Materials"

P. A. STERNE,* C. S. WANG, G. M. STOCKS, AND W. M. TEMMERMAN, "Electronic Structure and Antiferromagnetism in La_2CuO_4"

N. F. WRIGHT* AND W. H. BUTLER, "Structural Stability of High-Temperature Superconducting Materials"

N. F. WRIGHT,* G. S. PAINTER, W. R. BUSING, AND W. H. BUTLER, "Ionic Models for $YBa_2Cu_3O_7$"

Symposium on the Properties of Stainless Steels in Elevated Temperature Service, ASME Annual Winter Meeting, Boston, Massachusetts, December 13–18, 1987:

V. K. SIKKA, "Superplasticity and Its Application to Near-Net Shaping of Intermetallic Alloys"

J. M. VITEK* AND S. A. DAVID, "The Aging Behavior of Types 308 and 308CRE Stainless Steels and Its Effect on Mechanical Properties"

Structure and Properties of Disperse Systems in Industrial Applications Symposium, sponsored by Colgate-Palmolive Company, Princeton, New Jersey, January 7–8, 1988:

A. BLEIER, "Effect of Colloidal Phenomena on the Stability and Rheological Properties of Unary and Binary Suspensions Containing Oxide Solids: Secondary Minimum Interactions and Heterocoagulation"

Indo-U.S. Advanced Study Workshop, Hyderabad, India, January 15–21, 1988:

S. A. DAVID* AND J. M. VITEK, "Microstructural Modification During Laser Welding"

12th Annual Conference on Composites and Advanced Ceramics, Cocoa Beach, Florida, January 17–20, 1988:

C. H. HSUEH,* P. F. BECHER, AND P. ANGELINI, "Effects of Interfacial Film on Residual Thermal Stresses of Whisker Reinforced Ceramics"

Seminar, Department of Materials Science and Engineering, University of Tennessee, Knoxville, Tennessee, January 19, 1988:

M. H. YOO, "Strengthening Mechanisms in Ordered Intermetallic Compounds"

1988 TMS-AIME Annual Meeting, Phoenix, Arizona, January 25–29, 1988:

J. A. HORTON,* P. VEYSSIERE, I. BAKER, AND M. H. YOO, "Superlattice Dislocation Structures in Ordered Intermetallic Alloys"

L. K. MANSUR* AND E. H. LEE, "Ion-Beam-Stimulated Microstructural Evolution"

L. MARTINEZ* AND J. H. SCHNEIBEL, "Influencing the Shape of Creep Cavities in Nickel Aluminides by Stress Changes"

W. D. PORTER AND W. C. OLIVER,* "Aluminum Based Cubic Intermetallics Having the LI_2 Structure"

V. K. SIKKA, "Fabrication Technology for Nickel Aluminides"

C. J. SPARKS,* A. DHERE, M. HASAKA, B. CAVIN, G. E. ICE, AND A. HABENSCHUSS, "X-Ray Diffraction Study of Defects in Ni_3Al as a Function of Al and B Concentration"

M. TAKEYAMA* AND C. T. LIU, "Effect of Grain Size on Yield Strength of Ni_3Al and Some Other Alloys"

M. H. YOO,* J. A. HORTON, AND C. T. LIU, "Micromechanisms of Deformation in Ordered Intermetallics"

17th Annual Symposium of the Florida Chapter of the American Vacuum Society, Applied Vacuum Science and Technology, Clearwater Beach, Florida, February 1–3, 1988:

L. HEATHERLY* AND R. E. CLAUSING, "The Deposition and Removal of Diamond-Like Hard Carbon Films Using DC Glow Discharge and RF Plasmas"

WATTec '88, Knoxville, Tennessee, February 14–19, 1988:

S. A. DAVID, "Recent Advances in Welding Science"

The International Conference on High-Temperature Superconductors and Materials and Mechanisms of Superconductivity, Interlaken, Switzerland, February 29–March 4, 1988:

G. M. STOCKS,* W. M. TEMMERMAN, Z. SZOTEK, G. Y. GUO, AND P. J. DURHAM, "Ground State Properties and Electronic Structure of High T_c Superconductors"

Joint U.S.-French Workshop on Electron-Beam Induced Spectroscopies at Very High Spatial Resolution, Aussois, France, February 29–March 4, 1988:

J. BENTLEY, "Contributions to a Joint U.S.-French Workshop on Electron-Beam Induced Spectroscopies at Very High Spatial Resolution"

Indian Institute of Technology (ITT), Kanpur, India, March 7, 1988:

J. H. SCHNEIBEL, "Surface Energy Measurements"

Bhabha Atomic Research Center (BARC), Trombay, Bombay, India, March 9, 1988:

J. H. SCHNEIBEL, "Surface Energy Measurements"

Cornell University, Department of Materials Science and Engineering, Ithaca, New York, March 10, 1988:

P. S. SKLAD, "The Characterization of Al_2O_3 After Ion Implantation"

Seminar, Drexel University, Philadelphia, Pennsylvania, March 10, 1988:

S. A. DAVID, "Welding and Weldability of Ductile Intermetallic Alloys"

Indian Institute of Science (IISC), Bangalore, India, March 11, 1988:

J. H. SCHNEIBEL, "Surface Energy Measurements"

National Bureau of Standards, Gaithersburg, Maryland, March 18, 1988:

P. P. CAMUS, "Atom Probe Field-Ion Microscopy of Fe-Cr-(Co) Alloys"

1988 Meeting of the American Physical Society, New Orleans, Louisiana, March 21–25, 1988:

R. A. BROWN,* P. B. ALLEN, D. M. NICHOLSON, AND W. H. BUTLER, "A First-Principles Calculation of the Electronic Structure and Transport Properties of a Strong Scattering, Disordered Alloy"

W. H. BUTLER,* D. M. NICHOLSON, J. C. SWIHART, AND F. J. PINSKI, "Electrical Resistivity of Random Transition Metal Alloys"

R. A. DEFAZIO,* P. L. TAYLOR, AND N. F. WRIGHT, "Interchain Energy and Phase Transition in Isotactic Polypropylene"

C. L. FU* AND A. J. FREEMAN, "Total Energy Determination of the H-Induced c(2x2)-W(001) Multilayer Surface Reconstruction"

A. GONIS,* X.-G. ZHANG, D. M. NICHOLSON, AND C. L. FU, "Multiple Scattering Theory for General Space-Filling Cell Potentials"

F. W. KUTZLER* AND G. S. PAINTER, "Cooperative Effect Between Nonlocal Density Functionals and Nonspherical Charge Densities in Atomic Total Energies"

D. M. NICHOLSON,* G. M. STOCKS, F. J. PINSKI, A. GONIS, B. L. GYORFFY, AND D. D. JOHNSON, "Concentration Functional Theory of Short-Range Order"

G. S. PAINTER* AND F. W. AVERILL, "Effects of First-Row Impurities on the Cohesive Properties of Nickel Clusters"

F. J. PINSKI,* D. D. JOHNSON, AND G. M. STOCKS, "Equilibrium Properties of $Fe_{1-x}Ni_x$"

W. A. SHELTON, F. J. PINSKI,* AND G. M. STOCKS, "Electronic Structure of Compositionally Disordered $Ba(Bi_{1-x}Pb_x)O_3$"

E. D. SPECHT,* C. J. SPARKS, A. G. DHERE, J. BRYNESTAD, O. B. CAVIN, D. M. KROEGER, AND H. A. OYE, "Effect of Oxygen Pressure on the Orthorhombic-Tetragonal Transition in the High-Temperature Superconductor $YBa_2Cu_3O_x$"

F. J. WALKER,* K. B. ALEXANDER, AND R. A. MCKEE, "The Growth of fcc Titanium on Amorphous NiTi Substrates"

N. F. WRIGHT,* W. H. BUTLER, AND G. S. PAINTER, "Ionic Models for $YBa_2Cu_3O_7$ and $YBa_2Cu_3O_6$"

International Symposium on Technology of Future-Materials Development and Technology Innovation, Kobe, Japan, March 22–25, 1988:

P. F. BECHER, "Whisker Reinforced Ceramic Matrix Composites: Toughening Behavior and Properties"

Workshop on the Effects of Recoil Energy Spectrum and Nuclear Transmutations on the Evolution of the Microstructure, Lugano, Switzerland, March 23, 1988:

D. F. PEDRAZA,* P. J. MAZIASZ, AND R. L. KLUEH, "Helium Effects in Reactor Irradiated Ferritic and Austenitic Steels"

NGK Spark Plug Company, Ltd., Nagoya, Japan, March 26, 1988:

P. F. BECHER, "Whisker Reinforced Ceramic Matrix Composites: Toughening Behavior and Properties"

Japan Fine Ceramics Association, Tokyo, Japan, March 28, 1988:

P. F. BECHER, "Whisker Reinforced Ceramic Matrix Composites: Toughening Behavior and Properties"

Hitachi Ltd., Hitachi City, Japan, March 29, 1988:

P. F. BECHER, "Whisker Reinforced Ceramic Matrix Composites: Toughening Behavior and Properties"

Seminar, Department of Physics, University of Wisconsin, Milwaukee, Wisconsin, March 30, 1988:

C. L. FU, "Local Density Functional Theory of Surface Structural and Electronic Properties"

Materials Research Society 1988 Spring Meeting, Reno, Nevada, April 5–9, 1988:

A. BLEIER, "Chemical and Physical Principles of Processing that Affect Microstructure and Mechanical Properties of Al_2O_3-ZrO_2"

E. P. GEORGE* AND D. P. POPE, "Impurity-Induced Changes in Interfacial Strength and Their Role in Creep Fracture"

D. M. KROEGER,* J. BRYNESTAD, R. A. PADGETT, AND J. O. SCARBROUGH, "Grain Boundary Compositions in $YBa_2Cu_3O_7$ Determined from Auger Electron Spectroscopy of Fracture Surfaces"

C. T. LIU, "Grain Boundary Design of Ll_2 Ordered Intermetallic Alloys"

F. J. WALKER,* R. A. MCKEE, AND F. A. LIST, "Amorphous Interface Between Crystalline Nickel and Titanium Films"

N. F. WRIGHT,* W. H. BUTLER, AND G. S. PAINTER, "Ionic Models for $YBa_2Cu_3O_7$ and $YBa_2Cu_3O_6$"

M. H. YOO* and A. H. King, "Interaction of Slip with Grain Boundary in the Ll_2 Ordered Structure-A Sigma = 9 (122) Tilt Boundary"

Seminar, Ohio State University, Columbus, Ohio, April 6, 1988:

S. A. DAVID, "Effect of Cooling Rate on Weld Metal Microstructures and Its Influence on the Constitution Diagram"

European Physical Society Meeting, Budapest, Hungary, April 6–9, 1988:

G. M. STOCKS* AND D. M. NICHOLSON, "Ab Initio Theory of Alloy Phase Stability: The PdRh Phase Diagram"

Physics Department, University of Kentucky, Lexington, Kentucky, April 12, 1988:

C. L. FU, "Local Density Functional Theory of Surface Structural and Electronic Properties"

69th Annual American Welding Society Meeting, New Orleans, Louisiana, April 17–22, 1988:

J. M. VITEK* AND S. A. DAVID, "The Effect of Cooling Rate on Ferrite Content and Composition"

University of Salford, Salford, England, April 20, 1988:

C. J. MCHARGUE, "Structure and Mechanical Properties of Ion Implanted Ceramics"

University of Salford, Salford, England, April 21, 1988:

C. J. MCHARGUE, "Iron Ion Implantation Effects in Sapphire"

Oak Ridge Chapter Sigma Xi Meeting, Oak Ridge, Tennessee, April 26, 1988:

W. H. BUTLER, "High Temperature Superconductors"

American Society for Metals/Edison Welding Institute Power Beam Conference, San Diego, California, May 1–5, 1988:

S. A. DAVID,* J. M. VITEK, AND J. F. KING, "Microstructural Characterization and Properties of 3Cr-1.5Mo-0.1V Thick Section Electron Beam Welds"

90th Annual Meeting of the American Ceramic Society, Cincinnati, Ohio, May 1–5, 1988:

W. R. ALLEN* AND M. B. LEWIS, "Studies of Ion-Implanted Helium in MgO and Al_2O_3"

P. ANGELINI,* P. F. BECHER, AND T. N. TIEGS, "Influence of Sintering Aids on Microstructure and Mechanical Properties of SiC Whisker Reinforced Alumina and Mullite"

P. F. BECHER,* C. H. HSUEH, P. ANGELINI, AND T. N. TIEGS, "Toughening Behavior in Whisker Reinforced Ceramic Matrix Composites"

W. H. BUTLER,* D. M. NICHOLSON, G. S. PAINTER, G. M. STOCKS, AND N. F. WRIGHT, "The Electronic Structure of High Temperature Superconductors and Its Relation to Atomics Structure and Superconductivity"

C. H. HSUEH, "Evaluation of Interfacial Shear Strength at Fiber-Coating Interfaces"

K. L. MORE, "Defects in Beta-SiC Thin Films Grown on Alpha SiC Substrates"

G. M. PHARR AND W. C. OLIVER,* "Elastic Displacement During Indentation of Ceramics and Glasses"

J. H. SCHNEIBEL* AND L. MARTINEZ, "Coble Creep, Cavity Sintering, and Cavity Growth"

8th Annual Symposium of the Tennessee Valley Chapter of the American Vacuum Society, Oak Ridge, Tennessee, May 3–5, 1988:

D. L. JOSLIN,* R. E. CLAUSING, AND C. J. MCHARGUE, "The Mechanical Properties of Diamond-Like Carbon Films"

B. E. WILLIAMS,* J. T. GLASS, K. L. MORE, AND J. BENTLEY, "The Growth and Characterization of Diamond Thin Films"

ASM, Lehigh Valley Chapter, Reading, Pennsylvania, May 12, 1988:

C. T. LIU, "Ordered Intermetallics for Structural Use"

Auburn University, Auburn, Alabama, May 13, 1988:

D. M. NICHOLSON, "Short-Range Order in Alloys"

Third International Conference on Supercomputing, Boston, Massachusetts, May 15–20, 1988:

F. J. PINSKI,* D. M. NICHOLSON, G. M. STOCKS, W. H. BUTLER, D. D. JOHNSON, AND B. L. GYORFFY, "The Theory of Random Alloys"

20th Polish Seminar on Positron Annihilation, Piechowice, Poland, May 15–21, 1988:

Z. SZOTEK,* W. M. TEMMERMAN, B. L. GYORFFY, AND G. M. STOCKS, "On Positron Annihilation in Concentrated Random Alloys and Superconducting"

Ion Implantation and Plasma-Assisted Processes for Industrial Applications, Atlanta, Georgia, May 22–25, 1988:

C. J. MCHARGUE, "Use of Mossbauer Spectroscopy to Study Implanted Surfaces"

W. C. OLIVER* AND C. J. MCHARGUE, "Thin Film and Near-Surface Characterization Using a Mechanical Properties Microprobe"

P. S. SKLAD, "The Use of Analytical Electron Microscopy in the Study of Ion Implanted Materials"

Workshop on Composite Materials, Brown University, Providence, Rhode Island, May 30–June 3, 1988:

P. F. BECHER,* P. ANGELINI, C. H. HSUEH, AND T. N. TIEGS, "Theoretical and Experimental Analysis of the Toughening Behavior in Whisker Reinforced Ceramics"

University of Kentucky, Lexington, Kentucky, June 2, 1988:

D. M. NICHOLSON, "Short-Range Order in Alloys"

American Society of Metals International Conference on Whisker- and Fiber-Toughened Ceramics, Oak Ridge Associated Universities, Oak Ridge, Tennessee, June 7–9, 1988:

P. F. BECHER,* C. H. HSUEH, P. ANGELINI, AND T. N. TIEGS, "Factors Influencing the Toughening Behavior of Whisker Reinforced Ceramics"

P. HUBER, E. M. DELISO,* S. C. DANFORTH, AND A. BLEIER, "Processing Parameters for Whisker-Reinforced Composites"

American Society for Engineering Education (ASEE) 1988 Annual Conference, University of Portland, Portland, Oregon, June 19–23, 1988:

D. M. KROEGER, "Critical Current Densities in Superconducting Oxides"

14th International Symposium on Effects of Radiation on Materials, Andover, Massachusetts, June 27–29, 1988:

W. R. ALLEN* AND M. B. LEWIS, "Ion Beam Studies of Implanted Helium in Selected Ceramics"

A. J. JACOBS,* R. E. CLAUSING, L. HEATHERLY, AND R. M. KRUGER, "Irradiation-Assisted Stress Corrosion Cracking and Grain Boundary Segregation in Heat Treated Type 304SS"

E. H. LEE* AND N. H. PACKAN, "Swelling Suppression in Phosphorous-Modified Fe-Cr-Ni Alloys During Neutron Irradiation"

L. K. MANSUR* AND W. A. COGHLAN, "Isotopically Alloyed Injector Foils for Helium Effects Research in Mixed-Spectrum Reactors"

M. K. MILLER* AND M. G. BURKE, "Fine-Scale Microstructural Characterization of Pressure Vessel Steels and Related Materials Using APFIM"

R. E. STOLLER* AND L. K. MANSUR, "The Influence of Other Microstructural Features on Void Formation and Void Growth in Irradiated Materials"

35th International Field Emission Symposium, Oak Ridge, Tennessee, July 18–23, 1988:

M. G. BURKE* AND M. K. MILLER, "Solute Clustering and Precipitation in Pressure Vessel Steels Under Low Fluence Irradiation Conditions"

P. P. CAMUS,* I. BAKER, J. A. HORTON, AND M. K. MILLER, "Grain Boundary Chemistry of NiAl"

P. P. CAMUS* AND M. K. MILLER, "Practical Applications of FIM Simulations"

M. G. HETHERINGTON* AND M. K. MILLER, "Statistical Analysis of the Early Stages of Phase Decomposition by Atom Probe"

E. A. KENIK, "SHaRE - A Collaborative Approach to Materials Science Research"

D. M. KROEGER, "Grain Boundaries and Critical Current Densities in Oxide Superconductors"

M. K. MILLER* AND M. G. BURKE, "Identification of a B8-Ordered BeFe Phase"

M. K. MILLER,* A. J. MELMED, AND K. L. MORE, "Can APFIM Contribute to the Understanding of High Temperature Superconductors?"

M. K. MILLER* AND K. L. MORE, "FIM Simulation of $MBa_2Cu_3O_{7-x}$ Superconductors"

M. K. MILLER* AND K. F. RUSSELL, "An Atom Probe Study of Phase Decomposition in the Cape York Meteorite"

M. K. MILLER* AND K. F. RUSSELL, "The Effects of Image Gas on Atom Probe Analysis"

K. L. MORE* AND M. K. MILLER, "Microstructural Characterization of Udimet 720: A Nickel-Base Alloy"

E. M. PERRY,* D. L. COCKE, AND M. K. MILLER, "Atom Probe Investigation of the Oxidation of Ni-Zr Intermetallic Compounds"

S. SPOONER* AND M. K. MILLER, "A Comparison of Autocorrelograms Determined from SANS and APFIM Data"

Fine Particle Society Annual Meeting, Symposium on Aqueous and Nonaqueous Electrokinetic Phenomena, Santa Clara, California, July 19–22, 1988:

E. M. DELISO,* L. GECZI, AND A. BLEIER, "An Electrophoretic Explanation for the Effect of an Amine Additive on Submicron Silicon Power Suspensions"

1988 International Conference on Magnetism, Paris, France, July 25–29, 1988:

C. L. FU AND A. J. FREEMAN,* "Surface Magnetism of the Clean Surface Ni(111) and of a Ni Monolayer on Cu(111)"

F. J. PINSKI,* D. D. JOHNSON, AND G. M. STOCKS, "Collapse of Ferromagnetism in Ni_xFe_{1-x}"

W. A. SHELTON, JR.* AND G. M. STOCKS, "Magnetic Moment Formation in Compositionally Disordered $(Co_{1-x}Fe_x)_3V$"

Sintering Problems, Lawrence Berkeley Laboratory, University of California, Berkeley, California, July 29, 1988:

C. H. HSUEH, "Constraint of Stresses Due to Sintering with Rigid Inclusions"

International Conference on Nuclear Methods in Magnetism, Munich, West Germany, August 1–4, 1988:

C. L. FU,* A. J. FREEMAN, AND S. C. HONG, "Hyperfine Interactions at Surfaces and Interfaces"

46th Annual Meeting of the Electron Microscopy Society of America, Milwaukee, Wisconsin, August 7–12, 1988:

K. B. ALEXANDER,* F. J. WALKER, R. A. MCKEE, AND F. A. LIST, "Characterization of Amorphization in Ni-Ti Multilayers"

P. ANGELINI,* P. S. SKLAD, J. C. SEVELY, AND K. HSSEIN, "Evaluation of Amorphous and Crystalline SiC by Extended Energy Loss Fine Structure (EXELFS) Analysis"

J. BENTLEY, "Electron Microscopy of Modulated and Ordered Alloys"

M. G. BURKE AND M. K. MILLER,* "A Combined TEM/APFIM Approach to the Study of Phase Transformations: Phase Identification in the Fe-Be System"

E. A. KENIK AND K. L. MORE,* "SHaRE: Collaborative Materials Science Research"

E. A. KENIK* AND M. NASTASI, "Disordering and Phase Decomposition of a Nickel-Aluminum Intermetallic Under Low Temperature Electron Irradiation"

K. R. LAWLESS, J. V. CATHCART, AND E. A. KENIK,* "In Situ Oxidation of Ni_3Al Alloys"

Y. J. LIN,* M. L. MECARTNEY, AND P. ANGELINI, "Analytical TEM Study of a Yttria Stabilized Zirconia/Glass Composite"

L. K. MANSUR* AND E. H. LEE, "Ion Beam Stimulated Reactions in Metallic Alloys"

C. G. MCKAMEY, D. M. KROEGER, D. S. EASTON, J. A. HORTON, AND P. ANGELINI,* "Crystallization of Zr-Ni Metallic Glasses"

P. S. SKLAD,* P. ANGELINI, AND J. SEVELY, "The Characterization of Amorphous Al_2O_3 by Extended Energy Loss Fine Structure (EXELFS) Analysis"

International Conference on Critical Currents in High Temperature Superconductors, Snowmass Village, Colorado, August 16–19, 1988:

D. M. KROEGER,* J. BRYNESTAD, R. A. PADGETT, AND J. O. SCARBROUGH, "Effects of Grain Boundary Composition on Critical Current Density and Normal State Resistivity of $YBa_2Cu_3O_{7-x}$"

NATO Advanced Study Institute on Structure-Property Relationships in Ion-Beam Surface-Modified Ceramics - Theory and Applications, Castelvecchio Pascoli, Italy, August 28–September 9, 1988:

W. R. ALLEN* AND M. B. LEWIS, "Ion Scattering Studies of Helium Implanted in Alumina and Magnesium Oxide"

D. L. JOSLIN,* C. J. MCHARGUE, AND W. C. OLIVER, "Thin Film and Near Surface Characterization Using a Mechanical Properties Microprobe"

C. J. MCHARGUE, "Ion Beam Mixing of Metals and Ceramics - Material Considerations"

C. J. MCHARGUE, "The Mechanical Properties of Ion Implanted Ceramics"

J. E. PAWEL* AND C. J. MCHARGUE, "Modified Pull Test for the Testing of Very Adherent Films"

Society of Chemical Industry, Colloid and Surface Chemistry Group, Particle Deposition at the Solid-Liquid Interface Symposium, London, England, September 12–14, 1988:

A. BLEIER, "Secondary Minimum Interactions and Heterocoagulation Encountered in the Aqueous Processing of α-Al_2O_3:m-ZrO_2"

International Conference on Surface Modification of Metals by Ion Beams, Riva Del Garda, Italy, September 12–16, 1988:

C. J. MCHARGUE,* M. E. O'HERN, C. W. WHITE, AND M. B. LEWIS, "Ion Implantation in Ceramics - Residual Stress and Properties"

Cambridge University, Cambridge, England, September 13, 1988:

J. M. VITEK, "Laser Welding of Stainless Steel Weld Filler Metals at High Cooling Rates"

The Welding Institute, Abington, England, September 14, 1988:

J. M. VITEK, "Laser Welding of Stainless Steel Weld Filler Metals at High Cooling Rates"

Sixth International Symposium on Superalloys, Seven Springs Mountain Resort, Champion, Pennsylvania, September 18–22, 1988:

V. K. SIKKA* AND E. A. LORIA, "Industrial Scale Processing and Elevated Temperature Properties of Ni_3Al-Cr-Zr-B Alloys"

Max-Planck-Institut für Metallforschung, Stuttgart, West Germany, September 19, 1988:

J. M. VITEK, "Aging Behavior of Type 308 Stainless Steels"

Staatlichematerialsprüfungsanstalt, Stuttgart, West Germany, September 20, 1988:

J. M. VITEK, "Aging Behavior of Type 308 Stainless Steels"

Ecole Polytechnique Fédérale de Lausanne, Lausanne, Switzerland, September 22, 1988:

J. M. VITEK, "Laser Welding of Stainless Steel Weld Filler Metals at High Cooling Rates"

1988 TMS-AIME Fall Meeting, Chicago, Illinois, September 25–29, 1988:

M. G. BURKE* AND M. K. MILLER, "Atom Probe Field-Ion Microscopy Investigations of Neutron-Irradiated Pressure Vessel Steels"

E. A. KENIK, "Analytical Electron Microscopy and Radiation Damage Studies"

M. K. MILLER* AND M. G. BURKE, "Atom Probe Field-Ion Microscopy - Imaging at the Atomic Level"

M. K. MILLER* AND M. G. BURKE, "Atom Probe Field-Ion Microscopy - A Technique for Microstructural Characterization of Irradiated Materials on the Atomic Scale"

D. F. PEDRAZA, "Irradiation as a Tool for Studying Solid State Amorphization Phenomena"

C. J. SPARKS,* A. DHERE, AND G. E. ICE, "Synchrotron Radiation Gives New Information from Profile Analysis of X-Ray Diffraction Lines"

R. E. STOLLER, "Modeling Dislocation Evolution in Irradiated Alloys"

M. TAKEYAMA* AND C. T. LIU, "Grain-Boundary Contamination and Ductility Loss in Boron-Doped Ni_3Al"

M. H. YOO, "Deformation and Fracture in Superlattice Structures"

American Society of Metals 1988 World Materials Congress, Chicago, Illinois, September 25–30, 1988:

G. M. STOCKS,* B. L. GYORFFY, F. J. PINSKI, AND D. D. JOHNSON, "First-Principles Mean-Field Theory of Alloy Phase Stability"

M. H. YOO,* M. S. DAW, AND M. I. BASKES, "Atomistic Simulation of Superdislocation Dissociation in Ni_3Al"

M. H. YOO* AND A. H. KING, "Intergranular Fracture by Slip/Grain Boundary Interaction"

1988 ASM Materials Science Seminar, Science of Advanced Materials, Chicago, Illinois, September 26–29, 1988:

C. T. LIU, "Ordered Intermetallics for Structural Use"

Fourth International Colloquium on Welding and Melting by Electron and Laser Beams, Cannes, France, September 26–30, 1988:

J. M. VITEK* AND S. A. DAVID, "Laser Welding of Stainless Steel Weld Filler Metals at High Cooling Rates"

University of Missouri, Department of Physics, Columbia, Missouri, September 30, 1988:

C. J. SPARKS, "Synchrotron Radiation Provides for New Information About Surfaces and Interfaces from Profile Analysis"

International Symposium on the Electron Structure of High T_c Superconductors, Rome, Italy, October 4–7, 1988:

W. M. TEMMERMAN,* G. Y. GUO, Z. SZOTEK, P. J. DURHAM, AND G. M. STOCKS, "On the Validity of the Band Model for High T_c Superconductors"

Workshop on Mechanisms of Embrittlement of Pressure Vessel Steels, organized by International Group on Irradiation Damage Mechanisms in Pressure Vessel Steels, Harwell, England, October 5–7, 1988:

M. K. MILLER, "Atom Probe Studies of Clustering in Fe-Cu Alloys"

M. K. MILLER, "FIM Investigations on Gundremmigen KRB-A Archive and Vessel Trepan Material"

Technology Transfer Conference, Oak Ridge, Tennessee, October 10–11, 1988:

P. F. BECHER* AND G. M. BEGUN, "Transformation Toughened Zirconia Ceramics: Grain Size and Alloying Effects"

Surfaces-Materiaux-Technologie Societe Francaise du Vide, Lyon, France, October 10–14, 1988:

G. MAREST,* C. J. MCHARGUE, AND A. PEREZ, "Caracterisation de αk-Al_2O_3 Apre Implantation Ionique"

16th Midwest Solid State Theory Symposium, Cincinnati, Ohio, October 14–15, 1988:

G. M. STOCKS, "Towards a First-Principles Theory of Alloy Phase Stability"

H. J. YANG,* J. C. SWIHART, AND D. M. NICHOLSON, "The Calculation of the Density of States of the Ni_3P Amorphous Alloy"

International Symposium on Interface-Structure and Reactions, San Francisco, California, October 23–26, 1988:

J. BENTLEY, "AEM Characterization of Interfaces in Ceramics"

K. L. MORE,* H. S. KONG, AND J. T. GLASS, "Comparison of Defects in β-SiC Thin Films Grown on Si and α-SiC"

The 41st Pacific Coast Regional Meeting, American Ceramic Society, San Francisco, California, October 23–26, 1988:

C. H. HSUEH, "Interfacial Friction Analysis for Fiber-Reinforced Ceramic Composites during Fiber Push-Down (Indentation)"

Symposium on Advanced Characterization Techniques for Ceramics, San Francisco, California, October 23–26, 1988:

P. ANGELINI,* T. A. NOLAN, AND C. E. BAMBERGER, "Analytical Electron Microscopy of TiN and CrN Whiskers"

P. S. SKLAD,* C. J. MCHARGUE, C. W. WHITE, AND G. C. FARLOW, "Precipitate Characterization in Al_2O_3 Implanted with Nickel"

Seminar, Tennessee Technological University, Cookeville, Tennessee, October 28, 1988:

G. S. PAINTER, "The Microchemistry of Impurities in Metals: A Theoretical View of Grain Boundary Segregation"

American Nuclear Society Winter Meeting, Washington, D.C., October 30–November 3, 1988:

J. L. SNELGROVE,* G. L. HOFMAN, AND G. L. COPELAND, "Fuel for the Advanced Neutron Source-Performance Testing and Fabrication Development"

Seminar, University of Illinois, Materials Research Laboratory, Champaign, Illinois, November 1–3, 1988:

C. T. LIU, "Ordered Intermetallics for Structural Use"

Seminar on Microindentation Work, Vanderbilt University, Nashville, Tennessee, November 2, 1988:

W. C. OLIVER, "New Techniques Using the Mechanical Properties Microprobe"

Seminar, Department of Materials Science and Engineering, University of Tennessee, Knoxville, Tennessee, November 3, 1988:

C. J. MCHARGUE, "Ion Implantation and Ion Beam Mixing"

ASTM Symposium on Evaluation and Techniques in Fractography, Atlanta, Georgia, November 6–11, 1988:

J. H. SCHNEIBEL* AND L. MARTINEZ, "Evaluation and Extrapolation of Creep Damage"

ASM Meeting, Detroit, Michigan, November 7, 1988:

W. C. OLIVER, "New Techniques Using the Mechanical Properties Microprobe"

American Physical Society Meeting, 10th Conference on the Application of Accelerators in Research and Industry, Denton, Texas, November 7–9, 1988:

R. A. BUHL* AND N. H. PACKAN, "Modular Target Chamber for the ORNL Triple Ion Beam Accelerator Facility"

M. B. LEWIS, W. R. ALLEN,* R. A. BUHL, N. H. PACKAN, AND S. W. COOK, "A Triple Ion Beam Accelerator Facility for Materials Research"

1988 TMS Extractive and Process Metallurgical Fall Meeting, International Symposium on Casting of Near Net Shape Products, Honolulu, Hawaii, November 13–17, 1988:

V. K. SIKKA, "Near-Net-Shape Casting of Sheet and Bar of Ordered Nickel Aluminide Alloys"

ANS Corrosion Workshop, EG&G Idaho, Idaho Falls, Idaho, November 16–17, 1988:

R. E. PAWEL, "ANS Corrosion Tests at ORNL"

Materials Research Society Fall Meeting, Boston, Massachusetts, November 28–December 3, 1988:

K. B. ALEXANDER,* J. BENTLEY, D. M. KROEGER, AND J. BRYNESTAD, "Grain Boundary Chemistries of Stoichiometric and Non-Stoichiometric $YBa_2Cu_3O_{7-x}$"

P. ANGELINI,* P. S. SKLAD, C. J. MCHARGUE, AND M. B. LEWIS, "Chemical Aspects of Ion Implantation - Al_2O_3 Implanted with Zr and Cr"

J. BENTLEY,* P. S. SKLAD, AND P. ANGELINI, "Radial Distribution Functions of Amorphous Materials Determined from Direct Measurements of Electron Intensity Profiles"

R. H. BROWN,* P. B. ALLEN, D. M. NICHOLSON, AND W. H. BUTLER, "A First-Principles Calculation of the Resistivity and Diffusion Thermopower in Strong-Scattering Systems"

C. L. FU* AND M. H. YOO, "Crystal Elasticity of the Ll_2 Ordered Structure - An All-Electron Total-Energy Calculation"

E. P. GEORGE,* W. D. PORTER, H. M. HENSON, W. C. OLIVER, AND B. F. OLIVER, "Cleavage Fracture in an Al_3Ti-Base Alloy Having the Ll_2 Structure"

J. A. HORTON AND M. K. MILLER,* "An Atom Probe Study of the Behavior of Boron in Ni_3Al"

T. R. JERVIS,* J.-P. HIRVONEN, M. NASTASI, T. G. ZOCCO, J. A. MARTIN, G. M. PHARR, AND W. C. OLIVER, "Surface Mechanical Properties of Ti Alloys Produced by Excimer Laser Mixing of Ti on AISI 304 Stainless Steel"

E. A. KENIK* AND M. NASTASI, "Phase Stability of Ni_2Al_3 Under Electron Irradiation"

E. H. LEE* AND L. K. MANSUR, "Effects of Simultaneous B^+ and N^+ Implantation on Microhardness, Fatigue Life, and Microstructure in Fe-13Cr-15Ni Base Alloys"

M. K. MILLER* AND G. D. W. SMITH, "Atom Probe Microanalysis: Principles and Applications to Materials Problems"

W. C. OLIVER,* F. A. LIST, AND R. A. MCKEE, "The Influence of Thickness and Wavelength on the Mechanical Properties of a Compositionally Modulated Ceramic Thin Film"

W. D. PORTER,* K. HISATSUNE, C. J. SPARKS, W. C. OLIVER, AND A. DHERE, "Phase and Microstructure of Fe Modified Al_3Ti"

S. I. RAO,* C. R. HOUSKA, K. GRABOWSKI, J. CLAUSSEN, G. ICE, AND A. HABENSCHUSS, "X-Ray Diffraction from Ion Implanted Zones"

J. H. SCHNEIBEL* AND W. D. PORTER, "Mechanical Properties of Intermetallic Alloys Based on Al_3Zr and Al_3Nb"

P. S. SKLAD,* P. ANGELINI, AND J. SEVELY, "Analysis of Amorphous Phases in Ion-Implanted α-Al_2O_3"

P. S. SKLAD,* J. D. MCCALLUM, S. J. PENNYCOOK, C. J. MCHARGUE, C. W. WHITE, AND A. PEREZ, "Microstructural Characterization of α-Al_2O_3 Implanted with Iron"

C. J. SPARKS, "X Rays for Microprobe Analyses of Materials"

M. TAKEYAMA* AND C. T. LIU, "Effects of Preoxidation and Grain Size on Ductility of a Boron-Doped Ni_3Al at Elevated Temperatures"

M. H. YOO, "Deformation Twinning in Ordered Intermetallic Compounds"

7th International Symposium on Ceramics, Bologna, Italy, December 14–16, 1988:

P. F. BECHER, "Whisker Reinforced Ceramics: Toughening Behavior and Properties"

13th Annual Conference on Composites and Advanced Ceramics, Cocoa Beach, Florida, January 15–18, 1989:

P. A. HUBER,* E. M. DELISO, AND A. BLEIER, "Processing Parameters for Whisker Reinforced Composites"

Department of Metallurgy, Ohio State University, Columbus, Ohio, January 17, 1989:

S. A. DAVID, "Recent Advances in Welding Science"

Seminar, National Taiwan University, Taipei, Taiwan, January 23, 1989:

C. T. LIU, "The Influence of Alloy Variables on Crystal Structures and Mechanical Properties of Ordered Intermetallics"

Golden Gate Materials Technology Conference, Santa Clara, California, February 7–9, 1989:

M. K. MILLER, "Applications of the Atom Probe Field-Ion Microscope"

WATTec, Knoxville, Tennessee, February 16, 1989:

S. A. DAVID, "Welding and Weldability of Ductile Intermetallic Alloys"

1989 TMS/AIME Annual Meeting, Las Vegas, Nevada, February 27–March 3, 1989:

S. A. DAVID* AND J. M. VITEK, "Microstructural Modification during Laser Welding"

K. FARRELL, "On the Origin of Intergranular Creep Cavities in Metals"

K. FARRELL* AND H. T. LIN, "Effects of Helium Bubbles on Recrystallization and Grain Growth in 316 Stainless Steel"

J. A. HORTON, "Deformation and Fracture Experiments in Transmission Electron Microscopes"

H. T. LIN AND K. FARRELL,* "Weld Response of Helium-Atomized and Helium-Doped Austenitic Stainless Steels"

L. MARTINEZ* AND J. H. SCHNEIBEL, "Numerical Modelling of Cavity Growth Controlled by Diffusion and Plasticity"

M. K. MILLER* AND K. F. RUSSELL, "An Atom Probe Study of Phase Decompositon in the Cape York Meteorite"

J. H. SCHNEIBEL,* P. F. BECHER, AND J. A. HORTON, "Microstructure and Fracture Toughness of Powder-Processed Al_3Nb"

J. H. SCHNEIBEL* AND J. A. HORTON, "Inverse Creep in a Nickel Aluminide"

J. H. SCHNEIBEL* AND L. MARTINEZ, "Crack-Like Creep Cavitation in a Nickel Aluminide"

J. M. VITEK,* M. RAPPAZ, S. A. DAVID, AND L. A. BOATNER, "Evaluation of Electron Beam Welds of Single Crystal Fe-15Ni-15Cr Alloy"

Division of Materials Sciences, Sandia National Laboratories, Albuquerque, New Mexico, March 3, 1989:

C. J. MCHARGUE, "Structure and Mechanical Properties of Ion Implanted Ceramics"

Engineering Foundation Conference on Structural Ceramics - Science & Technology, Palm Coast, Florida, March 12–17, 1989:

P. F. BECHER, "Mechanical Behavior of Whisker-Reinforced Ceramics"

Graduate Seminar Series, University of Tennessee, Knoxville, Tennessee, March 14, 1989:

E. P. GEORGE,* W. D. PORTER, AND J. H. SCHNEIBEL, "Fracture Studies of Trialuminides"

Technology Transfer Seminar, Copenhagen, Denmark, March 17, 1989:

J. R. WEIR, JR., "Technology Transfer in the United States"

Swiss Materials Workshop, Neuchatel, Switzerland, March 19–22, 1989:

C. T. LIU, "Grain-Boundary Engineering of Ordered Intermetallics"

1989 Meeting of the American Physical Society, St. Louis, Missouri, March 20–24, 1989:

R. H. BROWN,* W. H. BUTLER, D. M. NICHOLSON, AND P. B. ALLEN, "A Comparison of Supercell and Coherent-Potential Approximation Methods in Substitutionally Disordered Alloys"

C. L. FU* AND K. M. HO, "Theoretical Prediction of External Field Induced Surface Reconstruction of Ag(110)"

B. L. GYORFFY, J. B. STAUNTON, AND G. M. STOCKS,* "Local Pairing and Superconductivity in the Hubbard Model with Attractive Interactions"

E. D. ISAACS,* D. B. MCWHAN, C. PETERS, G. E. ICE, D. P. SIDDONS, J. P. HASTINGS, C. VETTIER, AND O. VOGT, "Resonant Magnetic X-Ray Scattering in UAs"

G. S. PAINTER* AND F. W. KUTZLER, "Local and Non-Local Density Functional Calculations for 3d Transition Metal Atoms"

W. A. SHELTON, JR.,* G. M. STOCKS, AND F. J. PINSKI, "Electronic Structure of Compositionally Disordered $Bi(Ba_{0.5}K_{0.5})O_3$"

G. M. STOCKS, D. M. NICHOLSON,* F. J. PINSKI, D. D. JOHNSON, J. B. STAUNTON, AND B. L. GYORFFY, "Electronic Mean Field Theory of Compositional Rearrangements: Short-Range Order and Alloy Phase Diagrams"

N. F. WRIGHT* AND W. H. BUTLER, "Point Dipole Model for the Structural Stability and Phonon Spectrum of $YBa_2Cu_3O_7$"

H. J. YANG,* J. C. SWIHART, AND D. M. NICHOLSON, "The Calculation of the Density States of the $Ni_{80}P_{20}$ Amorphous Alloy"

5th International Al-Li Conference, Williamsburg, Virginia, March 28–31, 1989:

T. ZACHARIA,* S. A. DAVID, J. M. VITEK, AND R. P. MARTUKANITZ, "Weldability and Microstructural Characterization of Al-Li Alloys"

Advanced Joining Technologies for New Materials Conference, Washington, D.C., March 29–31, 1989:

S. A. DAVID AND M. L. SANTELLA,* "Problems in Joining Advanced Metals II: Welding and Weldability Ductile Intermetallic Alloys"

Seminar, Clemson University, Clemson, South Carolina, April 2, 1989:

A. BLEIER, "The Colloidal and Surface Chemical Aspects of Ceramic Processing that Affect the Development of Microstructure in Composites: The Al_2O_3-ZrO_2"

70th Annual American Welding Society Meeting, Washington, D.C., April 2–7, 1989:

S. A. DAVID, J. A. HORTON, D. PHILLIPS, AND G. M. GOODWIN,* "Welding and Weldability of Titanium Aluminide"

S. A. DAVID, J. M. VITEK,* J. R. KEISER, D. J. ALEXANDER, AND R. K. NANSTAD, "Low Temperature Ferrite Decomposition in Austenitic Stainless Steel Welds and Its Influence on Weld Metal Impact Properties"

J. M. VITEK,* M. RAPPAZ, S. A. DAVID, AND L. A. BOATNER, "Microstructural Development in Fe-15Ni-15Cr Single Crystal Welds"

T. ZACHARIA,* S. A. DAVID, J. M. VITEK, AND T. DEBROY, "Experimental and Computational Study of GTA and Laser Welds Using Type 304 Stainless Steel"

1989 Spring Meeting (104th) of Japanese Institute of Metals, Yokohama, Japan, April 4–6, 1989:

M. H. YOO, "Deformation and Fracture of Ordered Intermetallic Compounds"

SCANNING/EM West, Long Beach, California, April 5–7, 1989:

K. B. ALEXANDER, J. BENTLEY,* D. M. KROEGER, AND J. BRYNESTAD, "Grain Boundary Compositions in Stoichiometric and Non-Stoichiometric $YBa_2Cu_3O_{7-x}$"

J. BENTLEY, "Practical Considerations in the Application of the Alchemi Technique to Intermetallic Alloys"

D. C. JOY, "Monte Carlo Simulations for Microcomputers"

D. C. JOY, "Optimizing Probe Forming Optics in the Low Voltage SEM"

General Electric, Cincinnati, Ohio, April 14, 1989:

J. H. SCHNEIBEL, "Microstructure, Crystallography and Mechanical Properties of Trialuminides"

16th International Conference on Metallurgical Coatings (ICMC '89), San Diego, California, April 17–21, 1989:

M. E. O'HERN,* R. H. PARRISH, AND W. C. OLIVER, "Evaluation of Mechanical Properties of TiN Films by Ultra-Low Load Indentation"

91st Annual Meeting and Exposition, The American Ceramic Society, Inc., Indianapolis, Indiana, April 23–27, 1989:

P. ANGELINI,* P. F. BECHER, AND T. N. TIEGS, "Microstructural Changes in Elevated Temperature Static Fatigue Specimens of SiC Whisker Reinforced Alumina"

P. F. BECHER,* G. M. BEGUN, AND M. V. SWAIN, "Grain Size Dependent Transformation Behavior in Polycrystalline Tetragonal Zirconia Ceramics"

A. BLEIER, "Colloidal and Surface Chemical Aspects of Ceramic Processing that Affect the Development of Microstructure in Al_2O_3-ZrO_2 Composites"

E. M. DELISO,* L. S. GECZI, AND A. BLEIER, "Nonaqueous Processing of Silicon for Reaction Bonded Silicon Nitride"

C. H. HSUEH, "Fiber Pullout Versus Push-down for Fiber-Reinforced Ceramic Composites with Frictional Interfaces"

Materials Research Society Spring Meeting, San Diego, California, April 24–29, 1989:

N. F. WRIGHT* AND W. H. BUTLER, "Point Dipole Model for the Structural Stability of $YBa_2Cu_3O_7$"

Lehigh University, Bethlehem, Pennsylvania, April 25, 1989:

M. K. MILLER, "Atom Probe Field-Ion Microscopy: Principles and Applications to Materials Problems"

Spring Meeting of the Korean Institute of Metals, Chonju, Korea, April 27–29, 1989:

M. H. YOO, "Deformation and Fracture of Ordered Intermetallic Compounds"

Appendix B

PUBLICATIONS

Compiled by Jamie Bain

K. B. ALEXANDER AND D. E. LAUGHLIN

"AEM Determination of Composition Profiles Formed during Cellular Precipitation in Ni-In Alloys," pp. 61–64 in *Analytical Electron Microscopy - 1987,* proceedings of symposium held at Kona, Hawaii, July 13–17, 1987, ed. D. C. Joy, San Francisco Press, Inc., 1987.

K. B. ALEXANDER, F. J. WALKER, R. A. MCKEE, AND F. A. LIST

"Characterization of Amorphization in Ni-Ti Multilayers," pp. 452–3 in *Proceedings of the 46th Annual Meeting of the Electron Microscopy Society of America, Milwaukee, Wisconsin, August 7–12, 1988,* ed. G. W. Bailey, San Franciso Press, Inc., 1988.

A. AL-LEHAIBI, J. C. SWIHART, W. H. BUTLER, AND F. J. PINSKI

"Electron-Phonon Interaction Effects in Tantalum," *Phys. Rev. B* **36**(8), 4103–11 (September 15, 1987).

C. Y. ALLISON, R. E. STOLLER, AND E. A. KENIK

"Electron Microscopy of Electron Damage in Tantalum Carbide," *J. Appl. Phys.* **63**(5), 1740–3 (March 1, 1988).

S. AMADOR, P. S. PERSHAN, H. STRAGIER, B. S. SWANSON, D. J. TWEET, L. B. SORENSEN, E. B. SIROTA, G. E. ICE, AND A. HABENSCHUSS

"Synchrotron Studies of the First-Order Melting Transitions of Hexatic Monolayers and Multilayers in Freely Suspended Liquid-Crystals Films," *Phys. Rev. A* **39**(5), 2703–8 (March 1, 1989).

P. ANGELINI AND P. F. BECHER

"In Situ Fracture of SiC-Whisker-Reinforced Al_2O_3," pp. 148–9 in *Proceedings of the 45th Annual Meeting of the Electron Microscopy Society of America, Baltimore, Maryland, August 2–7, 1987,* ed. G. W. Bailey, San Francisco Press, Inc., 1987.

P. ANGELINI, J. C. SEVELY, K. HSSEIN, AND G. ZANCHI
"EXELFS of Amorphous and Crystalline SiC," pp. 267–9 in *Analytical Electron Microscopy - 1987,* proceedings of symposium held at Kona, Hawaii, July 13–17, 1987, ed. D. C. Joy, San Francisco Press, Inc., 1987.

P. ANGELINI, P. S. SKLAD, J. C. SEVELY, AND D. K. HSSEIN
"Evaluation of Amorphous and Crystalline SiC by Extended Energy Loss Fine Structure (EXELFS) Analysis," pp. 466–7 in *Proceedings of the 46th Annual Meeting of the Electron Microscopy Society of America, Milwaukee, Wisconsin, August 7–12, 1988,* ed. G. W. Bailey, San Francisco Press, Inc., 1988.

F. W. AVERILL AND G. S. PAINTER
"Pseudospherical Integration Scheme for Electronic-Structure Calculations," *Phys. Rev. B* **39**(12), 8115–21 (April 15, 1989).

S. BAIK AND P. F. BECHER
"Effect of Oxygen Contamination on Densification of TiB_2," *J. Am. Ceram. Soc.* **70**(8), 527–30 (August 1987).

S. BAIK AND R. RAJ
"Liquid-Phase Bonding of Silicon Nitride Ceramics," *J. Am. Ceram. Soc.* **70**(5), C–105–7 (1987).

S. BAIK AND C. L. WHITE
"Anisotropic Calcium Segregation to the Surface of Al_2O_3," *J. Am. Ceram. Soc.* **70**(9), 682–8 (1987).

I. BAKER, J. A. HORTON, AND E. M. SCHULSON
"Some Comments on Dislocation Bowing and Partial Separation During In-Situ Straining of γ' Ni_3Al," *Philos. Mag. Lett.* **55**(1), 3–6 (1987).

C. E. BAMBERGER, C. S. MACDOUGALL, AND O. B. CAVIN
"Formation of Molybdenum Carbides by Reaction of Molybdenum Compounds with Molten Sodium Cyanide," *React. Solids* **6**, 369–72 (1989).

P. F. BECHER
"Whisker Reinforced Ceramic Matrix Composites: Toughening Behavior and Properties," pp. 191–222 in *International Symposium on Basic Technologies for Future Industries: Material Development and Technology Innovation, Kobe, Japan, March 22–25, 1988,* The Secretariate of the International Symposium, Japan Industrial Technology Association, March 1988.

P. F. BECHER, G. M. BEGUN, AND E. F. FUNKENBUSCH
"Transformation Toughening Behavior in Ceramics," pp. 645–51 in *Advances in Ceramics, Vol. 24: Science and Technology of Zirconia Ceramics,* ed. S. Somiya, N. Yamamoto, and H. Yanagida, American Ceramic Society, Westerville, Ohio, 1988.

P. F. BECHER, C. H. HSUEH, P. ANGELINI, AND T. N. TIEGS
"Factors Influencing the Toughening Behavior of Whisker Reinforced Ceramics," pp. 109–11 in *Proceedings of Conference on Whisker- and Fiber-Toughened Ceramics*, ed. R. A. Bradley, D. Larsen, and J. O. Stiegler, ASM International, Metals Park, Ohio, 1988.

P. F. BECHER, C. H. HSUEH, P. ANGELINI, AND T. N. TIEGS
"Theoretical and Experimental Analysis of the Toughening Behavior of Whisker Reinforcement in Ceramic Matrix Composites," *Mater. Sci. Eng.* **A107**, 257–9 (1989).

P. F. BECHER, C. H. HSUEH, P. ANGELINI, AND T. N. TIEGS
"Toughening Behavior in Whisker Reinforced Ceramics," *J. Am. Ceram. Soc.* **71**(12), 1050–61 (1988).

P. F. BECHER AND T. N. TIEGS
"Toughening Behavior Involving Multiple Mechanisms: Whisker Reinforcement and Zirconia Toughening," *J. Am. Ceram. Soc.* **70**(9), 651–4 (1987).

J. E. BENCI, D. P. POPE, AND E. P. GEORGE
"Creep Damage Nucleation Sites in Ferrous Alloys," *Mater. Sci. Eng.* **A103**, 97–102 (1988).

J. BENTLEY
"Electron Microscopy of Modulated and Ordered Alloys," pp. 768–9 in *Proceedings of the 46th Annual Meeting of the Electron Microscopy Society of America, Milwaukee, Wisconsin, August 7–12, 1988,* ed. G. W. Bailey, San Francisco Press, Inc., 1988.

J. BENTLEY
"Electron Microscopy of Phase Transformations in Spinodal and Ordered Alloys," *Ultramicroscopy* **30**, 157–71 (1989).

J. BENTLEY
"X-Ray Detectors," pp. 235–6 in *Electron Beam Induced Spectroscopies with High Spatial Resolution,* proceedings of the NSF/CNRS Workshop, held at Aussois, France, February 28–March 5, 1988, ed. C. Colliex and M. Isaacson, 1988.

J. BENTLEY
"X-Ray Detectors," *Ultramicroscopy* **28**, 211–2 (1989).

J. BENTLEY, A. T. FISHER, C. P. HALTOM, J. BRYNESTAD, R. J. LAUF, R. K. WILLIAMS, AND D. M. KROEGER
"Electron Microscopy of High-Temperature Oxide Superconductors," pp. 52–53 in *Proceedings of the 45th Annual Meeting of the Electron Microscopy Society of America, Baltimore, Maryland, August 2–7, 1987,* ed. G. W. Bailey, San Francisco Press, Inc., 1987.

J. BENTLEY AND M. K. MILLER
"Phase Transformations in Aged CF 8 and CF 8M Stainless Steels," pp. 73–75 in *Analytical Electron Microscopy - 1987,* proceedings of symposium held at Kona, Hawaii, July 13–17, 1987, ed. D. C. Joy, San Francisco Press, Inc., 1987.

T. M. BESMANN, R. E. CLAUSING, R. L. HEESTAND, M. L. SANTELLA, AND C. TSAI,
Plasma Processing of Materials, ORNL/TM-10607, April 1988.

R. BLACK, R. CAROLAN, C. Y. LI, V. K. SIKKA, AND C. T. LIU
"Load Relaxation Studies of Grain Boundary Effects in Two Ni_3Al Alloys at Elevated Temperatures," *Scr. Metall.* **21**, 1675–80 (1987).

A. BLEIER AND C. G. WESTMORELAND
"Chemical and Physical Principles of Processing that Affect Microstructure of Al_2O_3-ZrO_2 Composites," pp. 145–54 in *Mater. Res. Soc. Symp. Proc., Vol. 21,* symposium held at Reno, Nevada, April 5–9, 1988, Materials Research Society, Pittsburgh, 1988.

A. BLEIER AND C. G. WESTMORELAND
"Effects of Adsorption of Polyacrylic Acid on the Stability of α-Al_2O_3, m-ZrO_2 and Their Binary Suspensions Systems," pp. 217–36 in *Interfacial Phenomena in Biotechnology and Materials Processing,* proceedings of the symposium held at Boston, Massachusetts, August 3–7, 1987, ed. Y. A. Attia, B. M. Moudgil, and S. Chander, Elsevier Science Publishers, Amsterdam, 1988.

H. G. BOHN, J. M. WILLIAMS, J. H. BARRETT, AND C. T. LIU
"Lattice Location of Boron and Hafnium Dopants in an Ordered Nickel Aluminide by Use of Ion Channeling/Nuclear Reaction Analyses," pp. 127–33 in *High-Temperature Ordered Intermetallic Alloys II,* proceedings of symposium held at Boston, Massachusetts, December 1–6, 1986, ed. N. S. Stoloff, C. C. Koch, C. T. Liu, and O. Izumi, Materials Research Society, Pittsburgh, 1987.

A. S. BOMMANNAVAR, C. J. SPARKS, A. HABENSCHUSS, G. E. ICE, A. DHERE, H. MORKOC, AND H. ZABEL
"X-Ray Diffraction Study of Thin GaAs Film on Si(100)," pp. 223–7 in *Materials Research Society Symposium Proceedings, Boston, Massachusetts, November 30–December 5, 1987, Vol. 102,* Materials Research Society, Pittsburgh, 1988.

M. G. BURKE, L. J. CUDDY, J. PILLER, AND M. K. MILLER
"Combined APFIM-TEM Study of Nb(CN) Precipitation in HSLA Steel," *Mater. Sci. Technol.* **4**, 113–6 (February 1988).

M. G. BURKE AND M. K. MILLER
"A Combined TEM/APFIM Approach to the Study of Phase Transformations: Phase Identification in the Fe-Be System," pp. 780–1 in *Proceedings of the 46th Annual Meeting of the Electron Microscopy Society of America, Milwaukee, Wisconsin, August 7–12, 1988,* ed. G. W. Bailey, San Francisco Press, Inc., 1988.

M. G. BURKE AND M. K. MILLER
"Comparison of TEM and APFIM in Microstructural Characterization and Interpretation: An Overview," *J. Electron Microsc. Technique* **8**, 201–10 (1988).

M. G. BURKE AND M. K. MILLER
"Solute Clustering and Precipitation in Pressure Vessel Steels Under Low Fluence Irradiation Conditions," *J. de Phys.* **49**, C6–283–8 (November 1988).

B. C. CAI, Y. T. CHOU, AND A. DASGUPTA
"Flux Pinning by a Special Grain Boundary in a Niobium Bicrystal," *Philos. Mag. B* 55(1), 67–73 (1987).

B. C. CAI, Y. T. CHOU, AND A. DASGUPTA
"Flux Pinning by Symmetrical Grain Boundaries in Niobium Bicrystals," *Philos. Mag. B* 55(1), 55–66 (1987).

P. P. CAMUS
"Atom Probe Analysis of Solute Clustering Above a Miscibility Gap," *J. de Phys.* **48**, C6–331–6 (November 1987).

P. P. CAMUS, I. BAKER, J. A. HORTON, AND M. K. MILLER
"Grain Boundary Chemistry of NiAl," *J. de Phys.* **49**(11), C6–329–33 (November 1988).

W. D. CARTER, P. H. HOLLOWAY, C. WHITE, AND R. CLAUSING
"Boron Distribution in Sintered Silicon Carbide," *Adv. Ceram. Mater.* 3(1), 62–65 (1988).

J. CESARANO III, I. A. AKSAY, and A. BLEIER
"Stability of Aqueous α-Al_2O_3 Suspensions with Poly(methacrylic acid) Polyelectrolyte," *J. Am. Ceram. Soc.* 71(4), 250–5 (April 1988).

A. CHOUDHURY
The Intergranular Segregation of Boron in Substoichiometric Ni_3Al, ORNL/TM-10508, December 1987.

S. J. COLLOCOTT, G. K. WHITE, S. X. DOU, AND R. K. WILLIAMS
"Thermal Properties of the High-T_c Superconductors $La_{1.85}Sr_{0.15}CuO_4$ and $YBa_2Cu_3O_7$," *Phys. Rev. B* 36(10), 5684–5 (1987).

S. A. DAVID
BES Welding Science Contractors Summary Report 1987–88, September 1988.

S. A. DAVID, J. F. KING, AND J. M. VITEK
"Microstructural Characterization and Properties of 3Cr-1.5Mo-0.1V Thick Section Electron Beam Welds," pp. 61–66 in *Power Beam Processing, Electron, Laser, Plasma-Arc,* proceedings of the International Power Beam Conference held at San Diego, California, May 2–4, 1988, ed. E. A. Metzbower and D. Hauser, American Society for Metals, Metals Park, Ohio, 1988.

S. A. DAVID, M. L. SANTELLA, AND G. M. GOODWIN
"Welding and Weldability of Ductile Intermetallic Alloys," pp. 1–13 in *The Influence of New Materials Development on Weldability,* proceedings of 1987 Annual North America Welding Research Seminar, held at Columbus, Ohio, September 29–30, 1987, Edison Welding Institute and The Welding Institute, Columbus, Ohio, 1987.

S. A. DAVID AND J. M. VITEK, EDS.
BES Welding Science Newsletter (No. 2), Materials Joining Group, Oak Ridge National Laboratory, Oak Ridge, Tennessee, November 1987.

S. A. DAVID AND J. M. VITEK, EDS.
BES Welding Science Newsletter (No. 3), Materials Joining Group, Oak Ridge National Laboratory, Oak Ridge, Tennessee, November 1988.

S. A. DAVID, J. M. VITEK, AND T. L. HEBBLE
"Effect of Rapid Solidification on Stainless Steel Weld Metal Microstructures and Its Implications on the Schaeffler Diagram," *Weld J.* **66**(10), 289s–300s (October 1987).

S. A. DAVID, J. M. VITEK, J. R. KEISER, AND W. C. OLIVER
"Nanoindentation Microhardness Study of Low-Temperature Ferrite Decomposition in Austenitic Stainless Steel Weld," *Weld. J.* **66**(8), 235s–40s (August 1987).

S. A. DAVID, J. M. VITEK, J. R. KEISER, AND W. C. OLIVER
"Use of a Mechanical Properties Microprobe in the Study of Weld Transformations," *Metall. Trans. A* **18A**, 1996–9 (November 1987).

S. A. DAVID, J. M. VITEK, R. W. REED, AND T. L. HEBBLE
Effect of Rapid Solidification on Stainless Steel Weld Metal Microstructures and Its Implications on the Schaeffler Diagram, ORNL/TM-10487, September 1987.

E. M. DELISO AND A. BLEIER
"Colloidal Stability of Oxidized Silicon Particles in Ethanolic and Aqueous Media," pp. 171–86 in *Interfacial Phenomena in Biotechnology and Materials Processing,* proceedings of symposium held at Boston, Massachusetts, August 3–7, 1987, ed. Y. A. Attia, B. M. Moudgil, and S. Chander, Elsevier Science Publishers, Amsterdam, The Netherlands, 1988.

K. FARRELL AND E. H. LEE
"Ion Damage in a Fe-10Cr-6Mo-0.5Nb Ferritic Steel," pp. 498–507 in *Radiation-Induced Changes in Microstructure: 13th International Symposium (Part I), ASTM STP 955,* proceedings of ASTM Symposium on the Effects of Radiation on Materials, held at Seattle, Washington, June 23–25, 1986, ed. F. A. Garner, N. H. Packan, and A. D. Kumar, American Society for Testing and Materials, Philadelphia, 1987.

C. L. FU AND M. H. YOO
"All-Electron Total-Energy Theory of Crystal Elasticity - Li_2 Ordered Alloys," *Philos. Mag. Lett.* **58**, 199–204 (1988).

F. A. GARNER, N. H. PACKAN, AND A. S. KUMAR, EDS.
913 pp., *Radiation-Induced Changes in Microstructure, 13th International Symposium, Part 1, ASTM STP 955*, symposium held at Seattle, Washington, June 23–25, 1986, American Society for Testing and Materials, Philadelphia, December 1987.

E. P. GEORGE AND D. P. POPE
"Impurity-Induced Changes in Interfacial Strength and Their Role in Creep Fracture," pp. 391–7 in *Interfacial Structure, Properties and Design,* proceedings of symposium held at Reno, Nevada, April 5–8, 1988, Materials Research Society, Pittsburgh, 1988.

E. P. GEORGE, W. D. PORTER, H. M. HENSON, W. C. OLIVER, AND B. F. OLIVER
"Cleavage Fracture in an Al_3Ti-Based Alloy Having the LI_2 Structure," *J. Mater. Res.* **4**(1), 78–84 (Jan./Feb. 1989).

A. GONIS, X.-G. ZHANG, A. J. FREEMAN, P. TURCHI, G. M. STOCKS, AND D. M. NICHOLSON
"Configurational Energies and Effective Cluster Interactions in Substitutionally Disordered Binary Alloys," *Phys. Rev. B* **36**(9), 4630–46 (September 1987).

A. GONIS, X.-G. ZHANG, AND D. M. NICHOLSON
"Electronic-Structure Method for General Space-Filling Cell Potentials," *Phys. Rev. B* **38**(5), 3564–7 (August 15, 1988).

G. Y. GUO, W. M. TEMMERMAN, AND G. M. STOCKS
"On the Metal-Semiconductor Transition and Antiferromagnetism in La_2CuO_4," *J. Phys. C: Solid State Phys.* **21**, L103–8 (1988).

A. HABENSCHUSS, G. E. ICE, C. J. SPARKS, AND R. A. NEISER
"The ORNL Beamline at the National Synchrotron Light Source," *Nucl. Instrum. Methods Phys. Res.* **A266**, 215–9 (1988).

M. G. HETHERINGTON AND M. K. MILLER
"On the Statistical Analysis of Atom Probe Data," *J. de Phys.* **48**, C6–559–64 (November 1987).

M. G. HETHERINGTON AND M. K. MILLER
"Statistical Analysis of the Early Stages of Phase Decomposition by Atom Probe," *J. de Phys.* **49**, C6–427–32 (November 1988).

A. W. HEWAT, E. A. HEWAT, J. BRYNESTAD, H. MOOK, AND E. D. SPECHT
"Structure and Superstructure of the Superconductor $Tl_2Ca_1Ba_2Cu_2O_8$ by Neutron and Electron Diffraction," *Physica C* **152**, 438–44 (1988).

S. C. HONG, A. J. FREEMAN, AND C. L. FU
"Structural, Electronic, and Magnetic Properties of Clean and Ag-Covered Fe Monolayers on W(110)," *Phys. Rev. B* **38**, 2156–63 (1988).

L. L. HORTON AND J. BENTLEY
"Dislocation Evolution in Fe-10% Cr," pp. 466–77 in *Radiation-Induced Changes in Microstructure: 13th International Symposium, (Part I), ASTM STP 955,* proceedings of symposium held at Seattle, Washington, June 23–26, 1986, ed. F. A. Garner, N. H. Packan, and A. S. Kumar, American Society for Testing and Materials, Philadelphia, 1987.

C. H. HSUEH
"Analytical Evaluation of Interfacial Shear Strength for Fiber-Reinforced Ceramic Composites," *J. Am. Ceram. Soc.* **71**(6), 490–3 (1988).

C. H. HSUEH
"Comment on Sintering with Rigid Inclusions," *J. Am. Ceram. Soc.* **71**(6), C314–5 (June 1988).

C. H. HSUEH
"Effects of Aspect Ratios of Ellipsoidal Inclusions on Elastic Stress Transfer of Ceramic Composites," *J. Am. Ceram. Soc.* **72**(2), 344–7 (1989).

C. H. HSUEH
"Elastic Load Transfer from Partially Embedded Axially Loaded Fibre to Matrix," *J. Mater. Sci. Lett.* **7**(5), 497–500 (1988).

C. H. HSUEH
"Some Considerations of Evaluation of Interfacial Frictional Stress from the Indentation Technique for Fibre-Reinforced Ceramic Composites," *J. Mater. Sci. Lett.* **8**, 739–42 (1989).

C. H. HSUEH AND P. F. BECHER
"Evaluation of Bridging Stress from R-Curve Behavior for Nontransforming Ceramics," *J. Am. Ceram. Soc.* **71**(5), C234–7 (May 1988).

C. H. HSUEH AND P. F. BECHER
"Some Considerations of Nonideal Transformation-Zone Profile," *J. Am. Ceram. Soc.* **71**(6), 494–7 (1988).

C. H. HSUEH AND P. F. BECHER
"Thermal Expansion Coefficients of Unidirectional Fiber-Reinforced Ceramics," *J. Am. Ceram. Soc.* **71**(10), C438–41 (1988).

C. H. HSUEH, P. F. BECHER, AND P. ANGELINI
"Effects of Interfacial Films on Residual Thermal Stresses in Whisker Reinforced Ceramics," *J. Am. Ceram. Soc.* **71**(11), 929–33 (1988).

B. HWANG, C. R. HOUSKA, G. E. ICE, AND A. HABENSCHUSS
"Residual Strain Gradients in a Fully Stabilized Zirconia Sample," *J. Appl. Phys.* **63**(11), 5351–6 (June 1988).

B. HWANG, C. R. HOUSKA, G. E. ICE, AND A. HABENSCHUSS
"X-Ray Analysis of the Near-Surface Phase Distribution Applied to Wear on a PSZ Disk," *Adv. Ceram. Mater.* **3**(2), 180–3 (March 1988).

G. E. ICE AND C. J. SPARKS
"A Simple Cantilevered Mirror for Focusing Synchrotron Radiation," *Nucl. Instrum. Methods Phys. Res.* **A266**, 394–8 (1988).

D. D. JOHNSON, F. J. PINSKI, AND G. M. STOCKS
"Effects of Chemical and Magnetic Disorder in $Fe_{.50}Mn_{.50}$," *J. Appl. Phys.* **63**(8), 3490–2 (April 15, 1988).

E. A. KENIK, M. J. GODBOLE, D. H. LOWNDES, A. J. PEDRAZA, AND D. F. PEDRAZA
"Structure of Rapidly Solidified NiTi," pp. 76–78 in *Analytical Electron Microscopy - 1987,* proceedings of symposium held at Kona, Hawaii, July 13–17, 1987, ed. D. C. Joy, San Francisco Press, Inc., 1987.

E. A. KENIK AND K. L. MORE
"SHaRE: Collaborative Materials Science Research," pp. 804–5 in *Proceedings of the 46th Annual Meeting of the Electron Microscopy Society of America, Milwaukee, Wisconsin, August 7–12, 1988,* ed. G. W. Bailey, San Francisco Press, Inc., 1988.

E. A. KENIK AND M. NASTASI
"Disordering and Phase Decomposition of a Nickel-Aluminum Intermetallic Under Low Temperature Electron Irradiation," pp. 774–5 in *Proceedings of the 46th Annual Meeting of the Electron Microscopy Society of America, Milwaukee, Wisconsin, August 7–12, 1988,* ed. G. W. Bailey, San Francisco Press, Inc., 1988.

E. A. KENIK AND M. NASTASI
"Phase Stability of Ni_2Al_3 Under Electron Irradiation," pp. 333–8 in *Processing and Characterization of Materials Using Ion Beams,* proceedings of the Materials Research Society Symposium, held at Boston, Massachusetts, November 28–December 2, 1988, Materials Research Society, Pittsburgh, 1989.

E. A. KENIK, T. A. ZAGULA, M. K. MILLER, AND J. BENTLEY
"Ordering in Ni_4Mo by TEM and APFIM," pp. 214–5 in *Proceedings of the 45th Annual Meeting of the Electron Microscopy Society of America, Baltimore, Maryland, August 2–7, 1987,* ed. G. W. Bailey, San Francisco Press, Inc., 1987.

P. A. A. KHAN, T. DEBROY, AND S. A. DAVID
"Laser Beam Welding of High-Manganese Stainless Steels - Examination of Alloying Element Loss and Microstructural Changes," *Weld. J.* **67**(1), 1s–7s (January 1988).

T. KIMOTO, E. H. LEE, AND L. K. MANSUR
"Effects of Helium Injection Mode on Void Formation in Fe-Ni-Cr Alloys," *J. Nucl. Mater.* **158**, 166–78 (1988).

D. M. KROEGER, J. BRYNESTAD, AND R. A. PADGETT
"Changes in Fracture Surface Composition and Morphology with Time in Vacuum in $YBa_2Cu_3O_{7-x}$," *Appl. Phys. Lett.* **52**(15), 1266–7 (April 1988).

D. M. KROEGER, J. BRYNESTAD, R. K. WILLIAMS, R. A. PADGETT, AND J. O. SCARBROUGH
"Effects of Small Deviations from Stoichiometry on Grain Boundary Compositions in $YBa_2Cu_3O_{7-x}$," pp. 521–6 in *Mater. Res. Soc. Symp., Vol. 122,* held at Reno, Nevada, April 5–8, 1988, Materials Research Society, Pittsburgh, 1988.

D. M. KROEGER, A. CHOUDHURY, J. BRYNESTAD, R. K. WILLIAMS, R. A. PADGETT, AND W. A. COGHLAN
"Grain-Boundary Compositions in $YBa_2Cu_3O_{7-x}$ from Auger Electron Spectroscopy of Fracture Surfaces," *J. Appl. Phys.* **64**(1), 331–5 (July 1, 1988).

V. P. KUJANPAA, S. A. DAVID, AND C. L. WHITE
"Characterization of Heat-Affected Zone Cracking in Austenitic Stainless Steel Welds," *Weld. J.* **66**(8), 221s–8s (August 1987).

F. W. KUTZLER AND G. S. PAINTER
"Energies of Atoms with Nonspherical Charge Densities Calculated with Nonlocal Density-Functional Theory," *Phys. Rev. Lett.* **59**(12), 1285–8 (September 21, 1987).

F. W. KUTZLER AND G. S. PAINTER
"Nonlocality in the Density-Functional Description of Bonding in Li_2, N_2, O_2, and F_2," *Phys. Rev. B* **37**(6), 2850–5 (February 15, 1988).

P. LAMPARTER, S. STEEB, D. M. KROEGER, AND S. SPOONER
"Neutron- and X-Ray-Small Angle Scattering with Fe-Base Metallic Glasses," *Mater. Sci. Eng.* **97**, 227–30 (1988).

K. R. LAWLESS, J. V. CATHCART, AND E. A. KENIK
"In Situ Oxidation of Ni_3Al Alloys," pp. 542–3 in *Proceedings of the 46th Annual Meeting of the Electron Microscopy Society of America, Milwaukee, Wisconsin, August 7–12, 1988,* ed. G. W. Bailey, San Francisco Press, Inc., 1988.

E. H. LEE AND E. A. KENIK
"Nucleation and Amorphization of Radiation-Produced Phases in a Modified Austenitic Stainless Steel During Ni-Ion Irradiation," *J. Mater. Res.* **3**(5), 840–4 (September/October 1988).

M. B. LEWIS
"Diffusion of Ion Implanted Helium in Vanadium and Niobium," *J. Nucl. Mater.* **152**, 114–22 (1988).

M. B. LEWIS AND W. R. ALLEN
"Range Distributions of 200 keV Helium in Selected Metals and Ceramics," *Nucl. Instrum. Methods Phys. Res. B* **35**, 10–16 (1988).

M. B. LEWIS, W. R. ALLEN, R. A. BUHL, N. H. PACKAN, S. W. COOK, AND L. K. MANSUR
Triple Ion Beam Irradiation, ORNL/TM-10867, December 1988.

C. LI, A. J. FREEMAN, AND C.-L. FU
"Electronic Structure and Surface Magnetism of fcc Co(001)," *J. Magn. Magn. Mater.* **75**, 53–60 (1988).

C. LI, A. J. FREEMAN, AND C.-L. FU
"Monolayer Magnetism: Electronic and Magnetic Properties of Fe/Au(001)," *J. Magn. Magn. Mater.* **75**, 201–8 (1988).

P. L. LI, E. P. GEORGE, AND D. P. POPE
"The Effects of Austenitization Temperature on the High Temperature Ductility of Fe-P-S Alloys," *Metall. Trans. A* **19A**, 887–92 (April 1988).

Y. T. LIN, P. ANGELINI, AND M. L. MECARTNEY
"Analytical TEM Study of a Yttria Stabilized Zirconia/Glass Composite," pp. 572–73 in *Proceedings of the 46th Annual Meeting of the Electron Microscopy Society of America, Milwaukee, Wisconsin, August 7–12, 1988,* ed. G. W. Bailey, San Francisco Press, Inc., 1988.

C. T. LIU
"Grain-Boundary Design of Ll_2 Ordered Intermetallic Alloys," pp. 429–41 in *Mater. Res. Soc. Symp. Proc., Vol. 122,* symposium held at Reno, Nevada, April 5–8, 1988, Materials Research Society, Pittsburgh, 1988.

C. T. LIU

"Phase Stability and Alloy Design of Ordered Intermetallics," pp. 7–21 in *Alloy Phase Stability,* proceedings of symposium held at Chania, Crete, Greece, June 14, 1987, ed. G. M. Stocks and A. Gonis, Kluwer Academic Publishers, Dordrecht, The Netherlands, 1989.

C. T. LIU AND B. F. OLIVER

"Effect of Grain Shape on Environmental Embrittlement in Ni_3Al Tested at Elevated Temperatures," *J. Mater. Res.* **4**(2), 294–9 (March/April 1989).

L. K. MANSUR AND E. H. LEE

"Ion Beam Stimulated Reactions in Metallic Alloys," pp. 490–1 in *Proceedings of the 46th Annual Meeting of the Electron Microscopy Society of America, Milwaukee, Wisconsin, August 7–12, 1988,* ed. G. W. Bailey, San Francisco Press, Inc., 1988.

G. MAREST, C. J. MCHARGUE, AND A. PEREZ

"Caracterisation de Alpha-Al_2O_3 Apres Implantation Ionique," pp. 119-25 in *Le Vide, les Couches Minces,* proceedings of Surfaces, Materials, and Technology Meeting, held at Lyon, France, October 10–14, 1988, October 1988.

J. E. MARION, C. H. HSUEH, AND A. G. EVANS

"Liquid-Phase Sintering of Ceramics," *J. Am. Ceram. Soc.* **70**(10), 708–13 (1987).

D. B. MARSHALL AND W. C. OLIVER

"Measurement of Interfacial Mechanical Properties in Fiber-Reinforced Ceramic Composites," *J. Am. Ceram. Soc.* **70**(8), 542–8 (August 1987).

P. J. MAZIASZ, N. H. PACKAN, D. F. PEDRAZA, AND E. H. LEE

"A TEM Study of Amorphization in NiTi Irradiated with Ni^{2+} Ions at Room Temperature," pp. 220–1 in *Proceedings of the 45th Annual Meeting of the Electron Microscopy Society of America, Baltimore, Maryland, August 2–7, 1987,* ed. G. W. Bailey, San Francisco Press, Inc., 1987.

C. J. MCHARGUE

"The Mechanical Properties of Ion Implanted Ceramics - A Review," *Defect and Diffusion Forum* **57/58**, 359–80 (1988).

C. J. MCHARGUE

"Use of Mossbauer Spectroscopy to Study Implanted Surfaces," pp. 171–6 in *Ion Implantation and Plasma Assisted Processes, Atlanta, Georgia, May 22–25, 1988,* ed. R. F. Hochman, H. Solnick-Legg, and K. O. Legg, American Society for Metals, Metals Park, Ohio, 1988.

C. J. MCHARGUE, P. S. SKLAD, C. W. WHITE, G. C. FARLOW, A. PEREZ, N. KORNILIOS, AND G. MAREST

"The Charge State of Iron Implanted into Sapphire," pp. 245–54 in *Materials Modification by High-fluence Ion Beams,* proceedings of symposium held at Viana Do Castelo, Portugal, August 24–September 4, 1987, ed. R. Kelly and M. Fernanda da Silva, Kluwer Academic Publishers, Dordrecht, The Netherlands, 1989.

C. J. MCHARGUE, P. S. SKLAD, C. W. WHITE, G. C. FARLOW, A. PEREZ, N. KORNILIOS, AND G. MAREST

"The Charge State of Iron Ions Implanted Into Sapphire," pp. 119–24 in *Proceedings of the Materials Research Society Symposium A, Boston, Massachusetts, November 30–December 5, 1987, Vol. 100,* Materials Research Society, Pittsburgh, 1988.

C. G. MCKAMEY, D. M. KROEGER, D. S. EASTON, AND J. A. HORTON

"Crystallization of Zr-Ni Metallic Glasses," pp. 456–7 in *Proceedings of the 46th Annual Meeting of the Electron Microscopy Society of America, Milwaukee, Wisconsin, August 7–12, 1988,* ed. G. W. Bailey, San Francisco Press, Inc., 1988.

M. L. MECARTNEY AND P. ANGELINI

"Analytical TEM of Grain Boundary Phases in Yttria-Zirconia Ceramics," pp. 166–7 in *Proceedings of the 45th Annual Meeting of the Electron Microscopy Society of America, Baltimore, Maryland, August 3–7, 1987,* ed. G. W. Bailey, San Francisco Press, Inc., 1987.

D. E. MELTZER, F. J. PINSKI, AND G. M. STOCKS

"Rare Gas Impurities in Alkali Metals-Relation to Optical Absorption," *Phys. Rev. B* **37**(11), 6011–8 (1988).

M. K. MILLER

"Analysis at the Atomic Level: The Atom Probe Field-Ion Microscope," pp. 374–6 in *J. Research of National Bureau of Standards, Vol. 93,* proceedings of symposium on Accuracy in Trace Analysis, held at Gaithersburg, Maryland, September 28, 1987, May-June 1988.

M. K. MILLER

"Determination of the Site Occupation Probability and the Degree of Order by APFIM," *J. Microsc.* **147**, 159–67 (August 1987).

M. K. MILLER

"The Effects of Local Magnification and Trajectory Aberrations on Atom Probe Analysis," *J. de Phys.* **48**, C6–565–70 (November 1987).

M. K. MILLER

"Morphology of Low Temperature Phase Transformations in the Iron-Chromium System," pp. 39–43 in *Phase Transformations '87*, symposium held at Cambridge, England, July 6–10, 1987, ed. G. D. Lorimer, Institute of Metals, England, 1988.

M. K. MILLER

"Ultrahigh-Resolution Chemical Analysis with the Atom Probe," *Int. Mater. Rev.* **32**(5), 221–40 (1987).

M. K. MILLER AND J. BENTLEY

"Characterization of Fine-Scale Microstructures in Aged Primary Coolant Pipe Steels," pp. 341–9 in *Environmental Degradation of Materials in Nuclear Power Systems - Water Reactors*, symposium held at Traverse City, Michigan, August 30–September 3, 1987, ed. G. J. Theus and J. R. Weeks, The Metallurgical Society, New York, 1988.

M. K. MILLER AND M. G. BURKE

"Characterization of Irradiated A533B Pressure Vessel Steel Weld," *J. de Phys.* **48**, C6–429–34 (November 1987).

M. K. MILLER AND M. G. BURKE

"Characterization of Low-Temperature Phase Transformations in the Iron-Beryllium System," pp. 199–202 in *Phase Transformations '87*, symposium held at Cambridge, England, July 6–10, 1987, ed. G. D. Lorimer, Institute of Metals, England, 1988.

M. K. MILLER AND M. G. BURKE

"Identification of an Ordered Hexagonal BeFe Phase," *J. de Phys.* **49**, C6–373–8 (November 1988).

M. K. MILLER AND M. G. BURKE

"Microstructural Characterization of Irradiated PWR Steels Using the Atom Probe Field-Ion Microscope," pp. 141–9 in *Environmental Degradation of Materials in Nuclear Power Systems - Water Reactors*, symposium held at Traverse City, Michigan, August 30–September 3, 1987, ed. G. J. Theus and J. R. Weeks, The Metallurgical Society, New York, 1988.

M. K. MILLER, D. T. HOELZER, F. EBRAHIMI, J. R. HAWTHORNE, AND M. G. BURKE

"Characterization of Irradiated Model Pressure Vessel Steels," *J. de Phys.* **48**, C6–423–8 (November 1987).

M. K. MILLER, D. T. HOELZER, F. EBRAHIMI, J. R. HAWTHORNE, AND M. G. BURKE

"Microstructural Characterization of Irradiated Fe-Cu-Ni-P Model Steels," pp. 133–9 in *Environmental Degradation of Materials in Nuclear Power Systems - Water Reactors*, symposium held at Traverse City, Michigan, August 30–September 3, 1987, ed. G. J. Theus and J. R. Weeks, The Metallurgical Society, New York, 1988.

M. K. MILLER AND J. A. HORTON

"Direct Observation of Boron Segregation to Line and Planar Defects in Ni_3Al," *J. de Phys.* **48**, C6–379–84 (November 1987).

M. K. MILLER, E. A. KENIK, AND T. A. ZAGULA
"Ordering in Ni_4Mo: An APFIM/TEM/HVEM Study," *J. de Phys.* **48**, C6–385–90 (November 1987).

M. K. MILLER, A. J. MELMED, AND K. L. MORE
"An APFIM/FEM Investigation of Planar Defects in High Temperature Superconductors," *J. de Phys.* **49**, C6–447–52 (November 1988).

M. K. MILLER AND A. R. MCDONALD
Atom Probe Field-Ion Microscopy and Related Topics: A Bibliography 1978–87, ORNL/TM-11157, April 1989.

M. K. MILLER AND K. L. MORE
"FIM Simulation of $RBa_2Cu_3O_{7-x}$ Superconductors," *J. de Phys.* **49**, C6–483–8 (November 1988).

M. K. MILLER AND K. F. RUSSELL
"An Atom Probe Study of Phase Decomposition in the Cape York Meteorite," *J. de Phys.* **49**, C6–397–402 (November 1988).

M. K. MILLER AND K. F. RUSSELL
"The Effects of Image Gas on Atom Probe Analysis," *J. de Phys.* **49**, C6–81–86 (November 1988).

K. L. MORE, J. BENTLEY, C. H. CARTER, JR., AND R. F. DAVIS
"Analytical Electron Microscopy Characterization of Boron in Sintered α-SiC," pp. 299–302 in *Analytical Electron Microscopy - 1987,* proceedings of symposium held at Kona, Hawaii, July 13–17, 1987, ed. D. C. Joy, San Francisco Press, Inc., 1987.

K. L. MORE, J. BENTLEY, AND R. F. DAVIS
"Antiphase Boundaries in Beta-SiC Thin Films," pp. 283–4 in *Proceedings of the 45th Annual Meeting of the Electron Microscopy Society of America, Baltimore, Maryland, August 2–7, 1987,* ed. G. W. Bailey, San Francisco Press, Inc., 1987.

K. L. MORE AND M. K. MILLER
"Microstructural Characterization of Udimet 720: A Nickel-Base Alloy," *J. de Phys.* **49**, C6–391–6 (November 1988).

N. NAITO AND C. H. HSUEH
"Residual Stress and Strain in Pyrolytic Boron Nitride Resulting from Thermal Anisotropy," *J. Mater. Sci.* **23**(6), 1901–5 (1988).

M. NASTASI, J.-P. HIRVONEN, T. R. JERVIS, G. M. PHARR, AND W. C. OLIVER
"Surface Mechanical Properties of Carbon Implanted Nickel," *J. Mater. Res.* **3**, 226–32 (March/April 1988).

T. G. NIEH, A. R. PELTON, W. C. OLIVER, AND J. WADSWORTH
"Characterization of the Aging Response of a Melt-Spun Al-Be-Li Alloy Ribbon," *Met. Trans. A* **19A**, 1173–8 (May 1988).

W. C. OLIVER, F. A. LIST, AND R. A. MCKEE
"The Influence of Thickness and Wavelength on the Mechanical Properties of a Compositionally Modulated Ceramic Thin Film," pp. 99–104 in *Mater. Res. Soc. Symp., Vol. 130,* proceedings of symposium held at Boston, Massachusetts, November 28–December 2, 1988, Materials Research Society, Pittsburgh, 1989.

W. C. OLIVER AND C. J. MCHARGUE
"Characterizing the Hardness and Modulus of Thin Films Using a Mechanical Properties Microprobe," *Thin Solid Films* **161**, 117–22 (1988).

W. C. OLIVER AND C. J. MCHARGUE
"Thin Films and Near-Surface Characterization Using a Mechanical Properties Microprobe," pp. 157–61 in *Ion Implantation and Plasma Assisted Processes, Atlanta, Georgia, May 22–25, 1988,* ed. R. F. Hochman, H. Solnick-Legg, K. O. Legg, American Society for Metals, Metals Park, Ohio, 1988.

W. C. OLIVER, J. WADSWORTH, AND T. G. NIEH
"Characterization of Rapidly Solidified Al-Be-Li and Al-Be Ribbons," *Scr. Metall.* **21**, 1429–33 (1987).

W. C. OLIVER AND C. L. WHITE
"The Segregation of Boron and Its Effect on the Fracture of an Ni_3Si Based Alloy," pp. 241–6 in *Mater. Res. Soc. Symp., Vol. 81,* proceedings of symposium held at Boston, Massachusetts, December 1–6, 1986, Materials Research Society, Pittsburgh, 1987.

N. H. PACKAN, L. HEATHERLY, W. KESTERNICH, AND H. SCHROEDER
"Radiation-Induced Segregation in Light-Ion Bombarded Ni-8% Si," pp. 617–27 in *Radiation-Induced Changes in Microstructure: 13th International Symposium (Part I), ASTM STP 955,* proceedings of ASTM Symposium on the Effects of Radiation on Materials, held at Seattle, Washington, June 23–25, 1986, ed. F. A. Garner, N. H. Packan, and A. D. Kumar, American Society for Testing and Materials, Philadelphia, 1987.

G. S. PAINTER AND F. W. AVERILL
"Impurity Effects on Metallic Cohesion: Lithium-Row Atoms in Nickel Clusters," *Phys. Rev. B* **39**(11), 7522–35 (April 15, 1989).

G. S. PAINTER AND F. W. AVERILL
"Reply to Comment on the Effects of Segregation on Grain Boundary Cohesion: A Density Functional Cluster Model of Boron and Sulfur in Nickel," *Phys. Rev. Lett.* **60**(19), 1982 (May 9, 1988).

R. H. PARRISH, J. J. WERT, W. C. OLIVER, AND P. S. SKLAD
"The Effect of Varying Sputtering Parameters on the Microstructure and Mechanical Properties of 10%Ni+TiB_2 Thin Films," pp. 18-1–7 in *Proceedings of the 7th International Conference on Erosion by Liquid and Solid Impact, Cambridge, United Kingdom, September 7, 1987*, 1987.

J. E. PAWEL AND C. J. MCHARGUE
"Testing of the Adhesion of Thin Films to Substrates," *J. Adhes. Sci. Technol.* **2**, 369–83 (1988).

J. E. PAWEL AND C. J. MCHARGUE
"Use of the Scratch Test to Measure Changes in Adhesion of Cr/Al_2O_3 Due to Ion Beam Mixing," *J. Adhes. Sci. Technol.* **2**, 385–93 (1988).

A. J. PEDRAZA, M. J. GODBOLE, E. A. KENIK, D. H. LOWNDES, AND J. R. THOMPSON, JR.
"Laser Enhanced Adhesion of Copper Films to Sapphire Substrates," *J. Vac. Sci. Technol. A* **6**(3), 1763–7 (May/June 1988).

D. F. PEDRAZA
"Effect of Simultaneous Heavy-Ion and Electron Bombardment on the Amorphization Kinetics of Intermetallics," *Phys. Rev. B* **38**(7), 4803–9 (September 1, 1988).

D. F. PEDRAZA
"Radiation-Induced Collapse of the Crystalline Structure," *J. Less-Common Met.* **140**, 219–30 (1988).

D. F. PEDRAZA AND P. J. MAZIASZ
"Void-Precipitate Association During Neutron Irradiation of Austenitic Stainless Steel," pp. 161–94 in *Radiation-Induced Changes in Microstructure: 13th International Symposium (Part I), ASTM STP 955,* proceedings of ASTM Symposium on the Effects of Radiation on Materials, held at Seattle, Washington, June 23–25, 1986, ed. F. A. Garner, N. H. Packan, and A. D. Kumar, American Society for Testing and Materials, Philadelphia, 1987.

J. P. PERDEW, M. LEVY, G. S. PAINTER, S. WEI, AND J. B. LAGOWSKI
"Chemical Bond as a Test of Density-Gradient Expansions for Kinetic and Exchange Energies," *Phys. Rev. B* **37**(2), 838–43 (January 15, 1988).

E. M. PERRY, D. L. COCKE, AND M. K. MILLER
"Atom Probe Investigation of the Oxidation of Ni-Zr Intermetallic Compounds," *J. de Phys.* **49**, C6–385–90 (November 1988).

J. B. PETHICA AND W. C. OLIVER
"Mechanical Properties of Nanometre Volumes of Material: Use of the Elastic Response of Small Area Indentations," pp. 13–23 in *Mater. Res. Soc. Symp., Vol. 130,* proceedings of symposium held at Boston, Massachusetts, November 28–December 2, 1988, Materials Research Society, Pittsburgh, 1989.

F. J. PINSKI
"Chemical Disorder and Magnetism in Alloys," pp. 30–31 in *Projects in Scientific Computing,* Pittsburgh Supercomputing Center, Pittsburgh, 1987.

F. J. PINSKI, D. M. NICHOLSON, G. M. STOCKS, W. H. BUTLER, D. D. JOHNSON, AND B. L. GYORFFY
"The Theory of Random Alloys," pp. 321–30 in *Supercomputing '88: Supercomputing Projects, Applications, and Artificial Intelligence, Vol. 1*, proceedings of the Third International Conference on Supercomputing, held at Boston, Massachusetts, May 15–20, 1988, ed. L. P. Kartashev and S. I. Kartashev, International Supercomputing Institute, Inc., St. Petersburg, Florida, 1988.

D. P. POPE AND C. T. LIU
"Strength and Ductility of Intermetallic Compounds," pp. 583–624 in *Superalloys, Supercomposites and Superceramics,* Academic Press, Inc., New York, 1989.

J. H. SCHNEIBEL, P. F. BECHER, AND J. A. HORTON
"Microstructure and Fracture Toughness of Powder-Processed Al_3Nb," *J. Mater. Res.* **3**(6), 1272–6 (Nov./Dec. 1988).

J. H. SCHNEIBEL AND J. A. HORTON
"Evolution of Dislocation Structure During Inverse Creep of a Nickel Aluminide: Ni-23.5Al-0.5Hf-0.2B (at. %)," *J. Mater. Res.* **3**(4), 651–6 (July/August 1988).

J. H. SCHNEIBEL AND L. MARTINEZ
"Creep Cavitation in a Nickel Aluminide," pp. 203–16 in *Creep and Fracture of Engineering Materials and Structures,* proceedings of the Third International Conference held at University College, Swansea, U.K., April 5–10, 1987, ed. B. Wilshire and R. W. Evans, The Institute of Metals, London, 1987.

J. H. SCHNEIBEL AND L. MARTINEZ
"Stochastic Processes in Creep Cavitation," *Metall. Trans. A* **18A**, 1835–42 (November 1987).

J. H. SCHNEIBEL AND W. D. PORTER
"Coble Creep in a Powder-Metallurgical Nickel Aluminide of Composition Ni-22.8Al-0.6Hf-0.1B (at. %)," *J. Mater. Res.* **3**(3), 403–6 (May/June 1988).

J. H. SCHNEIBEL, W. D. PORTER, AND J. A. HORTON
"Plastic Flow and Microstructure of Cast Nickel Aluminides at 1273 K," *Metall. Trans. A* **18A**, 2157–62 (December 1987).

J. SEVELY, P. ANGELINI, K. HSSEIN, AND G. ZANCHI

"EXELFS Analyses at 300 kV and 1 MV," pp. 106–8 in *Analytical Electron Microscopy - 1987,* proceedings of symposium held at Kona, Hawaii, July 13–17, 1987, ed. D. C. Joy, San Francisco Press, Inc., 1987.

J. E. SHIELD AND R. K. WILLIAMS

"The Study of the Pd-Rh System by Electrical Resistivity Measurements," *Scr. Metall.* **21**, 1475–9 (1987).

V. K. SIKKA

"Near-Net-Shape Casting of Sheet and Bar of Ordered Nickel Aluminide Alloys," pp. 315–33 in *Casting of Near Net Shape Products,* proceedings of symposium held at Honolulu, Hawaii, November 13–17, 1988, ed. Y. Sahai, J. E. Battles, R. S. Carbonara, and C. E. Mobley, The Metallurgical Society, New York, 1988.

V. K. SIKKA

"Superplasticity and Its Application to Near-Net Shaping of Intermetallic Alloys," pp. 451–67 in *Interdisciplinary Issues in Materials Processing and Manufacturing, Vol. 2,* proceedings of the Winter Annual Meeting of the American Society of Mechanical Engineers, Boston, Massachusetts, December 13–18, 1987, ed. S. K. Samanta, R. Komanduri, R. McMeeking, M. M. Chen, and A. Tseng, The American Society of Mechanical Engineers, New York, 1987.

V. K. SIKKA AND E. A. LORIA

"Industrial Scale Processing and Elevated Temperature Properties of Ni_3Al-Cr-Zr-B Alloys," pp. 203–12 in *Superalloys 1988,* proceedings of the Sixth International Symposium on Superalloys, held at Champion, Pennsylvania, September 18–22, 1988, ed. S. Reichman, D. N. Duhl, G. Maurer, S. Antolovich, and C. Lund, The Metallurgical Society, New York, 1988.

P. S. SKLAD

"Analytical Electron Microscopy of Alpha-Al_2O_3 Implanted with Iron," pp. 146–7 in *Proceedings of the 45th Annual Meeting of the Electron Microscopy Society of America, Baltimore, Maryland, August 2–7, 1987,* ed. G. W. Bailey, San Francisco Press, Inc., 1987.

P. S. SKLAD

"The Preparation of TEM Specimens from Hazardous or Difficult Materials," pp. 39–50 in *Specimen Preparation for Transmission Electron Microscopy of Materials,* Vol. 115, proceedings of Materials Research Society Symposium, held at Boston, Massachusetts, November 30–December 4, 1987, ed. J. C. Bravman, M. L. McDonald, and R. Anderson, Materials Research Society, Pittsburgh, 1988.

P. S. SKLAD

"The Use of Analytical Electron Microscopy in the Study of Ion Implanted Materials," pp. 149–56 in *Ion Implantation and Plasma Assisted Processes,* proceedings of conference held at Atlanta, Georgia, May 22–25, 1988, ed. R. F. Hochman, H. Solnick-Legg, and K. O. Legg, American Society for Metals, Metals Park, Ohio, 1989.

P. S. SKLAD, P. ANGELINI, C. J. MCHARGUE, AND C. W. WHITE

"An Analytical Electron Microscopy Investigation of Amorphous Structures in Ion-Implanted Al_2O_3," pp. 45–48 in *Analytical Electron Microscopy - 1987,* proceedings of symposium held at Kona, Hawaii, July 13–17, 1987, ed. D. C. Joy, San Francisco Press, Inc., 1987.

P. S. SKLAD, P. ANGELINI, AND J. SEVELY

"The Characterization of Amorphous Al_2O_3 by Extended Energy Loss Fine Structure (EXELFS) Analysis," pp. 468–9 in *Proceedings of the 46th Annual Meeting of the Electron Microscopy Society of America, Milwaukee, Wisconsin, August 7–12, 1988,* ed. G. W. Bailey, San Francisco Press, Inc., 1988.

J. SOULLARD, L. MARTINEZ, AND J. H. SCHNEIBEL

"Effect of Antimony on the Creep Fracture of Stainless Steel," *Metall. Trans. A* **19A**, 571–7 (March 1988).

C. J. SPARKS AND G. E. ICE

"X-Ray Microprobe for the Microcharacterization of Materials," pp. 223–33 in *Materials Research Society Symposium Proceedings, Vol. 143,* held at Boston, Massachusetts, November 28–December 2, 1988, Materials Research Society, Pittsburgh, 1989.

E. D. SPECHT, C. J. SPARKS, A. G. DHERE, J. BRYNESTAD, O. B. CAVIN, D. M. KROEGER, AND H. A. OYE

"Effect of Oxygen Pressure on the Orthorhombic-Tetragonal Transition in the High-Temperature Superconductor $YBa_2Cu_3O_x$," *Phys. Rev. B* **37**(13), 7426–34 (May 1, 1988).

S. SPOONER AND M. K. MILLER

"A Comparison of Autocorrelograms Determined from SANS and APFIM Data," *J. de Phys.* **49**, C6–405–10 (November 1988).

P. A. STERNE, C. S. WANG, G. M. STOCKS, AND W. M. TEMMERMAN

"Electronic Structure and Antiferromagnetism in La_2CuO_4," pp. 353–6 in *High-Temperature Superconductors, Vol. 99*, proceedings of symposium held at Boston, Massachusetts, November 30–December 4, 1987, ed. M. B. Brodsky, R. C. Dynes, K. Kitazawa, and H. L. Tuller, Materials Research Society, Pittsburgh, 1988.

J. O. STIEGLER AND C. T. LIU
"Aluminides for Structural Use," pp. 3–9 in *Encyclopedia of Materials Science and Engineering,* Suppl. Vol. 1, ed. R. W. Cahn and M. B. Bever, Pergamon Press, New York, September 1988.

G. M. STOCKS, D. M. NICHOLSON, F. J. PINSKI, D. D. JOHNSON, AND A. GONIS
"Electronic Structure of Random Alloys and the Theory of Ordering Processes," *Mater. Sci. Forum* **37**, 161–72 (1989).

G. M. STOCKS, W. M. TEMMERMAN, Z. SZOTEK, G. Y. GUO, AND P. J. DURHAM
"Ground State Properties and Electronic Structure of High T_c Superconductors," *Physica C* **153/155**, 1215–6 (1988).

G. M. STOCKS, W. M. TEMMERMAN, Z. SZOTEK, AND P. A. STERNE
"Density Functional Theory Total Energies and Equilibrium Volumes of La_2CuO_4 and $La_{1.5}Sr_{0.5}CuO_4$," *Supercond. Sci. Technol.* **1**, 57–63 (1988).

R. E. STOLLER AND G. R. ODETTE
"A Comparison of the Relative Importance of Helium and Vacancy Accumulation in Void Nucleation," pp. 358–70 in *Radiation-Induced Changes in Microstructure: 13th International Symposium (Part I), ASTM STP 955,* proceedings of ASTM Symposium on the Effects of Radiation on Materials, held at Seattle, Washington, June 23–25, 1986, ed. F. A. Garner, N. H. Packan, and A. D. Kumar, American Society for Testing and Materials, Philadelphia, 1987.

R. E. STOLLER AND G. R. ODETTE
"A Composite Model of Microstructural Evolution in Austenitic Stainless Steel Under Fast Neutron Irradiation," pp. 371–92 in *Radiation-Induced Changes in Microstructure: 13th International Symposium (Part I), ASTM STP 955,* proceedings of ASTM Symposium on the Effects of Radiation on Materials, held at Seattle, Washington, June 23–25, 1986, ed. F. A. Garner, N. H. Packan, and A. D. Kumar, American Society for Testing and Materials, Philadelphia, 1987.

R. E. STOLLER AND G. R. ODETTE
"Observations of Stacking Fault Tetrahedra in an Austenitic Alloy After High-Temperature Neutron Irradiation," *Philos. Mag. A* **58**, 523–32 (1988).

N. S. STOLOFF, C. C. KOCH, C. T. LIU, AND O. IZUMI, EDS.
515 pp., *High-Temperature Ordered Intermetallic Alloys II,* proceedings of the Materials Research Society Symposia, held at Boston, Massachusetts, December 2–4, 1986, Vol. 81, Materials Research Society, Pittsburgh, 1987.

J. C. SWIHART AND W. H. BUTLER
"Transport in Metal Alloys and Resistivity Saturation," pp. 285–96 in *Condensed Matter Theories, Vol. 2,* proceedings of the 10th International Workshop on Condensed Matter Theories, held at Argonne National Laboratory, Argonne, Illinois, July 21–28, 1986, ed. P. Vashishta, R. K. Kalia, and R. F. Bishop, Plenum Press, New York, 1987.

Z. SZOTEK, W. M. TEMMERMAN, B. L. GYORFFY, AND G. M. STOCKS
"Do Oxygen Vacancies Trap Positrons in the Superconducting Cuprates: $YBa_2Cu_3O_7$ and $YBa_2Cu_3O_6$?," *J. Phys. C: Solid State Phys.* **21**, L509–14 (1988).

M. TAKEYAMA AND C. T. LIU
"Effect of Grain Size on Yield Strength of Ni_3Al and Other Alloys," *J. Mater. Res.* **3**(4), 665–74 (July/August 1988).

M. TAKEYAMA AND C. T. LIU
"Effects of Grain Size and Test Temperature on Ductility and Fracture Behavior of a B-Doped Ni_3Al Alloy," *Acta Metall.* **36**(5), 1241–9 (1988).

M. TAKEYAMA AND C. T. LIU
"Surface Oxidation and Ductility Loss in Boron-Doped Ni_3Al at 760°C," *Scr. Metall.* **23**, 727–31 (1989).

W. M. TEMMERMAN, P. J. DURHAM, G. M. STOCKS, AND P. A. STERNE
"Electronic Structure of La-Cu and Y-Ba-Cu Oxides: Ground-State Properties and Photoemission Spectra," *J. Phys. F: Met. Phys.* **17**, L135–40 (1987).

W. M. TEMMERMAN, G. Y. GUO, Z. SZOTEK, AND G. M. STOCKS
"Local Spin Density Calculations for the High T_c Superconductors," *Physica Scr.* **T25**, 78–79 (1989).

W. M. TEMMERMAN, Z. SZOTEK, P. J. DURHAM, G. M. STOCKS, AND P. A. STERNE
"Electronic Structure of Y-Ba-Cu Oxides and Fluorides," *J. Phys. F: Met. Phys.* **17**, L319–27 (1987).

J. R. THOMPSON, J. BRYNESTAD, D. M. KROEGER, Y. C. KIM, S. T. SEKULA, D. K. CHRISTEN, AND E. D. SPECHT
"Superconductivity, Intergrain and Intragrain Critical Current Densities of $Tl_2Ca_2Ba_2Cu_3O_{10+\delta}$ and $Tl_2CaBa_2Cu_2O_{8+\delta}$ Materials," *Phys. Rev. B* **39**(10), 6652–9 (April 1, 1989).

J. Z. TISCHLER, J. D. BUDAI, G. E. ICE, AND A. HABENSCHUSS
"Multiple Scattering and the 200 Reflection in Silicon and Germanium," *Acta Cryst.* **A44**, 22–25 (1988).

H. TRINKAUS AND M. H. YOO
"Nucleation Under Time-Dependent Supersaturation," *Philos. Mag. A* **55**(3), 269–89 (1987).

P. E. A. TURCHI, G. M. STOCKS, W. H. BUTLER, D. M. NICHOLSON, AND A. GONIS
"First-Principles Study of Ordering Properties of Substitutional Alloys Using the Generalized Perturbation Method," *Phys. Rev. B* **37**(10), 5982–5 (April 1, 1988).

P. VEYSSIERE, J. A. HORTON, M. H. YOO, AND C. T. LIU
"APB Dragging in Ni_3Al Deformed at Intermediate Temperature," *Philos. Mag. Lett.* **57**(1), 17–23 (1988).

J. M. VITEK
"Diffraction Effects from Interfaces," pp. 38–41 in *Proceedings of the 45th Annual Meeting of the Electron Microscopy Society of America, Baltimore, Maryland, August 2–7, 1987,* ed. G. W. Bailey, San Francisco Press, Inc., 1987.

J. M. VITEK AND S. A. DAVID
"The Aging Behavior of Homogenized Type 308 and 308CRE Stainless Steel," *Metall. Trans. A* **18A**, 1195–201 (July 1987).

J. M. VITEK AND S. A. DAVID
"The Aging Behavior of Types 308 and 308CRE Stainless Steels and Its Effect on Mechanical Properties," pp. 157–71 in *Properties of Stainless Steels in Elevated Temperature Service, MPC-VOL. 26, PVP-VOL. 132,* proceedings of the Winter Annual Meeting of the American Society of Mechanical Engineers, Boston, Massachusetts, December 13–18, 1987, ed. M. Prager, The American Society of Mechanical Engineers, New York, December 1987.

J. M. VITEK AND S. A. DAVID
"The Effect of Cooling Rate on Ferrite in Type 308 Stainless Steel Weld Metal," *Weld. J.* **67**(5), 95s–102s (May 1988).

J. M. VITEK AND S. A. DAVID
"Laser Welding of Stainless Steel Weld Filler Metals at High Cooling Rates," pp. 369–76 in *4th International Colloquium on Welding and Melting by Electron and Laser Beams, Cannes, France, September 26-30, 1988,* ed. M. Contre, M. Kuncevic, C. Charissoux, and A. Blanchard, French Welding Institute, France, 1988.

J. M. VITEK AND S. A. DAVID
"Time-Dependent Composition Behavior of Precipitates in Aged Stainless Steels," pp. 21–24 in *Analytical Electron Microscopy - 1987,* proceedings of symposium held at Kona, Hawaii, July 13–17, 1987, ed. D. C. Joy, San Francisco Press, Inc., 1987.

J. M. VITEK, M. VAUDIN, M. RUHLE, AND S. L. SASS
"Diffraction Effects Along the Normal to a Grain Boundary," *Scr. Metall.* **23**, 349–54 (1989).

C. L. WHITE, S. A. DAVID, AND M. W. RICHEY

"Application of Auger Electron Spectroscopy to the Study of Trace Element Effects on Weldability," pp. 101–14 in *Welding Metallurgy of Structural Steels,* proceedings of an International Symposium on Welding Metallurgy of Structural Steels, sponsored by the TMS Ferrous Metallurgy Committee and the Heat Treatment Committee, and co-sponsored by the Edison Welding Institute, held at the Annual Meeting of the Metallurgical Society, Inc., Denver, Colorado, February 22–26, 1987, ed. J. Y. Koo, The Metallurgical Society, Inc., New York, 1987.

C. L. WHITE, C. T. LIU, AND R. A. PADGETT, JR.

"Free Surface Segregation in Boron Doped Ni_3Al," *Acta Metall.* **36**(8), 2229–38 (1988).

C. W. WHITE, L. A. BOATNER, P. S. SKLAD, C. J. MCHARGUE, J. RANKIN, G. C. FARLOW, AND M. J. AZIZ

"Ion Implantation and Annealing of Crystalline Oxide Ceramic Materials," *Nucl. Instr. Methods Phys. Res. B* **32**, 11–22 (1988).

R. K. WILLIAMS, R. S. GRAVES, F. J. WEAVER, AND D. W. YARBROUGH

"Effect of Point Defects on the Phonon Thermal Conductivity of BCC Iron," *J. Appl. Phys.* **62**(7), 2778–83 (October 1, 1987).

S. P. WITHROW, K. MORE, J. A. EDMOND, H. S. KONG, P. J. MAZIASZ, AND R. F. DAVIS

"Damage Production in β-SiC During Ion Implantation," pp. 373–8 in *Beam-Solid Interactions and Transient Processes, Vol. 74,* proceedings of symposium held at Boston, Massachusetts, December 1–4, 1986, ed. M. O. Thompson, S. T. Picraux, and J. S. Williams, Materials Research Society, Pittsburgh, 1987.

N. F. WRIGHT, G. S. PAINTER, W. R. BUSING, AND W. H. BUTLER

"Ionic Models for $YBa_2Cu_3O_7$," pp. 539–42 in *High-Temperature Superconductors, Vol. 99,* proceedings of symposium held at Boston, Massachusetts, November 30–December 4, 1987, ed. M. B. Brodsky, R. C. Dynes, K. Kitazawa, and H. L. Tuller, Materials Research Society, Pittsburgh, 1988.

M. H. YOO

"Deformation Twinning in Superlattice Structures," *J. Mater. Res.* **4**(1), 50–54 (Jan./Feb. 1989).

M. H. YOO

"Reply to 'On the Stability of Superdislocations'," *Scr. Metall.* **22**, 117 (1988).

M. H. YOO

"Stability of Superdislocations and Shear Faults in LI_2 Ordered Alloys," *Acta Metall.* **35**(7), 1559–69 (1987).

M. H. YOO, W. A. T. CLARK, AND C. L. BRIANT, EDS.
605 pp., *Interfacial Structure, Properties, and Design,* proceedings of Materials Research Society Symposium, held at Reno, Nevada, April 5–8, 1988, Vol. 122, Materials Research Society, Pittsburgh, 1988.

M. H. YOO, J. A. HORTON, AND C. T. LIU
Micromechanisms of Deformation and Fracture in Ordered Intermetallic Alloys - I. Strengthening Mechanisms, ORNL/TM-10709, July 1988.

M. H. YOO, J. A. HORTON, AND C. T. LIU
"Micromechanisms of Yield and Flow in Ordered Intermetallic Alloys," *Acta Metall.* **36**(11), 2935–46 (1988).

M. H. YOO AND A. H. KING
"Slip, Twinning, and Fracture at a Grain Boundary in the $L1_2$ Ordered Structure – $A\Sigma$ = Tilt Boundary," *J. Mater. Res.* **3**(5), 848–55 (September/October 1988).

M. H. YOO AND C. T. LIU
"Effect of Prestress on Tensile Yield Strength of a Ni_3Al Alloy," *J. Mater. Res.* **3**(5), 845–7 (September/October 1988).

C. S. YUST, C. J. MCHARGUE, AND L. A. HARRIS
"The Friction and Wear of Ion Implanted TiB_2," *Mater. Sci. Eng.* **A105/106**, 489–96 (November 1988).

Appendix C

PENDING PUBLICATIONS

Compiled by Jamie Bain

K. B. ALEXANDER, F. J. WALKER, R. A. MCKEE, AND F. A. LIST III
"Multilayer Ceramic Thin Films," submitted to *J. Am. Ceram. Soc.*

P. F. BECHER
"Advanced Ceramics: Whisker Reinforced Ceramic Composites," International Symposium on Technology of Future: Materials Development and Technology Innovation, Kobe, Japan, March 22–25, 1988, to be published in proceedings.

P. F. BECHER, P. ANGELINI, C. H. HSUEH, AND T. N. TIEGS
"Whisker Reinforced Ceramics: Toughening Behavior and Properties," 7th International Symposium on Ceramics, Bologna, Italy, December 14–16, 1988, to be published in proceedings.

P. F. BECHER, M. V. SWAIN, AND G. BEGUN
"Grain Size Dependent Transformation Behavior in Polycrystalline Tetragonal Zirconia Ceramics," submitted to *J. Am. Ceram. Soc.*

P. F. BECHER, T. N. TIEGS, AND P. ANGELINI
"Whisker Toughened Ceramic Composites," submitted to *Fiber Reinforced Ceramics,* ed. K. S. Masdiyasni, Noyes Publication, Inc.

J. BENTLEY, P. ANGELINI, P. S. SKLAD, AND A. T. FISHER
"Radial Distribution Functions from Diffracted Electron Intensities," The 47th Annual Meeting of the Electron Microscopy Society of America, San Antonio, Texas, August 6–11, 1989, to be published in proceedings.

J. BENTLEY AND K. HISTASUNE
"Sublattice Occupancies of Pd in $Cu_{0.5}Au_{0.5-x}Pd_x$," The 47th Annual Meeting of the Electron Microscopy Society of America, San Antonio, Texas, August 6–11, 1989, to be published in proceedings.

A. BLEIER

"Colloidal Properties of Alumina," submitted to *Alumina Chemicals: Science and Technology Handbook,* Lee Hart, Editor-in-Chief, Pam Achter, Managing Editor, The American Ceramic Society.

A. BLEIER

"Secondary Minimum Interactions and Heterocogulation Encountered in the Aqueous Processing of α-Al_2O_3:m-ZrO_2 Ceramic Composites," submitted to *Colloids and Surfaces.*

R. H. BROWN, P. B. ALLEN, D. M. NICHOLSON, AND W. H. BUTLER

"A First-Principles Calculation of the Resistivity and Thermopower in Strong-Scattering Alloys," Materials Research Society Symposium, Boston, Massachusetts, November 28–December 2, 1988, to be published in proceedings.

R. H. BROWN, P. B. ALLEN, D. M. NICHOLSON, AND W. H. BUTLER

"Resistivity of Strong-Scattering Alloys: Comparison of Exact Supercell and Coherent-Potential Approximation Approaches," submitted to *Phys. Rev. Lett.*

M. G. BURKE AND M. K. MILLER

"A Combined TEM/APFIM Approach to the Study of Phase Transformations: Phase Identification in the Fe-Be System," submitted to *Ultramicroscopy.*

S. J. CHANG AND P. F. BECHER

"Crack Tip Toughening by Inclusions with Pairs of Shear Transformations," American Society of Mechanical Engineers Winter Annual Meeting, San Francisco, California, December 1989, to be published in proceedings.

S. A. DAVID, J. A. HORTON, C. G. MCKAMEY, T. ZACHARIA, AND R. W. REED

"Welding of Iron Aluminides," submitted to *Weld. J.*

S. A. DAVID AND J. M. VITEK

"Correlation Between Solidification Parameters and Weld Microstructures," submitted to *Int. Mater. Rev.*

S. A. DAVID AND J. M. VITEK

"Microstructural Modification During Laser Welding," Indo-U.S. Advanced Study Workshop, Hyderabad, India, January 15–21, 1988, to be published in proceedings.

D. S. EASTON

"Melt Spinning of Lithium Hydride," DOE Workshop on Glass and Ceramic Processing Lithium Materials Processing, Los Alamos National Laboratory, Los Alamos, New Mexico, November 17–19, 1987, to be published in proceedings.

C. L. FU AND A. J. FREEMAN
"Covalent Bonding of Sulfur on Ni(001): The Prototype Adsorbate Poisoner," submitted to *Phys. Rev. Lett.*

C. L. FU AND A. J. FREEMAN
"Surface Magnetism of the Clean Ni(111) Surface and of a Ni Monolayer on Cu(111)," submitted to *J. de Phys.*

C. L. FU AND M. H. YOO
"Stacking Fault Energies, Crystal Elasticity and Their Relation to the Mechanical Properties of Ll_2-Ordered Alloys," Materials Research Society 1988 Fall Meeting, Boston, Massachusetts, November 28–December 2, 1988, to be published in proceedings.

E. P. GEORGE, C. T. LIU, AND R. A. PADGETT
"Comparison of Grain Boundary Compositions in B-Doped and B-Free Ni_3Al," submitted to *Scr. Metall.*

E. P. GEORGE, W. D. PORTER, AND D. C. JOY
"Identification of Cleavage Planes in Al_3Ti-Base Alloy by Electron Channeling in the SEM," Materials Research Society Fall Meeting, Boston, Massachusetts, November 28–December 2, 1988, to be published in proceedings.

B. L. GYORFFY, D. D. JOHNSON, F. J. PINSKI, D. M. NICHOLSON, AND G. M. STOCKS
"The Electronic Structure and the State of Compositional Order in Metallic Alloys," NATO ASI Series on Alloy Phase Stability, Chania, Crete, Greece, June 14–27, 1987, to be published in proceedings.

P. M. HAZZLEDINE, M. H. YOO, AND Y. Q. SUN
"The Geometry of Glide in Ni_3Al at Temperatures Above the Flow Stress Peak," submitted to *Acta Metall.*

S. C. HONG, A. J. FREEMAN, AND C. L. FU
"Magnetism and Hyperfine Interactions of Fe/W(110) and Ag-Covered Fe/W(110)," submitted to *J. de Phys.*

J. A. HORTON, M. K. MILLER, C. T. LIU, E. P. GEORGE, AND J. BENTLEY
"Effect of Aluminum Level of Boron Clustering in Ni_3Al," Materials Research Society Symposium, Boston, Massachusetts, November 28–December 2, 1988, to be published in proceedings.

C. H. HSUEH
"Analogy of Constitutive Equations for Elastic, Viscoelastic and Sintering Behaviors," submitted to *Acta Metall.*

C. H. HSUEH
"Analytical Analyses of Stress Transfer in Fiber-Reinforced Composites with Bonded and Debonded Fiber Ends," submitted to *J. Mater. Sci.*

C. H. HSUEH
"Effects of Interfacial Bonding on Sliding Phenomena During Compressive Loading of an Embedded Fiber," submitted to *J. Mater. Sci.*

C. H. HSUEH
"Evaluation of Interfacial Shear Strength, Residual Clamping Stress and Coefficient of Friction for Fiber-Reinforced Ceramic Composites," submitted to *Acta Metall.*

C. H. HSUEH
"Fiber Pullout Versus Push-down for Fiber-Reinforced Ceramic Composites with Frictional Interfaces," submitted to *J. Mater. Sci.*

C. H. HSUEH
"Interfacial Friction Analysis for Fiber-Reinforced Ceramic Composites During Fiber Push-Down (Indentation)," submitted to *J. Mater. Sci.*

C. H. HSUEH AND P. F. BECHER
"Some Considerations of Bridging Stresses for Whisker-Reinforced Ceramics," submitted to *J. Am. Ceram. Soc.*

C. H. HSUEH, P. F. BECHER, AND P. ANGELINI
"Effects of Interfacial Films on Thermal Stresses in Whisker Reinforced Ceramics," 12th Annual Conference on Composites and Advanced Ceramics, Cocoa Beach, Florida, January 17–20, 1988, to be published in proceedings.

C. H. HSUEH, M. K. FERBER, AND P. F. BECHER
"Stress-Displacement Relation of Fiber for Fiber-Reinforced Ceramic Composites During (Indentation) Loading and Unloading," submitted to *J. Mater. Res.*

C. H. HSUEH AND M. C. LU
"Elastic Stress Transfer from Fiber to Coating in Fiber/Coating System," submitted to *Mater. Sci. Eng.*

E. D. ISAACS, D. B. MCWHAN, C. PETERS, G. E. ICE, D. P. SIDDONS, J. B. HASTINGS, C. VETTIER, AND O. VOGT
"X-Ray Resonance Exchange Scattering in UAs," submitted to *Phys. Rev. Lett.*

A. J. JACOBS, R. E. CLAUSING, L. HEATHERLY, AND R. M. KRUGER
"Irradiation-Assisted Stress Corrosion Cracking and Grain Boundary Segregation in Heat Treated Type 304SS," ASTM 14th International Symposium of the Effects of Radiation on Materials, Andover, Massachusetts, June 27–29, 1988, to be published in proceedings.

E. A. KENIK

"Analytical Electron Microscopy Studies of Radiation Damage," accepted for publication in *Met. Trans.*

E. A. KENIK

"Loss of Grain Boundary Segregant During Ion Milling," Microbeam Analysis Society Meeting, Asheville, North Carolina, July 16–21, 1989, to be published in proceedings.

E. A. KENIK AND M. NASTASI

"Disordering and Phase Decomposition of Ni_2Al_3 Under Low Temperature Electron Irradiation," accepted for publication in *Ultramicroscopy.*

W. KESTERNICH, N. H. PACKAN, AND H. SCHROEDER

"Radiation-Induced Precipitation at Grain Boundaries in Ni-8 at.%Si," submitted to *Phil. Mag.*

H. E. KIM, S. J. ZINKLE, AND W. R. ALLEN

"Preparation and Characterization of ^{17}O-Enriched Al_2O_3 for Nuclear Fusion Damage Experiment," submitted to *J. Am. Ceram. Soc.*

J. KRISHNASWAMY, A. RENGAN, J. NARAYAN, K. VEDAM, AND C. J. MCHARGUE

"Thin Film Deposition by a New Laser-Ablation and Plasma Hybrid Technique," submitted to *J. Appl. Phys. Lett.*

E. H. LEE AND L. K. MANSUR

"Effect of Residual and Injected Oxygen on Swelling in Irradiated Fe-Ni-Cr Alloys," submitted to *Phil. Mag.* (In Press).

E. H. LEE AND L. K. MANSUR

"Effect of Simultaneous B^+ and N_2^+ Implantation on Microhardness, Fatigue Life, and Microstructure in Fe-13Cr-15Ni Base Alloys," submitted to *J. Mater. Res.*

E. H. LEE AND L. K. MANSUR

"Mechanisms of Swelling Suppression in Cold-Worked Phosphorous-Modified Fe-Ni-Cr Alloys," submitted to *Phil. Mag.* (In Press).

E. H. LEE AND N. H. PACKAN

"Swelling Suppression in Phosphorous-Modified Fe-Cr-Ni Alloys During Neutron Irradiation," ASTM 14th International Symposium of the Effects of Radiation on Materials, Andover, Massachusetts, June 27–29, 1988, to be published in proceedings.

J. I. LEE, A. J. FREEMAN, AND C. L. FU

"Enhanced Surface and Interface Magnetism of bcc Ni Overlays on Fe(001)," submitted to *Phys. Rev. B.*

M. B. LEWIS, W. R. ALLEN, R. A. BUHL, N. H. PACKAN, S. W. COOK, AND L. K. MANSUR

"Triple Ion Beam Irradiation Facility," submitted to *Nucl Instrum. Methods B.* (In Press).

C. T. LIU

"Grain-Boundary Design of Ll_2 Ordered Intermetallic Alloys," Materials Research Society Meeting, Reno, Nevada, April 5–8, 1988, to be published in proceedings.

C. T. LIU, E. H. LEE, AND C. G. MCKAMEY

"An Environmental Effect as the Major Cause for Room-Temperature Embrittlement in FeAl," submitted to *Scr. Metall.*

M. C. LU AND C. H. HSUEH

"Effects of Friction in Ceramic Coating/Fiber Composites," submitted to *J. Composite Mater.*

L. K. MANSUR AND W. A. COGHLAN

"Isotopically Alloyed Injector Foils for Helium Effects Research in Mixed-Spectrum Reactors," ASTM 14th International Symposium of the Effects of Radiation on Materials, Andover, Massachusetts, June 26–30, 1988, to be published in proceedings.

L. K. MANSUR AND M. L. GROSSBECK

"Mechanical Property Changes Induced in Structural Alloys by Neutron Irradiations with Different Helium to Displacement Ratios," submitted to *J. Nucl. Mater.*

L. K. MANSUR AND D. J. MICHEL

"Irradiation-Enhanced Materials Science and Engineering: Report on the Symposium," submitted to *Adv. Mater. Processes.*

L. MARTINEZ AND J. H. SCHNEIBEL

"Influencing the Shape of Creep Cavities in Nickel Aluminides by Stress Changes," submitted to *J. Mater. Res.*

C. J. MCHARGUE

"Ion Beam Mixing of Metals and Ceramics - Material Considerations," NATO-Advanced Study Institute on Structure-Property Relationships in Ion-Beam Surface-Modified Ceramics - Theory and Applications, Castelvecchio Pascoli, Italy, August 28–September 9, 1988, to be published in proceedings.

C. J. MCHARGUE

"Ion Implantation and Ion Beam Mixing," submitted to *Surface Engineering,* ed. R. Kossowsky and published by CRC Publications.

C. J. MCHARGUE

"The Mechanical Properties of Ion Implanted Ceramics," NATO-Advanced Study Institute on Structure-Property Relationships in Ion-Beam Surface-Modified Ceramics - Theory and Applications, Castelvecchio Pascoli, Italy, August 28–September 9, 1988, to be published in proceedings.

C. J. MCHARGUE

"Wear Resistant Thin Films and Surfaces Produced by Ion Beam Processes," submitted to *Ceram. Films Coatings.*

C. J. MCHARGUE, M. E. O'HERN, C. W. WHITE, AND M. B. LEWIS

"Ion Implantation in Ceramics-Residual Stress and Properties," International Conference on Surface Modification of Metals by Ion Beams, Riva Dela Garda, Italy, September 12–16, 1988, proceedings to be published in *Mater. Sci. Engr.*

C. J. MCHARGUE, C. W. WHITE, P. S. SKLAD, M. E. O'HERN, D. L. JOSLIN, AND G. C. FARLOW

"Structure-Mechanical Property Relationships in Ion Implanted Ceramics," 2nd International Seminar on Surface Engineering by High Energy Beams, Lisbon, Portugal, September 5–7, 1989, to be published in proceedings.

M. K. MILLER AND M. G. BURKE

"Atom Probe Field-Ion Microscopy - Imaging at the Atomic Level," submitted to *Imaging of Materials*, ed. D. B. Williams, A. Gronsky, and A. R. Pelson, Oxford University Press.

M. K. MILLER AND M. G. BURKE

"Fine-Scale Microstructural Characterization of Pressure Vessel Steels and Related Materials Using APFIM," 14th International Symposium on Effects of Radiation on Materials, Andover, Massachusetts, June 27–29, 1988, to be published in proceedings.

M. K. MILLER, M. G. HETHERINGTON, AND M. G. BURKE

"Atom Probe Field-Ion Microscopy - A Technique for Microstructural Characterization of Irradiated Materials on the Atomic Scale," submitted to *Metall. Trans.*

K. L. MORE AND M. K. MILLER

"Composition and Microstructure of a Nickel-Base Superalloy, UDIMET 720," 47th Annual Meeting of the Electron Microscopy Society of America, San Antonio, Texas, August 6–11, 1989, to be published in proceedings.

M. E. O'HERN, R. H. PARRISH, AND W. C. OLIVER

"Evaluation of Mechanical Properties of TiN Films by Ultra-Low Load Indentation," International Conference on Metallurgical Coatings, San Diego, California, April 17–21, 1989, to be published in proceedings.

W. C. OLIVER
"Mechanical Properties Microprobe," submitted to *Encyclopedia of Materials Science.*

T. F. PAGE, C. J. MCHARGUE, AND C. W. WHITE
"SEM Electron Channelling Patterns as a Technique for the Characterization of Ion Implantation Damage," submitted to *J. Mater. Res.*

T. F. PAGE, W. C. OLIVER, AND C. J. MCHARGUE
"The Unusual Deformation Behavior of Ceramic Crystals Subjected to Very Low Load Indentations," submitted to *J. Mater. Sci.*

J. E. PAWEL AND C. J. MCHARGUE
"Modified Pull Test for the Testing of Very Adherent Films," NATO-Advanced Study Institute on Structure-Property Relationships in Ion-Beam Surface-Modified Ceramics - Theory and Applications, Castelvecchio Pascoli, Italy, August 28–September 9, 1988, to be published in proceedings.

D. F. PEDRAZA
"Irradiation as a Tool for Studying Solid State Amorphization Phenomena," TMS/AMS Fall Meeting, Chicago, Illinois, September 25–29, 1988, to be published in proceedings.

D. F. PEDRAZA
"Radiation Induced Microstructural Evolution and Amorphization of Intermetallic," to be submitted to *Radiat. Eff. and Defects in Solids.* (In Press).

D. F. PEDRAZA, P. J. MAZIASZ, AND R. K. KLUEH
"Helium Effects on the Microstructural Evolution of Reactor Irradiated Ferritic and Austenitic Steels," submitted to *Radiation Effects*, proceedings of Workshop on the Effects of Recoil Energy Spectrum and Nuclear Transmutations on the Evolution of the Microstructure, Lugano, Switzerland, March 23, 1988.

J. B. PETHICA AND W. C. OLIVER
"Tip Surface Interactions in STM and AFM," submitted to *Physica Scr.*

G. M. PHARR AND W. C. OLIVER
"Nanoindentation of Silver - Relations Between Hardness and Dislocation Structure," submitted to *J. Mater. Res.*

W. D. PORTER, K. HISATSUNE, C. J. SPARKS, W. C. OLIVER, AND A. DHERE
"Phase and Microstructure of Fe Modified Al_3Ti," Materials Research Society Symposium, Boston, Massachusetts, November 28–December 2, 1988, to be published in proceedings.

W. D. PORTER, L. MARTINEZ, AND J. H. SCHNEIBEL
"Cavitation and Coble Creep in a Powder-Metallurgical (PM) Nickel Aluminide of Composition Ni-22.8Al-0.6Hf-0.1B (at. %)," submitted to *Scr. Metall.*

S. I. RAO, C. R. HOUSKA, K. GRABOWSKI, J. CLAUSSEN, G. ICE, AND A. HABENSCHUSS

"X-Ray Diffraction from Ion Implanted Zones," Materials Research Society Symposium, Boston, Massachusetts, November 28–December 3, 1988, to be published in proceedings.

M. RAPPAZ, S. A. DAVID, J. M. VITEK, AND L. A. BOATNER

"Development of Microstructures in Fe-15Ni-15Cr Single Crystal Electron Beam Welds," submitted to *Metall. Trans.*

R. REBONATO, G. E. ICE, A. HABENSHCUSS, AND J. C. BILELLO

"High-Resolution Microdiffraction Study of Notch-Tip Deformation in Mo Single Crystals Using X-Ray Synchrotron Radiation," submitted to *Scr. Metall.*

K. A. RITLEY, R. C. WARD, AND N. F. WRIGHT

"The Madelung Energy of the Superconductor $YBa_2Cu_3O_7$," submitted to *Am. J. Phys.*

J. H. SCHNEIBEL AND L. MARTINEZ

"Coble Creep, Cavity Sintering, and Cavity Growth," Symposium on the Sintering of Advanced Ceramics at the 90th Annual Meeting of the American Ceramic Society, Cincinnati, Ohio, May 1–5, 1988, to be published in proceedings.

J. H. SCHNEIBEL AND L. MARTINEZ

"Crack-Like Creep Cavitation in a Nickel Aluminide," accepted for publication in *Acta Metall.*

J. H. SCHNEIBEL AND W. D. PORTER

"Microstructure and Mechanical Properties of Ll_2-Structure Alloys Based on Al_3Zr," Materials Research Society Fall Meeting, Boston, Massachusetts, November 28–December 2, 1988, to be published in proceedings.

T. SCHOBER AND K. FARRELL

"Helium Bubbles in α-Ti and Ti Tritide Arising from Tritium Decay: A TEM Study," accepted by *J. Nucl. Mater.*

V. K. SIKKA

"Advances in Processing Techniques for Nickel Aluminides," ASM European Technical Conference, Advanced Materials and Processing Techniques for Structural Applications, Paris, France, September 7–9, 1987, to be published in proceedings.

P. S. SKLAD

"In-Situ Observations of the Amorphous to Gamma Transformation in Ion Implanted Al_2O_3," The 47th Annual Meeting of the Electron Microscopy Society of America, San Antonio, Texas, August 6–11, 1989, to be published in proceedings.

P. S. SKLAD

"The Use of Analytical Electron Microscopy in the Study of Ion Implanted Materials," Ion Implantation and Plasma Assisted Processes for Industrial Application, Atlanta, Georgia, May 21–25, 1988, to be published in proceedings.

P. S. SKLAD, J. D. MCCALLUM, S. J. PENNYCOOK, C. J. MCHARGUE, C. W. WHITE, AND A. PEREZ

"Microstructural Characterization of α-Al_2O_3 Implanted with Iron," Materials Research Society Symposium, Boston, Massachusetts, November 28–December 2, 1988, to be published in proceedings.

J. L. SNELGROVE, G. L. HOFMAN, AND G. L. COPELAND

"Fuel for the Advanced Neutron Source-Performance Testing and Fabrication Development," American Nuclear Society Winter Meeting, Washington, D.C., October 30–November 3, 1988, to be published in proceedings.

G. M. STOCKS AND A. GONIS, EDS.

"NATO ASI on Alloy Phase Stability," NATO ASI Series on Alloy Phase Stability, Chania, Crete, Greece, June 14–27, 1987, Martinus Nijhoff Publishers, The Netherlands, editors of proceedings to be published.

R. E. STOLLER AND L. K. MANSUR

"The Influence of Other Microstructural Features on Void Formation and Void Growth in Irradiated Materials," ASTM 14th International Symposium of the Effects of Radiation on Materials, Andover, Massachusetts, June 26–30, 1988, to be published in proceedings.

Z. SZOTEK, W. M. TEMMERMAN, B. L. GYORFFY, AND G. M. STOCKS

"On Positron Annihilation in Concentrated Random Alloys and Superconducting Cuprates," 20th Polish Seminar on Positron Annihilation, Piechowice, Poland, May 15–21, 1988, to be published in proceedings.

M. TAKEYAMA AND C. T. LIU

"Effect of Preoxidation and Grain Size on Ductility of a Boron-Doped Ni_3Al at Elevated Temperatures," submitted to *Acta Metall.*

M. TAKEYAMA AND C. T. LIU

"Effect of Preoxidation and Grain Size on Ductility of a Boron-Doped Ni_3Al at Elevated Temperatures," Materials Research Society Fall Meeting, Boston, Massachusetts, November 28–December 2, 1988, to be published in proceedings.

M. TAKEYAMA AND C. T. LIU

"Grain-Boundary Contamination and Ductility Loss in Boron-Doped Ni_3Al," submitted to *Metall. Trans.*

W. M. TEMMERMAN, G. Y. GUO, Z. SZOTEK, P. J. DURHAM, AND G. M. STOCKS
"On the Validity of the Band Model for High T_c Superconductors," International Symposium on the Electron Structure of High T_c Superconductors, Rome, Italy, October 4–7, 1988, to be published in proceedings.

P. E. A. TURCHI, A. GONIS, X. ZHANG, AND G. M. STOCKS
"Configurational Energies in Terms of Effective Cluster Interactions in Binary Substitutional Alloys: Connection Between the Embedded Cluster Method and the Generalized Perturbation Method," NATO Advanced Study Institute on Alloy Phase Stability Conference, Maleme, Crete, Greece, June 14–27, 1987, to be published in proceedings.

F. J. WALKER, R. A. MCKEE, AND F. A. LIST
"Amorphous Interface Between Crystalline Nickel and Titanium Films," submitted to *J. Mater. Sci.*

C. W. WHITE, C. J. MCHARGUE, P. S. SKLAD, L. A. BOATNER, AND G. C. FARLOW
"Ion Implantation and Annealing of Insulating Materials," submitted to *Mater. Sci. Reports.*

M. H. YOO
"The Force on a Dislocation in Superlattice Structure," submitted to *Philos. Mag.*

M. H. YOO, M. S. DAW, AND M. I. BASKES
"Atomistic Simulation of Superdislocation Dissociation in Ni_3Al," Atomistic Modelling in Materials-Beyond Pair-Potentials, Chicago, Illinois, September 27–30, 1988, to be published in proceedings.

M. H. YOO, C. L. FU, AND J. K. LEE
"Deformation Twinning in Ordered Intermetallic Compounds," Materials Research Society Meeting, Boston, Massachusetts, November 28–December 2, 1988, to be published in proceedings.

M. H. YOO AND A. H. KING
"Interaction of Slip with Grain Boundary in the Ll_2 Ordered Structure - A Σ=9 Tilt Boundary," Materials Research Society Meeting, Reno, Nevada, April 5–8, 1988, to be published in proceedings.

M. H. YOO AND A. H. KING
"Intergranular Fracture by Slip/Grain Boundary Interaction," submitted to *Metall. Trans.*

H. ZABEL, N. LUCAS, AND C. J. SPARKS
"X-Ray Characterization of Heteroepitaxial GaAs on Si (001)," submitted to *J. Electrochem. Soc.*

T. ZACHARIA, S. A. DAVID, J. M. VITEK, AND T. DEBROY
"Heat Transfer During Nd:YAG Pulsed Laser Welding and Its Effect on Solidification Structure of Austenitic Stainless Steels," submitted to *Metall. Trans.*

T. ZACHARIA, S. A. DAVID, J. M. VITEK, AND T. DEBROY
"Weld Pool Development During GTA and Laser Welding of Type 304 Stainless Steel. Part I - Theoretical Analysis," submitted to *Weld. J.*

T. ZACHARIA, S. A. DAVID, J. M. VITEK, AND T. DEBROY
"Weld Pool Development During GTA and Laser Welding of Type 304 Stainless Steel. Part II - Experimental Correlation," submitted to *Weld. J.*

T. ZACHARIA, S. A. DAVID, J. M. VITEK, AND R. P. MARTUKANITZ
"Weldability and Microstructural Characterization of Al-Li Alloys," Fifth International Aluminum - Lithium Conference, Williamsburg, Virginia, March 28–21, 1989, to be published in proceedings.

T. ZACHARIA, A. H. ERASLAN, D. K. AIDUN, AND S. A. DAVID
"Three Dimensional, Transient Model for Arc Welding Process," submitted to *Metall. Trans.*

S. ZINKLE AND K. FARRELL
"Void Swelling and Defect Cluster Formation in Reactor-Irradiated Copper," submitted to *J. Nucl. Mater.*

ORNL/TM–11281
Distribution
Category UC–404

INTERNAL DISTRIBUTION

1-2. Central Research Library
3. Document Reference Section
4-5. Laboratory Records Department
6. Laboratory Records, ORNL RC
7. ORNL Patent Section
8-57. M&C Records Office
58. D. J. Alexander
59. K. B. Alexander
60. P. Angelini
61. B. R. Appleton
62. P. F. Becher
63. J. Bentley
64. T. M. Besmann
65. A. Bleier
66. E. E. Bloom
67. R. A. Bradley
68. V. R. Bullington
69. W. H. Butler
70. P. T. Carlson
71. A. Choudhury
72. D. F. Craig
73. S. A. David
74. J. R. DiStefano
75. C. K. DuBose
76. L. M. Ferris
77. E. L. Fuller
78. E. P. George
79. M. L. Grossbeck
80. F. M. Haggag
81. R. L. Heestand
82. J. A. Horton
83. L. L. Horton
84. C. Hsueh
85. C. R. Hubbard
86. G. E. Ice
87. M. A. Janney
88. M. G. Jenkins
89. D. R. Johnson
90. R. R. Judkins
91. M. A. Karnitz
92. E. A. Kenik
93. D. J. Kim
94. H. E. Kim
95. O. F. Kimball
96. E. H. Lee
97. C. T. Liu
98-100. L. K. Mansur
101. P. J. Maziasz
102. D. J. McGuire
103. C. J. McHargue
104. C. G. McKamey
105. M. K. Miller
106. A. J. Moorhead
107. K. L. More
108. R. K. Nanstad
109. M. E. O'Hern
110. O. O. Omatete
111. N. H. Packan
112. D. F. Pedraza
113. M. L. Poutsma
114. P. L. Rittenhouse
115. A. F. Rowcliffe
116. A. C. Schaffhauser
117. M. A. Schmidt
118. V. K. Sikka
119. P. S. Sklad
120. G. M. Slaughter
121. C. J. Sparks
122. E. D. Specht
123-127. J. O. Stiegler
128. R. E. Stoller
129. V. J. Tennery
130. P. F. Tortorelli
131. D. B. Trauger
132. L. J. Turner
133. J. M. Vitek
134. J. R. Weir
135. F. W. Wiffen

136. M. K. Wilkinson
137. D. F. Wilson
138. S. G. Winslow
139. N. F. Wright
140. M. H. Yoo
141. F. W. Young
142. T. Zacharia
143. S. J. Zinkle
144. A. Zucker
145. A. D. Brailsford (Consultant)
146. H. D. Brody (Consultant)
147. D. P. Pope (Consultant)
148. M. L. Savitz (Consultant)
149. E. R. Thompson (Consultant)
150. J. B. Wachtman, Jr. (Consultant)

EXTERNAL DISTRIBUTION

151-153. AERE, Harwell, Didcot, Oxon, OX11, ORB, England

J. P. Charlesworth, Chemistry Division
A. B. Lidiard, Theoretical Physics Division
S. F. Pugh, Metallurgy Division

154-155. AMES LABORATORY, Iowa State University, Ames, IA 50011

B. N. Harmon
R. B. Thompson

156-162. ARGONNE NATIONAL LABORATORY, 9700 South Cass Ave., Argonne, IL 60439

M. B. Brodsky
B. Dunlap
B. R. T. Frost
D. M. Gruen
E. N. Kaufmann
R. Weeks
H. Wiedersich

163-164. ARIZONA STATE UNIVERSITY, Tempe, AZ 85287

R. W. Carpenter
J. B. Wagner

165-168. ASM INTERNATIONAL, Metals Park, OH 44073

H. David Chafe, Director
J. Griffiths
E. L. Langer
W. W. Scott, Jr., Technical Director

169. AUBURN UNIVERSITY, Department of Mechanical Engineering, Auburn, AL 36849

B. A. Chin

170. AUSTRALIAN ATOMIC ENERGY COMMISSION, Lucas Heights, NSW, Australia

A. Jostsons

171-173. BROOKHAVEN NATIONAL LABORATORY, Upton, NY 11973

A. N. Goland, Department of Applied Science
M. Knotek
K. Lynn

174-175. BROWN UNIVERSITY, Division of Engineering, Providence, RI 02912

J. Gurland
M. H. Richman

176. CARNEGIE-MELLON UNIVERSITY, Schenley Park, Pittsburgh, PA 15213

H. I. Aaronson

177. CASE-WESTERN RESERVE UNIVERSITY, Metallurgy and Materials Science, Cleveland, OH 44106

A. H. Heuer

178. CENTRAL ELECTRICITY GENERATING BOARD, Berkeley Nuclear Laboratories, Berkeley, Gloucestershire, CL13 9PB, England

J. E. Harris

179. CENTRE d'Etúdes Nucléaires, Fontenay-aux-Roses, France

Y. Queré, Section d'Etúdes des Solides Irradies

180-181. CORNELL UNIVERSITY, Department of Materials Science and Engineering, Ithaca, NY 14853

C. Y. Li
J. W. Mayer

182-185. EG&G IDAHO, INC., P.O. Box 1625, Idaho Falls, ID 83415

D. W. Keefer
D. D. Keiser
J. F. Key
V. W. Storhok

186-187. E. I. DU PONT de NEMOURS & COMPANY, INC., Experimental Station, E356/323, Chestnut Run 702, Wilmington, DE 19898

J. E. Berkowitch, Manager, Technology Transfer
R. R. H. French

188. FOSTER-MILLER, INC., 350 Second Avenue, Waltham, MA 02254

P. Stark

189. GEORGIA INSTITUTE OF TECHNOLOGY, School of Materials Engineering, Atlanta, GA 30332–0245

S. D. Antolovich

190-191. GEORGIA INSTITUTE OF TECHNOLOGY, Department of Chemical Engineering, Atlanta, GA 30332

B. R. Livesay
R. A. Young

192. GLCA DENISON UNIVERSITY, Main Street, Granville, OH 43023

R. R. Winters, Director, Oak Ridge Science Semester

193. HANFORD ENGINEERING DEVELOPMENT LABORATORY, P.O. Box 1970, Richland, WA 99352

R. Powell

194. ILLINOIS INSTITUTE OF TECHNOLOGY, Department of Metallurgical and Materials Engineering, Chicago, IL 60612

N. N. Brever

195-198. INSTITUTE FüR FESTKöRPERFORSCHUNG, Kernforschungsanlage Jülich, Postfach 1913, D-5170, Federal Republic of Germany

H. G. Bohn
W. Schilling
H. Ullmaier
H. Wenzl

199. INSTITUTE FüR METALLPHYSIK, University of Göttingen, Federal Republic of Germany

P. Haasen

200. INSTITUTE FüR REAKTORWERKSTOFFE, Kernforschungsanlage Jülich, Postfach 1913, D-5170, Jülich, Federal Republic of Germany

H. Nickel, Director

201. INSTITUTE FüR THEORETISCHE und ANGEWANDTE PHYSIK, UNIVERSITäT STUTTGART, 7000 Stuttgart 80-Pfaffenwaldring 57/V1, Federal Republic of Germany

A. Seeger

202-205. LAWRENCE BERKELEY LABORATORY, One Cyclotron Road, Mail Stop 62-203, Materials and Molecular Research Division, Berkeley, CA 94720

K. Berkner
J. W. Morris, Jr.
N. E. Phillips
R. O. Ritchie

206. LAWRENCE LIVERMORE NATIONAL LABORATORY, University of California, P.O. Box 808, Livermore, CA 94550

T. Sugihara

207-211. LOS ALAMOS NATIONAL LABORATORY, P.O. Box 1663, Los Alamos, NM 87545

F. A. Morse
D. Parkin
D. J. Sandstrom
J. F. Smith
E. Wewerka

212. LOUGHBOROUGH UNIVERSITY OF TECHNOLOGY, 51 Tynedale Road, Loughborough, Leicestershire, England LE113TA

R. G. Faulkner

213. MASSACHUSETTS INSTITUTE OF TECHNOLOGY, Department of Materials Science, 77 Massachusetts Avenue, Cambridge, MA 02139

R. L. Coble

214-215. MICHIGAN TECHNOLOGICAL UNIVERSITY, Department of Metallurgical Engineering, Houghton, MI 49931

L. A. Heldt
C. L. White

216. MOLY CORPORATION, P.O. Box 54945, Los Angeles, CA 90054

A. Levy

217. NATIONAL INSTITUTE OF STANDARDS AND TECHNOLOGY, Gaithersburg, MD 20899

S. J. Dapkunas

218. NATIONAL UNIVERSITY OF ATHENS, Institute of Mineralogy and Petrology, Panepistimiopolis, Ano Ilissia, Athens 621, Greece

C. N. Koumelis

219. NAVAL RESEARCH LABORATORY, Washington, DC 20375

D. J. Michel, Metallurgy Division, Code 6397

220-222. NORTH CAROLINA STATE UNIVERSITY, Department of Materials Engineering, Raleigh, NC 27607

R. B. Bensen, Jr.
J. J. Hren
C. C. Koch

223-224. NORTHWESTERN UNIVERSITY, Department of Materials Science and Engineering, Evanston, IL 60201

M. Meshii
J. R. Weertman

225-226. OAK RIDGE ASSOCIATED UNIVERSITIES, P.O. Box 117, Oak Ridge, TN 37831

J. L. Gumnick, University Programs Division
K. Newport

227. OFFICE OF NAVAL RESEARCH, Metals and Ceramics Program, Code 471, 800 N. Quincy Street, Arlington, VA 22217

R. C. Pohanka

228-229. OHIO STATE UNIVERSITY, 116 W. 19th Street, Columbus, OH 45469

R. Mills, Department of Physics
R. R. Rapp, Department of Metallurgical Engineering

230. PACIFIC NORTHWEST LABORATORY, P.O. Box 999, Richland, WA 99352

G. L. McVary

231. PENNSYLVANIA STATE UNIVERSITY, Department of Materials Science, University Park, PA 16802

K. Spear

232. PHOTON PHYSICS, 3175 Penobscot Building, Detroit, MI 48226

G. Keros

233-234. RENSSELAER POLYTECHNIC INSTITUTE, Materials Engineering Department, MRC 104, Troy, NY 12180

M. E. Glicksman
N. P. Stoloff

235. RESEARCH LABORATORY OF ENGINEERING MATERIALS, 4259 Nagatsuta, Midori, Yokohama 227, Japan

Shigeyuki Somiya, Laboratory of Engineering Materials

236. RICE UNIVERSITY, P.O. Box 192, Department of Materials Science, Houston, TX 77001

R. B. McLellan

237. SANDIA NATIONAL LABORATORIES, P.O. Box 5800, Albuquerque, NM 87185

R. L. Schwoebel, Director, Material and Process Sciences

238-240. SANDIA NATIONAL LABORATORIES, Livermore, CA 94550

W. Bauer, Physical Research
P. Mattern
R. W. Rohde

241. SCIENCE, 1515 Massachusetts Ave. NW, Washington, DC 20005

P. H. Abelson

242. SCK/CEN, B 2400 Mol, Belgium

S. Amelinckx

243. SOLAR ENERGY RESEARCH INSTITUTE, Golden, CO 80401

D. Feucht

244. STANFORD SYNCHROTRON RADIATION LABORATORY, P.O. Box 4349, Bin 69, Stanford, CA 94309–0210

A. I. Bienenstock

245-246. STANFORD UNIVERSITY, Department of Materials Science and Engineering, Stanford, CA 94305

R. H. Bube
R. Sinclair

247. TECHNISCHE HOCHSCHULE AACHEN, Aachen, Federal Republic of Germany

K. Lücke

248. TOYOTA CENTRAL RESEARCH AND DEVELOPMENT LABORATORIES, INC., 41-1 Nagakute, Aichi-ken, Aichi, 480-11, Japan

T. Hioki

249. UNIVERSITY OF ALABAMA, Department of Materials Engineering, Birmingham, AL 35294

C. S. Hartley

250. UNIVERSITY OF BIRMINGHAM, Department of Physical Metallurgy and Science and Materials, Birmingham, B152TT England

R. E. Smallman

251. UNIVERSITY OF CONNECTICUT, Department of Metallurgy, Storrs, CT 06268

P. C. Clapp

252. UNIVERSITY OF CRETE, Physics Department, P.O. Box 470, Iraklion, Crete, Greece

G. Kiriakidis

253. UNIVERSITY OF FLORIDA, Department of Materials Science and Engineering, Gainesville, FL 32611

E. D. Vernik, Jr.

254. UNIVERSITY OF HOUSTON, Department of Physics, Houston, TX 77004

S. C. Moss

255-257. UNIVERSITY OF ILLINOIS, 104 South Goodwin Avenue, Urbana, IL 61801

C. G. Bergeron
H. K. Birnbaum, Materials Research Laboratory
H. Zabel

258. UNIVERSITY OF KENTUCKY, Department of Materials Science and Engineering, Lexington, KY 40506

P. Gillis

259. UNIVERSITY OF LANCASTER, Department of Physics, Lancaster LA1 4YB, England

H. M. Pollock

260. UNIVERSITY OF MARYLAND, Chemical and Nuclear Engineering Bldg., College Park, MD 20742–1572

R. J. Arsenault

261. UNIVERSITY OF MEXICO, Instituto de Fisica, A.P. 20-364, 01000 Mexico, D.F. Mexico

J. A. Soullard

262-263. UNIVERSITY OF MICHIGAN, Department of Materials and Metallurgical Engineering, Ann Arbor, MI 48109

W. C. Bigelow
R. D. Pehlke

264. UNIVERSITY OF MINNESOTA, Department of Chemical Engineering and Materials Science, Minneapolis, MN 55455

W. W. Gerberich

265. UNIVERSITY OF MISSISSIPPI, Department of Mechanical Engineering, University, MS 38677

J. G. Vaughan

266-267. UNIVERSITY OF MISSOURI-ROLLA, 222 Fulton Hall, Rolla, MO 64501

H. U. Anderson
H. W. Weart, Department of Metallurgical Engineering

268. UNIVERSITY OF OSLO, Department of Chemistry, Blindern, Oslo, Norway

K. Kofstad

269-272. UNIVERSITY OF TENNESSEE, Department of Materials Science and Engineering, Knoxville, TN 37996

J. Danko
B. F. Oliver
J. E. Spruiell
E. E. Stansbury

273. UNIVERSITY OF TEXAS, Department of Mechanical Engineering, Austin, TX 78712

H. L. Marcus

274-276. UNIVERSITY OF VIRGINIA, Department of Material Science, Thornton Hall, Charlottesville, VA 22901

W. A. Jesser
K. R. Lawless
H. G. F. Wilsdorf

277. UNIVERSITY OF VIRGINIA, School of Engineering and Applied Science, Thornton Hall, Charlottesville, VA 22901

E. A. Starke, Jr.

278. UNIVERSITY OF WASHINGTON, Department of Metallurgical Engineering, Seattle, WA 98195

D. H. Polonis

279. UNIVERSITY OF WISCONSIN, Department of Metallurgical and Mineral Engineering, Madison, WI 53706

R. A. Dodd

280. VANDERBILT UNIVERSITY, Mechanical Engineering and Materials Science, Nashville, TN 37235

J. J. Wert

281-282. VIRGINIA POLYTECHNIC INSTITUTE AND STATE UNIVERSITY, Department of Materials Engineering, Blacksburg, VA 24061

R. W. Hendricks
C. W. Spencer

283. DOE, DIVISION OF MAGNETIC FUSION ENERGY, Washington, DC 20545

T. C. Reuther (ER-533, J224/GTN)

284-287. DOE, DIVISION OF MATERIALS SCIENCES, Washington, DC 20545

J. B. Darby (ER-131, J321/GTN)
R. J. Gottschall (ER-131, J321/GTN)
R. W. Heckel (ER-131, J314/GTN)
I. L. Thomas (ER-132, J321/GTN)

288. DOE, OFFICE OF FOSSIL ENERGY, Washington, DC 20545

M. I. Singer (FE-30)

289. DOE, OAK RIDGE OPERATIONS OFFICE, P.O. Box 2001, Oak Ridge, TN 37831-8600

Office of Assistant Manager for Energy Research and Development

290-339. DOE, OFFICE OF SCIENTIFIC AND TECHNICAL INFORMATION, P.O. Box 62, Oak Ridge, TN 37831

For distribution as shown in DOE/OSTI-4500, Distribution Category UC-404 (Materials).